ULB FACULTÉ DES SCIENCES

UNIVERSITÉ LIBRE DE BRUXELLES

# Very-high resolution earth observation data and open-source solutions for mapping urban areas in sub-Saharan Africa.

*Implementation of an operational framework for production of geoinformation : Application on Ouagadougou (Burkina Faso) and Dakar (Senegal).*

**Thesis presented by Taïs GRIPPA**

with a view to obtaining the PhD Degree in Geography (”Docteur en Sciences Géographiques”)

Année académique 2018-2019

Supervisor : Professor Eléonore WOLFF

Laboratoire d’Analyse Géospatiale (ANAGEO)

**Thesis jury :**

Jean-Michel DECROLY (Université libre de Bruxelles, Chair)
Eléonore WOLFF (Université libre de Bruxelles, Secretary)
Marius GILBERT (Université libre de Bruxelles)
Catherine LINARD (Université de Namur)
Frank CANTERS (Vrije Universiteit Brussel)

belspo

# Very-high resolution earth observation data and open-source solutions for mapping urban areas in sub-Saharan Africa.

Implementation of an operational framework for production of geoinformation: Application on Ouagadougou (Burkina Faso) and Dakar (Senegal).

January 2019

Thesis presented by **Taïs Grippa** with a view to obtaining the PhD Degree in Geography.



Funded by the Belgian Federal Science Policy Office (BELSPO) in the frame of the STEREO III program, as part of the MAUPP (SR/00/304) project.

DOI: 10.5281/zenodo.2584142

*To my parents.*

# Abstract

Nowadays, in sub-Saharan Africa (SSA), about 40% of the population is urban and this region is expected to face the highest growth rates during the next decades. By 2100, the three most populated cities in the world will be located in SSA. As a consequence of the extremely fast transformations experienced during the last decades, SSA cities are facing social and environmental issues combined with a lack of financial means and capacity in urban planning and management. The poorest often constitute a large part of the urban population that is extremely vulnerable to health and disaster risks.

In SSA cities, up-to-date and spatially detailed geographic information is often missing. This lack of information is an important issue for many scientific studies focusing on different urban issues and there is a real need to improve the availability of geoinformation for these cities in order to support urban planning, urban management, environment monitoring, epidemiology or risk assessment, etc... The work presented in this thesis aims to develop different frameworks for the production of geoinformation. For this purpose, advantage is taken of Very-High Resolution Remote Sensing imagery (0.5 meters) and open-source software. These frameworks implement cutting-edge methods and can handle a large amount of data in a semi-automated fashion to produce maps covering very large areas of interest. In the spirit of open science, the processing chains are entirely based on open-source software and are released publicly in open-access for any interested researchers, in order to make the methods developed completely transparent and in order to contribute to the creation of a pool of common tools and scientific knowledge. These frameworks are used to produce very detailed land-cover and land-use maps that provide essential information such as the built-up density, or the fact that a neighborhood is residential or not. This detailed geoinformation is then used as indicators of presence of populated places to improve existing population models at the intra-urban level.

# Résumé

Aujourd'hui, près de 40% de la population en Afrique subsaharienne vit en ville, et on prévoit que ces pays connaitront la plus forte croissance urbaine au cours des prochaines décennies. D'ici 2100, les trois villes les plus peuplées au monde seront probablement des villes d' Afrique subsaharienne. La conséquence des transformations extrêmement rapides que ces villes ont subies au cours des dernières décennies est qu'elles doivent faire face aujourd'hui à de nombreux problèmes liés à l'environnement, la planification urbaine ou encore le développement des inégalités. Une partie très importante des populations urbaines des grandes métropoles d' Afrique subsaharienne vit dans une extrême pauvreté et est très vulnérable aux risques naturels et sanitaires.

Dans ces villes, des données géographiques spatialement détaillées sont souvent indisponibles et leur mise à jour pose problème. Ce manque d'information est un problème important pour de nombreuses études scientifiques s'intéressant aux différents problèmes urbains. Il y a donc un réel besoin d'améliorer la production et la disponibilité des données géographiques pour ces villes, pour aider la planification et la gestion des services urbains, pour la surveillance de l'environnement, les études épidémiologiques et d'évaluation du risque, etc. . . Le travail présenté dans cette thèse a pour objectif de développer différents "frameworks" pour la production d'information géographique. À cette fin, nous avons tiré avantage des données satellitaires à très haute résolution spatiale (0.5m). Ces frameworks mettent en oeuvre des méthodes à la pointe de la recherche, notamment pour la cartographie de l'occupation du sol, et sont capables de traiter de façon semi-automatisée de grandes quantités de données afin de couvrir des zones d'intérêt très étendues. Ces chaînes de traitement reposent entièrement sur des logiciels libres (open source) et sont mises librement à disposition des chercheurs intéressés, dans un souci de transparence et pour contribuer à la mutualisation des outils et des connaissances scientifiques, dans l'esprit de l'open science. Ces frameworks sont utilisés, ici, afin de produire des cartes d'occupation et d'utilisation du sol avec des niveaux de détails très élevés, fournissant ainsi des informations essentielles comme la densité du bâti, ou le fait qu'un quartier soit résidentiel ou non. Ces informations sont ensuite utilisées comme indicateurs de la présence de population, ce qui permet d'améliorer les modèles de

population existants.

# Remerciements

Tout d'abord je voudrais remercier ma femme, Giusi, qui a toujours été là pour moi depuis 10 ans et qui a été mon pilier durant ces derniers mois tourmentés. Merci aussi à mes parents... Ensuite, je voudrais remercier tous mes amis et toute ma famille (et belle famille ;)) pour m'avoir supporté. Désolé que vous ne m'ayez pas beaucoup vu parfois quand les deadlines se faisaient plus proches. Je voudrais également remercier Éléonore Wolff, ma promotrice, qui m'a donné la chance de réaliser cette thèse et qui est toujours restée bienveillante et de bon conseil. Je voudrais pour finir remercier tous les collègues. Je pense que c'est vraiment incroyable de pouvoir travailler chaque jour dans un cadre aussi particulier que celui de l'IGEAT. Enfin, je voudrais particulièrement remercier Moritz, sans qui cette thèse n'aurait pas eu la même saveur de liberté, et qui a toujours été là quand j'avais besoin d'aide avec mes bugs dans GRASS GIS (et il y en a eu un tas...), mais aussi Mathieu, Sabine et Nicholus qui ont bien voulu relire et commenter les différentes versions de ce manuscrit.

# Acronyms

**AOI** Area Of Interest.

**DL** Deep Learning.

**FOSS4G** Free and Open Source Software for Geospatial.

**GEOBIA** Geographic Object-Based Image Analysis.

**GIS** Geographic Information Systems.

**HPC** High-performance computing.

**HR** High Resolution.

**HRRS** High Resolution Remote sensing.

**LC** Land Cover.

**LU** Land Use.

**MDG** Millennium Development Goals.

**nDSM** normalized Digital Surface Model.

**OBIA** Object-Based Image Analysis.

**OSM** OpenStreetMap.

**RS** Remote Sensing.

**RTAE** Relative Total Absolute Error.

**SDG** Sustainable Development Goals.

**SSA** sub-Saharan Africa.

**UN** United Nations.

**USPO** Unsupervised Segmentation Parameter Optimization.

**VGI** Volunteered Geographic Information.

**VHR** Very-High Resolution.

**VHRRS** Very-High Resolution Remote Sensing.

# Contents

# Chapter 1

# Introduction

Contrary to what one might think, African urban history dates back to a long time before the European colonization. Indeed, the first cities in western Africa probably appeared in Ghana between the $6^{th}$ and $7^{th}$ centuries but remained very small [1]. During the precolonial period, Gao, Tombouctou and Djenné – all of them located in the Mali empire – were the most populated cities of this region and counted between 70,000 and 80,000 inhabitants only[1] [2]. At that time, cities were primarily trading places, and this is why most of them were located along major trade routes or at their end, as in the Sudano-Sahelian zone which was crossed by trans-Saharan trade routes.

Sub-Saharan Africa (SSA) has experienced significant and widespread urbanization only very late in comparison to what happened in Latin America or Asia. It was the European colonization in the $18^{th}$ and $19^{th}$ centuries that laid the foundations for an important urban development. However, cities remained few and limited in size at this stage. They started to reach higher growth rates after World War II, especially after the 1960s when SSA countries gained their independence, and recorded globally unprecedented urban growth rates with about 6 to 10% per year [2]. From the 1970s, the phenomenon experienced a certain slowdown, but the rates remain quite high until now. Reader interested in an exhaustive background about urbanization in SSA may refer to Coquery-Vidrovitch (1991).

Nowadays, about 40% of the population is urban in SSA and the region is expected to face the highest growth rates during the next decades, and reach urbanization rates of 47% by 2030 and 58% by 2050 [4]. A recent study claimed[2] that three African cities - Lagos (Nigeria), Kinshasa (Democratic republic of Congo) and Dar es Salaam (The united republic of Tanzania) - could be the most populated

[1]The information available for the precolonial period are very insufficient and it is therefore difficult to have reliable population figures.

[2]Since they had to deal with several uncertain data and the task to make such predictions for such a distant future could be hazardous, the authors concede that their finding should be used with caution.

cities in the world by 2100, and that 30 to 40 out of the 100 biggest cities in the world could be located in SSA [5].

As a consequence of the extremely fast transformations experienced during the last decades, SSA cities are facing social and environmental issues that are sometime lumped together and called the "urban crisis". These issues are mostly due to the important population increase combined with a lack of financial means and of capacity in urban planning and management [6]. SSA cities have to face growing environmental issues such as water and air pollution, inadequate waste collection and disposal, noise pollution etc... [7]. In the same time, the spatial segregation that had been developed on a racial basis during the colonial period has evolved into a spatial segregation based on socio-economic characteristics [7, 8]. It results in dual cities with important intra-urban inequalities. Slum-like areas - where people live with insufficient living space, without tenure security and adequate sanitation or access to water - coexist with rich neighborhoods having higher living standards. The poorest often constitute a large part of the urban population that is extremely vulnerable to health and disaster risks [9]. According to the United Nations, SSA has the highest proportion of urban population living in slum conditions [7].

In SSA cities, up-to-date and spatially detailed geographic information (hereafter called "geoinformation") is often missing. This shortage is an important issue for many scientific studies focusing on different urban issues and there is a real need to improve the availability of geoinformation for these cities in order to support urban planning, urban management, environmental monitoring, etc...

For a long time, geoinformation has been produced thanks to air-borne (from airplanes) or space-borne (from satellites) imagery. These are important sources of information for geographers as they have the ability to capture and record the exact configuration of a territory in one single picture. Hand-made visual photo-interpretation combined with field surveying have long been used as the common procedure to transform these images into valuable geoinformation. However, these methods remain cost- and labor-intensive and are not well adapted for fast and regular map updates. With the increasing amount of Very-High Resolution Remote Sensing (VHRRS) data and the improving computing capabilities, it is now possible to implement cost-effective solutions for the production of geoinformation in order to map the urban environment with a fine level of spatial and thematic details in highly automated procedures. These solutions are relevant for the SSA cities that are characterized by limited financial capabilities and where the pace of change and urban growth imply frequent map updates. In this thesis, a specific emphasis is laid on using only Free and Open Source Software for Geospatial (FOSS4G) in the proposed solutions for limiting the costs and allowing anyone to review and adapt

them to their needs[3].

Land cover and land use are the most common geoinformation that can be derived from Remote Sensing (RS) images. The first refers to the composition and physical characteristics of earth surface elements such as vegetation, soils, water or artificial surfaces, while the second informs about the type of functions and activities that people decided to carry out in some places.

In this thesis, the first two objectives are to implement two automated frameworks for the production of land-cover and land-use maps, allowing for the processing of large images covering complex heterogeneous urban environments, in a context of lack of geoinformation as usually the case in SSA cities. What we mean by "framework" is a compilation of tools and methods which provide a generic functionality that could serve multiple different domains of application, that could be applied on different case studies and data sets with limited adaptation and that can be improved by adding user-written code. The form of the frameworks developed in this thesis is described in more details in chapter 2. These two objectives are included under the encompassing research question[4] established as follows: "How to produce geoinformation for SSA cities, using VHRRS data and open-source solutions ?". The main research questions and the resulting scientific objectives of this thesis are highlighted in figure 1.1.

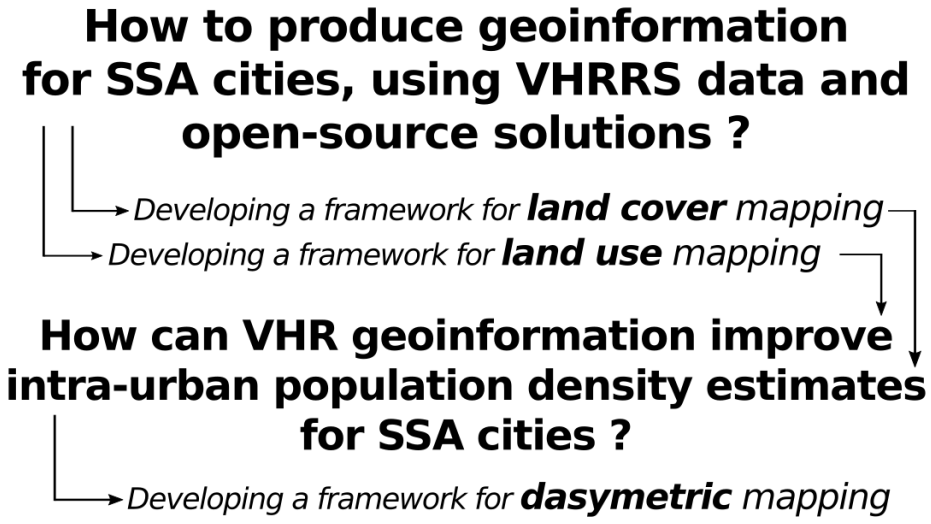


Figure 1.1: Main research questions of this thesis and resulting scientific objectives.

While there is a prolific scientific literature on land cover and land use mapping, the work undertaken in this thesis to fulfill these objectives proved more difficult than

[3]These points are discussed in more detailed in section 1.5.

[4]In fact this question does not wait for a clear and unequivocal answer. Rather, it suggests to implement and test different approach and to use those which are the most relevant in the context of mapping SSA cities to create and share different frameworks for the production of geoinformation.

initially expected, for several reasons: i) Most studies do not operate on data-poor contexts such as SSA and the proposed methods were sometimes found difficult or impossible to apply. ii) The authors do not systematically release publicly the code they used to conduct their analyses, leading to a lack of reproducibility. iii) The validity of the methods proposed in the literature is often evaluated on small areas and may be inefficient for the large-scale applications considered in this thesis.

The land cover and land use are meaningful and valuable geoinformation by themselves. However, in this thesis, we decided to go further and to use them for improving the results of population density estimates. This leads to another research question phrased as follows: "How can VHR geoinformation improve intra-urban population density estimates for SSA cities ?". Accessibility to and quality of population data are important issues for many applications in different fields of research, such as epidemiology and risk assessment. However, in SSA, population data are marred by several challenges, notably the fact that data released by official institutions are only available in coarse administrative units that do not match the level of spatial detail required for studies at the intra-urban level. Existing spatial modeling methods provide a workaround to this limitation. Using ancillary data such as the location of the settlement or the built-up density, it is possible to model and to estimate population densities at a finer spatial resolution than in official data and to map them as a continuous variable in gridded layers (raster) instead of homogeneously distributed in areal administrative units. Unfortunately, currently available gridded population models for SSA suffer from limitations and fail to provide population estimates with the spatial details required by research operating at the intra-urban level. As explained below, this is mainly due to the relatively coarse spatial resolution of the input data used in these models. Spatial and thematic detailed geoinformation derived from VHRRS data is likely to be a valuable source of information for population modeling purpose, but it remains largely unexplored according to literature review on the state of the art. For this reason, we decided to fill this gap and made the hypothesis that leveraging geographic information derived from VHRRS data can improve the accuracy and the spatial detail of existing population models.

In summary, the overall goal of this thesis is to develop and to implement open-source methodological frameworks for the detailed mapping of the land cover and land use of SSA urban areas using VHRRS data and to assess how these pieces of geoinformation can improve the quality of intra-urban population models.

The following sections of this general introduction lay the theoretical foundation of this thesis and provide some background to assist the reader in the general understanding of the research conducted and of the methodological and technical development presented in the subsequent chapters. Section 1.1 presents a brief de-

scription of the case studies. Section 1.2 introduces the general background on land cover mapping using VHRRS data and summarizes the different methodological issues we faced and the solutions we propose. The method implemented to map the land use in a data-scarce context is briefly presented in section 1.3. Section 1.4 presents the potential of land cover and land use information for improving existing population models. Finally, the issue of reproducibility and the importance of open science is addressed in section 1.5, while the specific objectives and the thesis outline are presented in section 1.6.

## 1.1 Case studies

The methods developed in this thesis were applied for testing on two west-African cities, namely Ouagadougou and Dakar, the capitals of Burkina Faso and Senegal, respectively. The selection of the Area Of Interest (AOI) - i.e., the geographical extension that is considered as relevant for the study - is an exercise that remains quite subjective since there is no consensus for establishing criteria for the delineation of the limit between rural and urban areas [10]. Here, the AOIs were selected through visual interpretation of VHR imagery and are not strictly restricted to the administrative units. Indeed, they cover both the core city and the peri-urban areas, allowing us to capture the different economic activities and the extension of the urban sprawl [11]. The AOI covered 615 $km^2$, and 418 $km^2$ in 2015[5], for Ouagadougou and Dakar, respectively. In terms of the geographic extent covered by the land cover mapping using VHRRS, these AOIs are most probably top-ranked in the scientific literature [12].

These cities have been undergoing an extensive and partly unregulated urban growth during the last decades [13, 14]. According to the last official count of the population, Ouagadougou has 1.9 million inhabitants (2012 [15]), while Dakar has about 3 million (2013 [16]). According to the United Nations, the population of Dakar grew by roughly 30% between 2005 and 2015, while the population of Ouagadougou grew by 65% during the same period [4]. They are characterized by a mix of very different urban patterns, e.g. administrative and industrial areas with large-sized buildings as well as planned and unplanned residential areas with smaller-sized buildings. In both case studies, an important part of the city is characterized by a landscape with a checkerboard design inherited from the French colonization. The urban fabric is more diverse and complex in Dakar than in Ouagadougou, especially in the city center.

From a remote sensing perspective, these cities present important challenges, especially because the built-up is usually very hard to discriminate from the bare

[5] At the time of satellite imagery acquisition

soil and the artificial ground surfaces with the available spectral information. This can be explained, among others, by the presence of dust on roof tops and by the use of similar construction materials - i.e., concrete - for flat roofs and artificial ground surfaces. Both cities have a typical Sahelian climate and are located in the same ecological region (Hot semi-arid - Bhs - according to the Köppen classification). Because of this arid climate, the period of the year selected for image acquisition is very important. The end of the rainy season is the most recommended since the bare soils are more covered with vegetation and thus easier to distinguish from the built-up areas.

These case studies were selected for several reason, namely because the probability of acquiring cloud-free images was higher than for cities located in equatorial zones, because of existing networks with local scientific teams and because of the opportunity to access recent and spatially detailed population data.

## 1.2 Land cover mapping and OBIA

As mentioned above, the first scientific objective of this thesis is to develop a framework for land cover mapping. Therefore, we use VHRRS data as input, for its ability to maps the urban environment with great spatial details. In this section, a light theoretical background of the most used approach for processing VHR images, called Object-Based Image Analysis (OBIA), is provided. An overview of the different issues we faced when applying state-of-the-art methods for mapping large and heterogeneous areas and the solutions that we propose are briefly presented in subsection 1.2.1. Also, since it is important with regard to population modeling, we briefly illustrate in subsection 1.2.2 how the height of off-ground objects is used to increase the thematic accuracy of the land cover maps produced. The complete methodological developments related to the implementation of the semi-automated framework for land cover classification are further presented in chapter 2.

In the early stages of remote sensing, spaceborne remote sensing images were typically available with a spatial resolution ranging from 10 to 30 meters [17] and were classified on a pixel-by-pixel basis (pixel-based paradigm). With time, the resolution increased and the launch of new sensors providing VHR images, around 2000, propelled the development of new strategies for processing these new data sets. As pixels became smaller, the geographical objects to be mapped - e.g., a house or a tree - spread over multiple pixels, as illustrated in Figure 1.2. Application of standard pixel-based approaches on VHR images led to speckled classification results [18], the so-called "salt-and-pepper" effect, where pixels belonging to a same geographical object (e.g., a building) were not assigned to the same label. As a mitigation, a new approach emerged, aiming at grouping images pixels to create images segments

corresponding to actual geographical objects (houses, trees, ...) which would then be classified. The process of segment creation is known as "segmentation" and has a significant impact on the quality of the final classification accuracy. The entire method is known as Geographic Object-Based Image Analysis (GEOBIA) (or simply OBIA) and has now been acknowledged as a standard for processing VHRRS data. An OBIA framework for land cover mapping usually consists of the main following steps: i) the segmentation (creation of objects), ii) the computation of segment statistics (spectral, morphological and contextual information), iii) optionally, the selection of the more discriminant statistics (feature selection), and finally iv) the classification.

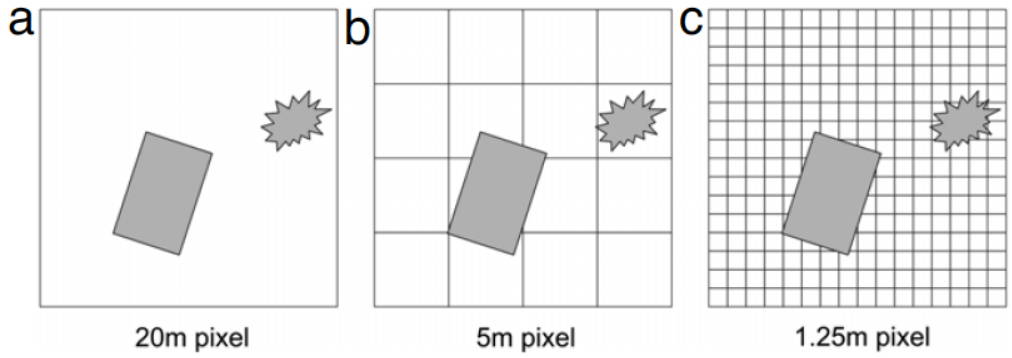


Figure 1.2: Relation between the spatial resolution of the images and the size of geographical objects to be mapped. Source: Blaschke [19].

Designing a methodological framework allowing for the operational production of land cover maps is a complex task, where many methodological problems arise. This is especially true when the objective is to produce a processing chain that is as automated as possible and able to handle very large areas (major cities in SSA easily sprawl over 300 $km^2$). It is important to note that, at the beginning of this thesis, there was a lack of methods that had proven their efficiency for large scale land cover mapping using VHR. While >95% of the scientific publications on land cover mapping have an AOI covering less than 3 $km^2$[12], the applicability/efficiency of common OBIA methods on large data set remained largely uncertain. For processing our data sets - covering more than 1.000 $km^2$ in total - and achieving sufficient accuracy, we had to push existing methods up to their limits and find new strategies for scaling them.

### 1.2.1 The need for scalable and automated segmentation

As already mentioned, segmentation is an important step that can impact significantly the quality of the final map. Segmentation can be performed using several

algorithms, and each needs tuning to provide a "good" segmentation result. As illustrated in Figure 1.3, the choice of the segmentation parameter values greatly influences the size, the shape and the spectral heterogeneity of the objects created (the image segments). When there are too many image segments (over-segmentation, see Figure 1.3 A)), one single geographical object - e.g., a building - can be made of many image objects, which leads to ineffective size and shape measures in the classification stage. On the contrary, when there are not enough image segments (under-segmentation, see Figure 1.3 C)), different geographical objects can be included in the same image segment which will reduce the quality of the final maps. An acceptable segmentation result should in fact be somewhere between these two extreme situations (see Figure 1.3 B)). But what exactly is a "good" segmentation ? Haralick and Shapiro (1985) first stated that a segmentation process should maintain uniformity of single objects while making them as different as possible from their neighbors [20].

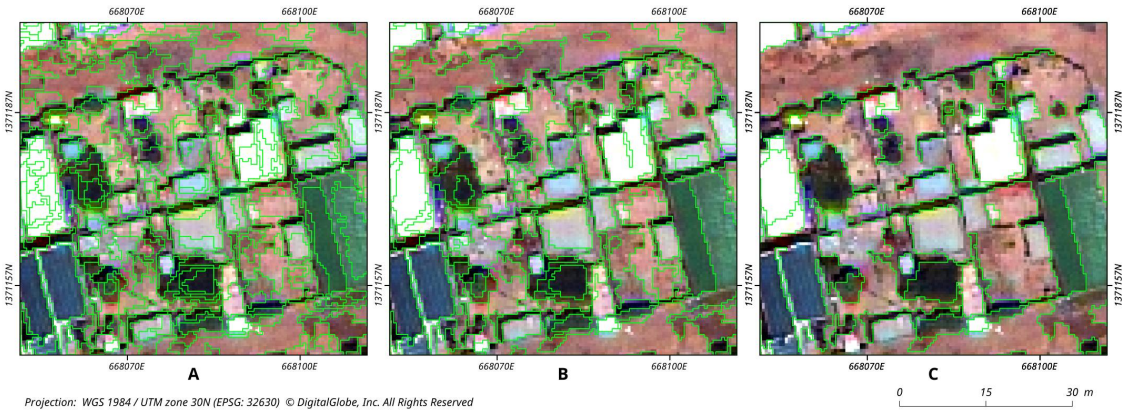


Figure 1.3: Impact of the choice of the parameter on the segmentation result. A) The result is over-segmented. B) The result is quite valid for further analyses (classification). C) The result is under-segmented.

In many studies, segmentation parameter values are often selected on a manual basis by trial-and-error refinement relying on visual assessment. This tedious, time-consuming and subjective approach proved to be marred by transferability issues and did not allow for any automation, since the validity of the selected parameters is usually restricted to the specific scene under study, or even to specific areas within this scene, and they have to be adapted for each dataset [21]. When looking for automation in an OBIA framework, the determination of the optimal segmentation parameters is the biggest challenge. In this work, we made use of state-of-the-art methods for determining the parameters in an unsupervised fashion, called Unsupervised Segmentation Parameter Optimization (USPO). In this thesis, we used an USPO method enabling the determination of segmentation parameters that satisfy an optimization function maximizing both intra-segment homogeneity and inter-

segment heterogeneity. More details are provided in chapter 2.

We created a semi-automated processing chain for OBIA land cover mapping that uses USPO methods for the segmentation. This processing chain, or framework, is implemented in Python and takes advantage of the existing open-source software GRASS GIS. A new add-on, called i.segment.uspo [22], has been developed in order to allow for the use of USPO methods in this software.

Ouagadougou was used as a case study for the development of the semi-automated framework. In the initial development stage, published in Grippa et al. (2017) (**paper 1** [21], in chapter 2), it was tested on a limited portion of the city covering 25 $km^2$, and it achieved a good classification accuracy. However, when applied to the entire scene of Ouagadougou (615 $km^2$), the results were not as good as expected. This was because the segmentation parameter optimization strategy was designed as a global approach, i.e., the whole image was segmented using the same parameter, without considering the existing spatial variations in terms of built-up patterns as illustrated in Figure 1.4.


Figure 1.4: Heterogeneity in built-up patterns in Ouagadougou

As the state-of-the-art methods used for mapping urban area using VHRRS data proved to under-perform when applied to large AOI with important heterogeneity of built-up patterns across the scene, existing methods have been adapted. A recent study, in which segmentation parameters where optimized at the agricultural plot level in Spain, showed that the optimal segmentation parameters could vary significantly depending on the type of crops cultivated in the field [23]. We made the assumption that the same should also be true for different types of built-up patterns in an urban context. Thus, we decided to divide the whole scene into smaller and more homogeneous (local) zones, through an expert-based visual interpretation process based on two criteria, namely built-up density and building size. Then, we used the USPO method to automatically select optimal segmentation parameters for each local zones. We called this approach the "local USPO". This strategy proved its ability to improve the quality of the segmentation and outperformed the

"classical" global approach in terms of classification accuracy, as illustrated in Figure 1.5. This comparison between both approaches is discussed in more detail in Grippa et al. (2017) (**paper 2** [24], in chapter 2).

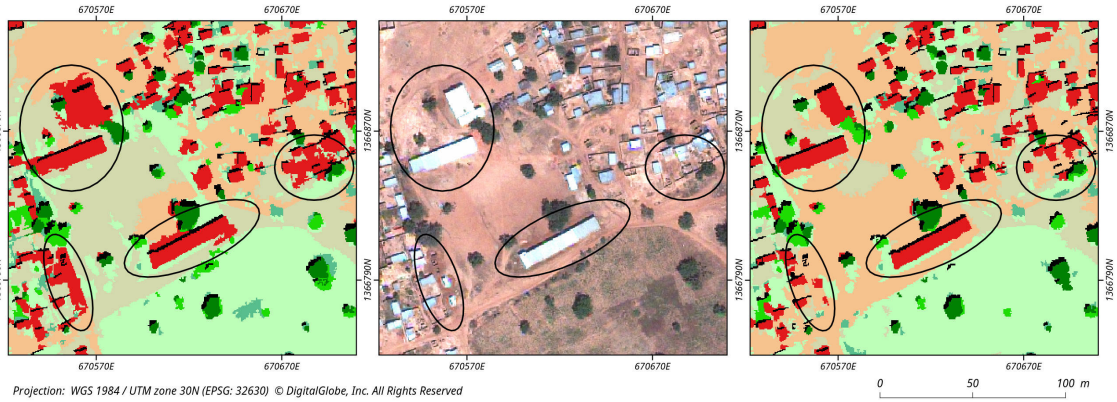


Figure 1.5: Impact of the global (left image) and local (right image) optimization of the segmentation parameters on the classified map. Applying local USPO reduces misclassifications, especially at the edges of buildings.

Although it succeeded in increasing the quality of the land-cover map produced, the method was still marred by the need to draw local zones manually, which creates a bottleneck for automation and reduces the ease for transferability on new case studies. For this reason, we pursued the improvement of the methods. We made the assumption that applying a local USPO approach on a dummy - i.e., non-expert guided - partition of the scene, could reach the same level of improvement as that obtained when applied on a partition created through a labor-intensive expert-based visual interpretation. To achieved this, we considered alternative solutions for the semi-automated partitioning of a large scene (see Figure 1.6). We compared the performance of our land cover mapping framework with expert-based local zone creation and grid-based and "cutline"-based scene partitioning. The last two led to similar improvements as using expert-based local zones, but the "cutline" partitioning was preferred since it delineates the landscape in a more meaningful way. Indeed, as illustrated in Figure 1.6, delineations between adjacent zones are more prone to follow linear patterns, such as roof edges and streets, and could mitigate "edge effect" problems. The results of the different approaches are further discussed in Georganos et al. (2018) [13] (**paper 3** in chapter 2).

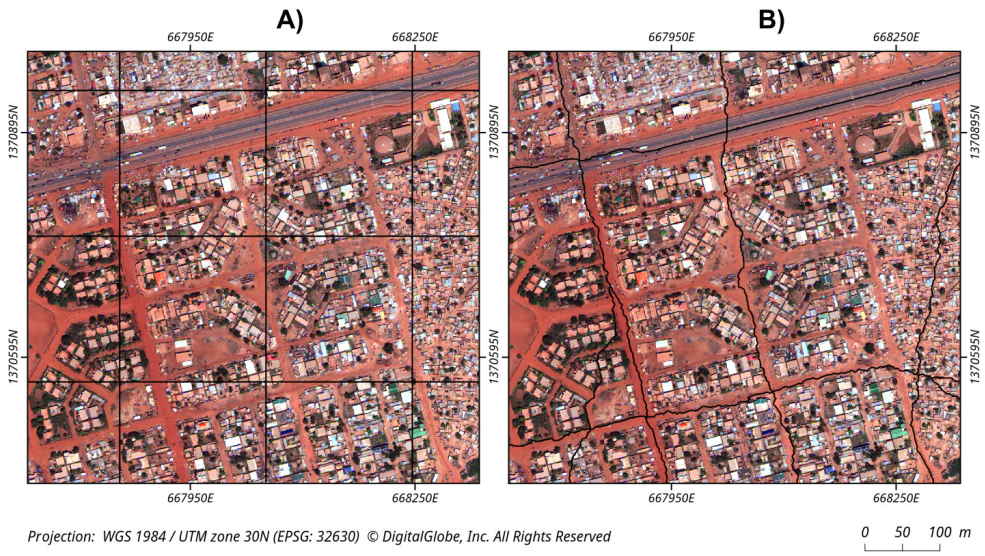


Figure 1.6: Automated partition of the scene tested for local optimization of segmentation parameters. A) Using regular grid. B) Using a "cutline" algorithm.

### 1.2.2 Using object height for increasing the thematic accuracy of building class

We just saw how existing segmentation methods were adapted for processing VHRRS images and mapping the land cover with fine spatial details in an urban environment. This spatial detail is often considered as the main added value of VHR. However, VHR data provide another very important added value compared to HRRS data. Indeed, when they are acquired in stereo pairs, object height information can be derived from VHR images (normalized Digital Surface Model (nDSM), Figure 1.7(B)). As illustrated in Figure 1.7, this can be used to classify different categories of buildings according to their mean height. This information is extremely important for many applications, such as urban planning. It is also of great value for population modeling and constitute a key predictor of improved population estimations because different building heights may impact the population densities. Interested readers can refer to Vanhuysse et al. (2017) [25] for more details about the procedure to create height information.

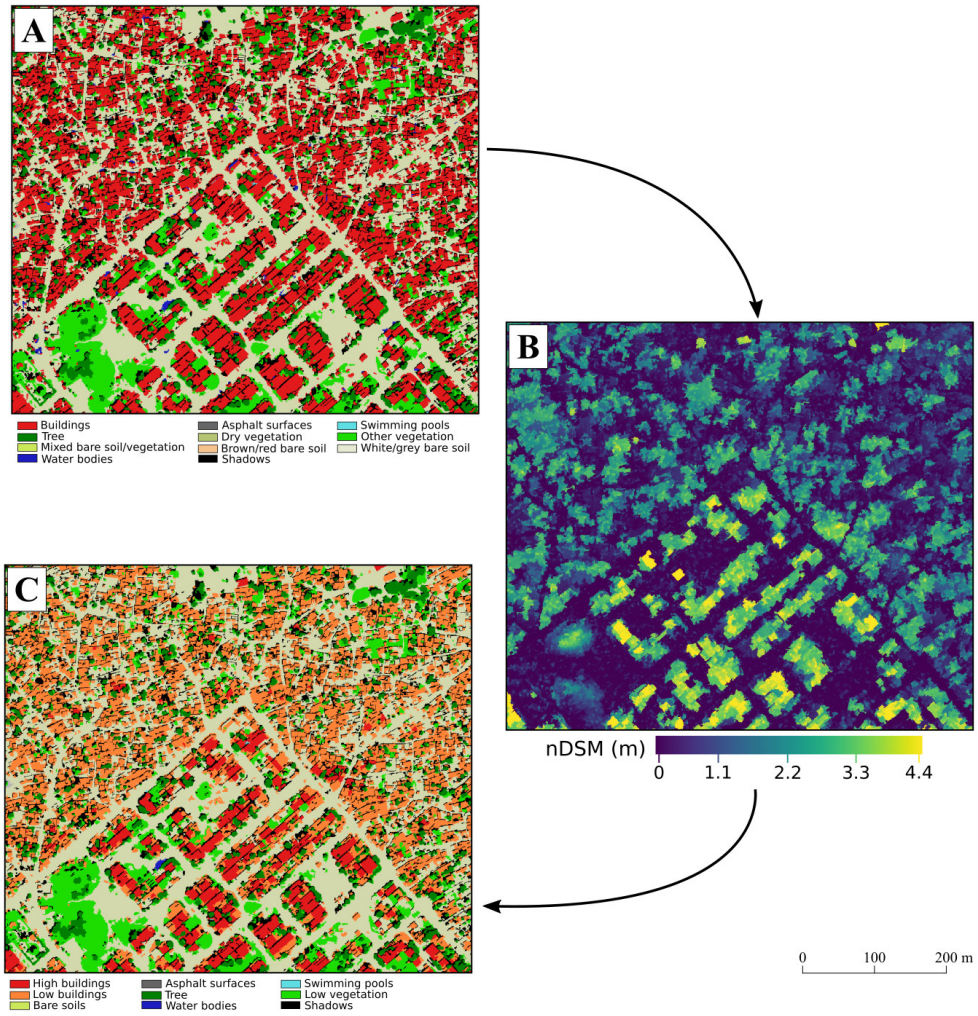


Figure 1.7: Use of nDSM for distinguishing high- from low-elevated buildings in a land cover classification. (A) Initial land cover classification with a single building class. (B) nDSM layer providing height information about above-ground objects. (C) Refined classification with building objects reclassified according to their mean height.

## 1.3 Mapping the urban land use at street block level

Aside from the development of a framework for land cover mapping, the second scientific objective of this thesis is to develop a framework for land use mapping, which is another essential piece of geoinformation that can be extracted from RS images. Up-to-date and reliable land-use information is essential for a variety of applications such as planning or monitoring of the urban environment as well as in support to scientific studies [11].

Many studies aiming at mapping the urban land use based on VHR data work at the street block [26–29] or even at the cadastral plot level [30–32]. The street blocks have been depicted as the most fundamental and appropriate unit in which

to map the urban structure, and they provide a spatial detail which is well adapted for urban planning [33–35]. However, street block geometries are most of the time unavailable to researchers working on SSA cities, either because they are difficult to access or because they do not exist. To overcome this lack of existing information, we developed a semi-automated procedure for the creation of street block geometries using OpenStreetMap (OSM) data [36]. This free and open-source Volunteered Geographic Information (VGI) source is improving rapidly, both in terms of completeness and of thematic accuracy, and it is going to become a key player in the coming decade for the production and access to high-quality geoinformation in developing countries [11].

In the literature, many studies aiming at mapping the land use operate in a context of good availability of ancillary data, and take advantage of official databases providing detailed and exhaustive spatial information on urban facilities (schools, hospitals, ...) to classify the urban functions [30–32, 37]. Unfortunately, these data were not available for our case studies, as is the case for many SSA cities. For this reason, we had to design strategies allowing us to map the land use in urban areas with a very limited set of ancillary data. For this purpose, we leveraged the valuable information previously produced. By analysing the land-cover maps, it was possible to determine the type of urban function, according to the composition (e.g., presence of absence of builings, vegetation, etc...) and the organization (e.g., the size and density of building or vegetation patches) of the land cover classes in each street block. Variables originally used in ecological studies, called "landscape metrics" were used to characterize street blocks in such a way. The whole methodology consisting of a semi-automated framework for the creation of street block geometries, their characterization using spatial metrics and their classification is presented in Grippa et al. (2018) (**paper 4** [11] in chapter 3).

From a population modeling point of view, access to information about on the location of urban functions throughout the city is extremely important. Indeed, urban areas are characterized by the concentration of various human activities and residential functions represent only a limited proportion of the built-up areas. The built-up density (computed from the land cover information) is usually among the top predictors in population models [38]. However, when the buildings are not dedicated to residential functions (e.g., industrial buildings as in Figure 1.8, top right), its use may result in an overestimation of the population. Land use information, providing a distinction between the different urban functions (residential, industrial, commercial, ...) could mitigate this issue. Thus, in this thesis, we make the hypothesis that land cover and land use provide complementary information and can be used together when designing population models.

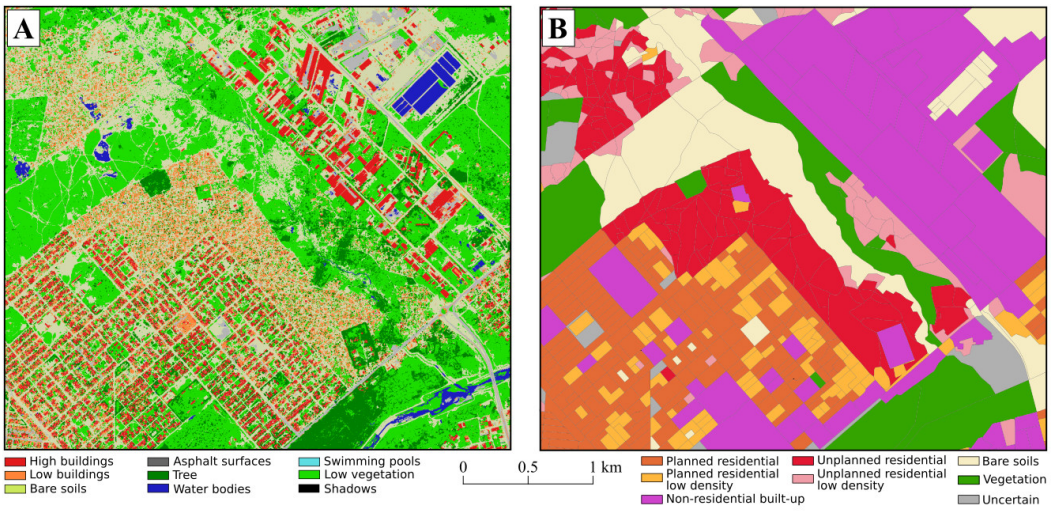


Figure 1.8: Land cover (A) and land use (B) are complementary geoinformation that can be combined to improve population estimations.

## 1.4 Improving the knowledge on intra-urban population distribution

As mentioned at the start of this introduction, the land cover and land use are valuable pieces of geoinformation by themselves for a multitude of application. Much time and effort was spent for the development of transferable semi-automated framework for their production. However, we decided to go further and to use them for improving the results of population density estimates, in view of answering the following research question: "How can VHR geoinformation improve intra-urban population density estimates for SSA cities ?". Indeed, population data currently available for SSA are often marred by a lack of sufficient detail, which limits the possibility of analysis for studies in epidemiology or risk assessment.

In this section, we briefly introduce why population data are essential information for many different fields of research and what are the problems related to the use of official census data. Next, we give an overview of how population modeling can be used to estimate fine-scale population densities. Finally, we highlight the main limitations of the currently available gridded population layers and the potential of VHRRS data to mitigate them.

### 1.4.1 Why population data is essential

There is a wide variety of applications depending, directly or indirectly, on information about human population and especially on its spatial distribution. Access to accurate and detailed population data is needed by public authorities, local organizations or academia for evidence-based decision-making and research. The present

research is conducted to meet needs explicitly expressed by researchers in the field of epidemiology and health assessment, but it is likely that the methods and maps produced may be worthwhile in many other fields of research. However, their potential use by public authorities in decision-making processes is more uncertain.

Without aiming to make an exhaustive inventory of all the possible applications, a selection of concrete examples - not limited to SSA - illustrating the importance of having accurate and detailed population data is presented hereafter.

a) Location decision for new public facilities

The spatial allocation of resources is a strategic issue in the implementation of public policies and public investments should, ideally, reach the greatest number of people who need them. When planning the establishment of new health facilities, such as medical centers or hospitals, an unavoidable question arising is "where should it be located". It has been shown that better access to health facilities can positively impact different health outcomes, such as maternal and infant mortality, vaccination coverage and treatment of infectious diseases [39].

Such a location decision-making process is subject to multiple conflicting criteria [40] and the final decision on the location for a new facility could be far from optimal [41] if not supported by an objective analysis of needs and constraints (evidence-based decision). Location-allocation models regroup different methods that have long been used to solve this kind of problems, e.g., multi-criteria decision analysis [40]. In this kind of decision-support models, the choice of the "best" candidate among a set of different possible locations is made according to an "objective" function. In the case of developing countries, the use of health services strongly varies with distance [42] and walking remains the main transport mode for an important part of the population [39] making the location decision even more essential. The objective function can remain quite simple, such as minimizing the mean travel time needed by the population to reach a health facility, e.g., by computing on a pixel-by-pixel basis the ratio of population density and travel time [40]. It is therefore essential to know where the population is located, with enough detail in terms of spatial resolution, so that public authorities can make objective decisions and allocate financial resources in the most optimal way[6].

b) Planning vaccination campaigns and managing outbreaks.

Vaccination is another health-related issue that requires access to population data. Vaccination campaigns can be organized on a regular basis or in response to an epidemic. Planning a vaccination campaign is a difficult task – mostly logistic -

[6]Resource allocation is always a question of political will, but such information can be valuable for decision support.

that requires accurate information about settled places as well as population densities. The micro-planning of vaccination campaigns usually operates by dividing a large area of interest into smaller geographic target areas that will be assigned to different vaccination teams [43]. Unfortunately, population data is often available for coarse administrative levels that do not correspond to the operational scale. As a consequence, it is difficult to correctly allocate human resources and to inform the vaccination team about the exact location they are expected to go, leading in some situation to "... highly inefficient and unbalanced work plan for the vaccination teams."[43, p. 104]. In addition to the location of inhabited areas, it is also necessary to estimate the number of inhabitants of a target area, so that field teams can carry enough vaccine doses to reach a minimum percentage of the population, in order to ensure the effectiveness of the campaign [7].

Recently, the Ebola outbreak in West Africa has been an opportunity to realize the poor quality of the population data, leading to difficulties because "... emergency responders struggled to identify the location and size of rural settlements, and could not accurately calculate infection rates since the denominator (i.e., the population at risk) was not known, an issue that is regularly encountered in emergencies and outbreaks situations..."[45, p. 2].

c) Vulnerability and risk assessment

Many populations are subject to potential hazard events that can have anthropogenic (e.g., nuclear power plant, for example), or natural (floods, earthquakes, landslides, tsunami, rising sea levels) origin. Quantifying the vulnerability of the population can be interesting in order to better prepare emergency plans and respond to hazard events. Risk assessment is usually performed to prepare emergency responses and/or try to modify the current configuration of a place in order to mitigate the potential damages. A risk can be defined as the combination of the probability of hazardous events to occur and the vulnerability - i.e., "... the susceptibility of elements at stake to suffer from damages in case of hazard occurrence."[46, p. 29]. Depending on the type of elements considered, vulnerability and risk assessment may focus on social or environmental aspects, the economy, etc...

Concerning risk assessment involving human populations, the spatial distribution of population density is the most basic and mandatory information required in the analysis. However, this may not be enough, since different population subcategories could be impacted differently by the same event. In this regard, it may be useful to have access to more disaggregated data in terms of age, gender, income, etc ... [47] for the evaluation of the vulnerability of the population at risk. The scale of the

[7] A vaccination campaign is effective if a least a certain proportion of the target population is reached, e.g. 95% of the population for measles outbreak [44].

analysis may differ depending on the type of risk. For some risks such as floods, landslides and volcanic eruptions, the relevant analytical scale is quite fine, and it will therefore be necessary to access detailed spatial population data or, at least, plausible estimates.

Several examples of scientific studies on vulnerability and risk assessment exist and are presented here. A study published in 2007 by McGranahan et al. put the emphasis on the population living in low elevation coastal zones that are faced by the threat of rising sea levels induced by climate change [48]. In this research, a risk analysis was performed using the spatial distribution of the population living in urban areas facing risk regarding sea-level rising. This was the first attempt to use a global gridded-population product to conduct such analysis. More recent research [49] highlighted the uncertainties that are inherent to these global products and their impact on final estimates. Another type of risk to which people living in coastal areas are subjected is a tsunami event. A study published by Wegscheider et al. (2011) aimed at mapping the tsunami-prone areas in Bali (Indonesia) in order to identify communities which faced higher risk, with the aim of developing their response capability [47]. The authors reported that they had to perform their analysis with population estimations since the available official population data at the lower administrative level did not meet the needs for a tsunami vulnerability assessment, in terms of spatial resolution. Michellier et al. published in 2016 the results of a research aiming at assessing the risk toward geo-hazard such as earthquakes, landslide or volcanic activity including lava flows in an area sprawling over several countries in central Africa [46]. The authors were faced with the fact that some population data were completely outdated and only available for administrative levels too coarse for their analysis. Also, even when data existed, their accessibility and availability for research purpose was difficult. To support their analysis, the authors had to estimate the population of the cities of Goma and Bukavu (Democratic republic of Congo), by combining remote sensing analysis and labor-intensive field surveying.

d) Measuring the progress toward the Sustainable Development Goals (SDG)

The SDG are widely referred to in the literature related to development and poverty reduction. Initially, the Millennium Development Goals (MDG) were established with the aim to centralize and reinforce the development agenda of several programs of the United Nations (UN) (UNDP, UNEP, WHO, UNICEF, UNESCO, etc...) [50]. They were replaced by the SDGs in 2015. In order to measure the progress toward the achievement of these goals, several sets of indicators were established. An important part of them rely on population figures as denominator, e.g.

the proportion of the population below the international poverty line. While the general objective of the MDGs was mainly oriented toward the reduction of inequalities between countries, nowadays, the SDGs increase the ambitions for reducing the inequalities at the intra-country level [45]. In this context, the SDGs indicators should also be computed on disaggregated levels, requiring population data with a more detailed geographical resolution [51, p. 7].

It should be noted that the ability to measure progress toward SDGs completely depends "(...) on the availability of data and capacity to measure them (...)"[50]. It is very unlikely that the least developed countries, such as those of SSA, might have the capacity to deliver accurate data that can be used to compute the SDGs indicators, since the reliability of the whole statistical data collection system is sometimes more than questionable. For this reason, the rationale and efficiency of use of SDGs for policy making and development aid are sometimes criticized [52].

### 1.4.2 The issues related to official population data

As highlighted in the previous section, there are many different applications that require population data to perform their analysis. One may wonder why we should model the population at fine scale instead of simply use existing census data. This section introduces the main issues related to official population data.

Worldwide, there is a general concern about privacy issues when official population data are released. While they are usually collected at the individual or the household level, data are spatially aggregated and released only at administrative units levels [53, 54]. On the one hand, it has the advantage of satisfying the privacy concerns and also improving the manipulation of the data thanks to a dramatic reduction of their volume. On the other hand, several issues arise from the aggregation of population data into administrative units. One of them is related to administrative units boundaries that result from subjective choices and are established according to "(...) operational requirements of the census, local political considerations, and government administration"[55, p. 4]. As a consequence, most of the time, their extent does not have any geographical or natural meaning and thus does not match the extent of the phenomenon under investigation. Another challenge encountered in research is the fact that administrative boundaries may be modified from one census to another, which complicates the comparisons over time [56]. Moreover, related to the previous points, the findings of analyses made using aggregated data may be dramatically different according to the size and shape of the aggregation unit. This problem, firstly described by Openshaw [55], is well known in the field of spatial analysis and called the "Modifiable Areal Unit Problem" (MAUP). Finally, and the most important point with regard to this thesis, is

the fact that aggregated data give information for whole administrative units and thus hide important spatial discrepancies that may exist within them [57].

Besides the aforementioned general issues, some others are more specific to the situation in SSA. In developed countries, we can generally rely on accessible, exhaustive and accurate population data which are detailed regarding to their spatial resolution and distinction between socio-economic subcategories (gender, age, incomes, etc..). We have to remember that carrying out a national census is a huge task that is hard to achieve, even for developed countries[8] [45], which explains - among other things - that they are usually performed only once in a decade. Conducting a national census in SSA countries is much more complicated since they lag behind developed countries, in terms of material and financial resources [58]. In addition, having an up-to-date knowledge of the current population could be considered as a risk of instigating political instability and could thus suffer from a lack of political will [45]. Regarding the situation of population data in SSA, three major issues can be highlighted: i) their outdatedness, ii) their unreliability and iii) their lack of spatial detail.

i) Many SSA countries do not manage to maintain the ten-year period between two censuses and population data are often outdated [59]. As illustrated in Figure 1.9, this can lead to extreme situations. For example, the last national census dates back to 1984 for the Democratic Republic of Congo, 1987 for Somalia and 1993 for Madagascar [60].

   In case of outdated data, population projections are sometimes used to obtain a more realistic estimation of population count for a specific year. These projections are usually made with demographic growth rate provided by international institutions, e.g., the UN, which could be used to estimate population count for the different administrative units within a country. However, since growth rates are provided only at the national level, this approach can hide important intra-national disparities and assume that the growth rates are the same countrywide[9].

   Aside from national censuses, more recent population counts are sometimes available for some specific areas. However, these pieces of information are poorly centralized and referenced, leading to a difficulty in accessing them

[8] In this regard, it is interesting to mention that the methods evolved in developed countries and that some are now able to produce census-like data by combining existing information (databases) collected via different sources, such as population registers, family allowance, unemployment register, individuals annual tax declarations, employers' social security contributions, etc.

[9] Usually growth rates are provided with a distinction between urban and rural populations. However, this implies that the distribution of urban and rural settlement should be known to adapt projections.

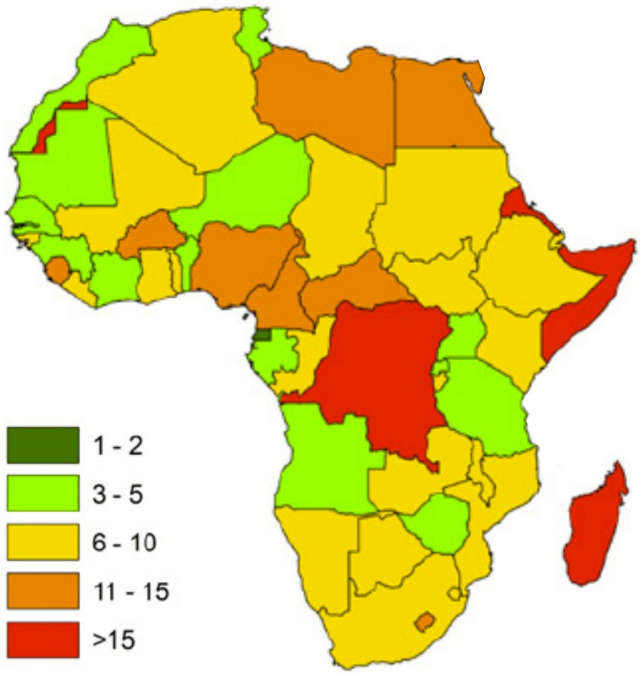


Figure 1.9: Using 2017 as the reference year, the figure shows the number of years since the latest national census for African countries. Figure adapted from Wardrop (2018) [45].

without having a reliable network of contacts among local public authorities and NGOs.

ii) Population data are often criticized concerning their reliability and several authors agree on the fact that caution is needed when dealing with population statistics on SSA [8, 61, 62]. Actually, all the official statistics are strongly criticized [58, 63]. The financial advantages that developing countries can obtain from diverse international agencies are conditioned to their socio-economic development measured by statistical indicators [45]. Since these indicators mainly depend on the official national statistics (population, gross domestic product, etc..), the political authorities may have an interest in increasing or reducing official population counts, depending on the situation, and using them as "(...) political weapon (...)"[62].

iii) Another issue is associated with the spatial resolution at which population data are accessible. In SSA the finest administrative level at which data are available is most of the time much coarser than one could access in developed countries. As aforementioned, available data may not correspond to the level of detail needed for different applications. It is obvious for urban areas where the variation of a phenomenon has to be measured at the intra-urban level.

The first three administrative levels in the national scheme, e.g., national, provincial, regional, are usually available. However, it is much more difficult to access population data linked to the spatial boundaries of the finest administrative level. In some cases, it is possible to access population data at this level in the form of non-spatial databases, i.e., spreadsheets not joined to administrative units limits as vector format for their use in Geographic Information Systems (GIS). Sometimes, spatial information is provided as points instead of the actual linear limits of the entities, which renders the use of population data difficult.

In this thesis, we aim at providing solutions to mitigate this last issue.

### 1.4.3 Population modeling to deal with imperfect official data

As highlighted, official population data can suffer from several shortcomings, which can be more or less troublesome depending on the situation and the type of analyses that need to be performed. To overcome these issues, several spatial modeling strategies have been proposed in the literature. These are referred to here as "population modeling" methods[10].

Before going further, it is important to stop for a moment and to "Remember that all models are wrong; the practical question is how wrong do they have to be to not be useful."[64, p. 74]. This statement, which may seem a bit sarcastic, must be understood as the fact that a model is only a simplification of a complex reality. If the aim of a model is to predict the "truth", as the "whole and absolute truth", then all the models are wrong. As a result, "The most that can be expected from any model is that it can supply a useful approximation to reality..." [65, p. 440].

Depending on the type of issue encountered in the population data, two types of approaches can be used: the bottom-up and top-down approaches.

#### Bottom-up approach

The first two aforementioned issues - i.e., population data being outdated and/or considered as unreliable - can be bypassed by implementing a bottom-up population modeling approach. As its name suggests and as shown in Figure 1.10, this approach consists in collecting population data during micro-survey on the field and combining them with ancillary data to estimate the total population of the territory.

Micro-surveying consists of field surveys carried out on limited areas with the objective of enumerating the population or collecting other census-like data. These

[10]It is important to mention that this term has a wider meaning in the literature and encompasses population growth models.

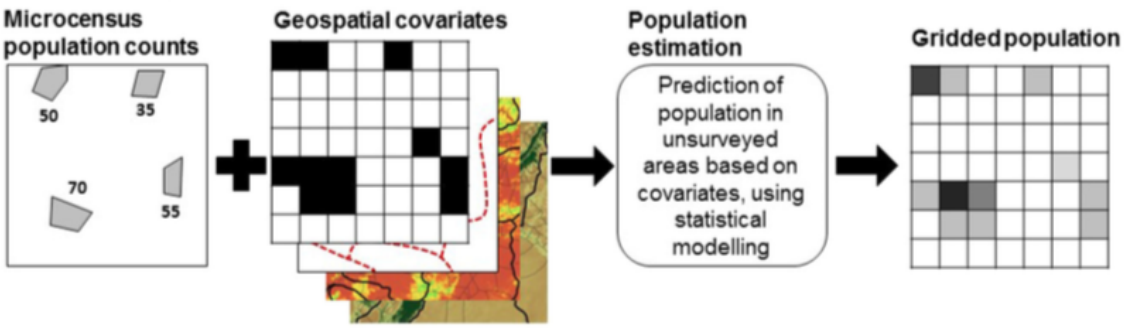


Figure 1.10: The bottom-up approach aims to estimate the whole population of a large area using existing information of micro-survey conducted on a limited portion of the area of interest. Figure adapted from Wardrop et al. [45].

micro-surveys should be performed in different areas scattered throughout the territory and representative of the diversity of situations that can be encountered (stratified sampling). Using statistical analyses, it is possible to highlight correlations between population density collected in the field and ancillary data[11], and then use them to estimate (predict) population densities in all the areas not covered by the micro-surveys. Micro-surveying is at the same time the main advantage and drawback of this approach. It enables the acquisition of up-to-date and reliable field data but with the limitation of cost-, labor- and time-intensiveness and the need for a workforce trained on standard techniques of census surveys. This approach is not the one we investigate in this thesis, but interested readers can refer to the publication of Wardrop et al. [45] for a more detailed explanation about bottom-up approaches.

### Top-down approach (Dasymetric mapping)

If the available official population data are affected only by insufficient spatial detail, a top-down approach is generally preferred to a bottom-up one because of ease of implementation. In this approach, also called "dasymetric mapping", official population data available in administrative units (source zones) are redistributed – disaggregated - into smaller zones (target zones). The method relies on "spatial reallocation weights", also called "weighting layers", which are used as approximations of the actual spatial distribution of population densities within the source zone. The main challenge in dasymetric mapping consists in using all the information provided by the ancillary data to improve the weighting layer so that it minimizes the errors of population estimates in target zones. For a long time, these weights have been subjectively determined by experts, according to existing information such as land-use

[11] There are plenty different variables that may be potential proxies for population densities, such as the land cover, land use, climate, slope, accessibility (to transportation networks, to schools, hospitals,...), night-lights, or other socio-economic or sociocultural indicators.

information or household characteristics. State-of-the-art research has now shifted towards the use of the power and the efficiency of machine learning algorithms to model the distribution of population densities without any expert-based knowledge.

Dasymetric mapping methods have been used for decades and extensive scientific literature is available on this subject [53, 54, 66–70]. Additional reviews on dasymetric methods can be found in [71, 72]. The main drawback of this approach is related to its dependence on existing population data and it is important to note that the population estimates derived using top-down dasymetric approach could be only as accurate as the "... the census data on which they are based."[45]. For this reason, this approach should be used only when existing population data are sufficiently recent and reliable.

In dasymetric mapping methods, target zones are usually completely included in source zones, which presents the advantage of being more convenient from a computational point of view. Moreover, it enables the "pycnophilactic" property to be satisfied, i.e., that the initial volume of population provided as input in the sources zones is maintained during the dasymetric procedure. It means that the total volume of the population predicted on target zones within the source zones has to be equal to the initial volume in those same source zones.

In the early stages of dasymetric mapping, the standard procedure was to use polygons as target zones - i.e., polygons corresponding to the actual limits of urban versus rural areas - with the assumption that the estimated population was homogeneously distributed in these target zones. Also, even if target polygons are generally more geographically meaningful, they might not be comparable with other information "... collected on several incompatible partitions of the zone of interest. ..."[72, p. 29], leading to a lack of interoperability in spatial analyses.

With the increasing spatial details provided by ancillary data, researchers succeeded in refining the size of target zones. Nowadays, most of the dasymetric mapping strategies aim at producing gridded population products, i.e., a raster layer whose pixel values refer to the (estimated) number of inhabitants, as illustrated in Figure 1.11. This format presents several advantages [59], such as enabling easier interoperability when combined with other grid-based datasets in the analyses or avoiding potential MAUP-related issues when polygons are used as target zones. Moreover, it allows for higher flexibility in practical applications since population estimates may be obtained for nearly any desired Area Of Interest (AOI), by summing all the pixel values within the AOI, as long as the size of the AOI is much larger than the spatial resolution of the grid layer (pixel size).

Using a simple example, initially proposed by Su et al. [54], the logic behind the main dasymetric mapping methods is described in Figure 1.12. In this example, we consider that we only have access to the information aggregated at the

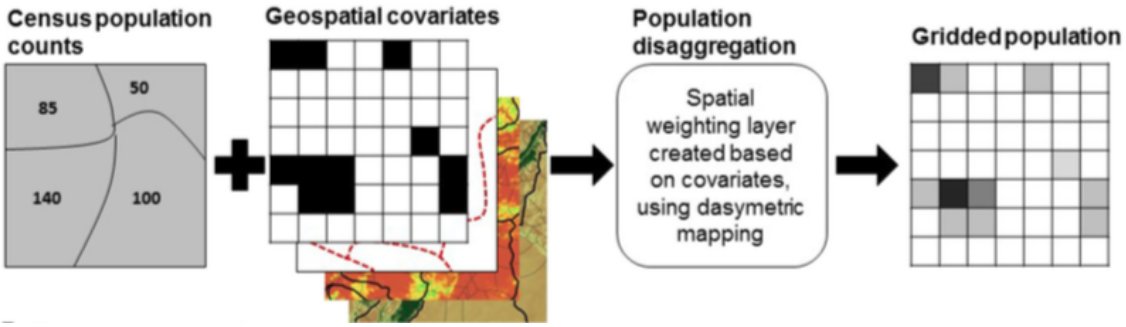


Figure 1.11: Top-down approaches (dasymetric mapping) start from existing population data available in administrative areas and aim to reallocate population counts at a finer level with a realistic distribution of population densities. Figure adapted from Wardrop et al. [45].

main unit level (the upper one), which contains 100 inhabitants (Figure 1.12(a)). Figure 1.12(b) depicts the actual spatial distribution of the inhabitants in this administrative unit, represented as points. The final objective here is to estimate the population counts in four subunits.

When no ancillary dataset is available, the best option is to conduct a "simple areal weighting", which is not considered properly as a dasymetric method in literature. This method (Figure 1.12(d)) assumes that population is homogeneously distributed within source zones and uses a redistribution weighting layer simply based on the percentage of the area of the original unit shared by the different subunits. In this example, the upper-left subunit represents 14% of the area of the main unit, and thus is reallocated with 14 inhabitants (14% of the population of the main unit). Comparison with the official data reveals that the actual aggregated count for this subunits is 10 (Figure 1.12(c)), which means that the error of prediction is of 4 inhabitants. Generally, the accuracy of the prediction is considered for the whole model and can be measured by the relative total absolute error RTAE[12] of prediction, which is here of 28%. It is this approach that is developed in the Gridded Population of the World (GPW) product [74].

The dasymetric mapping procedure can take advantage of available basic geographic information to improve the quality of population estimates. For this, the information should be considered as a good proxy of the actual population distribution, having thus a potential to improve the quality of the predictions. Such knowledge is usually provided by binary products giving the location of populated vs non-populated places (also called settlement layers). To improve the disaggregation, we could consider that the total amount of population of the initial unit is in fact entirely concentrated in populated places. Then, and since no other information

[12]RTAE is computed as the ratio between the sum of absolute errors and the total reference population or the whole territory under investigation [73].

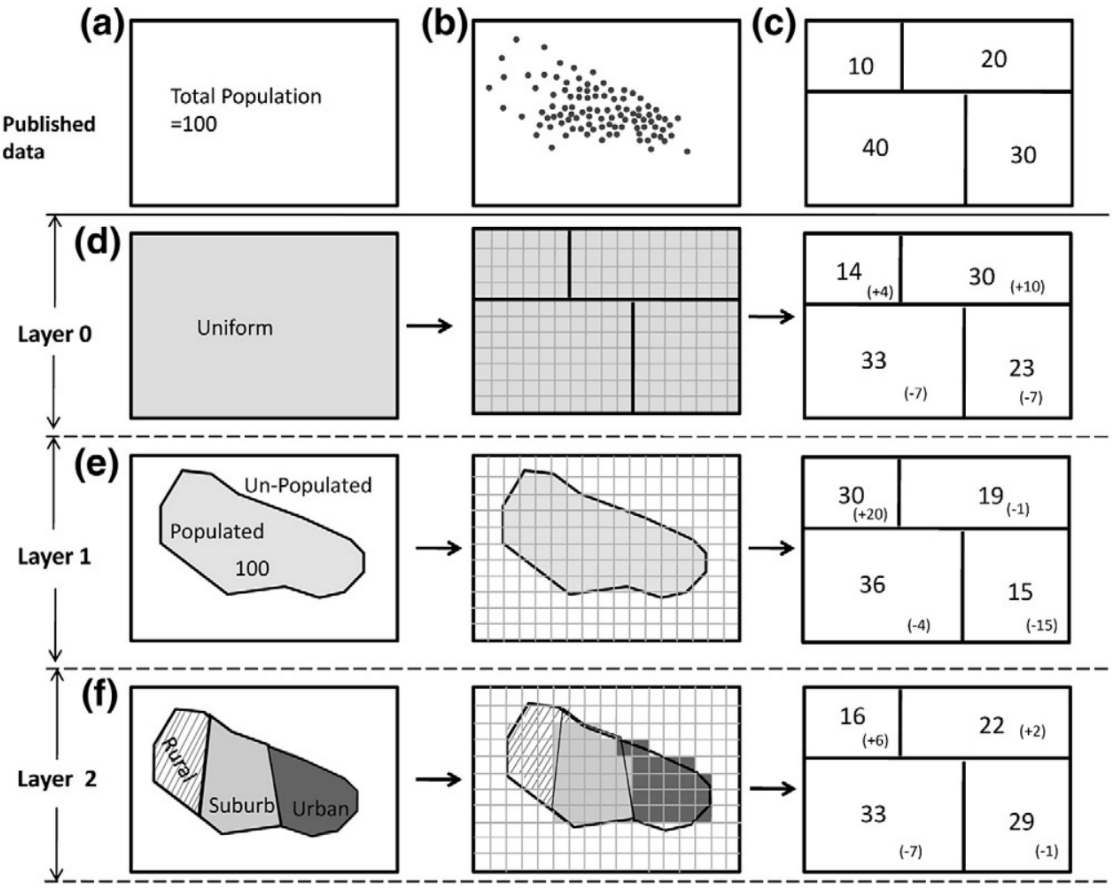


Figure 1.12: Simple examples depicting how dasymetric mapping models work. Source: Su et al. [54].

is available, a simple areal weighting can be performed on the populated place only (as illustrated in Figure 1.12(e)). While the distribution seems more realistic at first look, it is surprising to notice that the RTAE is more important than in the previous example and reaches 40%. The Global Rural Urban Mapping Project (GRUMP) [75] or the Global Human Settlement population Layer (GHSL-POP) [76] are two example of gridded population product that used this approach.

Population density obviously varies within populated places. For that reason, additional data providing a more useful thematic information can greatly improve the quality of the population model. In this example, adding ancillary information on the level of urbanization (urban, suburban, rural areas) enables to significantly reduce the RTAE which drops to 16% (Figure 1.12(f)).

Broadly speaking, while the detail of built-up masks remains limited, the quality of the prediction is likely to increase as more and more ancillary data are used in the dasymetric mapping strategy, which explains the development of new methods based on machine learning to incorporate a large number of covariates [77]. These novel methods are used in projects such as Landscan [78] or WorldPop [79].

Remote sensing (RS) data are an important source of useful geographic infor-

mation, derived by machine learning and image analysis methods. In the literature, many studies used RS-derived product such as built-up masks or land cover maps as the main ancillary information to be used for the creation of weighting layers. Other types of RS-derived information have also been used or have demonstrated their predictive power for population modeling, such as specific bands (thermal), bands ratios, image textures (either from active or passive sensor), vegetation indices, terrain slopes, elevation or height information (nDSM). For a more complete pictures of input data used in the literature for population modeling, interested readers can refer to [80].

An important advantage, especially for sub-Saharan countries where some regions could be faced with problems of accessibility or security, is that RS data allows for mapping very large areas. Moreover, in comparison with traditional mapping methods, RS-derived products are fast to produce and are considered relatively inexpensive with regards to their wide coverage [59].

### 1.4.4 Limitation of available global databases for SSA urban areas

As mentioned above, grid-based population data have several advantages, compared to more traditional polygon-based shapes, which makes them "... widely used [...] within the humanitarian aid and development community."[59].

As already mentioned, there are several projects that produce global gridded population products, including the Gridded Population of the World (GPW), with a 5km spatial resolution, the Global Rural Urban Mapping Project (GRUMP) and Landscan with, respectively, night-time and daytime estimates at 1km spatial resolution, the Global Human Settlement population Layer (GHSL-POP) with a spatial resolution of 250m and the WorldPop project with a spatial resolution of 100m.

Because of their coarser resolution, the first three products serve mostly for studies on the national or regional scales. For their part, GHSL and WorldPop population layers have a spatial resolution that better corresponds to what may be needed for urban applications. However, a detailed spatial resolution does not necessarily imply a model of good quality. When looking in Figure 1.13, we quickly realize that these products can only have very limited utility for intra-urban analyses: they are not enough spatially detailed to give a useful approximation of the actual population distribution. Figure 1.14 gives a closer look at the WorldPop layer, with the administrative units (in red) used as source zones during the dasymetric mapping. Since the population appears to be nearly homogeneously distributed within the administrative units, the advantage of using this dasymetric product instead of the original administrative unit is not obvious. This limitation can be

explained by the use of built-up masks that lack sufficient spatial details, as explained in subsection 1.4.5. As a direct consequence of the excessive homogeneity, these layers are marred by a significant "border effect", i.e., drops in population densities at the boundaries of the original administrative units. This is a common artifact in dasymetric mapping and different solutions have been proposed to mitigate it [81–83].

This lack of capacity to accurately model the spatial discontinuity of population densities inside administrative units is precisely the issues that this thesis aims to tackle, by making the hypothesis that satellite images with a higher resolution (VHR) could be leveraged for producing very detailed geoinformation to feed population models with more valuable ancillary data.

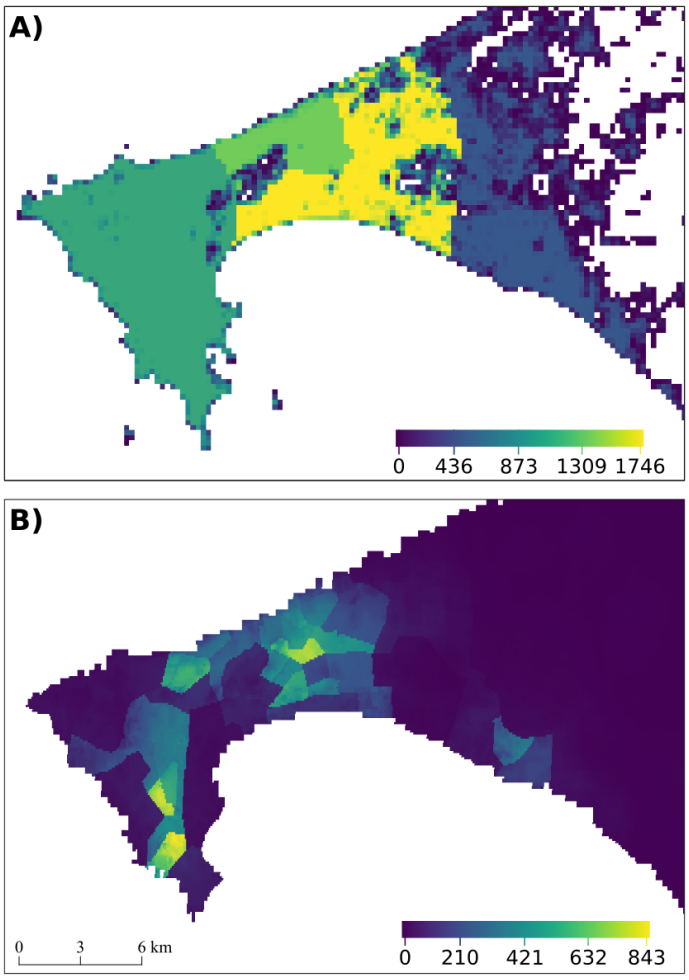


Figure 1.13: Population count estimates provided by several gridded population products on the city of Dakar. A)GHSL-POP (250m). B) WorldPop (100m).

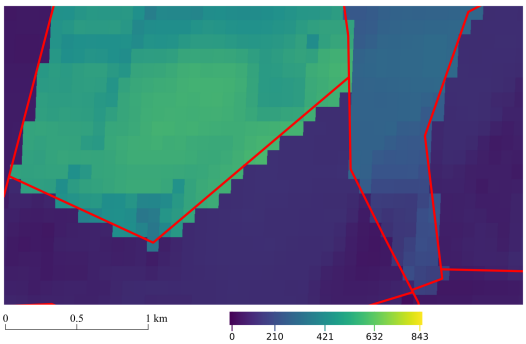


Figure 1.14: Population count estimates provided by the WorldPop project, superimposed with administrative units used as source zones in the dasymetric mapping procedure.

### 1.4.5 The potential of geoinformation derived from VHR

As we just demonstrated in the previous section, the best gridded population layers currently available for SSA are of limited quality. This is mainly because these dasymetric mapping models rely on layers of built-up areas with a relatively coarse resolution that appear among the most important predictors for the creation of weighting layers [38]. In this section we will highlight the potential of ancillary layers with a higher resolution (VHR) for supporting population modeling.

One should understand that the detail and the quality of the geoinformation that can be extracted from RS data highly depends on the spatial resolution of the input images. The difference between HR and VHR satellite images is illustrated in Figure 1.15. It is quite obvious that the increase in resolution can result in a huge difference for mapping intra-urban areas: While buildings are blurred on the HR image, all individual buildings may be distinguished on VHR.

To visualize the impact of the spatial resolution of ancillary data on dasymetric models, three different built-up layers are compared in Figure 1.16. The binary built-up masks have a spatial resolution of 0.5m(B), 10m(C) and 38m (D). The superimposed red lines correspond to a grid layer of 100*100m spatial resolution used to model population densities[13]. If we consider that these binary masks are the only available datasets, the most obvious strategy for the creation of weighting layers is to compute the proportion of built-up in each cell of the 100*100m grid. As can be seen in Figure 1.16, the percentage of the total area referred to as built-up greatly differs based on data source considered - close to 100% for the lower-resolution image, and probably below 60% for the highest-resolution image. The problem encountered by the coarser resolution product is related to the so-called "mixed-pixel" effect that happens when the size of the pixels is bigger than the

[13]Here, the resolution of 100*100m is chosen because it corresponds to the most spatially detailed currently available (WorldPop product).

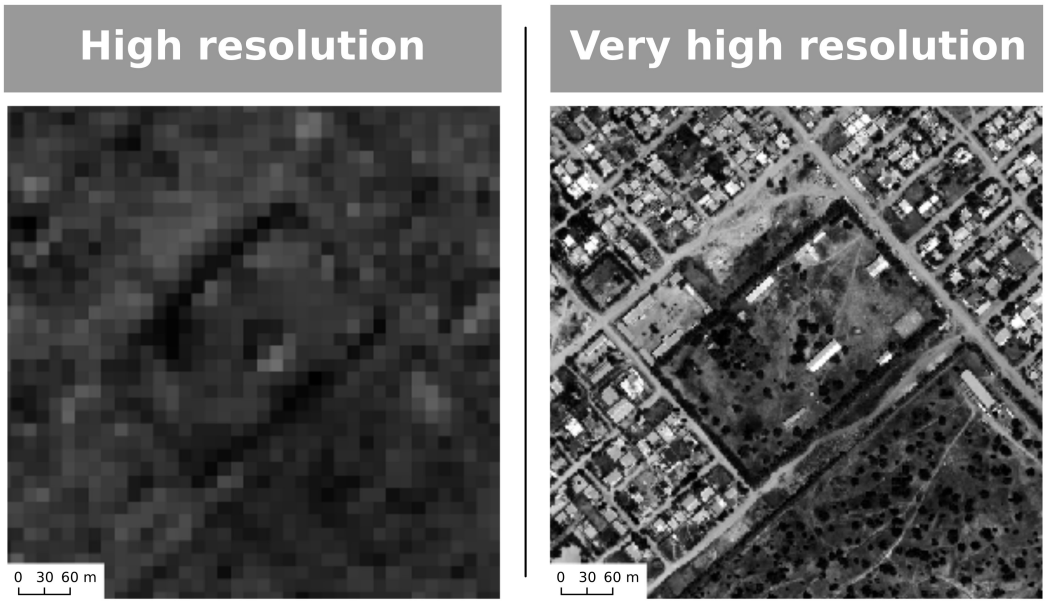


Figure 1.15: Difference between high resolution (Landsat - 15m in panchromatic) and very-high resolution (WorldView3 - 0.5m resampled product).

individual buildings and can include several land cover classes, as illustrated in Figure 1.2(a). As a consequence, coarse resolution products tend to classify pixels as "built" as soon as a small proportion of the underlying land surface is made of artificial elements. From a population modeling perspective, this results in a loss of the ability to appropriately capture the whole range of actual built-up densities.

It has been highlighted in the literature that both the quality [59] and the spatial resolution [54] of the ancillary products have a strong influence on the accuracy of the predictions of population models. In this regard, it is quite surprising to notice that the potential of VHRRS data for modeling intra-urban population in SSA still remains largely unexplored in the literature. This may be due to their higher costs and their processing power requirements, which are important factors limiting their use. However, with continuously decreasing prices and increasing computing capacity, there is a clear opportunity for the use of VHRRS data for improving the quality of the population models for urban areas.

In this thesis we leverage the potential of VHRRS-derived built-up masks as well as land cover and land use maps in order to quantify the gain in accuracy that VHR geoinformation could bring in comparison to HR. The results of this analysis are presented in Grippa et al. (2019) (**paper 5** [85], in chapter 4).

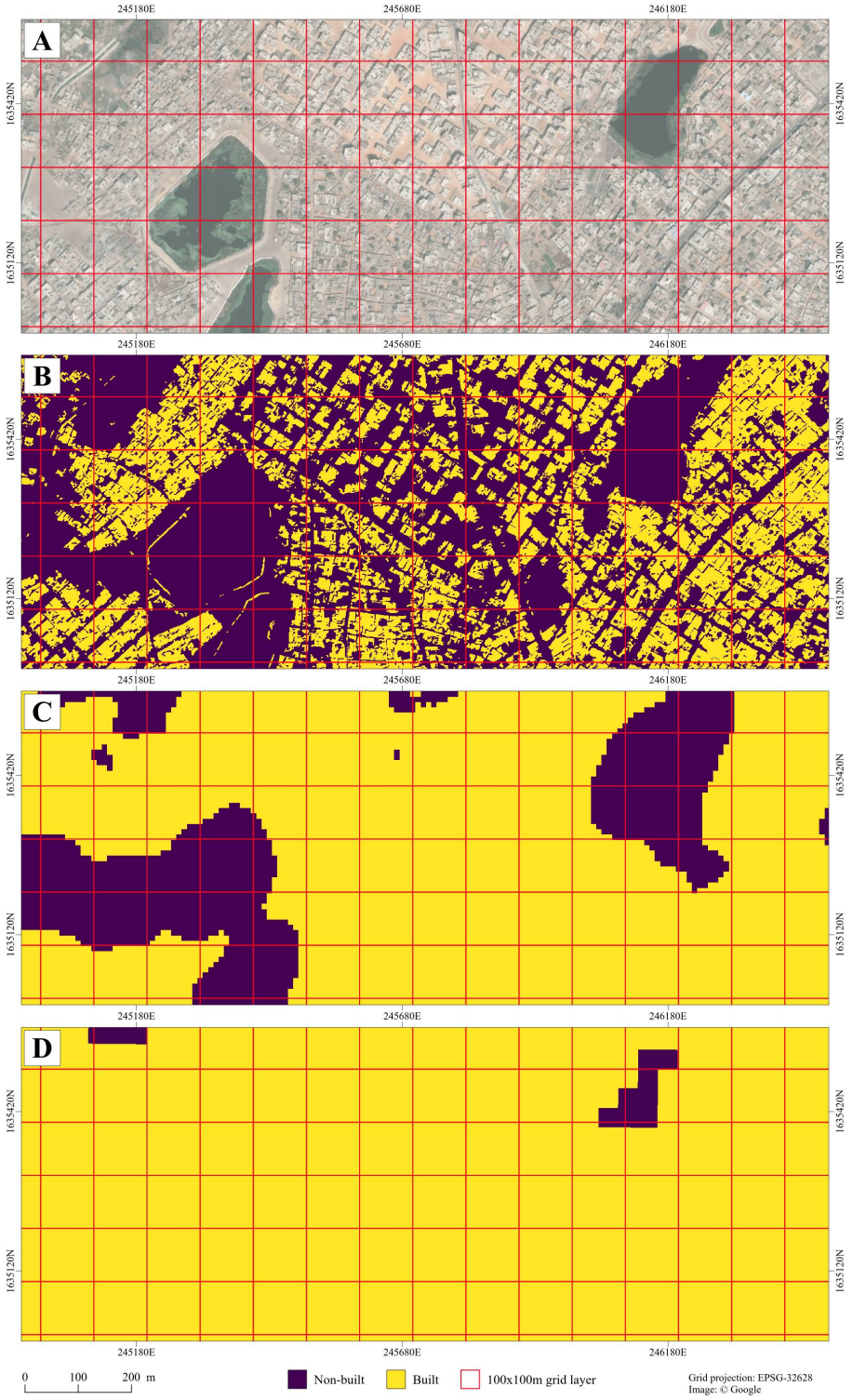


Figure 1.16: Built-up layers (binary masks) with different spatial resolutions. A) True color composite (VHR satellite imagery, 0.5m spatial resolution). B) Built-up mask at 0.5m spatial resolution, derived from A). C) Built-up mask at 10m spatial resolution [84]. D) Built-up mask at 38m spatial resolution (GHSL).

## 1.5 Toward open science in RS and GIS

In the research conducted in this thesis, we were several times faced with issues when attempting to reproduce results or methods published by other researchers. This reproducibility issue is not restricted to GIS or RS but concerns all the fields of scientific research. A recent survey revealed that more than 50% of researchers considered that there is currently a significant crisis in sciences regarding the reproducibility of research, and only 10% considered there was no crisis at all [86]. Although there is proof that the community is aware of the problem, the "... widespread adoption of [...][open science] practices has not yet been achieved."[87].

With regards to GIS and remote sensing, we argue that the academic community should dramatically intensify the efforts to push research forward on the path of open science. In this thesis, a special attention was given to applying the different principles of open sciences (see Figure 1.17), with the aim to allow other researchers to review, share, reuse or modify the proposed methods and results, but also in a spirit of equity toward those that have to work under financial constraints. Certain aspects of open access related specifically to remote sensing, as well as the importance of open source software, are further discussed in chapter 2 (**paper 1** [21]).


Figure 1.17: The six principles of open science. Source: Neuhold [88]

## 1.6 Specific objectives and outline of this thesis

For a variety of scientific studies and for urban planning and monitoring, VHR satellite images are not usable as input by themselves. To be useful, these raw data first need to be analyzed and processed using advanced methods to extract valuable geoinformation, such as land cover and land use maps. In SSA cities, these key pieces of information are often nonexistent of unavailable. Moreover, since SSA cities face fast urban growth and transformation and have to deal with limited financial means, there is a need to develop and share operational, transferable and cost-effective solutions for the production of geoinformation.

The main - global - research question of this thesis is "How to produce geoinformation for SSA cities, using VHRRS data and open-source solutions ?". In fact there is no clear and unequivocal answer to this question. Rather, it suggests the implementation and testing of different approaches and the selection of those which are the most relevant in the context of mapping SSA cities to create and share different framework for the production of geoinformation.

The first two objectives of this thesis are to develop different free and open-source frameworks for mapping the land cover and land use from VHRRS data. Land cover and land use mapping using VHR data is largely addressed in the remote sensing literature. Despite the fact that many articles are already published and that the different approaches and methods seem well established, their implementation is not as easy as expected, for several reasons:

i) First, while many authors publish and describe interesting methods, most of them fail to disclose all the information (scripts, formulas, computer code, parameters values used at each stages of the analyses, etc.) that would enable other researchers to replicate them easily. This constitutes an important obstacle to the transfer of cutting-edge methods into applied research projects.

ii) Second, a vast majority of scientific publications in GIS and RS focus on developed countries, especially for applications on urban areas. However, the characteristics of the European or North American cities are different, in many aspects, from SSA cities. As a result, some methods published in the literature are in fact not applicable at all when dealing with an SSA urban environment. In addition, working on case studies from developed countries also means working in a context of a better availability of existing geographic data. At the extreme opposite researchers working on SSA face an important lack of existing data and thus have to develop alternative methods less demanding in ancillary data.

iii) Third, many published remote sensing methods are tested and validated only on (very) small image snippets[14]. As a consequence, these methods often prove not as effective as initially announced, or may even completely fail to meet the requirements for applied studies that need to implement operational mapping strategies to cover very large study areas.

Considering the aforementioned problems identified in the literature, the following derivative objectives were considered, as often as possible, during this research:

[14] As already mentioned, >95% of publications on land cover mapping used concerned areas of less than $3\,km^2$[12].

i) Publishing all the methods in open access, either through open-access scientific peer-reviewed journals or by publishing author preprints on the University institutional repository.

ii) Implementing methods that rely only on open-source software, thus allowing anyone to replicate the proposed methods without having to spend money on proprietary software licenses.

iii) Giving open access to all the computer code used to perform the analyses, without any restriction (open-source license). This is a key condition toward a real open methodology as it allows other researchers to review the code and maybe propose to improve it. Also, it facilitates the reuse of the methods by other researchers and avoids spending time rewriting/re-coding what already exists.

iv) Releasing the results (produced maps) as open data that can be reused without any restrictions in other fields of research, such as epidemiology or risk assessment.

v) Designing mapping frameworks that remain parsimonious with the use of ancillary data, in order to be used on other data-poor case studies.

vi) Ensuring that proposed solutions are scalable and can be used to process very large areas of interests.

vii) Paying attention to the transferability of the frameworks to other locations and data sets.

viii) Creating computationally efficient frameworks, by implementing parallel processing for saving time and human resources.

In addition to the development of frameworks for land cover and land use mapping, we decided to use the geoinformation produced in the first stages to fill a gap in the field of population modeling and support urban-related research and applications such as epidemiology and risk assessment which suffer from the limitations of gridded population products currently available for SSA. In section 1.4 of this introduction we showed that these limitations are mainly due to the use of RS data with insufficient spatial resolution. Although VHRRS data allows for mapping urban areas with impressive spatial and thematic details and may be used to overcome these limitations, its potential for population redistribution is still largely unexplored. This observation leads to the second and main research question tackled in this thesis: "How can VHRRS data improve intra-urban population density estimates for SSA cities ?".

For the convenience of the reader, the main stages of the research workflow are presented in Figure 1.18, which briefly depicts the main processing steps of the research with their related input data and outcomes. The mains (sub-)objectives related to each chapter of this thesis are recapitulated in Figure 1.19.

This thesis is presented here as a compilation of several scientific articles, published in peer-reviewed journals or in conference proceedings. They constitute my main contributions, during the last four years, to a broader research project - "Modeling and forecasting African Urban Population Patterns for vulnerability and health assessments" (MAUPP) - funded by the program supporting research in Earth observation (STEREO III) of the Belgian Federal Science Policy Office (BELSPO). The main objective of MAUPP is to improve the knowledge of sub-Saharan African urban population patterns for a wider usage in vulnerability and health assessment studies. This project is conducted in partnership with the WorldPop project which aims at modeling the population at a spatial resolution of 100*100 meters, and the results of this thesis will be integrated in WorldPop population layers.

The arrangement of the next chapters corresponds to the actual workflow of this research, as presented in Figures 1.18 and 1.19, with the implementation of mapping frameworks for the production of geoinformation performed prior to the population modeling stage and tackling the main research question. **Chapter 2** presents consecutively the initial implementation of a semi-automated processing chain for mapping land cover from VHRRS (paper 1) as well as the methodological developments that were required to adapt state-of-the-art OBIA methods in order to process large and heterogeneous scene (papers 2,3). **Chapter 3** (papers 4) presents a semi-automated framework for the classification of urban land use at the street block level in data-poor context. It describes the creation of street blocks from OpenStreetMap (OSM) data and their classification in land-use classes based on their land cover composition. **Chapter 4** (paper 5) presents the final stage of the research workflow where a dasymetric mapping framework is created with the aim to answer the main research question by assessing the added value of VHR data against HR data in a dasymetric reallocation procedure. Finally, **chapter 5** provides a conclusion which summarizes the main achievements of this thesis as well as the remaining limitations and future perspectives.

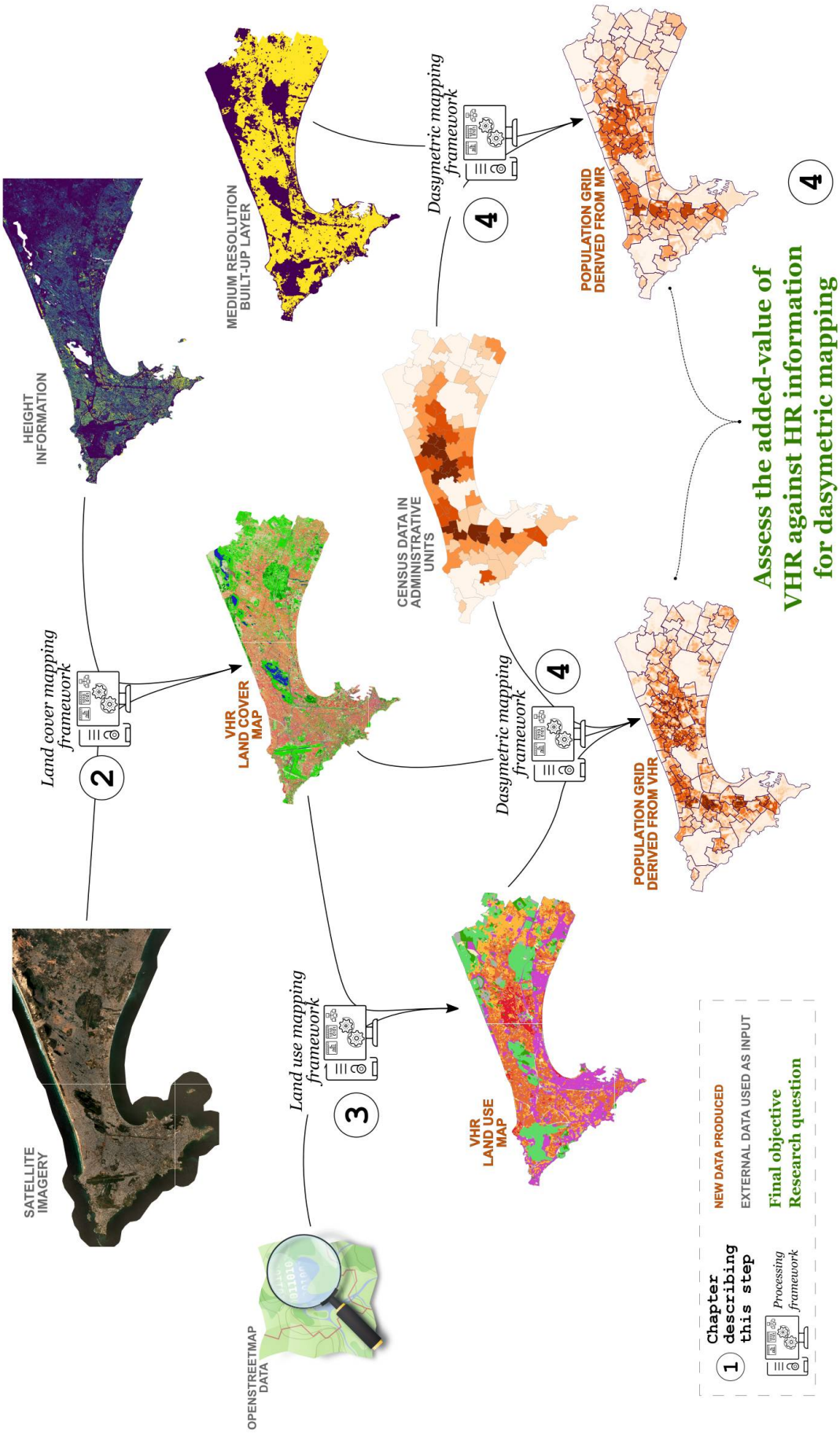


Figure 1.18: Conceptual flowchart of the achievements of this thesis.

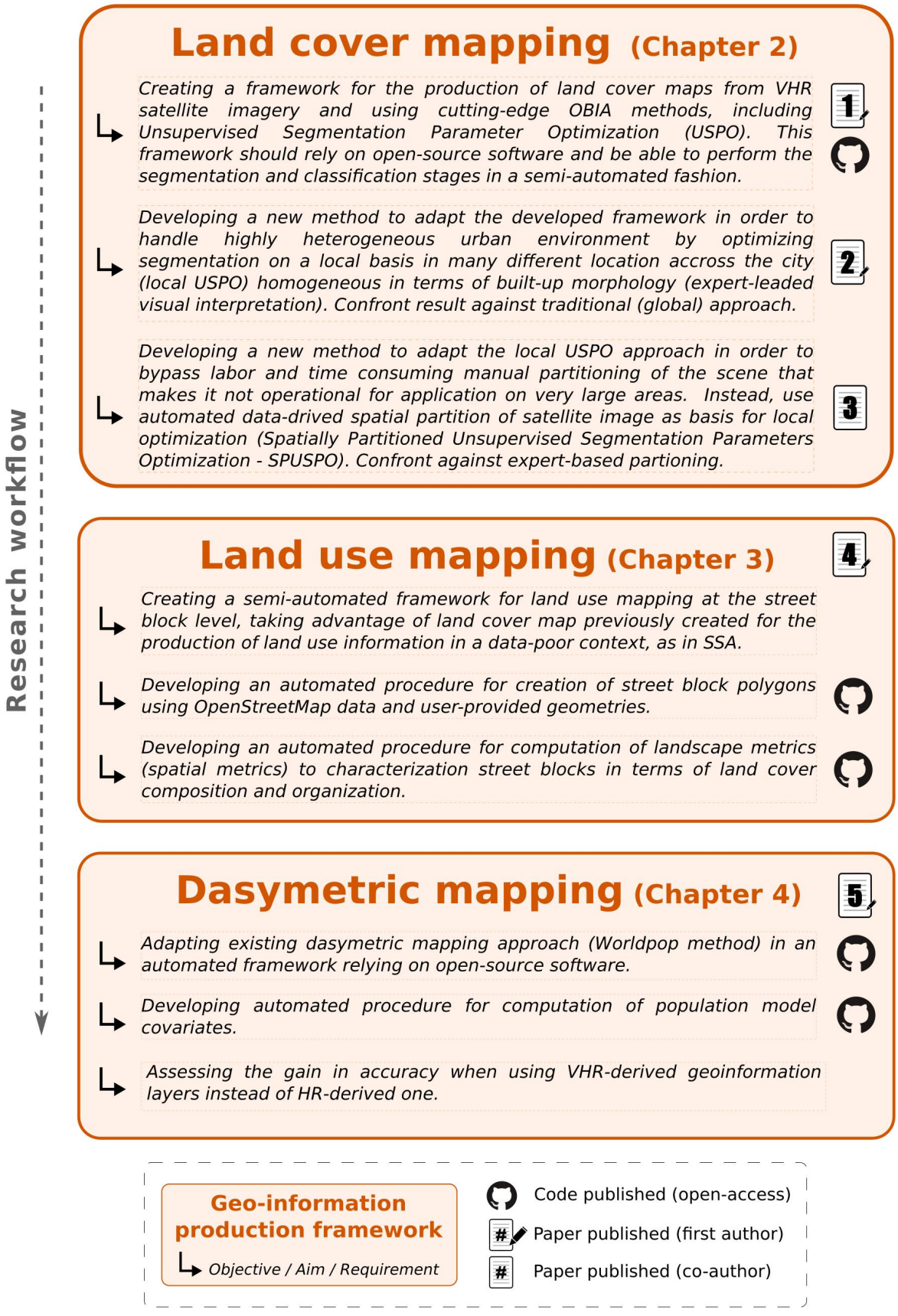


Figure 1.19: Frameworks development and related objectives and publications.

# Chapter 2

# Mapping the land cover from VHR remote sensing data with open-source solutions

## 2.1 Implementation of an open-source semi-automated processing chain for urban object-based land-cover classification

**Grippa, Taïs**, Moritz Lennert, Benjamin Beaumont, Sabine Vanhuysse, Nathalie Stephenne, and Eléonore Wolff. 2017. "**An Open-Source Semi-Automated Processing Chain for Urban Object-Based Classification.**" Remote Sensing 9 (4): 358. http://doi.org/10.3390/rs9040358.

*remote sensing*

MDPI

*Article*

# An Open-Source Semi-Automated Processing Chain for Urban Object-Based Classification

**Taïs Grippa [1,*], Moritz Lennert [1], Benjamin Beaumont [1,2], Sabine Vanhuysse [1], Nathalie Stephenne [2] and Eléonore Wolff [1]**

1 Department of Geoscience, Environment & Society, Université Libre De Bruxelles (ULB), 1050 Bruxelles, Belgium; mlennert@ulb.ac.be (M.L.); bbeaumon@ulb.ac.be (B.B.); svhuysse@ulb.ac.be (S.V.); ewolff@ulb.ac.be (E.W.)

2 Remote Sensing and Geodata Unit, Institut Scientifique de Service Public (ISSeP), 4000 Liège, Belgium; n.stephenne@issep.be

* Correspondence: tgrippa@ulb.ac.be; Tel.: +32-2-650-6806

Academic Editors: Norman Kerle, Markus Gerke, Sébastien Lefèvre and Prasad S. Thenkabail
Received: 19 December 2016; Accepted: 6 April 2017; Published: 11 April 2017

**Abstract:** This study presents the development of a semi-automated processing chain for urban object-based land-cover and land-use classification. The processing chain is implemented in Python and relies on existing open-source software GRASS GIS and R. The complete tool chain is available in open access and is adaptable to specific user needs. For automation purposes, we developed two GRASS GIS add-ons enabling users (1) to optimize segmentation parameters in an unsupervised manner and (2) to classify remote sensing data using several individual machine learning classifiers or their prediction combinations through voting-schemes. We tested the performance of the processing chain using sub-metric multispectral and height data on two very different urban environments: Ouagadougou, Burkina Faso in sub-Saharan Africa and Liège, Belgium in Western Europe. Using a hierarchical classification scheme, the overall accuracy reached 93% at the first level (5 classes) and about 80% at the second level (11 and 9 classes, respectively).

**Keywords:** OBIA; land cover; supervised classification; segmentation; optimization; GRASS GIS

## 1. Introduction

Land-use/land-cover (LULC) information extraction is one of the main use cases of remote sensing imagery. The advent of sub-meter resolution data brought about the revolution of methods from pixel-based to object-based image analysis (OBIA) involving image segmentation. The latter provides many new opportunities and highly increases the quality of the output, but there remains a number of challenges to address.

First of all, segmentation parameters are often selected after a tedious and time-consuming trial-and-error refinement [1,2]. This method consists of a manual step-by-step segmentation parameters adjustment, relying on subjective visual human interpretation. Despite such efforts, the validity of the selected parameters is usually restricted to the specific scene under study, or even to specific areas within this scene, and they have to be adapted for each dataset. Unsupervised optimization methods meet the requirements for automation in the OBIA process, as they can be used to automatically adjust the segmentation parameters [1].

Second, during the classification step, many authors use rule-based approaches, which can be efficient on a specific dataset (e.g., [3,4]). However, their transferability remains an issue [5,6] as they also generally rely on manual intervention by the authors, with many choices guided by scene specificities. As an alternative, machine-learning classifiers, e.g., random forest or support vector machines (see [7,8] for a review of applications in remote sensing), have proven their efficiency for

remote sensing data classification. While identification of the best performing classifier cannot rely on a priori knowledge, the combination of the results of multiple classifiers through an ensemble or voting schemes is a solution towards the development of more automated classification processes, as it "[...] makes the performance of the system more robust against the difficulties that each individual classifier may have on each particular data set". [9] (p. 705).

Third, much of the work presented on OBIA tool chains is black box. First, the specific decisions of authors concerning parameter settings in the manual processes described above are based on their subjective evaluation, which is not always easy to reproduce. Moreover, even if their procedures are well documented, algorithms implemented in proprietary software cannot be properly reviewed as their code is distributed as closed source. This concerns the core software and also, in some cases, extensions of that software (e.g., the 'Estimation of Scale Parameter' (ESP) tool published in [10]). Furthermore, only those who have access to the software can attempt the replication of the results. In times when the reproducibility of research is high on the discussion agenda [11], the use of free and open-source solutions, including access to the code developed by researchers in their work, becomes paramount.

Linked to the previous point, the question of access to the necessary tools is of great importance, especially for many researchers in poorer countries where the lack of resources reduces their options [12], and especially for research using remote sensing [13]. Again, free and open-source solutions provide an answer to this issue by creating common-pool resources that all researchers can use, but also contribute to. Licensing costs can also be an obstacle to the upscaling of processes, especially in times of big data with ever-increasing spatial, spectral, and temporal resolutions [13]. Free and open-source software can help researchers surmount this challenge by letting them run their programs on as many different cores or machines as necessary without having to worry about software costs.

In this paper, we present a complete semi-automated processing chain for urban LULC mapping from earth observation data, which responds at least partly to the above issues. This chain was initially presented at the GEOBIA 2016 conference [14]. Freely available to any potential user, it should be seen as a framework that can be reused, modified, or enhanced for further studies. The chain was developed in a completely free and open-source environment, using GRASS GIS (Geographical Resources Analysis Support System) [15] and R [16], and was immediately reinjected into the wider open-source community. It contains tools for unsupervised segmentation parameter optimization, statistical characterization of objects, and machine-learning techniques combined through a majority-voting scheme. Care was taken to make the use of this processing chain accessible even to novice programmers. The proposed framework was tested with similar datasets on two very different urban environments to assess its transportability, i.e., the ability to achieve accurate classification when applying the same generic framework to different scenes with similar datasets [17].

## 2. Methods and Tools

The processing chain mainly relies on the open-source software GRASS GIS, that has been in continuous development since the 1980s and is now one of the core components of the Open Source Geospatial software stack [18]. This multipurpose Geographical Information System is made of hundreds of small programs [19], called 'modules' or 'add-ons', enabling users to carry out a large variety of geospatial processes [18]. Thanks to its continuous review mechanism and to its active community that has strong links with academia, GRASS GIS is increasingly being used by researchers [20–25]. Since 2012, GRASS GIS has had major advances in object-based image analysis (OBIA).

The proposed chain is made of the core Python code linking GRASS GIS functions thanks to the GRASS Python scripting library. It is implemented in a 'Jupyter notebook' that enables researchers to easily share the computer code that they developed for their studies and that often remains unpublished [26]. This programming environment allows users to mix both explanatory text sections with the related computer code that can be executed in the same document (see Figure 1). Care was taken to clearly document the code and to refer to the official help and/or scientific references.

The Jupyter notebook is subdivided into several parts corresponding to the different processing steps (see Figure 1) which are summarized in the flowchart presented in Figure 2.

The GRASS GIS add-ons used in the processing chain are briefly presented below. For a more detailed description of those add-ons, interested readers may refer to the presentation made during the FOSS4G 2016 conference [27].

### *2.1. Segmentation and Unsupervised Segmentation Parameter Optimization (USPO) Tools*

The segmentation was performed using the i.segment module of GRASS GIS [28]. This module implements image segmentation with a region-growing algorithm or an experimental mean-shift algorithm which was added recently. The region-growing algorithm, which is used in this study, requires a standardized 'threshold' parameter below which regions are merged, and a 'minsize' parameter defining the minimum size of regions. As with most GRASS GIS modules, the i.segment module is designed to handle very large datasets while keeping a low memory footprint. As an example of the orders of magnitudes, we encountered an issue when exceeding 2 billion objects, and this issue was solved quite quickly by the responsive GRASS Development Team. Most of the elements in the processing chain offer the option of using parallel computing to accelerate the analyses. Scaling is thus possible across all available cores, within the limits of available memory and input-output restrictions.

```
    print "r.object.geometry have been installed on your computer"
else: print "r.object.geometry is already installed on your computer"
```

**Set list of raster from which to compute statistics with i.segment.stats**

Here after, a list of raster layer on which to compute statistics is saved. Please adapt those layers according to the raster you want to use for object statistics.

In [ ]:
```
## Display the name of rasters available in PERMANENT and CLASSIFICATION mapset
print grass.list_strings("raster", mapset="PERMANENT", flag='r')
print grass.list_strings("raster", mapset="CLASSIFICATION", flag='r')
```

In [ ]:
```
## Define the list of raster layers for which statistics will be computed
inputstats="opt_blue@PERMANENT"
inputstats+=",opt_green@PERMANENT"
inputstats+=",opt_nir@PERMANENT"
inputstats+=",opt_red@PERMANENT"
inputstats+=",NDVI@PERMANENT"
inputstats+=",Brightness@PERMANENT"
inputstats+=",nDSM@CLASSIFICATION"
print inputstats
```

**Compute statistics of segments with i.segment.stats**

In the following section, 'i.segment.stats' add on is used to compute object statistics. Please refer to the official help if you want to modify the parameters. Other raster statistics and morphological features could be used according to your needs.

In [ ]:
```
## Define computational region to match the extention of segmentation raster
grass.run_command('g.region', overwrite=True, raster="segments@CLASSIFICATION")

## Saving current time for processing time management
print ("Start computing statistics for training segments, using i.segment.stats on " + time.ctime())
begintime_isegmentstats=time.time()

## Compute statistics of objets using i.segment.stats only with .csv output (no vectormap output)
grass.run_command('i.segment.stats', overwrite=True, map="segments_training@CLASSIFICATION",
                  rasters=inputstats,
                  raster_statistics="min,max,range,mean,stddev,sum,coeff_var,first_quart,median,third_
quart,perc_90",
                  area_measures="area,perimeter,compact_circle",
                  csvfile="F:\\.....\\Classification\\i.segment.stats\\stats_training_sample.csv")

## Compute processing time and print it
print_processing_time(begintime_isegmentstats, "Segment statistics computed in :")
```

**Figure 1.** Excerpt of the "Jupyter notebook" consisting of a sequence of descriptive text parts that document the different processing steps and cells of the Python script that can be executed directly from the notebook.

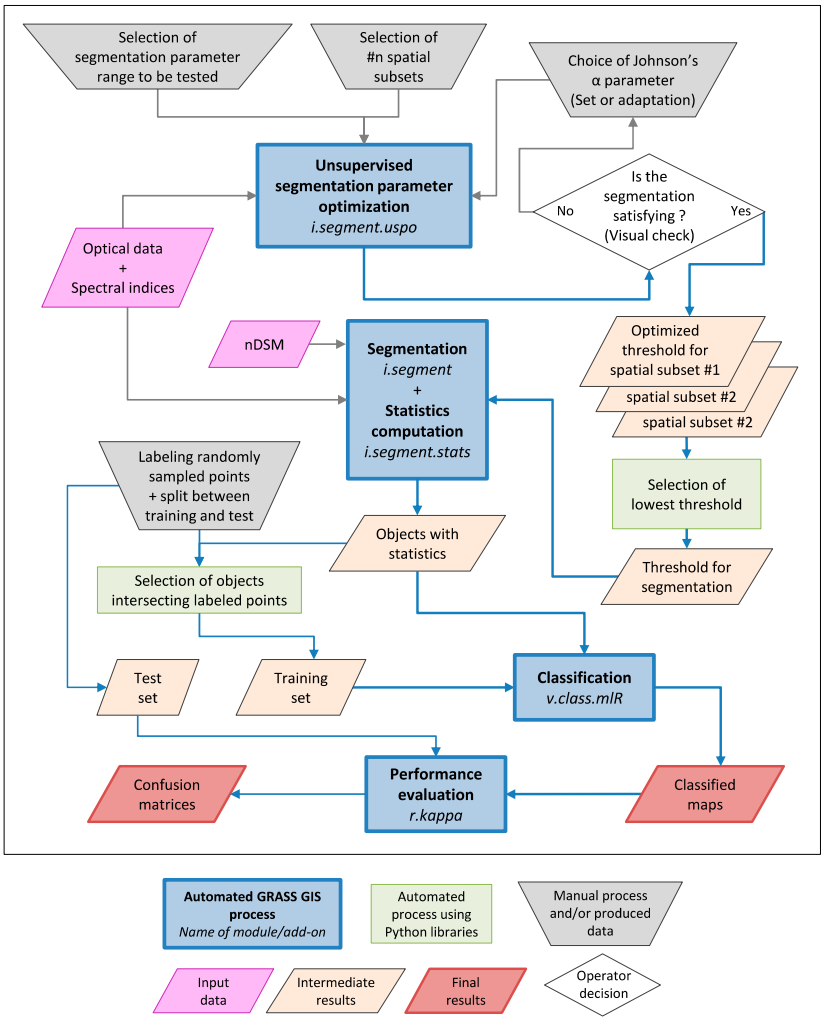


**Figure 2.** Flowchart of the processing chain.

The choice of segmentation parameters is an important step in OBIA. Indeed, the ultimate goal of segmentation is to cluster individual pixels into meaningful objects, i.e., objects that correspond as much as possible to the geographical objects of interest in the scene. Moreover, the impact of segmentation quality on the accuracy of the classification seems obvious, even though a recent study [29] argues that this link is not so straightforward.

Usually, the selection of segmentation parameters is carried out using a 'trial-and-error' approach that relies on the visual assessment of several naïve segmentation results, and gradual adjustment of the segmentation parameters. This method presents the disadvantages of being subjective and requiring a tedious and time-consuming effort.

When objectivity is required in the evaluation of the segmentation results, several empirical methods can be used. Among them, a distinction can be made between the supervised (empirical discrepancy methods) and the unsupervised approaches (empirical goodness methods), depending on the requirement of a reference object delineation [1,30]. Both supervised and unsupervised methods allow the comparison of different segmentation algorithms or of different parameters used in a single algorithm (segmentation parameter optimization).

Supervised evaluation methods assess the divergence between a segmented image and a reference segmentation layer using 'discrepancy measures'. Usually, the reference layer is created by delineating objects manually, thus requiring a time-consuming and highly subjective task.

In contrast, unsupervised evaluation methods assess the quality of a segmented image without the need of a reference or prior knowledge. This is the major advantage of these methods that can be used for automated segmentation parameter optimization [31]. Moreover, a recent study shows that they can achieve similar classification accuracy [32]. The evaluation relies on 'goodness measures' computed directly on the segmented image that represent the characteristics of a good segmentation. The uniformity of single objects (intra-segment homogeneity) and a significant difference between adjacent objects (inter-segment heterogeneity), firstly presented in [33] as desired characteristics of created objects, are now widely used in unsupervised evaluation methods. Several unsupervised approaches have been proposed in the literature, with different goodness measures and methods for combining them into a synthetic metric (see [1] for a review).

As we looked for automation, we elaborated a new GRASS GIS add-on for unsupervised segmentation parameter optimization (USPO) named i.segment.uspo [34]. Its working principle is illustrated on Figure 3. This tool is an implementation of the methods proposed by [31,35]. It relies on optimization functions combining measures of intra-object variance weighted by object size [32] (WV) as an intra-segment homogeneity quality measure, and spatial autocorrelation (SA) as an inter-segment heterogeneity quality measure [35]. For the latter, the user can choose between Moran's I [36] or Geary's C [37]. As the measure should be comparable for different segmentation results, both intra-segment homogeneity and inter-segment heterogeneity measures are normalized using the following function [35]:

$$F(x) = \frac{X_{max} - X}{X_{max} - X_{min}} \quad (1)$$

where $F(x)$ is the normalized value of either WV or SA, $X$ is the WV (or SA) value of the current segmentation result, and $X_{max}$ and $X_{min}$ are the maximum and minimum values of WV (or SA) for the whole stack of segmentation results to be evaluated. A high value for normalized WV ($WVnorm$) indicates higher undersegmentation, while a high value for normalized SA ($SAnorm$) highlights a higher oversegmentation.

The GRASS GIS add-on i.segment.uspo enables the combination of these WV and SA measures using two different optimization functions: a simple sum of the normalized criteria values as proposed by [35] or the F-function proposed by [31] that permits us to weight the two optimization criteria. The F-function is calculated as follows:

$$F = \left(1 + \alpha^2\right) \frac{AS_{norm} \times WV_{norm}}{\alpha^2 \times AS_{norm} + WV_{norm}} \quad (2)$$

where $F$ is the 'overall goodness', ranging from 0 (poor quality) to 1 (high quality) [31], to be used as a synthetic measure of the quality of the segmentation and $\alpha$ is a parameter that can be modified to give more weight to WV or to SA.

This overall goodness metric was designed in order to perform unsupervised segmentation parameter optimization for multi-scale OBIA (MS-OBIA) [31] (i.e., a process where different levels of segmentation are used together in the classification). In the semi-automated processing chain that was developed, the classification is performed using a single segmentation level. However, the chain could very easily be modified to enable MS-OBIA.

As highlighted in [38], the ability of USPO approaches to produce a good segmentation for specific features of interest in the scene is not straightforward, especially if those features are small-sized. Regarding this issue, we clearly recommend a visual check of the segmentation results to ensure that they are consistent with the objects of interest in the scene, as illustrated in the flowchart in Figure 2. If this is not the case, the $\alpha$ parameter in the Johnsons' optimization function can be adapted to give more importance either to intra-segment homogeneity (set the $\alpha$ parameter higher than 1 to avoid residual undersegmentation) or to inter-segment heterogeneity (set the $\alpha$ parameter lower than 1 to avoid residual oversegmentation) [31]. More generally, it is clear that the 'perfect' segmentation does not exist [1,39,40], even if optimization methods are used. In their conclusion,

Räsänen et al. argue that "[...] different segmentation evaluation methods should be used with care [...]. When segmentation evaluation is rigorously used, however, it can assist in finding a more optimal segmentation". [29] (p. 8623).

Based on a range of parameter values provided by the user, the i.segment.uspo tool creates a set of segmentation results that are then assessed using the optimization function (see Figure 3). We suggest setting the range of segmentation parameter values to be tested by identifying values resulting in clearly under-segmented and over-segmented results, and using them as extremes. In order to reduce computation time during the optimization process, the tool provides the possibility to optimize the segmentation parameters on several spatial subsets of the scene (i.e., several zones limited in terms of area).

Care is recommended during the selection of those spatial subsets to ensure that they represent the diversity of the landscape that can be found in the whole scene. Detailed results are available (WV and AS measures and optimization scores for each segmentation parameter combination and each spatial subset), enabling the user to make an informed choice. Provided that there are no extreme outliers among the distribution of segmentation parameters from the different spatial subsets, the choice amongst the results can be completely automated by, for example, selecting the lowest value of the threshold parameter (as illustrated in Figure 2). Even though this approach could result in oversegmentation in some parts of the scene, some studies [39,41] argue that oversegmentation is preferable to undersegmentation, as the former can be corrected during classification, contrary to the latter. Furthermore, some recent studies [32,42] highlight that oversegmentation, as long as it remains at an admissible level, could be a minor issue in regard to the final classification result. Insofar that the different spatial subsets were well chosen to ensure that they represent the diversity of landscapes in the whole scene, the presence of extreme outliers among the optimized segmentation parameter is an indication that segmentation using a single parameter for the whole scene is not recommended. In this case, the whole scene could be subdivided into several more homogeneous areas according to some specific criteria. These areas could then be used as tiles in the segmentation workflow to perform local optimizations of the segmentation parameters [43].

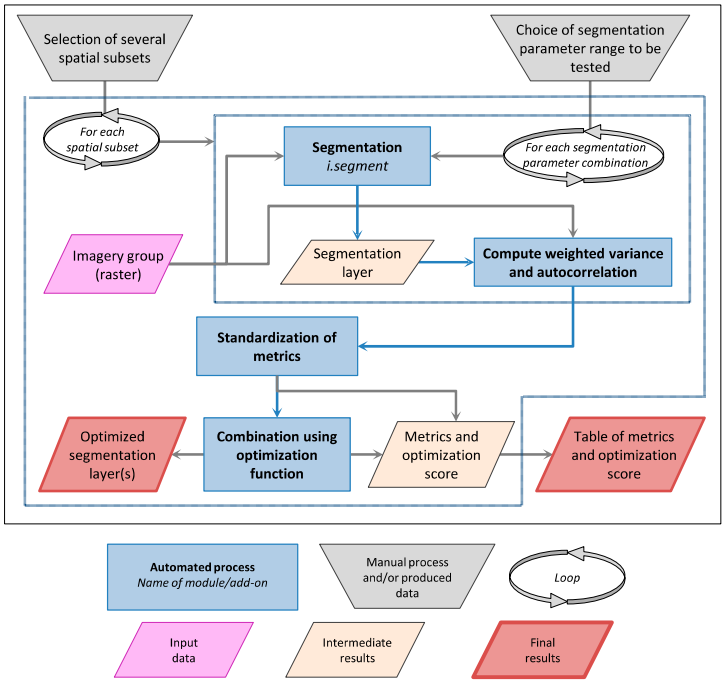


**Figure 3.** Selection of the optimized thresholds by i.segment.uspo.

The chain was designed to perform the segmentation process by dividing the scene using a vector layer provided by the user. This layer can consist of, e.g., arbitrary tiles or existing administrative boundaries. This implementation also allows users to manage very large datasets.

### *2.2. Object Statistics Computation*

Object statistics were computed using the i.segment.stats GRASS GIS add-on [44] and were used as features in the classification process. This tool computes both the spectral statistics (e.g., min, max, median, stddev) and morphological statistics of objects (e.g., area, perimeter, compactness, fractal dimension). In order to speed up the calculation of the latter, another add-on, r.object.geometry [45], was developed. This add-on eliminates the need for vectorizing segments when computing morphological statistics, resulting in a significant gain in time.

### *2.3. Classification by the Combination of Multiple Machine Learning Classifiers*

The classification stage of the processing chain uses the v.class.mlR GRASS GIS add-on [46]. It relies on the utilization of the "Caret" library of the R software [47], and enables the classification of data using Support Vector Machine (currently only with a radial kernel) (SVMradial), Random Forest (RF), Recursive partitioning (Rpart), and k-Nearest Neighbors (kNN) classifiers. This add-on automatically tunes classifiers' parameters using repeated cross-validation with, by default, 10 iterations of 5-fold cross-validation on the training data set. Predictions of individual classifiers are then combined using several types of majority vote.

Four voting systems are provided: "Simple Majority Vote" (SMV), "Simple Weighted Vote" (SWV), "Best Worst Weighted Vote" (BWWV), and "Quadratic Best Worst Weighted Vote" (QBWWV). SMV simply consists of retaining the most frequent prediction. In the other votes, the predictions of individual classifiers are weighted. In SWV, the weight used is strictly the accuracy of individual classifiers estimated through cross-validation. In BWWV, the worst classifier is assigned a zero weight and is thereby not taken into account, and the best classifier is assigned a unit weight. The remaining classifiers are weighted linearly between 0 and 1. The last vote, QBWWV, is designed similarly to the former but the remaining classifiers are weighted using a squared function, amplifying the importance of more accurate classifiers. Interested readers can refer to [9] for the votes presented here and to [48] for more advanced methods used in remote sensing field.

A noticeable advantage of GRASS GIS is that it can be connected directly to R [16,49], allowing the exploitation of several advanced statistics methods (e.g., deep learning methods) implemented in this open-source software.

## 3. Case Studies

### *3.1. Study Areas and Data*

In order to evaluate the transportability of the proposed processing chain, we applied it to two very different urban environments: Ouagadougou (Burkina Faso, in Sub-Saharan Africa) and Liège (Belgium, in Western Europe). More broadly, this work is linked with two research projects dealing with the production (Modelling and forecasting African Urban Population Patterns for vulnerability and health assessments project (MAUPP, http://maupp.ulb.ac.be/), focusing on African Sub-Saharan cities) and the update (SmartPop project, focusing on the Walloon region in Belgium, http://www.issep.be/smartpop/) of LULC maps. These maps will be used later as inputs in census population data disaggregation models.

The processing chain was first developed on Ouagadougou, the capital of Burkina Faso in Western Africa. Covering more than 615 $km^2$, this city has been facing intensive urban sprawl during the last few decades similar to most sub-Saharan African cities and is characterized by very different urban patterns, such as planned versus unplanned residential areas, among others. Then, the processing chain was applied to the Liège area (261 $km^2$), a Western European city located in Belgium which

shows strong land artificialization (more than 55% of the territory). Urban morphologies are more diversified (from isolated houses to 10+ storey buildings), but urban sprawl is limited and controlled in comparison with Africa.

The datasets consist of multi-spectral and height data. For Ouagadougou, a pan sharpened stereo WorldView-3 imagery (Visible and Near-InfraRed bands (VNIR), spatial resolution of 0.5 m) acquired during the wet season (October 2015) and a normalized digital surface model (nDSM) (spatial resolution of 0.5 m) produced by stereophotogrammetry from WorldView-3 stereo-pairs were used. For Liège, the data consisted of leaf-on VNIR aerial orthophotos with a spatial resolution of 0.25 m acquired in May 2012 and a leaf-off nDSM extracted from Light Detection And Ranging data (LiDAR) (with a point density between 1 and 3 points per square meter) that was acquired in the winter of 2013–14.

As our processing chain is under development, we focused the classification effort on a 25 km$^2$ subset for both cities (see Figure 4), representative of the diversity of landscapes and urban forms.

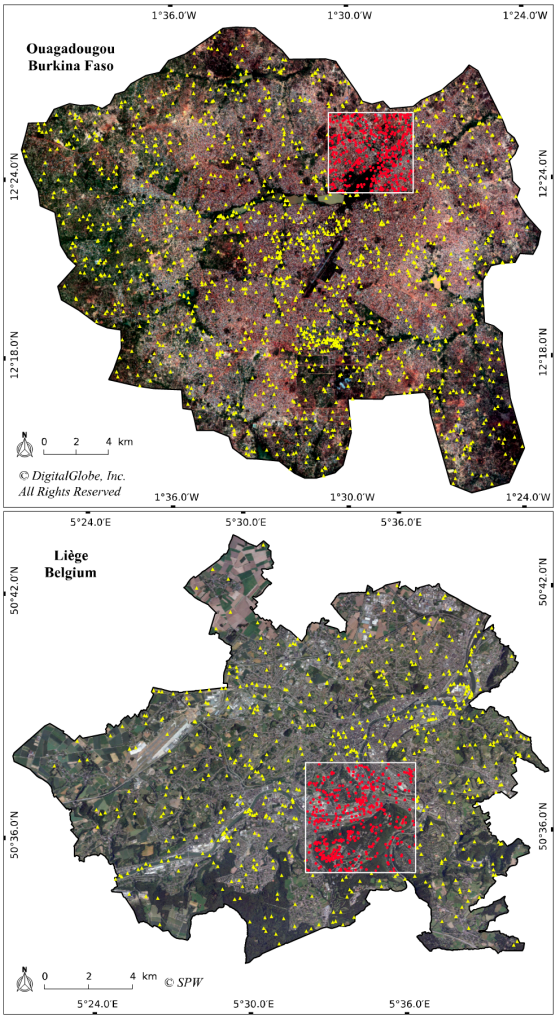


**Figure 4.** Ouagadougou and Liège case studies. True color composite is used as the background. For both cities, the classification was made on the white-squared subset. Training samples are in yellow while the test samples are in red.

### *3.2. Legend/Classification Scheme*

The classification scheme is organized in two hierarchical levels (see Table 1). The first level contains only land-cover (LC) classes, while the second level is a LULC mix of classes. At both

levels, an extra class is dedicated to shadows; their post-processing is out of the scope of this article. The classification was made based on the second-level classes, which were aggregated to match the first-level classes.

**Table 1.** Classification scheme and size of the training and test sets for Ouagadougou and Liège.

| Level 1 Classes Land Cover (LC) | Level 2 Classes Land Use/Land Cover (LULC) | Abbreviation | Training Set Size | Test Set Size |
|---|---|---|---|---|
| Ouagadougou–Burkina Faso | | | | |
| Artificial surfaces | Buildings | BU | 216 | 43 |
| | Swimming pools | SW | 90 | 31 |
| | Asphalt surfaces | AS | 119 | 30 |
| Natural material surfaces | Brown/red bare soil | RBS | 130 | 42 |
| | White/grey bare soil | GBS | 91 | 30 |
| Vegetation | Trees | TR | 91 | 32 |
| | Mixed bare soil/vegetation | MBV | 99 | 32 |
| | Dry vegetation | DV | 93 | 32 |
| | Other vegetation | OV | 218 | 36 |
| Water | Water bodies | WB | 115 | 31 |
| Shadow | Shadow | SH | 90 | 30 |
| Liège–Belgium | | | | |
| Artificial surfaces | Buildings | BU | 62 | 37 |
| | Asphalt surfaces | AS | 86 | 60 |
| Natural material surfaces | Bare soil | BS | 51 | 42 |
| Vegetation | Low vegetation (<1 m) | LV | 55 | 46 |
| | Medium vegetation (1–7 m) | MV | 49 | 48 |
| | High vegetation deciduous (>7 m) | HVD | 63 | 36 |
| | High vegetation coniferous (>7 m) | HVC | 49 | 43 |
| Water | Water bodies | WB | 72 | 37 |
| Shadow | Shadow | SH | 62 | 39 |

### *3.3. Sampling Scheme*

Sampling was conducted outside the processing chain, by generating random points and labelling them by hand, through visual image photo-interpretation. Although existing geodatabases were used for stratification, visual interpretation was needed to bypass thematic or spatial accuracy issues. In order to ensure a clear spatial independence, the training set was generated for the whole area excluding the 25 $km^2$ subset where the classification was produced. An independent test set was generated inside this subset for performance evaluation purposes (see Figure 4). This procedure avoids potential spatial autocorrelation between the training and test sets.

For Ouagadougou, the OpenStreetMap (OSM) dataset was used as far as possible according to the availability. These data were used only for stratification purposes and only for some specific classes, i.e., for second-level classes of 'buildings', 'asphalt surfaces', and 'water bodies'. When OSM datasets consisted of lines, as it is the case for asphalt roads and watercourses, buffers were created. Manual sampling was required for 'swimming pools' and 'shadow' classes. Intensive visual interpretation was needed for labelling each sampled point individually and to bypass mislabelled (cases where OSM attributes were false) and spatial inaccurate issues coming from the OSM data.

For Liège, existing official geodatabases from the national administration, i.e., 'TOP10V' (Institut Géographique National (IGN), 2010), and from the regional administration, i.e., 'Projet Informatique de Cartographie Continue' (PICC) (Service Public de Wallonie (SPW), 2007), were used for the stratification of the majority of second-level classes. Manual sampling was needed for the class 'shadow'. Given the production date of the geodatabases used, a visual validation of the samples was needed to match the 2012/2013 land-cover status. In total, 1352 training points and 369 test points were created for

Ouagadougou and 549 training points and 388 test points for Liège. The smaller size of the training set for Liège is explained by the reduced number of classes, their higher spectral consistency, and the intensive use of reference geodatabases. The class-distribution details are presented in Table 1.

Training and test points were used to automatically select intersecting segments and create the training and test sets. Although there is risk that some imperfect segments are used, the advantage of this strategy is that the same labelled set of points can be used with different segmentation results.

### *3.4. Segmentation*

The segmentation and unsupervised segmentation parameter optimization (USPO) steps were carried out using multispectral information. For Ouagadougou, NDVI was also used as an additional layer. The nDSM layer was not used for the segmentation because of its insufficient geometric precision. The "minsize" parameter was set in order to match a chosen minimum mapping unit. The latter was defined according to the geographical context based on the smallest house/shelter: 2 $m^2$ for Ouagadougou and 15 $m^2$ for Liège. The intervention of the operator in the USPO process was limited to identification of the range of "threshold" parameters to be tested (minimum, maximum, and intervals), by manually looking for the thresholds resulting in clearly over-segmented or under-segmented objects. The optimized threshold was then automatically determined via the i.segment.uspo add-on. When giving the same weight to both intra-object homogeneity and inter-object heterogeneity measures (with the Johnson's $\alpha$ parameter set to 1), objects of interest like small houses or trees were undersegmented. To avoid this issue, Johnson's $\alpha$ parameter was then set to 1.25 for both Ouagadougou and Liège, in order to give more importance to intra-object homogeneity in the optimization function.

### *3.5. Classification Feature*

For both case studies, the minimum, maximum, range, standard deviation, sum, and median statistics were computed for segments on the multispectral bands, NDVI and nDSM. These spectral statistics were completed with the morphological attributes of the objects (area, perimeter, and compactness).

## 4. Results

The classifications were performed at the second level of the legend scheme (see Table 1) using four individual machine learning classifiers that were combined using four voting systems. For each classification, the second-level classes were then aggregated to obtain the classes of the first level. The overall accuracy as well as Cohen's Kappa metric of individual classifiers and vote combinations are presented in Table 2.

**Table 2.** Performance evaluation of individual classifiers and the four different voting systems. For each line, the highest value is in bold. OA: Overall accuracy. L1 and L2: Levels of the classification scheme. kNN: k-Nearest Neighbors. Rpart: Recursive partitioning. SVMradial: Support Vector Machine with radial kernel. RF: Random Forest. SMV: Simple Majority Vote. SWV: Simple Weighted Vote. BWWV: Best Worst Weighted Vote. QBWWV: Quadratic Best Worst Weighted Vote.

| | | | **Individual Classifiers** | | | | **Votes** | | | |
|---|---|---|---|---|---|---|---|---|---|---|
| | | | **kNN** | **Rpart** | **SVMradial** | **RF** | **SMV** | **BWWV** | **QBWWV** | **SWV** |
| **Ouagadougou** | L1 | Kappa | 0.69 | 0.80 | 0.84 | **0.90** | 0.87 | **0.90** | **0.90** | **0.90** |
| | | OA | 77% | 85% | 88% | **93%** | 91% | 92% | 92% | **93%** |
| | L2 | Kappa | 0.45 | 0.69 | 0.72 | **0.79** | 0.76 | **0.79** | **0.79** | **0.79** |
| | | OA | 50% | 72% | 75% | **81%** | 78% | **81%** | **81%** | **81%** |
| **Liège** | L1 | Kappa | 0.75 | 0.83 | 0.87 | **0.89** | 0.88 | **0.89** | **0.89** | **0.89** |
| | | OA | 82% | 88% | 90% | 92% | 91% | 92% | 92% | **93%** |
| | L2 | Kappa | 0.44 | 0.71 | 0.71 | **0.77** | 0.74 | 0.76 | 0.76 | 0.76 |
| | | OA | 50% | 74% | 74% | **79%** | 77% | **79%** | **79%** | **79%** |

The ranking of individual classifiers' performance is the same for Ouagadougou and Liège, with Random Forest (RF) performing best (overall accuracy (OA) of 81% and 79%, respectively), followed by Support Vector Machine with radial kernel (SVMradial) (75% and 74% OA, respectively), then Recursive partitioning (Rpart) (72% and 74% OA, respectively), and finally K–Nearest Neighbors classifier (kNN) (both 50% OA).

In the proposed processing chain, the training set is created by selecting the objects that contain the manually labelled point (see Figure 2), without any visual check. This design could result in the presence of mis-segmented objects in the training set which could perturb the classifiers. This explains why RF outperformed SVM, as studies show that RF is very robust when trained with imperfect data [50], while SVM is very sensitive to the presence of noise in the training set [51].

The user's and producer's accuracy computed on second-level classes are provided for each classification in Tables A1 and A2. As assessing the performance with these measures can become very confusing, the F-score (harmonic mean of the user's and producer's accuracy) is used as a synthetic accuracy metric [52,53] in order to compare the classifiers' performance on a class basis. The 'buildings' class is of particular importance in the context of the MAUPP and SmartPop projects since their final objective is to disaggregate census population data using LULC maps in order to model the spatial distribution of population densities. Using RF, this class reached a high accuracy for both case studies, with an F-score of 0.93 for Ouagadougou and 0.91 for Liège (see Table 3). For Ouagadougou, RF impressively outperformed Rpart and SVM for the class 'buildings' (both reaching an F-score of 0.78). This is also true for asphalt surfaces, with an F-score of 0.83 for RF, 0.61 for Rpart, and 0.55 for SVM. Again, those observations can be explained by the robustness of RF when dealing with imperfect data.

**Table 3.** F-score for individual classes for the second level (L2) of the classification. For each line, the highest value is in bold. kNN: k-Nearest Neighbors. Rpart: Recursive partitioning. SVMradial: Support Vector Machine with radial kernel. RF: Random Forest. SMV: Simple Majority Vote. SWV: Simple Weighted Vote. BWWV: Best Worst Weighted Vote. QBWWV: Quadratic Best Worst Weighted Vote.

| | **Individual Classifiers** | | | | **Votes** | | | |
|---|---|---|---|---|---|---|---|---|
| **Level 2 Classes** | **kNN** | **Rpart** | **SVMradial** | **RF** | **SMV** | **SWV** | **BWWV** | **QBWWV** |
| **Ouagadougou–Burkina Faso** | | | | | | | | |
| Buildings | 0.62 | 0.78 | 0.78 | **0.93** | 0.86 | **0.93** | 0.92 | 0.92 |
| Swimming pools | 0.91 | 0.92 | 0.97 | **0.98** | **0.98** | **0.98** | **0.98** | **0.98** |
| Asphalt surfaces | 0.50 | 0.61 | 0.55 | **0.83** | 0.80 | **0.83** | **0.83** | **0.83** |
| Brown/red bare soil | 0.52 | 0.75 | 0.65 | **0.78** | 0.77 | 0.77 | 0.77 | 0.77 |
| White/grey bare soil | 0.26 | 0.69 | 0.71 | **0.72** | 0.65 | 0.70 | 0.70 | 0.70 |
| Trees | 0.58 | 0.83 | 0.83 | **0.85** | 0.82 | 0.84 | **0.85** | **0.85** |
| Mixed bare soil/vegetation | 0.29 | **0.62** | 0.59 | 0.56 | 0.57 | 0.58 | 0.58 | 0.58 |
| Dry vegetation | 0.08 | 0.48 | **0.65** | 0.61 | 0.64 | 0.63 | 0.62 | 0.62 |
| Other vegetation | 0.55 | 0.71 | 0.73 | 0.77 | 0.75 | 0.78 | **0.81** | **0.81** |
| Inland waters | 0.19 | 0.74 | 0.85 | **0.87** | 0.75 | 0.85 | 0.85 | 0.85 |
| Shadow | 0.75 | 0.72 | 0.93 | 0.94 | **0.95** | **0.95** | 0.94 | 0.94 |
| **Liège–Belgium** | | | | | | | | |
| Buildings | 0.51 | 0.92 | 0.83 | 0.91 | **0.93** | **0.93** | 0.91 | 0.91 |
| Asphalt surfaces | 0.64 | 0.71 | 0.77 | **0.82** | 0.78 | **0.82** | **0.82** | **0.82** |
| Low vegetation (<1 m) | 0.37 | 0.77 | 0.71 | **0.80** | **0.80** | 0.77 | 0.77 | 0.77 |
| Medium vegetation (1–7 m) | 0.34 | 0.67 | 0.62 | **0.69** | 0.67 | 0.67 | 0.67 | 0.67 |
| High vegetation deciduous (>7 m) | 0.29 | 0.61 | 0.59 | **0.63** | 0.60 | 0.62 | 0.62 | 0.62 |
| High vegetation coniferous (>7 m) | 0.36 | 0.72 | 0.67 | **0.73** | 0.68 | **0.73** | **0.73** | **0.73** |
| Bare soil | 0.49 | 0.63 | 0.71 | 0.74 | 0.66 | **0.75** | 0.74 | 0.74 |
| Inland waters | 0.81 | 0.89 | 0.92 | **0.97** | **0.97** | **0.97** | **0.97** | **0.97** |
| Shadow | 0.70 | 0.79 | 0.89 | **0.90** | **0.90** | **0.90** | **0.90** | **0.90** |

While satisfactory F-scores were obtained for specific classes such as 'buildings', 'asphalt surfaces', or 'water bodies', the accuracy is quite low for the other classes. It is also interesting to note that SVM and Rpart outperformed RF for specific classes in Ouagadougou ('dry vegetation' and 'mixed bare soil/vegetation', respectively).

The analysis of individual classifiers' confusion matrices (see Tables 4 and 5) revealed that, for both case studies, confusions occurred mainly between the different vegetation classes (46% and 61% of the whole confusions in Ouagadougou and Liège, respectively). In Ouagadougou, confusion also appeared between the bare soils classes (Brown/red bare soils; White/grey bare soils) and asphalt surfaces, shown in Table 4. Thanks to the hierarchical design of the legend, those confusions were greatly reduced when aggregating the second level classes to reach the first level of the legend. For this level, the overall accuracy is 93% for both case studies when considering the best performing voting scheme, i.e., the Simple Weighted Vote (SWV), shown in Table 2.

**Table 4.** Confusion matrix for the Simple Weighted Vote on Ouagadougou, Burkina Faso. Values are given as a percentage of the reference test set (column-based normalization). Diagonal values correspond to the producer accuracy. BU: Buildings, SW: Swimming pools, AS: Asphalt surfaces, RBS: Brown/red bare soil, GBS: White/grey bare soil, TR: Tree, MBV: Mixed bare soil/vegetation, DV: Dry vegetation, OV: Other vegetation, WB: Water bodies, SH: Shadow.

| | | **Reference** | | | | | | | | | | |
|---|---|---|---|---|---|---|---|---|---|---|---|---|
| | **L2 Classes** | **BU** | **SW** | **AS** | **RBS** | **GBS** | **TR** | **MBV** | **DV** | **OV** | **WB** | **SH** |
| **Simple Weighted Vote (SWV)** | BU | 97.7 | 0 | 0 | 0 | 6.67 | 0 | 0 | 0 | 0 | 9.68 | 0 |
| | SW | 0 | 96.8 | 0 | 0 | 0 | 0 | 0 | 0 | 0 | 0 | 0 |
| | AS | 0 | 0 | 90 | 11.9 | 0 | 0 | 0 | 9.38 | 0 | 0 | 0 |
| | RBS | 0 | 0 | 3.33 | 85.7 | 36.7 | 0 | 6.25 | 0 | 0 | 3.23 | 0 |
| | GBS | 0 | 0 | 0 | 0 | 53.3 | 0 | 0 | 0 | 0 | 0 | 0 |
| | TR | 0 | 0 | 0 | 0 | 0 | 90.6 | 0 | 3.13 | 19.4 | 0 | 0 |
| | MBV | 2.33 | 0 | 0 | 2.38 | 3.33 | 0 | 50 | 12.5 | 0 | 0 | 0 |
| | DV | 0 | 0 | 0 | 0 | 0 | 0 | 40.6 | 65.6 | 2.78 | 0 | 0 |
| | OV | 0 | 0 | 0 | 0 | 0 | 9.38 | 3.13 | 6.25 | 77.8 | 3.23 | 3.33 |
| | WB | 0 | 0 | 6.67 | 0 | 0 | 0 | 0 | 3.13 | 0 | 80.6 | 0 |
| | SH | 0 | 3.23 | 0 | 0 | 0 | 0 | 0 | 0 | 0 | 3.23 | 96.7 |

Despite the combination of individual predictions, majority votes do not perform better than the best individual classifier for the classes with high confusion, i.e., vegetation and bare soil classes. Conversely, the accuracy of other classes was improved by the votes. For example, it can be observed in Table 3 that the classes of 'buildings' and 'bare soil' benefit from the votes in Liège. The improvement resulting from the vote is more noticeable for the 'other vegetation' class in Ouagadougou, where the best-performing individual classifier (RF) reached an F-score of 0.77 while weighted votes (BWWV, QBWWV) reached 0.81. These balanced results, with votes outperforming individual classifiers for some classes and underperforming for others are consistent with the previous research [9]. The current method of attributing weight during the vote, using the overall accuracy of individual classifiers, is quite simple. Other methods might be implemented in order to take into account the performance of each classifier for specific classes (see [54] for a review of decision level fusion methods used in remote sensing).

Regarding segmentation, the use of an optimized segmentation parameter provided by i.segment.uspo achieved satisfactory results in our case studies. Even if the quantitative assessment of the segmentation's quality is not in the scope of this paper, a visual check of Figure 5 reveals that the images are segmented into meaningful objects.

Even though a rigorous comparison of the results using different datasets and training/test sets could not be performed, the results obtained by applying the proposed semi-automated processing chain on two very different urban contexts are similar and attest the transportability of the proposed framework.

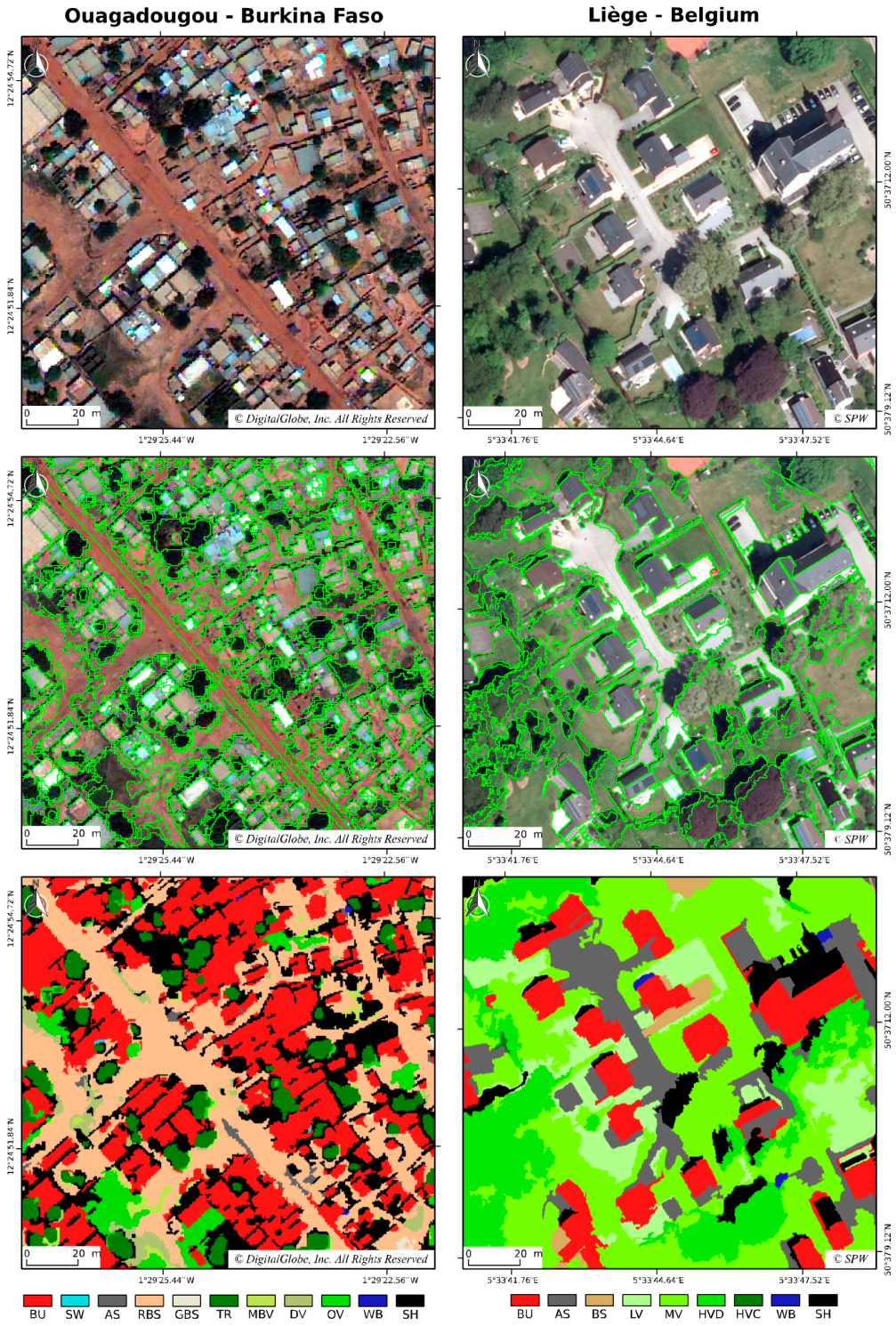


**Figure 5.** True color composite (top), results of segmentation with Unsupervised Segmentation Parameter Optimization USPO (middle), classification at the second level with SWV vote (bottom) on a subset for each case study. BU: Buildings, SW: Swimming pools, AS: Asphalt surfaces, BS: Bare soil, RBS: Brown/red bare soil, GBS: White/grey bare soil, TR: Tree, MBV: Mixed bare soil/vegetation, DV: Dry vegetation, LV: Low vegetation, MV: Medium vegetation, HVD: High vegetation deciduous, HVD: High vegetation coniferous, OV: Other vegetation, WB: Water bodies, SH: Shadow.

**Table 5.** Confusion matrix for the Simple Weighted Vote on Liège, Belgium. Values are given as a percentage of the reference test set (column-based normalization). Diagonal values correspond to the producer accuracy. BU: Buildings, AS: Asphalt surfaces, LV: Low vegetation, MV: Medium vegetation, HVD: High vegetation deciduous, HVD: High vegetation coniferous, BS: Bare soil, WB: Water bodies, SH: Shadow.

| | | Reference | | | | | | | | |
|---|---|---|---|---|---|---|---|---|---|---|
| | **L2 Classes** | **BU** | **AS** | **LV** | **MV** | **HVD** | **HVC** | **BS** | **WB** | **SH** |
| **Simple Weighted Vote (SWV)** | BU | 89.2 | 1.67 | 0 | 0 | 0 | 0 | 0 | 0 | 0 |
| | AS | 5.41 | 80 | 0 | 0 | 0 | 0 | 16.7 | 0 | 0 |
| | LV | 0 | 0 | 71.7 | 8.33 | 0 | 0 | 7.14 | 0 | 0 |
| | MV | 0 | 0 | 28.3 | 64.6 | 0 | 0 | 2.38 | 0 | 0 |
| | HVD | 0 | 0 | 0 | 25 | 75 | 27.9 | 0 | 0 | 0 |
| | HVC | 0 | 0 | 0 | 2.08 | 22.2 | 72.1 | 0 | 0 | 5.13 |
| | BS | 2.7 | 15 | 0 | 0 | 0 | 0 | 73.8 | 0 | 0 |
| | WB | 0 | 0 | 0 | 0 | 0 | 0 | 0 | 94.6 | 0 |
| | SH | 2.7 | 3.33 | 0 | 0 | 2.78 | 0 | 0 | 5.41 | 94.9 |

## 5. Discussion and Perspectives

The entire semi-automated processing chain for urban OBIA classification, relying on open-source solutions, is available on a dedicated Github repository (https://github.com/tgrippa/Opensource_OBIA_processing_chain). As it is shared under the CC-BY 4.0 Creative Common Licence, anyone interested can use and/or adapt it to match different project-specific needs, by integrating additional steps (e.g., automated image pre-processing, computation of spectral or textural indices, automated sampling based on existing reference geodatasets).

Other frameworks relying on open-source solutions have already been proposed for the extraction of valuable geographical information from remote sensing data [53,55–58]. Some of them are distributed as a plug-in or a toolbox for existing geographical information systems, mainly for QGIS [55,56,58], and present the advantage of providing a comforting environment for users, making their use quite simple.

For most of them, pixel-based image classification is their core task. However, some include basic object-based capabilities. For example, in the context of a pixel-based supervised classification, the Semi Automated Classification Plug-in (SACP) [55] enables the user to save time when creating regions of interest (ROI), as these are created using a region growing segmentation, starting from pixel seeds defined by the user. Another example is the 'Twinned Object and Pixel-based Automated Classification chain' (TWOPAC) plug-in that enables performing classification using object-based derived features, but considers the segmentation as well as the object features computation as pre-processing steps to be performed outside of the tool [59].

After our investigations, we found only one existing open-source framework that allowed us to perform a complete object-based image analysis from segmentation to classification [57]. It relies fully on Python libraries and is a highly modular solution for object-based image analysis, as it can be linked with a lot of existing functions and software. Unfortunately, it could be very difficult for researchers without strong programming skills to handle this kind of framework.

In this paper, we propose a contribution toward the development of a fully automated processing chain for object-based image analysis. The advantage of the framework we propose is that it relies on the open-source software GRASS GIS, which has had recent enhancements for object-based image analysis, enabling the development of more automated procedures. As GRASS GIS offers a graphical user interface (GUI), the different commands can be tested in the GUI during the script development stage, and can then be included in the processing chain thanks to the GRASS Python scripting library. Another key advantage of GRASS GIS is its users' and developers' community, which is usually helpful and responsive.

Even though enhancements are desirable, the semi-automated processing chain currently achieved interesting results, as shown through the two case studies presented in this paper. Perspectives on further developments are discussed below in this section.

The generation of training and validation samples still requires strong manual expert intervention. This remains a challenge to be overcome by future research looking for automation, especially when highly accurate reference geodatabases are not available. In that case, alternative data such as OpenStreetMap data could be used, but their quality is often inconsistent and they should therefore be assessed prior to any automated use. Issues of co-registration with VHR imagery might also arise when using such data sets. The practical implementation of an active learning strategy [60], which could help in building efficient training sets more rapidly, is currently under development in GRASS GIS.

In order to improve the segmentation and hence the resulting classification, we intend to implement a multi-scale segmentation strategy, which has proved its ability to enhance the classification performance in a previous study [31]. Segmentation strategies using superpixels could also be investigated for further enhancements, since a new add-on [61] implementing SLIC superpixels method has been developed recently. This approach has provided interesting results in recent research [42].

Another improvement method concerns the features used as inputs in the classification process. Currently, only relatively simple object statistics are used. Band ratios and several textural indices will be added. They will be automatically computed and submitted to a feature selection procedure for those classifiers that do not include feature selection inherently.

During parameter tuning, spatial autocorrelation between the training and test sets created in cross-validation can lead to undetected overfitting and an overvaluation of the accuracy [62,63]. To reduce this potential bias and obtain better bootstrap error estimates, we will investigate the possibility of implementing spatial cross-validation, i.e., a spatially-constrained partitioning of the training and test sets created in cross-validation [64]. In addition, more classifiers will also be included.

Moreover, we will explore the possibility of implementing other strategies for the combination of multiple classifiers (see [48,54,65] for a review). The voting systems currently used to combine predictions are based on weights derived from the overall accuracy or kappa of individual classifiers, but in some cases, the non-best classifiers outperformed the best classifier's performance for specific classes (see Table 3).

Since the performance of different LULC mapping methods is currently being assessed in the SmartPop project, our open-source semi-automated approach is being compared to a rule-based approach, developed in a proprietary software. The latter integrates existing ancillary vector layers (buildings, roads, rails, and water bodies) in the segmentation. Constrained segmentation using ancillary vector layers in GRASS GIS will be investigated in future studies.

In the near future, the processing chain will be tested on different datasets and/or cities. For the MAUPP project, Synthetic Aperture Radar (SAR) data will be added as an input in order to improve the accuracy and the chain will be applied to Ouagadougou (Burkina Faso), Dakar, and Saint-Louis (Senegal). For the SmartPop project, Pléiades imagery will be used instead of orthophotos in order to assess the comparative advantage of each dataset. Thereafter, the efficiency of the processing chain will be tested for the automated processing of a very large area (i.e., the Walloon Region in Belgium), taking advantage of the parallel computing options in the different modules.

## 6. Conclusions

In times when the reproducibility of research and the sharing of existing solutions is high on the discussion agenda, the development of free and open-source solutions becomes paramount. In this paper, a semi-automated processing chain for urban object-based classification is proposed as a contribution towards the development of a transparent and open-source fully automated processing chain for urban land-use/land-cover mapping from earth observation data. This processing chain, relying on existing open-source geospatial software, is very adaptable and transportable to similar datasets. It proved its ability of being quickly customizable in order to match the requirements of

different projects, with very different urban morphologies and different datasets. Freely available for anyone interested, it should be seen as a framework to be reused and enhanced for further studies. The results achieved on our case studies are very interesting, taking into account the complexity of the urban environments and the detail of the legend.

**Acknowledgments:** This work was funded by the Belgian Federal Science Policy Office (BELSPO) (Research Program for Earth Observation STEREO III, contract SR/00/304—as part of the MAUPP project—http://maupp.ulb.ac.be) and by the Moerman research program of ISSeP (SmartPop project—http://www.issep.be/smartpop). Service Public de Wallonie (SPW) is acknowledged for providing aerial orthophotos, LiDAR, and ancillary vector geodatabases (LIC 160128-1348, all rights reserved to SPW). WorldView3 data is copyrighted under the mention "©COPYRIGHT 2015 DigitalGlobe, Inc., Longmont CO USA 80503. DigitalGlobe and the DigitalGlobe logos are trademarks of DigitalGlobe, Inc. The use and/or dissemination of this data and/or of any product in any way derived there from are restricted. Unauthorized use and/or dissemination is prohibited". OpenStreetMap data are copyrighted under the mention "©OpenStreetMap contributors, CC BY-SA". The authors greatly thank the reviewers for their relevant comments which helped to improve this manuscript.

**Author Contributions:** Taïs Grippa, Moritz Lennert, Benjamin Beaumont, and Sabine Vanhuysse wrote the manuscript. Taïs Grippa is the main author who developed the processing chain and applied it on both case studies. Moritz Lennert implemented the new GRASS GIS add-ons and provided precious technical support. Benjamin Beaumont and Sabine Vanhuysse created the training and test sets. Nathalie Stephenne and Eléonore Wolff contributed actively to the revisions of the manuscript.

**Conflicts of Interest:** The authors declare no conflict of interest.

## Appendix

**Table A1.** Performance evaluation of the level-2 classification of Ouagadougou, Burkina Faso. Producer accuracy (PA) and User accuracy (UA) for each class of the second level of classification. For each line, the highest value is in bold. BU: Buildings. SW: Swimming pools. AS: Asphalt surfaces. RBS: Brown/red bare soil. GBS: White/grey bare soil. TR: Trees. MBV: Mixed bare soil/vegetation. DV: Dry vegetation. OV: Other vegetation. WB: Water bodies. SH: Shadow.

| | | Individual Classifiers | | | | Votes | | | |
|---|---|---|---|---|---|---|---|---|---|
| **Level 2 Classes** | **Accuracy** | **kNN** | **Rpart** | **SVMradial** | **RF** | **SMV** | **SWV** | **BWWV** | **QBWWV** |
| BU | PA: | 79.1% | 79.1% | **100.0%** | 95.3% | 97.7% | 97.7% | 95.3% | 95.3% |
| | UA: | 51.5% | 77.3% | 64.2% | **91.1%** | 76.4% | 89.4% | 89.1% | 89.1% |
| SW | PA: | 83.9% | 87.1% | 93.5% | **96.8%** | **96.8%** | **96.8%** | **96.8%** | **96.8%** |
| | UA: | **100.0%** | 96.4% | **100.0%** | **100.0%** | **100.0%** | **100.0%** | **100.0%** | **100.0%** |
| AS | PA: | 56.7% | 83.3% | 56.7% | **90.0%** | 86.7% | **90.0%** | **90.0%** | **90.0%** |
| | UA: | 44.7% | 48.1% | 53.1% | **77.1%** | 74.3% | **77.1%** | **77.1%** | **77.1%** |
| RBS | PA: | 57.1% | 83.3% | 64.3% | **85.7%** | **85.7%** | **85.7%** | **85.7%** | **85.7%** |
| | UA: | 47.1% | 68.6% | 65.9% | **72.0%** | 69.2% | 70.6% | 70.6% | 70.6% |
| GBS | PA: | 26.7% | **56.7%** | **56.7%** | **56.7%** | 50.0% | 53.3% | 53.3% | 53.3% |
| | UA: | 25.0% | 89.5% | 94.4% | **100.0%** | 93.8% | **100.0%** | **100.0%** | **100.0%** |
| TR | PA: | 50.0% | **96.9%** | 81.3% | 90.6% | 90.6% | 90.6% | 90.6% | 90.6% |
| | UA: | 69.6% | 72.1% | **83.9%** | 80.6% | 74.4% | 78.4% | 80.6% | 80.6% |
| MBV | PA: | 28.1% | **62.5%** | 46.9% | 46.9% | 50.0% | 50.0% | 50.0% | 50.0% |
| | UA: | 30.0% | 60.6% | **78.9%** | 68.2% | 66.7% | 69.6% | 69.6% | 69.6% |
| DV | PA: | 6.3% | 46.9% | **71.9%** | 62.5% | 65.6% | 65.6% | 65.6% | 65.6% |
| | UA: | 12.5% | 50.0% | 59.0% | 58.8% | **61.8%** | 60.0% | 58.3% | 58.3% |
| OV | PA: | 63.9% | 61.1% | 72.2% | **80.6%** | 69.4% | 77.8% | **80.6%** | **80.6%** |
| | UA: | 48.9% | **84.6%** | 74.3% | 74.4% | 80.6% | 77.8% | 80.6% | 80.6% |
| WB | PA: | 12.9% | 64.5% | 80.6% | **83.9%** | 64.5% | 80.6% | 80.6% | 80.6% |
| | UA: | 36.4% | 87.0% | 89.3% | 89.7% | **90.9%** | 89.3% | 89.3% | 89.3% |
| SH | PA: | 73.3% | 60.0% | 93.3% | **96.7%** | **96.7%** | **96.7%** | **96.7%** | **96.7%** |
| | UA: | 75.9% | 90.0% | 93.3% | 90.6% | **93.5%** | **93.5%** | 90.6% | 90.6% |
| OA | | 50,1% | 71.5% | 74.8% | **81.0%** | 78.3% | **81.0%** | **81.0%** | **81.0%** |
| Kappa | | 0.45 | 0.69 | 0.72 | **0.79** | 0.76 | **0.79** | **0.79** | **0.79** |

**Table A2.** Performance evaluation of the level-2 classification of Liège, Belgium. Producer accuracy (PA) and User accuracy (UA) for each class of the second level of classification. For each line, the highest value is in bold. BU: Buildings. AS: Asphalt surfaces. LV: Low vegetation (<1 m). MV: Medium vegetation (1–7 m). HVD: High vegetation deciduous (>7 m). HVC: High vegetation coniferous (>7 m). BS: Bare soil. WB: Water bodies. SH: Shadow.

| | | Individual Classifiers | | | | Votes | | | |
|---|---|---|---|---|---|---|---|---|---|
| **Level 2 Classes** | **Accuracy** | **kNN** | **Rpart** | **SVMradial** | **RF** | **SMV** | **SWV** | **BWWV** | **QBWWV** |
| BU | PA: | 48.6% | 89.2% | 81.1% | 86.5% | **91.9%** | 89.2% | 86.5% | 86.5% |
| | UA: | 52.9% | 94.3% | 85.7% | 97.0% | 94.4% | **97.1%** | 97.0% | 97.0% |
| AS | PA: | 78.3% | 70.0% | 76.7% | 78.3% | **81.7%** | 80.0% | 80.0% | 80.0% |
| | UA: | 54.7% | 72.4% | 76.7% | **85.5%** | 75.4% | 84.2% | 84.2% | 84.2% |
| LV | PA: | 32.6% | 69.6% | 65.2% | **78.3%** | **78.3%** | 71.7% | 71.7% | 71.7% |
| | UA: | 42.9% | **86.5%** | 76.9% | 81.8% | 81.8% | 82.5% | 82.5% | 82.5% |
| MV | PA: | 33.3% | **68.8%** | 58.3% | 64.6% | 62.5% | 64.6% | 64.6% | 64.6% |
| | UA: | 34.8% | 66.0% | 66.7% | **73.8%** | 73.2% | 68.9% | 68.9% | 68.9% |
| HVD | PA: | 33.3% | 72.2% | **75.0%** | **75.0%** | **75.0%** | **75.0%** | **75.0%** | **75.0%** |
| | UA: | 25.0% | 53.1% | 49.1% | **54.0%** | 50.0% | 52.9% | 52.9% | 52.9% |
| HVC | PA: | 34.9% | **74.4%** | 62.8% | 72.1% | 65.1% | 72.1% | 72.1% | 72.1% |
| | UA: | 37.5% | 69.6% | 71.1% | **73.8%** | 71.8% | **73.8%** | **73.8%** | **73.8%** |
| BS | PA: | 40.5% | 61.9% | 69.0% | **76.2%** | 57.1% | 73.8% | 73.8% | 73.8% |
| | UA: | 60.7% | 65.0% | 72.5% | 72.7% | **77.4%** | 75.6% | 73.8% | 73.8% |
| WB | PA: | 73.0% | **97.3%** | 91.9% | 94.6% | 94.6% | 94.6% | 94.6% | 94.6% |
| | UA: | 90.0% | 81.8% | 91.9% | **100.0%** | **100.0%** | **100.0%** | **100.0%** | **100.0%** |
| SH | PA: | 71.8% | 69.2% | 92.3% | **94.9%** | **94.9%** | **94.9%** | **94.9%** | **94.9%** |
| | UA: | 68.3% | **93.1%** | 85.7% | 86.0% | 86.0% | 86.0% | 86.0% | 86.0% |
| OA | | 50.3% | 74.0% | 74.0% | **79.4%** | 77.3% | 78.9% | 78.6% | 78.6% |
| Kappa | | 0.44 | 0.71 | 0.71 | **0.77** | 0.74 | 0.76 | 0.76 | 0.76 |

## References


1. Zhang, H.; Fritts, J.E.; Goldman, S.A. Image segmentation evaluation: A survey of unsupervised methods. *Comput. Vis. Image Underst.* **2008**, *110*, 260–280. [CrossRef]
2. Blaschke, T. Object based image analysis for remote sensing. *ISPRS J. Photogramm. Remote Sens.* **2010**, *65*, 2–16. [CrossRef]
3. Salehi, B.; Zhang, Y.; Zhong, M.; Dey, V. Object-Based Classification of Urban Areas Using VHR Imagery and Height Points Ancillary Data. *Remote Sens.* **2012**, *4*, 2256–2276. [CrossRef]
4. O'Neil-Dunne, J.P.M.; MacFaden, S.W.; Royar, A.R.; Pelletier, K.C. An object-based system for LiDAR data fusion and feature extraction. *Geocarto Int.* **2013**, *28*, 227–242. [CrossRef]
5. Kohli, D.; Warwadekar, P.; Kerle, N.; Sliuzas, R.; Stein, A. Transferability of Object-Oriented Image Analysis Methods for Slum Identification. *Remote Sens.* **2013**, *5*, 4209–4228. [CrossRef]
6. Belgiu, M.; Drăguţ, L.; Strobl, J. Quantitative evaluation of variations in rule-based classifications of land cover in urban neighbourhoods using WorldView-2 imagery. *ISPRS J. Photogramm. Remote Sens.* **2014**, *87*, 205–215. [CrossRef] [PubMed]
7. Mountrakis, G.; Im, J.; Ogole, C. Support vector machines in remote sensing: A review. *ISPRS J. Photogramm. Remote Sens.* **2011**, *66*, 247–259. [CrossRef]
8. Belgiu, M.; Drăgut, L. Random forest in remote sensing: A review of applications and future directions. *ISPRS J. Photogramm. Remote Sens.* **2016**, *114*, 24–31. [CrossRef]
9. Moreno-Seco, F.; Inesta, J.M.; De León, P.J.P.; Micó, L. Comparison of classifier fusion methods for classification in pattern recognition tasks. In *Joint IAPR International Workshops on Statistical Techniques in Pattern Recognition (SPR) and Structural and Syntactic Pattern Recognition*; Springer: Berlin/Heidelberg, Germany, 2006; pp. 705–713.
10. Drăguţ, L.; Csillik, O.; Eisank, C.; Tiede, D. Automated parameterisation for multi-scale image segmentation on multiple layers. *ISPRS J. Photogramm. Remote Sens.* **2014**, *88*, 119–127. [CrossRef] [PubMed]

11. Skaggs, T.H.; Young, M.H.; Vrugt, J.A. Reproducible Research in Vadose Zone Sciences. *Vadose Zone J.* **2015**, *14*. [CrossRef]
12. Walsham, G.; Sahay, S. Research on information systems in developing countries: Current landscape and future prospects. *Inf. Technol. Dev.* **2006**, *12*, 7–24. [CrossRef]
13. Haack, B.; Ryerson, R. Improving remote sensing research and education in developing countries: Approaches and recommendations. *Int. J. Appl. Earth Obs. Geoinf.* **2016**, *45*, 77–83. [CrossRef]
14. Grippa, T.; Lennert, M.; Beaumont, B.; Vanhuysse, S.; Stephenne, N.; Wolff, E. An open-source semi-automated processing chain for urban obia classification. In Proceedings of the GEOBIA 2016: Solutions and Synergies, Enschede, The Netherlands, 14–16 September 2016.
15. GRASS Development Team. Geographic Resources Analysis Support System (GRASS). Open Source Geospatial Foundation: Chicago, IL, USA, 2015. Available online: https://grass.osgeo.org/ (accessed on 13 June 2016).
16. R Development Core Team. *R: A Language and Environment for Statistical Computing*; R Foundation for Statistical Computing: Vienna, Austria, 2008.
17. Walker, J.S.; Blaschke, T. Object-based land-cover classification for the Phoenix metropolitan area: Optimization vs. transportability. *Int. J. Remote Sens.* **2008**, *29*, 2021–2040. [CrossRef]
18. Neteler, M.; Bowman, M.H.; Landa, M.; Metz, M. GRASS GIS: A multi-purpose open source GIS. *Environ. Model. Softw.* **2012**, *31*, 124–130. [CrossRef]
19. Neteler, M.; Beaudette, D.E.; Cavallini, P.; Lami, L.; Cepicky, J. Grass gis. In *Open Source Approaches in Spatial Data Handling*; Springer: Berlin/Heidelberg, Germany, 2008; pp. 171–199.
20. Hofierka, J.; Kaňuk, J. Assessment of photovoltaic potential in urban areas using open-source solar radiation tools. *Renew. Energy* **2009**, *34*, 2206–2214. [CrossRef]
21. Frigeri, A.; Hare, T.; Neteler, M.; Coradini, A.; Federico, C.; Orosei, R. A working environment for digital planetary data processing and mapping using ISIS and GRASS GIS. *Planet. Space Sci.* **2011**, *59*, 1265–1272. [CrossRef]
22. Sofina, N.; Ehlers, M. Object-based change detection using highresolution remotely sensed data and gis. In Proceedings of the International Archives Photogrammetry, Remote Sensing and Spatial Information Sciences-XXII ISPRS Congress, Melbourne, Australia, 25 August–1 September 2012; Volume 39, p. B7.
23. Rocchini, D.; Delucchi, L.; Bacaro, G.; Cavallini, P.; Feilhauer, H.; Foody, G.M.; He, K.S.; Nagendra, H.; Porta, C.; Ricotta, C.; et al. Calculating landscape diversity with information-theory based indices: A GRASS GIS solution. *Ecol. Inform.* **2013**, *17*, 82–93. [CrossRef]
24. Do, T.H.; Raghavan, V.; Vinayaraj, P.; Truong, X.L.; Yonezawa, G. Pixel Based and Object Based Fuzzy LULC Classification using GRASS GIS and RapidEye Imagery of Lao Cai Area, Vietnam. *Geoinformatics* **2016**, *27*, 104–105.
25. Petrasova, A.; Mitasova, H.; Petras, V.; Jeziorska, J. Fusion of high-resolution DEMs for water flow modeling. *Open Geospatial Data Softw. Stand.* **2017**, *2*, 6. [CrossRef]
26. Kluyver, T.; Ragan-Kelley, B.; Pérez, F.; Granger, B.; Bussonnier, M.; Frederic, J.; Kelley, K.; Hamrick, J.; Grout, J.; Corlay, S.; et al. Jupyter Notebooks—A publishing format for reproducible computational workflows. In *Positioning and Power in Academic Publishing: Players, Agents and Agendas*; IOS Press: Amsterdam, The Netherlands, 2016; pp. 87–90.
27. Lennert, M. A Complete Toolchain for Object-Based Image Analysis with GRASS GIS 2016. Available online: http://video.foss4g.org/foss4g2016/videos/index.html (accessed on 25 November 2016).
28. Momsen, E.; Metz, M.; GRASS Development Team Module i.segment. *Geographic Resources Analysis Support System (GRASS) Software, Version 7.3*; Open Source Geospatial Foundation: Chicago, IL, USA, 2015. Available online: https://grass.osgeo.org/grass73/manuals/i.segment.html (accessed on 25 November 2016).
29. Räsänen, A.; Rusanen, A.; Kuitunen, M.; Lensu, A. What makes segmentation good? A case study in boreal forest habitat mapping. *Int. J. Remote Sens.* **2013**, *34*, 8603–8627. [CrossRef]
30. Zhang, Y.J. A survey on evaluation methods for image segmentation. *Pattern Recognit.* **1996**, *29*, 1335–1346. [CrossRef]
31. Johnson, B.A.; Bragais, M.; Endo, I.; Magcale-Macandog, D.B.; Macandog, P.B.M. Image Segmentation Parameter Optimization Considering Within- and Between-Segment Heterogeneity at Multiple Scale Levels: Test Case for Mapping Residential Areas Using Landsat Imagery. *ISPRS Int. J. Geo-Inf.* **2015**, *4*, 2292–2305. [CrossRef]

32. Belgiu, M.; Drăgut, L. Comparing supervised and unsupervised multiresolution segmentation approaches for extracting buildings from very high resolution imagery. *ISPRS J. Photogramm. Remote Sens.* **2014**, *96*, 67–75. [CrossRef] [PubMed]
33. Haralick, R.M.; Shapiro, L.G. Image segmentation techniques. *Comput. Vis. Graph. Image Process.* **1985**, *29*, 100–132. [CrossRef]
34. Lennert, M.; GRASS Development Team Addon i.segment.uspo. *Geographic Resources Analysis Support System (GRASS) Software, Version 7.3*; Open Source Geospatial Foundation: Chicago, IL, USA, 2016. Available online: https://grass.osgeo.org/grass70/manuals/addons/i.segment.uspo.html (accessed on 25 November 2016).
35. Espindola, G.M.; Camara, G.; Reis, I.A.; Bins, L.S.; Monteiro, A.M. Parameter selection for region-growing image segmentation algorithms using spatial autocorrelation. *Int. J. Remote Sens.* **2006**, *27*, 3035–3040. [CrossRef]
36. Moran, P.A.P. Notes on Continuous Stochastic Phenomena. *Biometrika* **1950**, *37*, 17–23. [CrossRef] [PubMed]
37. Geary, R.C. The Contiguity Ratio and Statistical Mapping. *Inc. Stat.* **1954**, *5*, 115–145. [CrossRef]
38. Grybas, H.; Melendy, L.; Congalton, R.G. A comparison of unsupervised segmentation parameter optimization approaches using moderate- and high-resolution imagery. *GISci. Remote Sens.* **2017**, *0*, 1–19. [CrossRef]
39. Carleer, A.P.; Debeir, O.; Wolff, E. Assessment of very high spatial resolution satellite image segmentations. *Photogramm. Eng. Remote Sens.* **2005**, *71*, 1285–1294. [CrossRef]
40. Johnson, B.; Xie, Z. Unsupervised image segmentation evaluation and refinement using a multi-scale approach. *ISPRS J. Photogramm. Remote Sens.* **2011**, *66*, 473–483. [CrossRef]
41. Schiewe, J. Segmentation of high-resolution remotely sensed data-concepts, applications and problems. *Int. Arch. Photogramm. Remote Sens. Spat. Inf. Sci.* **2002**, *34*, 380–385.
42. Csillik, O. Fast Segmentation and Classification of Very High Resolution Remote Sensing Data Using SLIC Superpixels. *Remote Sens.* **2017**, *9*, 243. [CrossRef]
43. Cánovas-García, F.; Alonso-Sarría, F. A local approach to optimize the scale parameter in multiresolution segmentation for multispectral imagery. *Geocarto Int.* **2015**, *30*, 937–961. [CrossRef]
44. Lennert, M.; GRASS Development Team Addon i.segment.stats. *Geographic Resources Analysis Support System (GRASS) Software, Version 7.3*; Open Source Geospatial Foundation: Chicago, IL, USA, 2016. Available online: https://grass.osgeo.org/grass70/manuals/addons/i.segment.stats.html (accessed on 25 November 2016).
45. Metz, M.; Lennert, M.; GRASS Development Team Addon r.object.geometry. *Geographic Resources Analysis Support System (GRASS) Software, Version 7.3*; Open Source Geospatial Foundation: Chicago, IL, USA, 2016. Available online: https://grass.osgeo.org/grass72/manuals/addons/r.object.geometry.html (accessed on 25 November 2016).
46. Lennert, M.; GRASS Development Team Addon v.class.mlR. *Geographic Resources Analysis Support System (GRASS) Software, Version 7.3*; Open Source Geospatial Foundation: Chicago, IL, USA, 2016. Available online: https://grass.osgeo.org/grass70/manuals/addons/v.class.mlR.html (accessed on 25 November 2016).
47. Kuhn, M. Building Predictive Models in R Using the caret Package. *J. Stat. Softw.* **2008**, *28*, 115571. [CrossRef]
48. Du, P.; Xia, J.; Zhang, W.; Tan, K.; Liu, Y.; Liu, S. Multiple Classifier System for Remote Sensing Image Classification: A Review. *Sensors* **2012**, *12*, 4764–4792. [CrossRef] [PubMed]
49. Neteler, M.; Mitasova, H. Open Source GIS—A GRASS GIS Approach. Available online: http://link.springer.com.ezproxy.ulb.ac.be/book/10.1007%2F978-0-387-68574-8 (accessed 2 November 2014).
50. Folleco, A.; Khoshgoftaar, T.M.; Hulse, J.V.; Bullard, L. Identifying Learners Robust to Low Quality Data. In Proceedings of the 2008 IEEE International Conference on Information Reuse and Integration, Las Vegas, NV, USA, 13–15 July 2008; pp. 190–195.
51. Foody, G.; Pal, M.; Rocchini, D.; Garzon-Lopez, C.; Bastin, L. The Sensitivity of Mapping Methods to Reference Data Quality: Training Supervised Image Classifications with Imperfect Reference Data. *ISPRS Int. J. Geo-Inf.* **2016**, *5*, 199. [CrossRef]
52. Sokolova, M.; Lapalme, G. A systematic analysis of performance measures for classification tasks. *Inf. Process. Manag.* **2009**, *45*, 427–437. [CrossRef]
53. Inglada, J.; Vincent, A.; Arias, M.; Tardy, B.; Morin, D.; Rodes, I. Operational High Resolution Land Cover Map Production at the Country Scale Using Satellite Image Time Series. *Remote Sens.* **2017**, *9*, 95. [CrossRef]

54. Zeng, Y.; Zhang, J.; Van Genderen, J.L. Comparison and Analysis of Remote Sensing Data Fusion Techniques at Feature and Decision Levels. In Proceedings of the ISPRS Commission VII Mid-term Symposium Remote Sensing: From Pixels to Processes, Enschede, The Netherlands, 8–11 May 2006.
55. Congedo, L. *Semi-Automatic Classification Plugin User Manual, Release 5.3.6.1*; RoMEO: Paterson, NJ, USA, 2017.
56. Huth, J.; Kuenzer, C.; Wehrmann, T.; Gebhardt, S.; Tuan, V.Q.; Dech, S. Land Cover and Land Use Classification with TWOPAC: Towards Automated Processing for Pixel- and Object-Based Image Classification. *Remote Sens.* **2012**, *4*, 2530–2553. [CrossRef]
57. Clewley, D.; Bunting, P.; Shepherd, J.; Gillingham, S.; Flood, N.; Dymond, J.; Lucas, R.; Armston, J.; Moghaddam, M. A Python-Based Open Source System for Geographic Object-Based Image Analysis (GEOBIA) Utilizing Raster Attribute Tables. *Remote Sens.* **2014**, *6*, 6111–6135. [CrossRef]
58. Guzinski, R.; Kass, S.; Huber, S.; Bauer-Gottwein, P.; Jensen, I.; Naeimi, V.; Doubkova, M.; Walli, A.; Tottrup, C. Enabling the Use of Earth Observation Data for Integrated Water Resource Management in Africa with the Water Observation and Information System. *Remote Sens.* **2014**, *6*, 7819–7839. [CrossRef]
59. Huth, J.; Kuenzer, C. *TWOPAC Handbook: Twinned Object and Pixel-Based Automated Classification Chain*; RoMEO: Paterson, NJ, USA, 2013.
60. Tuia, D.; Volpi, M.; Copa, L.; Kanevski, M.; Munoz-Mari, J. A Survey of Active Learning Algorithms for Supervised Remote Sensing Image Classification. *IEEE J. Sel. Top. Signal Process.* **2011**, *5*, 606–617. [CrossRef]
61. Kanavath, R.; Metz, M.; GRASS Development Team Addon i.superpixels.slic. *Geographic Resources Analysis Support System (GRASS) Software, Version 7.3*; Open Source Geospatial Foundation: Chicago, IL, USA, 2017. Available online: https://grass.osgeo.org/grass72/manuals/addons/i.superpixels.slic.html (accessed on 20 February 2017).
62. Mannel, S.; Price, M.; Hua, D. Impact of reference datasets and autocorrelation on classification accuracy. *Int. J. Remote Sens.* **2011**, *32*, 5321–5330. [CrossRef]
63. Brenning, A. Spatial Cross-Validation and Bootstrap for the Assessment of Prediction Rules in Remote Sensing: The R Package Sperrorest. In Proceedings of the 2012 IEEE International Geoscience and Remote Sensing Symposium, Munich, Germany, 22–27 July 2012; pp. 5372–5375.
64. Brenning, A.; Long, S.; Fieguth, P. Detecting rock glacier flow structures using Gabor filters and IKONOS imagery. *Remote Sens. Environ.* **2012**, *125*, 227–237. [CrossRef]
65. Lisini, G.; Dell'Acqua, F.; Trianni, G.; Gamba, P. Comparison and Combination of Multiband Classifiers for Landsat Urban Land Cover Mapping. In Proceedings of the 2005 IEEE International Geoscience and Remote Sensing Symposium, Seoul, Korea, 25–29 July 2005; Volume 4, pp. 2823–2826.


## 2.2 Adaptative optimization of segmentation parameter for handling large-scale heterogeneous urban area

**Grippa, Tais**, Stefanos Georganos, Sabine Vanhuysse, Moritz Lennert, and Eléonore Wolff. 2017. "**A Local Segmentation Parameter Optimization Approach for Mapping Heterogeneous Urban Environments Using VHR Imagery.**" In Proceedings Volume 10431, Remote Sensing Technologies and Applications in Urban Environments II. IEEE. http://doi.org/10.1117/12.2278422. Available in open-access on the ULB institutional repository.

Georganos, Stefanos, **Tais Grippa**, Moritz Lennert, Sabine Vanhuysse, Brian Johnson, and Eléonore Wolff. 2018. "**Scale Matters: Spatially Partitioned Unsupervised Segmentation Parameter Optimization for Large and Heterogeneous Satellite Images.**" Remote Sensing 10 (9): 1440. https://doi.org/10.3390/rs10091440.

# A local segmentation parameter optimization approach for mapping heterogeneous urban environments using VHR imagery

Tais Grippa*[a], Stefanos Georganos[a], Moritz Lennert[a], Sabine Vanhuysse[a], Eleonore Wolff[a]
[a] Department of Geosciences Environment and Society - Institute for Environmental Management and Land-use Planning (DGES-IGEAT), Université libre de Bruxelles, Belgium

## ABSTRACT

Mapping large heterogeneous urban areas using object-based image analysis (OBIA) remains challenging, especially with respect to the segmentation process. This could be explained both by the complex arrangement of heterogeneous land-cover classes and by the high diversity of urban patterns which can be encountered throughout the scene. In this context, using a single segmentation parameter to obtain satisfying segmentation results for the whole scene can be impossible. Nonetheless, it is possible to subdivide the whole city into smaller local zones, rather homogeneous according to their urban pattern. These zones can then be used to optimize the segmentation parameter locally, instead of using the whole image or a single representative spatial subset. This paper assesses the contribution of a local approach for the optimization of segmentation parameter compared to a global approach. Ouagadougou, located in sub-Saharan Africa, is used as case studies. First, the whole scene is segmented using a single globally optimized segmentation parameter. Second, the city is subdivided into 283 local zones, homogeneous in terms of building size and building density. Each local zone is then segmented using a locally optimized segmentation parameter. Unsupervised segmentation parameter optimization (USPO), relying on an optimization function which tends to maximize both intra-object homogeneity and inter-object heterogeneity, is used to select the segmentation parameter automatically for both approaches. Finally, a land-use/land-cover classification is performed using the Random Forest (RF) classifier. The results reveal that the local approach outperforms the global one, especially by limiting confusions between buildings and their bare-soil neighbors.

**Keywords:** Object Based Image Analysis, Unsupervised Segmentation Parameters Optimization, Local Approach, Urban Area, Land Cover Mapping

## 1. INTRODUCTION

Land-use/land-cover (LULC) maps are essential decision-making tools as they can provide a picture of the current urban configuration, enabling the deployment of appropriate policies for urban planning and management. This is especially true in the sub-Saharan African urban context where cities undergo high growth rates and decision makers usually face the scarcity of reference information.

Nowadays, the availability of very-high-resolution (VHR) remote sensing (RS) imagery is higher than ever. This allows for unprecedented capabilities for the production of spatially and thematically detailed LULC maps. VHR RS data enable mapping a large diversity of elements of the urban landscape, such as buildings, roads or trees. However, the production of such detailed maps still remains a challenging task and requires the use of appropriate image analysis techniques in order to achieve accurate results. The processing of VHR RS imagery is usually performed using object-based image analysis (OBIA) techniques. While pixel-based techniques classify each pixel individually, OBIA groups similar pixels into segments (objects)[1] and classifies those new geographical entities. OBIA has been shown to outperform pixel-based analyses in several studies[2], due to the elimination of the so-called 'salt and paper' effect and the utilization of geometrical and contextual features.

This document is the authors version of the paper submitted to Proc. SPIE 10431, Remote Sensing Technologies and Applications in Urban Environments II, ; doi: 10.1117/12.2278422; http://dx.doi.org/10.1117/12.2278422 and available on www.spiedigitallibrary.org

Several studies[3–6] showed that the quality of the segmentation has an impact, even if not straightforward[4], on the accuracy of the final classified map and requires therefore a particular attention. Assessing the quality of the segmentation results can be achieved in a supervised way, either by visual interpretation of the segments, or by comparing these to a reference segmentation layer. Unfortunately, these approaches are time-consuming and subjective[7]. Recently, new techniques have appeared to enable the assessment of segmentation results in an unsupervised way[8–12]. Using these techniques, it is therefore possible to automate the selection of the segmentation parameter. These so-called 'unsupervised segmentation parameter optimization' (USPO) techniques mainly seek to maximize intra-segment homogeneity and inter-segment heterogeneity[7]. Their main advantage that they operate on a purely unsupervised manner, as they rely on metrics computed directly on the data, and usually produce results comparable to those of supervised methods[13].

Most of the time, when the area of interest is very large, both supervised and unsupervised optimization approaches are performed on a representative spatial subset, i.e., a limited portion of the whole scene, in order to reduce computational costs which can be a major issue. Although this approach may be acceptable for homogeneous areas, it would be rather unintuitive to assume that a single parameter, even optimized, can adequately segment different landscape patterns throughout large heterogeneous areas such as sub-Saharan African cities. In fact, it would be more reasonable to make the assumption that the optimal segmentation parameter can differ across the scene. As such, by using a single – global - parameter, the segmentation results may potentially add an unnecessary bias into the segmentation algorithm by forcing a single value for the whole image, while the most optimal parameter is likely to vary for different urban patterns.

In recent years, a few studies have tackled this issue, by employing more localized or regionalized optimization procedures. Cánovas-García and Alonso-Sarría (2015) demonstrated an improvement in segmentation quality by optimizing the segmentation parameter based on spatially differentiated agricultural plots, instead of selecting a single parameter for the whole scene[14]. Recently, Kavzoglu et al. (2016) proposed a regionalized multiscale approach in which an initial coarse segmentation was carried out in order to produce areas for further refinement of the segmentation parameters[15]. Classification results were shown to improve when the optimization of the segmentation parameter was performed regionally rather than globally. To our knowledge, no studies have tackled this issue in heterogeneous urban environments.

In this paper, we present a framework for investigating the contribution of a local segmentation parameter optimization approach compared to a global approach. The area of interest, located in the city of Ouagadougou in Burkina Faso, covers 94 square kilometers (km²) and is highly heterogeneous in terms of urban patterns. Firstly, a global approach was performed in which the whole scene was segmented based on a single parameter selected by USPO on a spatial subset representative of the diversity of the whole scene. Secondly, a local approach was carried out using a partition of the city into 283 local zones, homogeneous in terms of building size and building density. Each local zone was then segmented using a locally optimized segmentation parameter. The whole framework was based on an open source semi-automated processing chain[16].

The research presented in this paper is part of the 'Modeling and forecasting African Urban Population Patterns for vulnerability and health assessments' project (MAUPP – http://maupp.ulb.ac.be), focusing on production of LULC maps and estimations of human population densities in African cities.

## 2. MATERIAL AND METHODS

### 2.1 Processing chain, software and tools

The analysis was performed using the open-source software GRASS GIS[17] and R. The segmentation step was performed using 'i.segment' and 'i.segment.uspo' from GRASS GIS and the classification step using the 'caret' package of R. The whole processing was coded in Python and embedded in a 'Jupyter notebook'[18]. Python was used in order to chain commands of GRASS GIS and R directly in the same interface, and in a similar fashion as the chain presented in a previous publication[16] and publicly available.

This document is the authors version of the paper submitted to Proc. SPIE 10431, Remote Sensing Technologies and Applications in Urban Environments II, ; doi: 10.1117/12.2278422; http://dx.doi.org/10.1117/12.2278422 and available on www.spiedigitallibrary.org

## 2.2 Data

The dataset consists of a pan-sharpened stereo WorldView-3 imagery, with visible and near-infrared (VNIR) bands, re-sampled by the provider to a spatial resolution of 0.5 m. It was acquired during the wet season (October 2015) in order to enhance the spectral separability between bare soils and artificial surfaces. A normalized digital surface model (nDSM) was produced by photogrammetry from the WorldView-3 stereo-pairs and was used to provide height information. Additional indices were computed from the VNIR bands, i.e., the normalized vegetation index (NDVI), the normalized water index (NDWI)[19] and the Spectral Shape Index (SSI)[20]; they were used during the classification step.

## 2.3 Case study

We applied the analysis to a subset of the city of Ouagadougou in Burkina Faso. The city has been undergoing an extensive urban sprawl during the last decades and the number of inhabitants has doubled between 2004 and 2014 according to the United Nations[21]. It covered an area of around 615 km² at the time of imagery acquisition in 2015. The subset dedicated to the analysis is located northeast to the city center (see Figure 1) and covers 94 km². The extent of the AOI is very large compared to other studies and according to the spatial resolution of the data[22].

The city of Ouagadougou is an interesting case study for assessing the contribution of a locally optimized segmentation parameter approach as it is composed of highly contrasted neighborhoods in terms of urban patterns (see Figure 2).

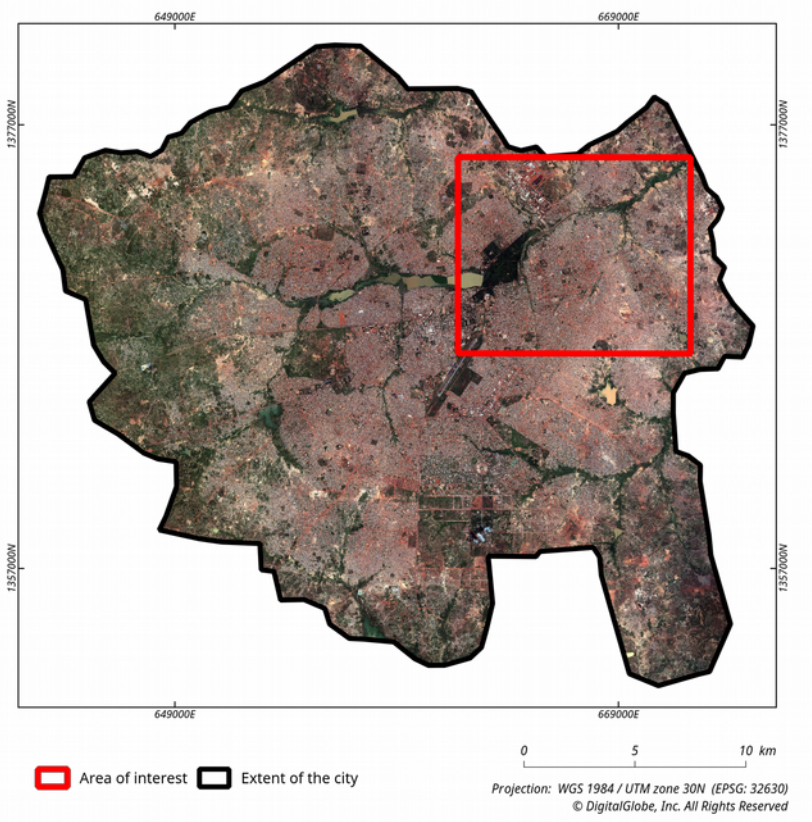


Figure 1: Extent of the city of Ouagadougou, Burkina Faso, and footprint of the area of interest used in this research.

This document is the authors version of the paper submitted to Proc. SPIE 10431, Remote Sensing Technologies and Applications in Urban Environments II, ; doi: 10.1117/12.2278422; http://dx.doi.org/10.1117/12.2278422 and available on www.spiedigitallibrary.org

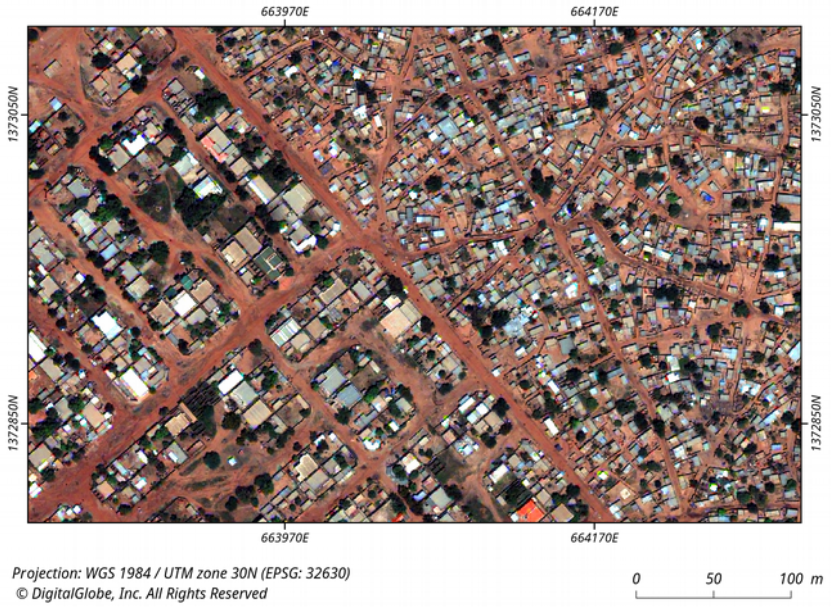


Figure 2: Subset of the area of interest with a clear opposition between unplanned and planned residential neighborhoods, with varying building sizes and densities.

### 2.4 Segmentation and Unsupervised Segmentation Parameter Optimization (USPO)

Segmentation is a very important step in an OBIA classification workflow. Indeed, the segmentation quality can affect the accuracy of the classification. In this paper, an unsupervised segmentation parameter optimization (USPO) method is used in order to automate the selection of the optimum segmentation parameter. The main advantage of such method is that it relies on 'goodness measures'[7] quantifying the desired characteristics a good segmentation should have, i.e., homogeneous objects which are different from their neighbors.

In this paper we used the 'i.segment' module of GRASS GIS software to perform the segmentation. The latter implements a region-growing segmentation algorithm which is ruled by two parameters. The main parameter is the 'threshold' which controls the tolerance for merging contiguous objects according to their proximity in the feature space. The second parameter is the 'minsize' which controls the minimum size of segments. It is implemented at the end of the segmentation process, and merges the objects that are too small with their most similar neighbors.

In GRASS GIS, unsupervised segmentation parameter optimization is possible using the 'i.segment.uspo' add-on. The latter was used in this study to automatically select the optimum threshold parameter. The minsize parameter was fixed in order to match the desired minimum mapping unit of the final map, i.e., 3.75 m². The add-on allows users to select different USPO approaches presented in previous studies[8,12] and its implementation is described in Grippa et al. (2017)[16]. It generates a stack of different segmentation results by varying the threshold parameter and selects the one that obtains the largest score for an optimization function. The score combines a measure of intra-object weighted variance (WV)[23] assessing the intra-segment homogeneity and a spatial autocorrelation (SA) measure assessing the inter-segment heterogeneity. For the SA measure, the user can choose between Geary's C[24] and Moran's I[25]. The latter was used in this paper. Both measures are normalized using the following function[8]:

$$WV_{norm} = \frac{WV_{Max} - WV}{WV_{Max} - WV_{Min}} \quad (1)$$

and

$$SA_{norm} = \frac{SA_{Max} - SA}{SA_{Max} - SA_{Min}} \quad (2)$$

Where $WV$ is the weighted variance and $SA$ is the spatial autocorrelation measure of the current segmentation

This document is the authors version of the paper submitted to Proc. SPIE 10431, Remote Sensing Technologies and Applications in Urban Environments II, ; doi: 10.1117/12.2278422; http://dx.doi.org/10.1117/12.2278422 and available on www.spiedigitallibrary.org

layer. $WV_{Max}$ , $WV_{Min}$ and $SA_{Max}$ , $SA_{Min}$ refer respectively to the maximum and minimum $WV$ and $SA$ value in the stack of segmentation.

The normalized measures are then combined using the F-function proposed by Johnson (2015)[12] which is computed as follows :

$$F=(1+\alpha^2)\times\frac{SA_{norm}\times WV_{norm}}{\alpha^2\times SA_{norm}+WV_{norm}} \quad (3)$$

Where $F$ is an 'overall goodness' measure, ranging from 0 (poor quality) to 1 (high quality). The segmentation result that reaches the highest value of $F$ is then selected as the optimum one. The $\alpha$ parameter can be used to modify the importance of $SA_{norm}$ in the optimization function. In our case this parameter was fixed to 1.

Recent research revealed that the overall goodness measure resulting from this USPO approach is highly dependent on the range of parameter considered during the optimization procedure[26]. Therefore, we performed some empirical tests to find parameters generating clearly over-segmented and under-segmented results. The range was fixed as starting at a threshold value of 0.004 and stopping at 0.030, using a incremental step of 0.001.

### 2.5 Segmentation parameter optimization using a global approach

First, we applied a procedure that aims to select a single globally optimized segmentation parameter. We call it the 'global approach'. Due to computation time issues, the segmentation parameter optimization was not applied to the whole area of interest (AOI), but to a limited subset. This design is frequently used when dealing with very large datasets and was applied in previous research[12]. We made sure that the selected spatial subset contains all the types of urban patterns which can be found in the whole scene (see Figure 3). This spatial subset covers more than 10% of the whole AOI (10.2 km² / 94 km²).

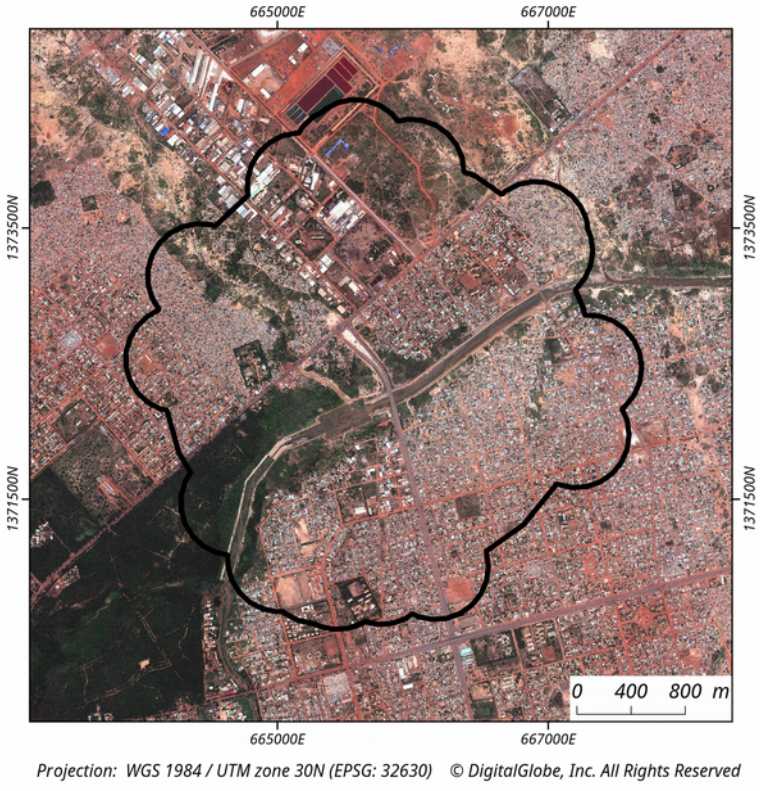


Figure 3: Spatial subset used for the global optimization of segmentation parameter. The subset covers more than 10% of the whole AOI and is representative of the diversity of urban patterns which can be found in the scene.

This document is the authors version of the paper submitted to Proc. SPIE 10431, Remote Sensing Technologies and Applications in Urban Environments II, ; doi: 10.1117/12.2278422; http://dx.doi.org/10.1117/12.2278422 and available on www.spiedigitallibrary.org

In this global approach, the segmentation parameter optimization was applied to the spatial subset, using the i.segment.uspo GRASS GIS add-on. The suggested threshold is assumed to be optimal for the whole scene. The latter was then segmented with the i.segment GRASS GIS module, using this globally-optimized threshold.

### 2.6 Segmentation parameter optimization using a local approach

Next, we applied a procedure in order to optimize the segmentation parameter for different 'local zones' (LZs) of the AOI. The reason for applying this procedure, named the 'local approach', is that the AOI presents a very high heterogeneity in terms of urban patterns (see Figure 2). Therefore, we assumed that segmenting different parts of the city using locally optimized segmentation parameters should enable the reduction of both over and under-segmentation, and thereby improve the quality of the final LULC map.

A partition of the area of interest in multiple zones was required in order to optimize the segmentation parameter locally. In developed countries, such reference geospatial data, e.g., city districts, street blocks or even cadastral plots, are often available. On the contrary, developing countries and especially African ones are known to suffer from a severe lack of available reference geospatial data. In the case of Ouagadougou, no preexisting reference data were available. In that context, the partition of the city into small homogeneous LZs was achieved manually, by visual interpretation based on criteria relating to building size and density. The full procedure was carried out by the same interpreter. We partitioned the AOI into multiple LZs according to the following criteria:

i. LZs should be homogenous, both in terms of building size and density, and should be visibly different from their neighboring LZs.

ii. LZs boundaries should follow, as far as possible, man-made or natural linear elements, e. g., roads, paths, rivers, streams, railways.

iii. Built-up LZs should be larger than 1.5 hectares (ha).

iv. Non-built-up LZs (vegetation, water, bare soils) should be larger than 15 ha when located in core urban areas, and larger than 20 ha when located in peri-urban areas. This criterion can be adapted on a case-by-case basis according to the situation and the judgment of the interpreter.

It should be noticed that the first two criteria are similar to those used in previous studies[27,28].

Then, we labeled LZs according to their urban morphology. For this purpose, a classification scheme combining the building sizes and density was used and named here 'morphological type'. Figures 4-5 illustrate the partition of the city into local homogenous zones and the membership of each zone to its morphological type. Snapshots of the urban pattern for some morphological type are presented on Figure 6.

This document is the authors version of the paper submitted to Proc. SPIE 10431, Remote Sensing Technologies and Applications in Urban Environments II, ; doi: 10.1117/12.2278422; http://dx.doi.org/10.1117/12.2278422 and available on www.spiedigitallibrary.org

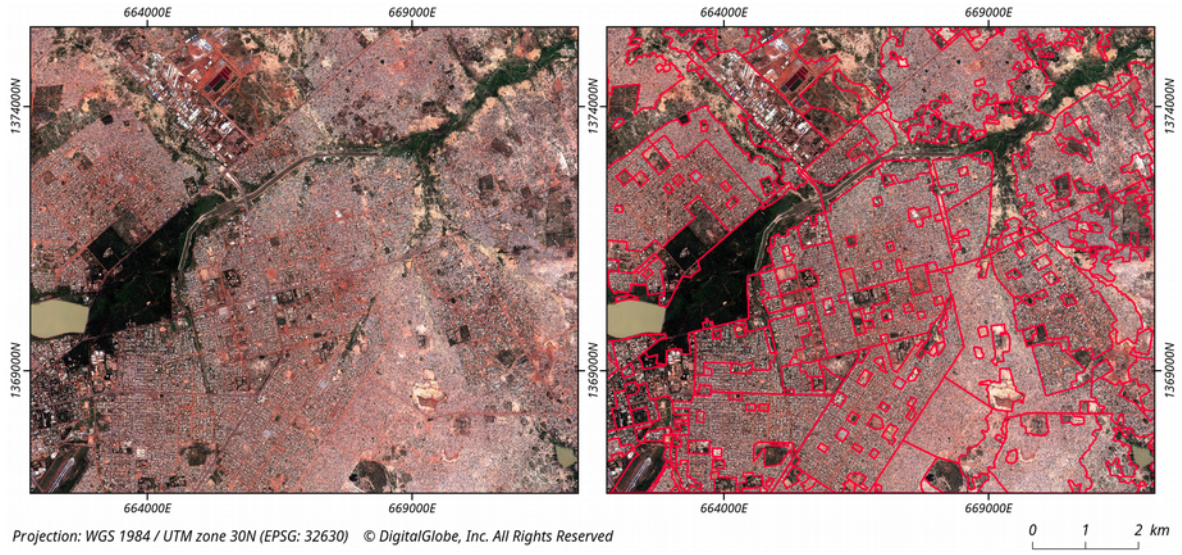


Figure 4: Partition of the city into smaller zones used for the locally optimized segmentation parameter approach.

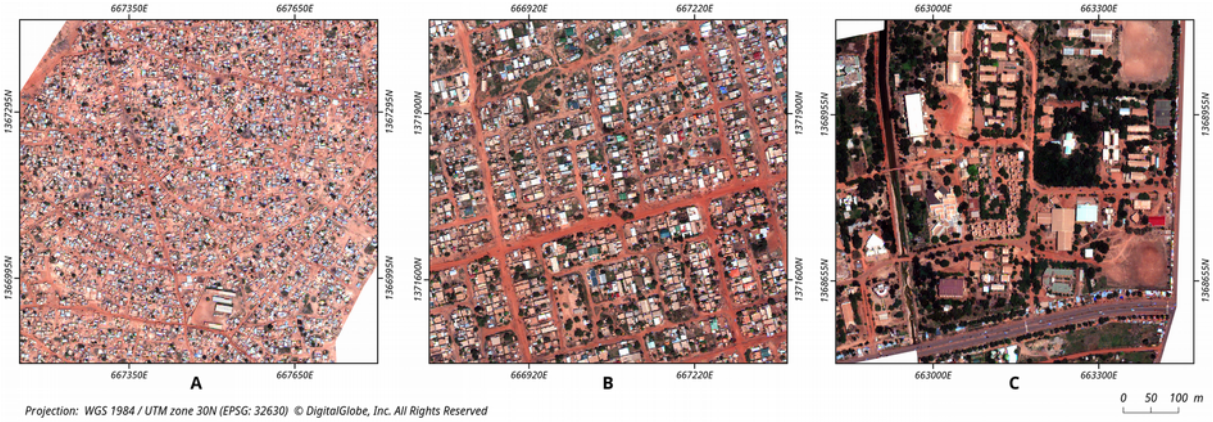


Figure 5: Examples of morphological types with different urban patterns. A) Small-sized high density built-up fabric B) Medium-sized high density built-up fabric C) Large-sized medium density built-up fabric.

This document is the authors version of the paper submitted to Proc. SPIE 10431, Remote Sensing Technologies and Applications in Urban Environments II, ; doi: 10.1117/12.2278422; http://dx.doi.org/10.1117/12.2278422 and available on www.spiedigitallibrary.org

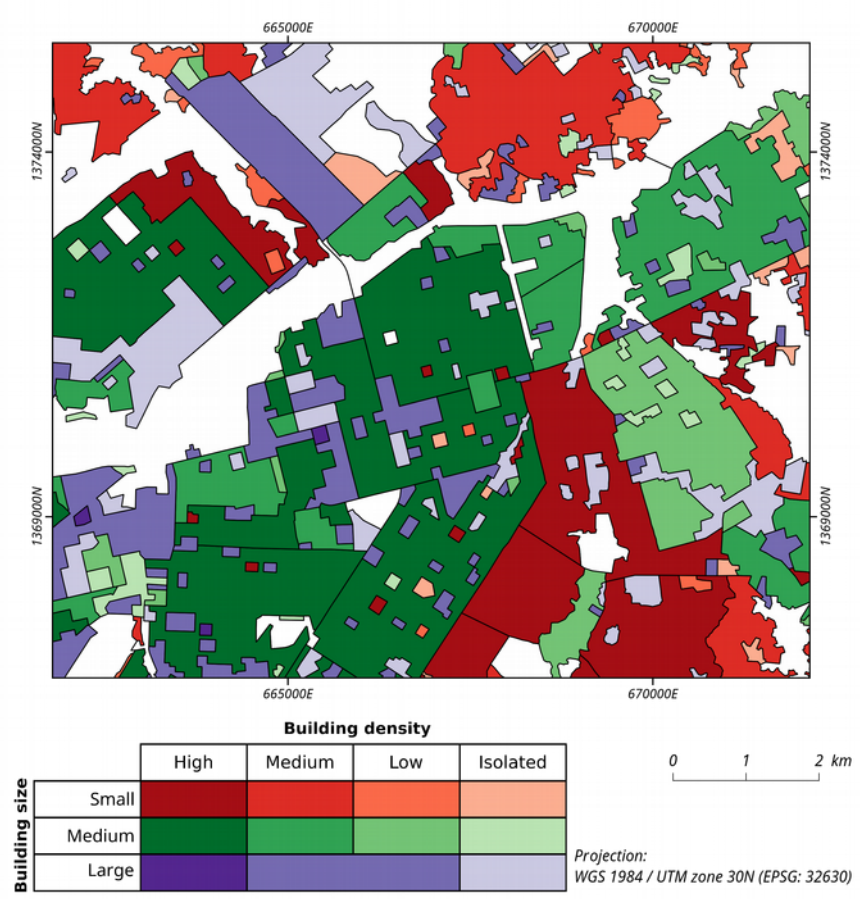


Figure 6: Membership of each local zone to its morphological type, consisting of a combination of categories of building size and density.

### 2.7 Legend, classification scheme and sampling

We considered 11 LULC classes in the classification scheme, as shown in Table 1. The 'caret' package of the R software was used to perform the classifications using a Random Forest (RF) classifier[29] with parameters optimized using cross validation and grid search.

The training and validation sets consisted of random samples generated automatically and labeled manually by the interpreter. In both the global and the local approach, training points were used to automatically select the segments in which they were included. A visual check of these segments was performed in order to eliminate those that mis-segmented objects and covered more than a single LULC class. This explains why small differences appear in the number of training samples for a same class (see Table 1). In total, 956 and 958 training points were used in the global and local approach, respectively. For each class of the legend, 40 points were dedicated to the validation. They were not used to train the classifier, in order to get a completely independent validation set. The validation points used to assess the classification performance of both approaches is strictly identical, allowing comparison of accuracy measures.

This document is the authors version of the paper submitted to Proc. SPIE 10431, Remote Sensing Technologies and Applications in Urban Environments II, ; doi: 10.1117/12.2278422; http://dx.doi.org/10.1117/12.2278422 and available on www.spiedigitallibrary.org

Table 1: Classification scheme and size of the training and validation sets.

| Level 1 classes land cover | Level 2 classes land use/land cover | Abbreviation | Training set size global approach | Training set size local approach | Validation set size |
|---|---|---|---|---|---|
| Artificial surfaces | Buildings | BU | 203 | 202 | 40 |
| | Swimming pools | SW | 72 | 72 | 40 |
| | Asphalt surfaces | AS | 63 | 63 | 40 |
| Natural material surfaces | Brown/red bare soil | RBS | 71 | 71 | 40 |
| | White/grey bare soil | GBS | 71 | 73 | 40 |
| Vegetation | Trees | TR | 95 | 95 | 40 |
| | Mixed bare soil/vegetation | MBV | 90 | 91 | 40 |
| | Dry vegetation | DV | 65 | 65 | 40 |
| | Other vegetation | OV | 77 | 78 | 40 |
| Water | Water bodies | WB | 75 | 72 | 40 |
| Shadow | Shadow | SH | 74 | 76 | 40 |
| | | **Total size:** | 956 | 958 | 440 |

## 3. RESULTS

The results show that the values of the segmentation parameter obtained using the local optimization approach differ noticeably from those resulting from the global approach. This is consistent with the results of previous studies on local optimization of segmentation parameter[14]. Figure 7 illustrates the variation of optimized 'threshold' parameter according to the membership of the LZ to the morphological type. The first observation that can be made relates to the non-built-up zones (i.e., morphological type 0) for which the optimum segmentation parameters are mostly lower than in the global approach. On the contrary, for a large majority of built-up zones the optimized threshold is higher than in the global approach. A higher 'threshold' makes the region-growing algorithm more tolerant for merging groups of pixels, resulting in a lower number of segments in the final segmentation result.

A second observation is that the distribution of locally optimized parameters by morphological type tends to be more dispersed when the building density decreases (see Figure 7). Mapping the locally optimized segmentation parameter, as in Figure 8, confirms this non-random distribution. Also, we noticed that the smaller-sized zones get the highest values of optimized 'threshold'. The visual assessment of those smaller zones revealed that the local optimization approach achieved most of the time better segmentation and classification results. Further research should be undertaken to better understand the relationship between the size of the zones to be used for local optimization approach and the resulting segmentation and classification results.

The quantitative evaluation of the classification showed that the local optimization approach slightly outperformed the global one regarding the overall accuracy (AO). For the second level of classification, using 11 classes, the OA reached 84.77% for the global approach and 85.45% for the local one (see Table 2). These results are both satisfying considering the high number of classes and the fact that some of them are spectrally very similar, e.g., classes 'Mixed bare soil/vegetation' and 'Dry vegetation'. When considering the 5 classes of the second level, the OA reached 94.77% for the global approach and 95.45% for the local one.

This document is the authors version of the paper submitted to Proc. SPIE 10431, Remote Sensing Technologies and Applications in Urban Environments II, ; doi: 10.1117/12.2278422; http://dx.doi.org/10.1117/12.2278422 and available on www.spiedigitallibrary.org

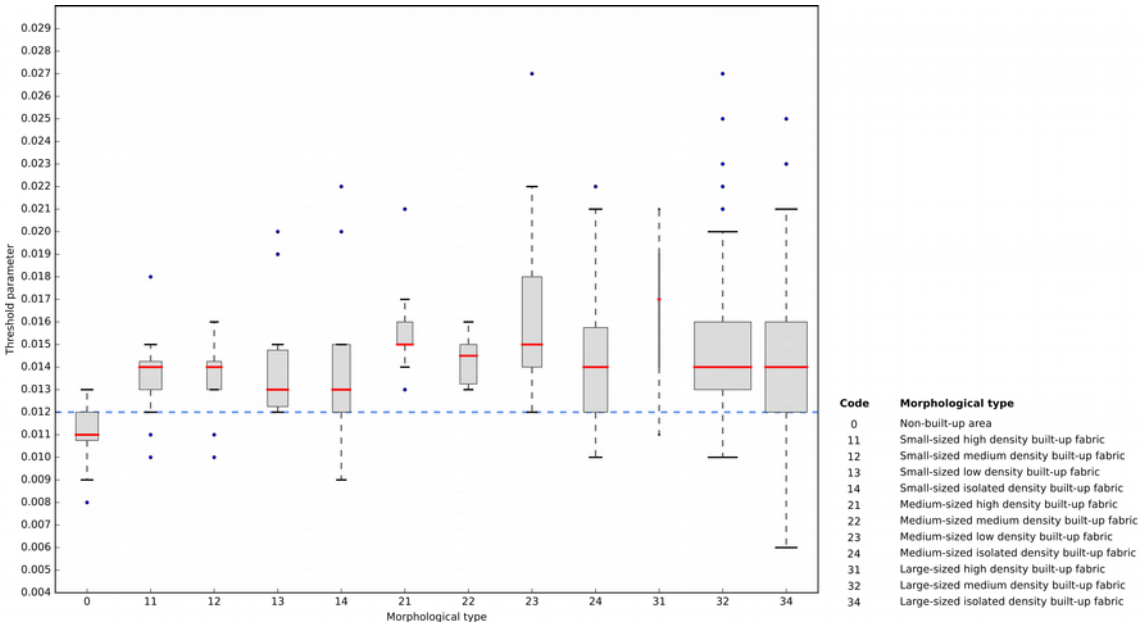


Figure 7: Boxplots representing the dispersion of locally optimized segmentation parameters by morphological type. The red lines refer to the median value. The lower and upper limits of the boxes refer to the first and third quartile, respectively. The range of the whiskers corresponds to the last observation whose value is included into 1,5 times the interquartile range. Observations with values beyond the whiskers are considered as outliers and represented by dots. The box widths are proportional to the square root[30] of the number of LZs of each morphological type. The straight dashed blue line refers to the 'threshold' derived from the global optimization approach.

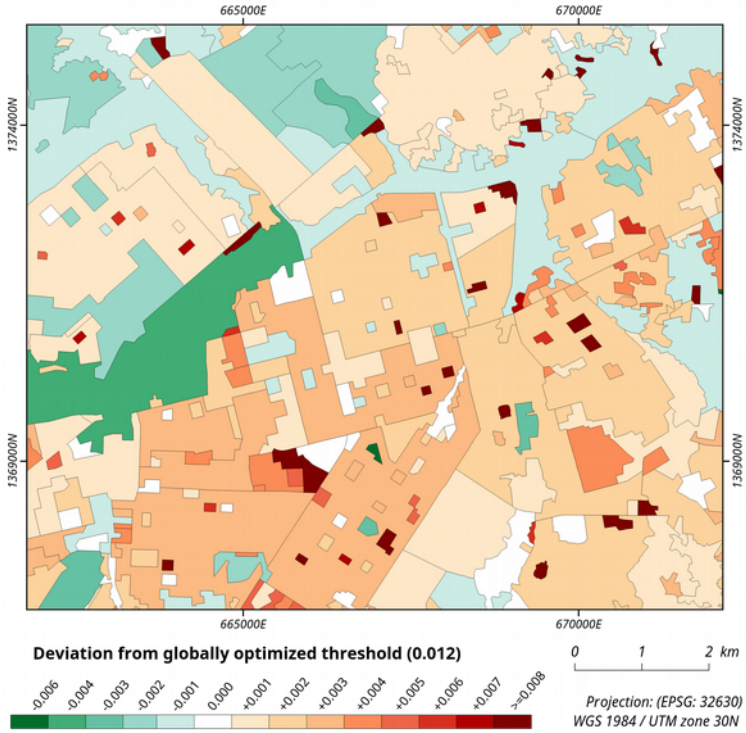


Figure 8: Spatial distribution of the locally optimized segmentation parameters. The values represent the deviation from the globally optimized segmentation parameter.

This document is the authors version of the paper submitted to Proc. SPIE 10431, Remote Sensing Technologies and Applications in Urban Environments II, ; doi: 10.1117/12.2278422; http://dx.doi.org/10.1117/12.2278422 and available on www.spiedigitallibrary.org

Table 2: Comparison of the performance evaluation of the classifications carried out using the global and the local segmentation parameter optimization approaches.

| | Classification level | Overall accuracy | Kappa |
|---|---|---|---|
| **Global optimization approach** | L1 (5 classes) | 94.77 % | 0.9297 |
| | L2 (11 classes) | 84.77 % | 0.8325 |
| **Local optimization approach** | L1 (5 classes) | 95.45 % | 0.9389 |
| | L2 (11 classes) | 85.45 % | 0.8400 |

Since the MAUPP project is mainly focused on the estimation of human population densities, the accuracy of the produced maps is particularly important with respect to the class 'Buildings'. For this reason, we mainly assessed the contribution of the local optimization approach for that specific class. The analysis of the F-score for each class of the second level of classification (see Table 3) revealed that the class 'Buildings' reaches a score of 0.92 and 0.93 using the global and the local approach, respectively. In general, the local approach achieved slightly better scores than the global one, except for the classes 'Brown/red bare soil' and 'Inland waters'.

Table 3: F-score for individual classes of the second level (L2) of the classification. For each class, if one approach outperforms the other, the F-score value is in bold.

| Level 2 Classes | Global optimization approach | Local optimization approach |
|---|---|---|
| Buildings | 0.92 | **0.93** |
| Swimming pools | 0.97 | 0.97 |
| Asphalt surfaces | 0.93 | **0.95** |
| Brown/red bare soil | **0.89** | 0.85 |
| White/grey bare soil | 0.85 | 0.85 |
| Trees | 0.81 | **0.82** |
| Mixed bare soil/vegetation | 0.69 | **0.72** |
| Dry vegetation | 0.67 | 0.67 |
| Other vegetation | 0.75 | **0.79** |
| Inland waters | **0.91** | 0.90 |
| Shadow | 0.95 | **0.96** |

Assessing the quality of the classification through quantitative performance evaluation appeared not sufficient to completely evaluate the differences appearing in the final map. Even though the classification results showed a slight OA improvement when using a local segmentation parameter optimization approach, we realized that some substantial differences occurred, especially regarding the 'Buildings' and 'Brown/red bare soils' classes. As the qualitative evaluation did not well capture some specific differences between the two approaches, we conducted a meticulous qualitative visual assessment of the classification results. Figures 9-11 present selected snapshots highlighting the main differences between the classifications resulting from both the global and the local approach.

We carefully carried out a visual analysis of the results. We discovered that, in most cases, the local segmentation optimization approach resulted in a more accurate LULC map. We can report that the most important improvement resides in the fact that the local approach better segmented bare-soil objects neighboring buildings. Those were often over-segmented using the global approach which created confusion with the 'Buildings' class. As a consequence, the local segmentation parameter optimization approach helped in limiting commission errors for the class 'Buildings'. Figures 9-10 illustrate how the delineation of buildings on the final map appears more accurate when using the local approach.

This document is the authors version of the paper submitted to Proc. SPIE 10431, Remote Sensing Technologies and Applications in Urban Environments II, ; doi: 10.1117/12.2278422; http://dx.doi.org/10.1117/12.2278422 and available on www.spiedigitallibrary.org

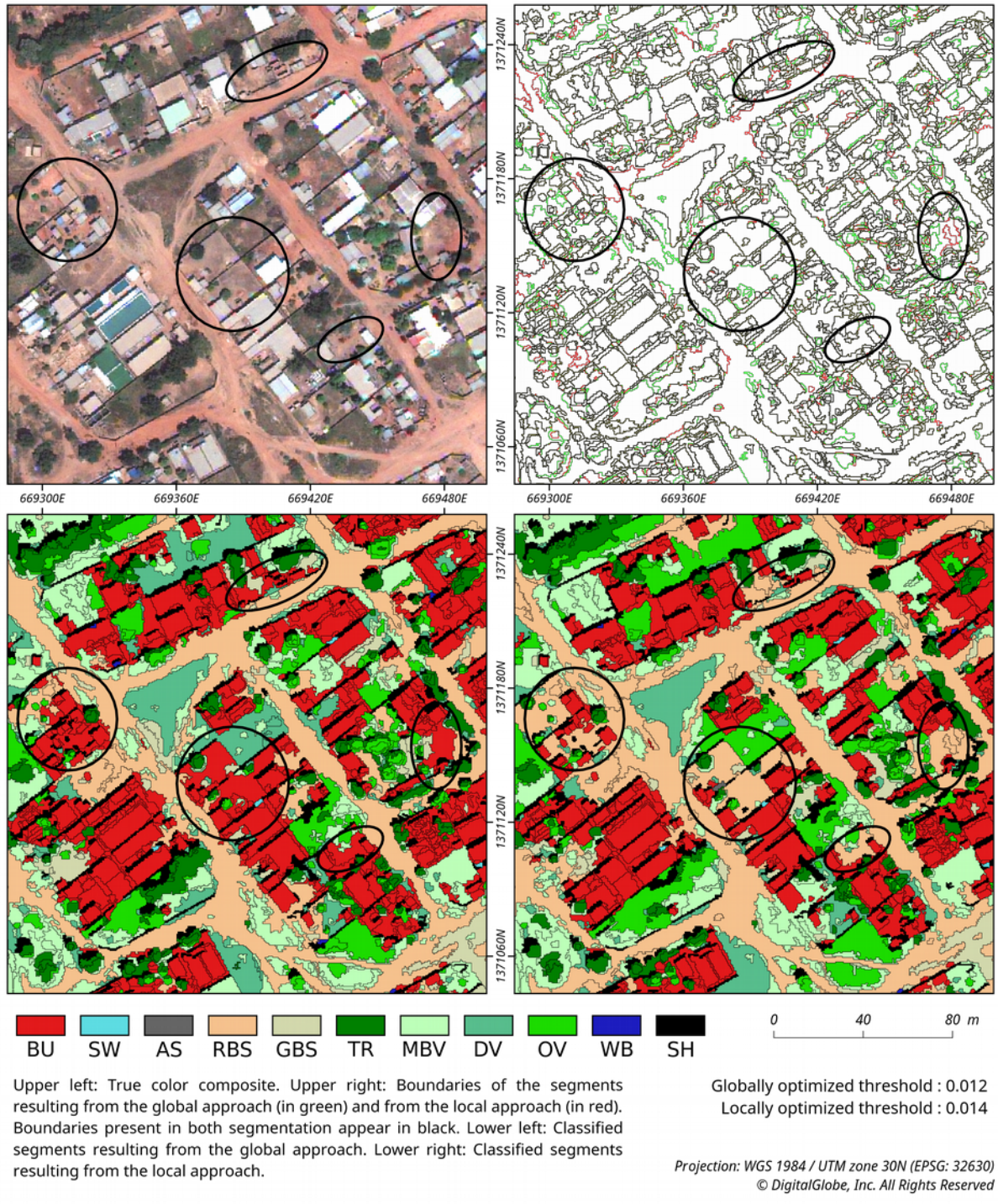


Figure 9: Subset of the AOI located in a LZ characterized by medium-sized low density built-up fabric. Bare-soil objects neighbors to the building are better classified using the local segmentation parameter optimization approach. BU: Buildings, SW: Swimming pools, AS: Asphalt surfaces, RBS: Brown/red bare soil, GBS: White/grey bare soil, TR: Tree, MBV: Mixed bare soil/vegetation, DV: Dry vegetation, OV: Other vegetation, WB: Water bodies, SH: Shadow.

This document is the authors version of the paper submitted to Proc. SPIE 10431, Remote Sensing Technologies and Applications in Urban Environments II, ; doi: 10.1117/12.2278422; http://dx.doi.org/10.1117/12.2278422 and available on www.spiedigitallibrary.org

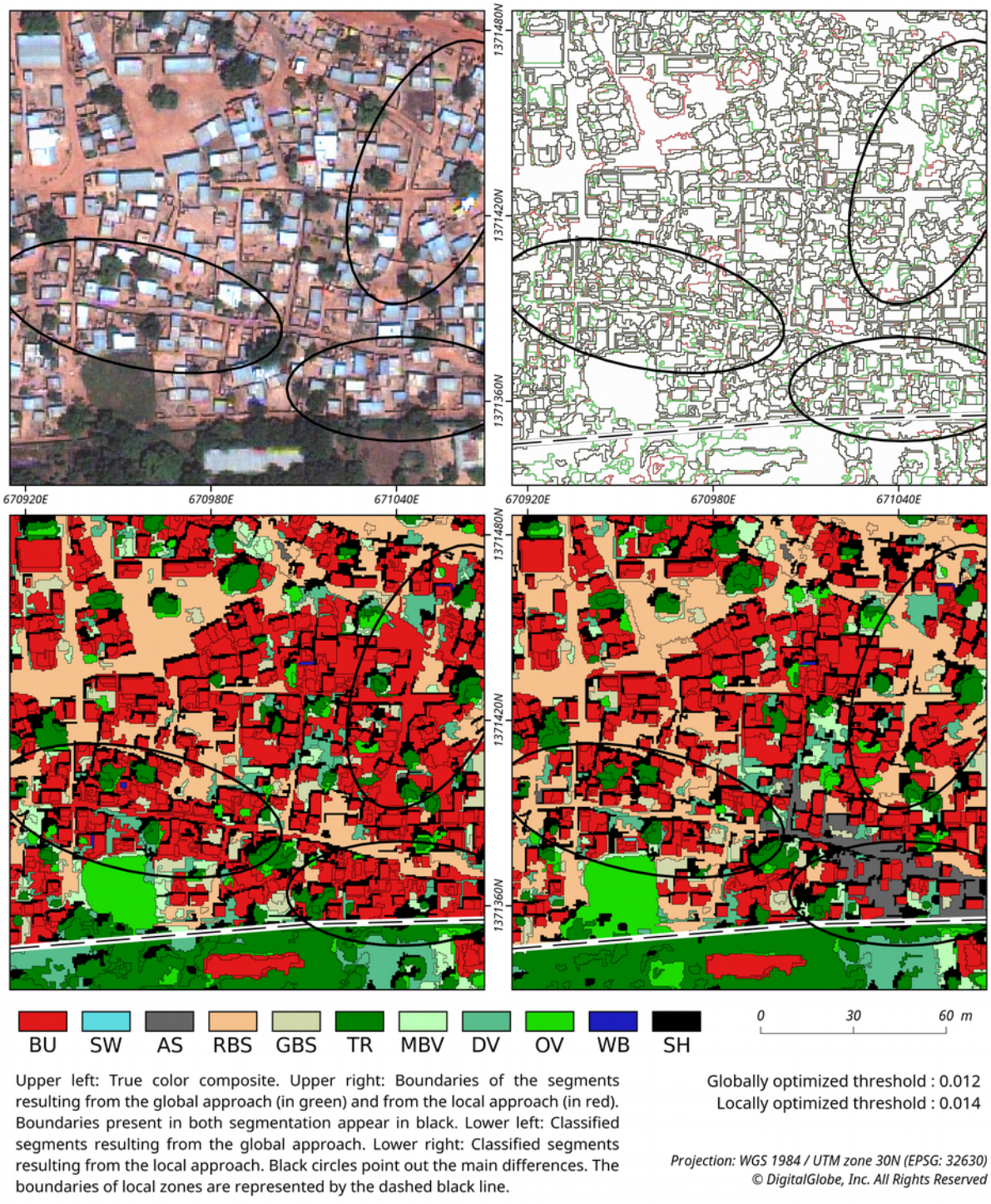


Figure 10: Subset of the AOI located in a LZ characterized by small-sized high density built-up fabric. Bare-soil objects neighbors to the building are better classified using the local segmentation parameter optimization approach. BU: Buildings, SW: Swimming pools, AS: Asphalt surfaces, RBS: Brown/red bare soil, GBS: White/grey bare soil, TR: Tree, MBV: Mixed bare soil/vegetation, DV: Dry vegetation, OV: Other vegetation, WB: Water bodies, SH: Shadow.

This document is the authors version of the paper submitted to Proc. SPIE 10431, Remote Sensing Technologies and Applications in Urban Environments II, ; doi: 10.1117/12.2278422; http://dx.doi.org/10.1117/12.2278422 and available on www.spiedigitallibrary.org

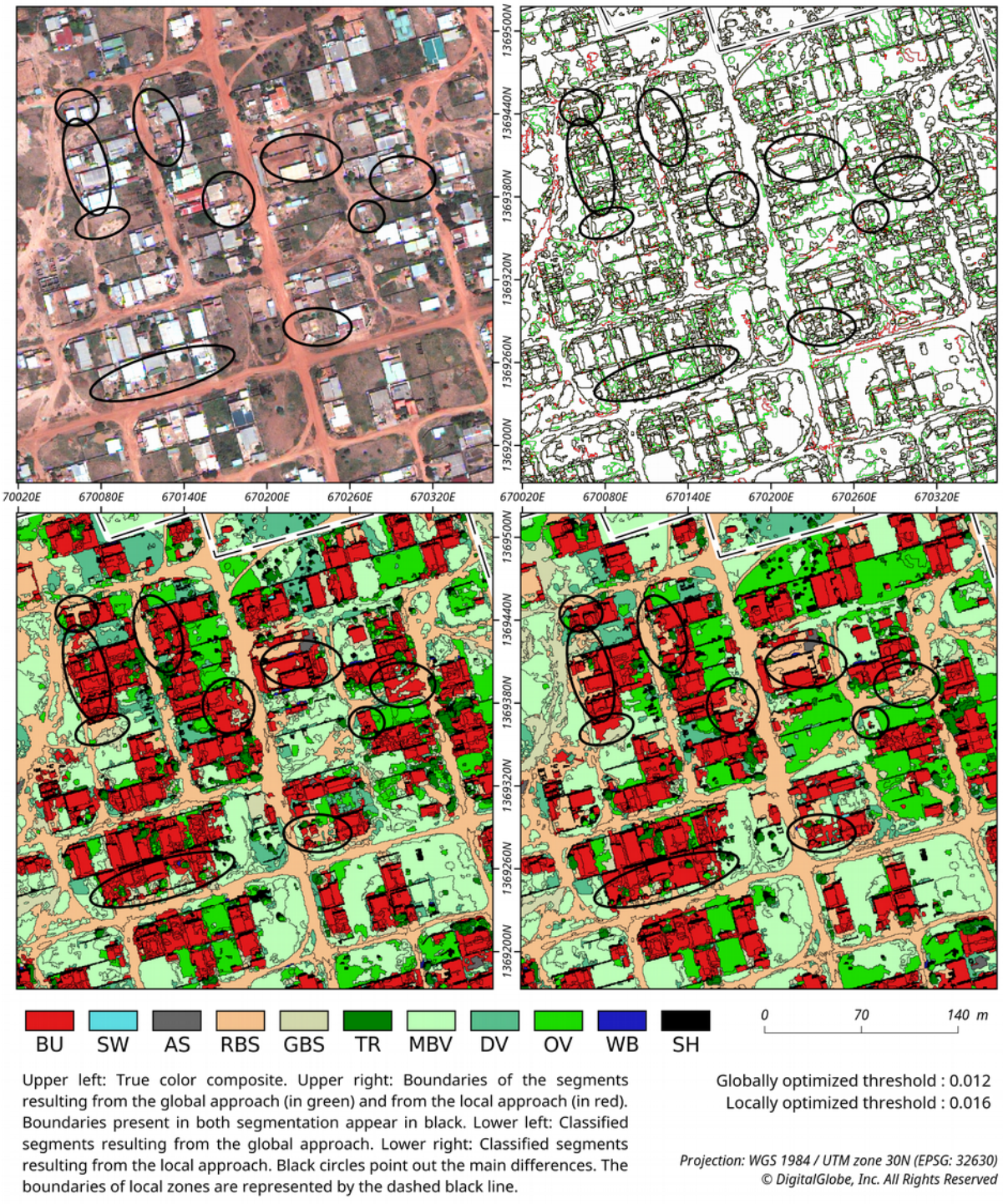


Figure 11: Subset of the AOI located in a LZ characterized by medium-sized low density built-up fabric. Here, some counter-examples illustrate the situation where local approach misclassified bare-soil objects neighboring of buildings, since the global approach accurately classified them. BU: Buildings, SW: Swimming pools, AS: Asphalt surfaces, RBS: Brown/red bare soil, GBS: White/grey bare soil, TR: Tree, MBV: Mixed bare soil/vegetation, DV: Dry vegetation, OV: Other vegetation, WB: Water bodies, SH: Shadow.

This document is the authors version of the paper submitted to Proc. SPIE 10431, Remote Sensing Technologies and Applications in Urban Environments II, ; doi: 10.1117/12.2278422; http://dx.doi.org/10.1117/12.2278422 and available on www.spiedigitallibrary.org

This confusion could be explained by the fact that the training samples for the bare-soil classes were very rarely located so close to the buildings. As such, bare-soil objects used for training were bigger and registered different feature characteristic than those over-segmented bare-soil objects neighboring buildings.

More generally, it appeared that the training set consisting of the objects created in the local approach better separated the different classes. Figure 12 illustrates the class separability in both training sets. The figure depicts the probability density function for the most important features in both RF models, i.e., the first quartile on NDVI values. It is clear that training objects of the same class are spectrally more homogeneous when using the local approach, leading to a higher intra-class homogeneity. As a consequence, the inter-class separability is higher with class centres appearing noticeably different for few classes, e.g. 'Buildings' or 'Trees'. It could also be noticed that class centres of 'Buildings' and 'Brown/red bare soils' are very similar in the global approach (around 0.15 and 0.13, respectively), which could create confusion between these classes. For the local approach, the class centres are better separated (around 0.04 and 0.10 respectively), which probably helps to clear up the confusion. These observations could explain the higher classification performance using the local approach.

Important differences appeared when we compared the percentage of the area of interest classified as 'Buildings' in both approaches (see Table 4). When considering the whole area of interest, 16.80% of the area is classified as 'Buildings' in both approach. This area increases to 17.99% (+1.19%) in the local approach, and to 19.93% (+3.13%) in the global one. The biggest difference between both approaches appears for smaller-sized high and medium density built-up areas.

Table 4: Comparison of the percentage of the area classified as 'Buildings' in both approaches

| Morphological Type | Code | Percentage (%) of the map classified as buildings | | |
|---|---|---|---|---|
| | | in both approaches | in local approach | in global approach |
| Non-built-up area | 0 | 0.86 | 1.3 (+0.44) | 1.4 (+0.54) |
| Small-sized high density built-up fabric | 11 | 24.07 | 26.04 (+1.97) | 29.62 (+5.55) |
| Small-sized medium density built-up fabric | 12 | 17.86 | 19.51 (+1.65) | 22.51 (+4.65) |
| Small-sized low density built-up fabric | 13 | 5.86 | 6.26 (+0.4) | 7.35 (+1.49) |
| Small-sized isolated density built-up fabric | 14 | 2.45 | 3.01 (+0.56) | 3.25 (+0.8) |
| Medium-sized high density built-up fabric | 21 | 34.84 | 36.78 (+1.94) | 40.33 (+5.49) |
| Medium-sized medium density built-up fabric | 22 | 20.24 | 21.49 (+1.25) | 23.66 (+3.42) |
| Medium-sized low density built-up fabric | 23 | 15.78 | 16.69 (+0.91) | 18.57 (+2.79) |
| Medium-sized isolated density built-up fabric | 24 | 2.1 | 2.32 (+0.22) | 2.77 (+0.67) |
| Large-sized high density built-up fabric | 31 | 47.76 | 51.23 (+3.47) | 53.02 (+5.26) |
| Large-sized medium density built-up fabric | 32 | 15.44 | 16.12 (+0.68) | 17.5 (+2.06) |
| Large-sized isolated density built-up fabric | 34 | 5.17 | 5.86 (+0.69) | 6.22 (+1.05) |
| | Total | 16.8 | 17.99 (+1.19) | 19.93 (+3.13) |

The main weakness of the local approach lies in the required processing time which was almost 2.5 times longer than in the global approach. More precisely, the optimization of the segmentation parameter and the segmentation itself required 6.1 hours for the global approach and 15.7 hours for the local one. The processing operations were carried out on a HP® Workstation Z620 equipped with two Intel® Xeon® E5-2680 processors (base frequency at 2.70GHz), both having 8 cores. The optimization step was performed in parallel, using 15 threads. Furthermore, in a context where existing geospatial data to be used as local zones are missing, partitioning the scene into homogeneous local zones proves a very time-consuming task. In this context, future research on local optimization of segmentation parameter could assess the ability to achieve similar results using a regular grid or very large superpixels as local zones for optimization.

The classification results obtained using the local approach are not perfect. Actually, in some situations, the local

This document is the authors version of the paper submitted to Proc. SPIE 10431, Remote Sensing Technologies and Applications in Urban Environments II, ; doi: 10.1117/12.2278422; http://dx.doi.org/10.1117/12.2278422 and available on www.spiedigitallibrary.org

approach failed in classifying correctly some bare-soil objects neighboring buildings whereas the global approach succeeded, as illustrated in Figure 11. However, after meticulous visual assessment, we can affirm that those counter-examples are very rare. Our analysis revealed that, in general, the LULC map produced with a local segmentation parameter optimization approach was more accurate, especially for the class 'Buildings' than that obtained using a global approach. However, more tests should be carried out to verify if that conclusion is consistent when applying the presented framework on different case studies.

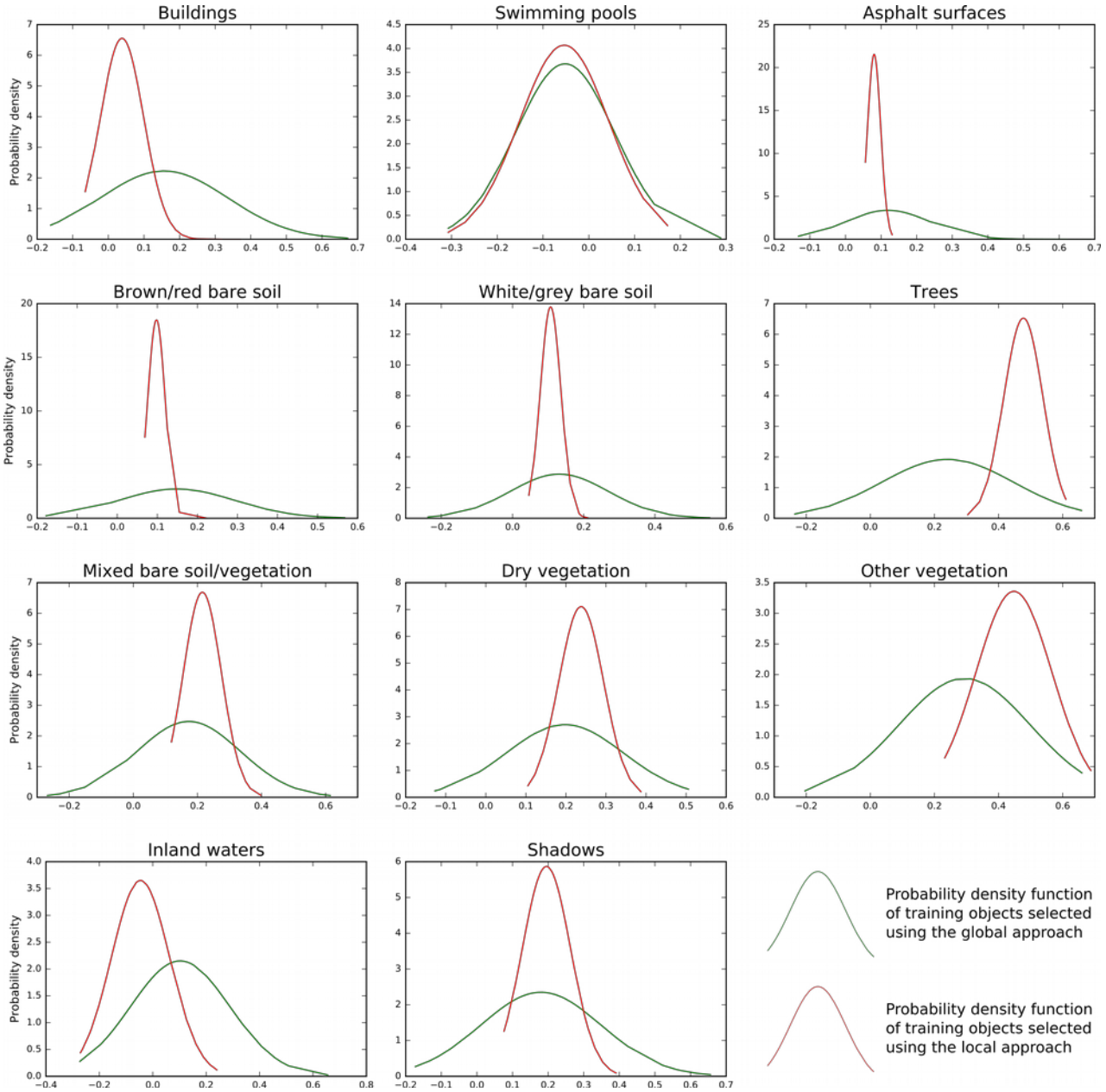


Figure 12: Probability density function of training object statistics for the different classes of the legend. The object feature presented here is the most important variable in the Random Forest classifier, i.e. first quartile on NDVI.

This document is the authors version of the paper submitted to Proc. SPIE 10431, Remote Sensing Technologies and Applications in Urban Environments II, ; doi: 10.1117/12.2278422; http://dx.doi.org/10.1117/12.2278422 and available on www.spiedigitallibrary.org

## 4. CONCLUSIONS

In this research, we assessed the contribution of a local approach for optimization of segmentation parameters for the production of land-use / land-cover maps in highly heterogeneous urban environments. First, the area of interest was segmented using a global segmentation parameter, which was optimized on a spatial subset representative of the diversity of urban patterns present throughout the whole scene. Then, the optimization of segmentation parameter was carried out for 283 local zones, homogeneous in terms of urban patterns. Both quantitative and qualitative assessments showed that the local approach outperformed the global one. The classification overall accuracy reached 94.77% and 95.45% for the global and the local approach, respectively, using 5 land-cover classes. When considering 11 land-use / land-cover classes, the overall accuracy reached 84.77% and 85.45% respectively. Analysis of training objects features revealed that the local approach helped in improving the separability of different classes. Furthermore, a qualitative assessment of the final maps revealed that the most important improvement of using a local approach resides in the huge reduction of classification errors for bare soils objects neighboring buildings objects, resulting in a better delineation of buildings in the final map. However, this improvement was not reflected by the overall accuracy measures. Therefore, in future work, we will focus on using more targeted methods of assessment. A second possible field of future research is the automation of the delineation of morphological areas, notably based on texture measures, possibly using lower resolution imagery.

## ACKNOWLEDGEMENTS

This work was funded by the Belgian Federal Science Policy Office (BELSPO) (Research Program for Earth Observation STEREO III, contract SR/00/304—as part of the MAUPP project—http://maupp.ulb.ac.be). WorldView3 data is copyrighted under the mention "©COPYRIGHT 2015 DigitalGlobe, Inc., Longmont CO USA 80503. DigitalGlobe and the DigitalGlobe logos are trademarks of DigitalGlobe, Inc. The use and/or dissemination of this data and/or of any product in any way derived there from are restricted. Unauthorized use and/or dissemination is prohibited".

## REFERENCES

[1] Blaschke, T., "Object based image analysis for remote sensing," ISPRS J. Photogramm. Remote Sens. **65**(1), 2–16 (2010).

[2] Blaschke, T., Hay, G. J., Kelly, M., Lang, S., Hofmann, P., Addink, E., Queiroz Feitosa, R., van der Meer, F., van der Werff, H., van Coillie, F. and Tiede, D., "Geographic Object-Based Image Analysis – Towards a new paradigm," ISPRS J. Photogramm. Remote Sens. **87**, 180–191 (2014).

[3] Gao, Y., Mas, J. F., Kerle, N. and Navarrete Pacheco, J. A., "Optimal region growing segmentation and its effect on classification accuracy," Int. J. Remote Sens. **32**(13), 3747–3763 (2011).

[4] Räsänen, A., Rusanen, A., Kuitunen, M. and Lensu, A., "What makes segmentation good? A case study in boreal forest habitat mapping," Int. J. Remote Sens. **34**(23), 8603–8627 (2013).

[5] Cheng, J., Bo, Y., Zhu, Y. and Ji, X., "A novel method for assessing the segmentation quality of high-spatial resolution remote-sensing images," Int. J. Remote Sens. **35**(10), 3816–3839 (2014).

[6] Yang, J., Li, P. and He, Y., "A multi-band approach to unsupervised scale parameter selection for multi-scale image segmentation," ISPRS J. Photogramm. Remote Sens. **94**, 13–24 (2014).

[7] Zhang, H., Fritts, J. E. and Goldman, S. A., "Image segmentation evaluation: A survey of unsupervised methods," Comput. Vis. Image Underst. **110**(2), 260–280 (2008).

[8] Espindola, G. M., Camara, G., Reis, I. A., Bins, L. S. and Monteiro, A. M., "Parameter selection for region-growing image segmentation algorithms using spatial autocorrelation," Int. J. Remote Sens. **27**(14), 3035–3040 (2006).

[9] Drăguț, L., Tiede, D. and Levick, S. R., "ESP: a tool to estimate scale parameter for multiresolution image segmentation of remotely sensed data," Int. J. Geogr. Inf. Sci. **24**(6), 859–871 (2010).

[10] Drăguț, L., Csillik, O., Eisank, C. and Tiede, D., "Automated parameterisation for multi-scale image segmentation on multiple layers," ISPRS J. Photogramm. Remote Sens. **88**, 119–127 (2014).

[11] Johnson, B. and Xie, Z., "Unsupervised image segmentation evaluation and refinement using a multi-scale approach," ISPRS J. Photogramm. Remote Sens. **66**(4), 473–483 (2011).

[12] Johnson, B. A., Bragais, M., Endo, I., Magcale-Macandog, D. B. and Macandog, P. B. M., "Image Segmentation Parameter Optimization Considering Within- and Between-Segment Heterogeneity at Multiple Scale Levels: Test Case for Mapping Residential Areas Using Landsat Imagery," ISPRS Int. J. Geo-Inf. **4**(4), 2292–2305 (2015).

[13] Belgiu, M., Drăguț, L. and Strobl, J., "Quantitative evaluation of variations in rule-based classifications of land cover in urban neighbourhoods using WorldView-2 imagery," ISPRS J. Photogramm. Remote Sens. **87**, 205–215 (2014).

[14] Cánovas-García, F. and Alonso-Sarría, F., "A local approach to optimize the scale parameter in multiresolution segmentation for multispectral imagery," Geocarto Int. **30**(8), 937–961 (2015).

[15] Kavzoglu, T., Yildiz Erdemir, M. and Tonbul, H., "A region-based mutli-scale approach for object-based image analysis," ISPRS - Int. Arch. Photogramm. Remote Sens. Spat. Inf. Sci. **XLI-B7**, 241–247 (2016).

[16] Grippa, T., Lennert, M., Beaumont, B., Vanhuysse, S., Stephenne, N. and Wolff, E., "An Open-Source Semi-Automated Processing Chain for Urban Object-Based Classification," Remote Sens. **9**(4), 358 (2017).

[17] Neteler, M., Bowman, M. H., Landa, M. and Metz, M., "GRASS GIS: A multi-purpose open source GIS," Environ. Model. Softw. **31**, 124–130 (2012).

[18] Kluyver, T., Ragan-Kelley, B., Pérez, F., Granger, B., Bussonnier, M., Frederic, J., Kelley, K., Hamrick, J., Grout, J., Corlay, S., Ivanov, P., Avila, D., Abdalla, S., Willing, C. and Jupyter Development Team., "Jupyter Notebooks - a publishing format for reproducible computational workflows," Proc. 20th Int. Conf. Electron. Publ., 87–90, Göttingen, Germany (2016).

[19] McFeeters, S. K., "The use of the Normalized Difference Water Index (NDWI) in the delineation of open water features," Int. J. Remote Sens. **17**(7), 1425–1432 (1996).

[20] Chen, Y., Su, W., Li, J. and Sun, Z., "Hierarchical object oriented classification using very high resolution imagery and LIDAR data over urban areas," Adv. Space Res. **43**(7), 1101–1110 (2009).

[21] United Nations., "World Urbanization Prospects: The 2014 Revision, CD-ROM Edition," United nations, Department of Economic and Social Affairs, Population Division (2014).

[22] Ma, L., Li, M., Ma, X., Cheng, L., Du, P. and Liu, Y., "A review of supervised object-based land-cover image classification," ISPRS J. Photogramm. Remote Sens. **130**, 277–293 (2017).

[23] Belgiu, M. and Drăgut, L., "Comparing supervised and unsupervised multiresolution segmentation approaches for extracting buildings from very high resolution imagery," ISPRS J. Photogramm. Remote Sens. **96**, 67–75 (2014).

[24] Geary, R. C., "The Contiguity Ratio and Statistical Mapping," Inc. Stat. **5**(3), 115 (1954).

[25] Moran, P. A. P., "Notes on Continuous Stochastic Phenomena," Biometrika **37**(1/2), 17 (1950).

[26] Böck, S., Immitzer, M. and Atzberger, C., "On the Objectivity of the Objective Function—Problems with Unsupervised Segmentation Evaluation Based on Global Score and a Possible Remedy," Remote Sens. **9**(8), 769 (2017).

[27] Herold, M., Scepan, J. and Clarke, K. C., "The use of remote sensing and landscape metrics to describe structures and changes in urban land uses," Environ. Plan. A **34**(8), 1443–1458 (2002).

[28] Liu, X., Clarke, K. and Herold, M., "Population density and image texture," Photogramm. Eng. Remote Sens. **72**(2), 187–196 (2006).

[29] Breiman, L., "Random Forests," Mach. Learn. **45**(1), 5–32 (2001).

This document is the authors version of the paper submitted to Proc. SPIE 10431, Remote Sensing Technologies and Applications in Urban Environments II, ; doi: 10.1117/12.2278422; http://dx.doi.org/10.1117/12.2278422 and available on www.spiedigitallibrary.org

[30] McGill, R., Tukey, J. W. and Larsen, W. A., "Variations of Box Plots," Am. Stat. **32**(1), 12 (1978).

*remote sensing*

MDPI

*Article*

# Scale Matters: Spatially Partitioned Unsupervised Segmentation Parameter Optimization for Large and Heterogeneous Satellite Images

**Stefanos Georganos [1,*], Tais Grippa [1], Moritz Lennert [1], Sabine Vanhuysse [1], Brian Alan Johnson [2] and Eléonore Wolff [1]**

[1] Department of Geosciences, Environment & Society, Université libre de Bruxelles (ULB), 1050 Bruxelles, Belgium; tgrippa@ulb.ac.be (T.G.); mlennert@ulb.ac.be (M.L.); svhuysse@ulb.ac.be (S.V.); ewolff@ulb.ac.be (E.W.)

[2] Natural Resources and Ecosystem Services Area, Institute for Global Environmental Strategies, 2108-11 Kamiyamaguchi, Hayama, Kanagawa 240-0115, Japan; johnson@iges.or.jp

* Correspondence: sgeorgan@ulb.ac.be; Tel.: +32-2-650-6806

Received: 13 August 2018; Accepted: 5 September 2018; Published: 9 September 2018


**Abstract:** To classify Very-High-Resolution (VHR) imagery, Geographic Object Based Image Analysis (GEOBIA) is the most popular method used to produce high quality Land-Use/Land-Cover maps. A crucial step in GEOBIA is the appropriate parametrization of the segmentation algorithm prior to the classification. However, little effort has been made to automatically optimize GEOBIA algorithms in an unsupervised and spatially meaningful manner. So far, most Unsupervised Segmentation Parameter Optimization (USPO) techniques, assume spatial stationarity for the whole study area extent. This can be questionable, particularly for applications in geographically large and heterogeneous urban areas. In this study, we employed a novel framework named Spatially Partitioned Unsupervised Segmentation Parameter Optimization (SPUSPO), which optimizes segmentation parameters locally rather than globally, for the Sub-Saharan African city of Ouagadougou, Burkina Faso, using WorldView-3 imagery (607 km$^2$). The results showed that there exists significant spatial variation in the optimal segmentation parameters suggested by USPO across the whole scene, which follows landscape patterns—mainly of the various built-up and vegetation types. The most appropriate automatic spatial partitioning method from the investigated techniques, was an edge-detection cutline algorithm, which achieved higher classification accuracy than a global optimization, better predicted built-up regions, and did not suffer from edge effects. The overall classification accuracy using SPUSPO was 90.5%, whilst the accuracy from undertaking a traditional USPO approach was 89.5%. The differences between them were statistically significant ($p < 0.05$) based on a McNemar's test of similarity. Our methods were validated further by employing a segmentation goodness metric, Area Fit Index (AFI)on building objects across Ouagadougou, which suggested that a global USPO was more over-segmented than our local approach. The mean AFI values for SPUSPO and USPO were 0.28 and 0.36, respectively. Finally, the processing was carried out using the open-source software GRASS GIS, due to its efficiency in raster-based applications.

**Keywords:** unsupervised segmentation parameter optimization; GRASS GIS; image classification; land cover; urban areas; big data

## 1. Introduction

Accurate and precise Land-Use/Land-Cover (LULC) maps derived from remotely sensed imagery are crucial for applications spanning several fields, including spatial planning, population estimation, environmental monitoring, and socio-economic and epidemiological modelling [1–4]. These map

products not only provide useful information on their own, but also through their use as an input to secondary models (e.g., population distribution models [3], hydrological models [5], or LULC change models [6–8]. As such, maximizing the accuracy of LULC maps is a critical methodological facet in reducing error propagation and enhancing the effectiveness of science-based policy-making.

For the classification of high- and very-high resolution (VHR) imagery in particular, Geographic Object-Based Image (GEOBIA) analysis has been established as a superior method over traditional pixel-based approaches [9], as it produces a semantic representation of data closer to reality than the arbitrary nature of pixels [10]. Recent studies have attempted to establish a formal ontological framework to further advance the use of objects as spatial representation units [11]. In GEOBIA, the most crucial step before classification is the clustering of neighboring image pixels into segments based on spatial, spectral, and contextual criteria [12]. These segments should ideally represent real world objects or LC categories (e.g., building rooftops, or agricultural fields) that are larger than the original image resolution [13]. As several studies have demonstrated, GEOBIA classification accuracy is not only affected by the classification algorithm itself [14], but also by the quality of the extracted image segmentation [15–18]. Consequently, the selection of an appropriate segmentation (i.e., object-creating) algorithm, as well as its parametrization, are crucial with respect to the final output [19–21].

Region-growing (RG) segmentation techniques are the most popular in GEOBIA literature, mainly due to their implementation through the multiresolution segmentation algorithm [22], implemented in the popular software eCognition (Definiens) [16,23–26]. The most important parameter in RG segmentation is the Threshold Parameter (TP; e.g., the Scale Parameter of the multiresolution segmentation algorithm in eCognition), which governs the average size of the created segments. The selection of the parameter is most commonly attempted through a time consuming, user dependent, trial and error process [27,28], in which the quality of the produced segmentations is assessed visually [29], or through a quantitative comparison against reference data (i.e., manually digitized polygons based on visual image interpretation) [30–32]. These approaches have been criticized for being untenable due to their subjective nature and time inefficiency, whilst at the same time, the improvement they can offer in classification accuracy might be limited [33]. Therefore, other research has been directed towards the development of objectively defined Unsupervised Segmentation Parameter Optimization (USPO) techniques, which evaluate individual segmentations based on geostatistical metrics and do not require reference data [34–36]. To do so, various USPO metrics have been proposed, such as the rate of change in local variance implemented through the estimation of scale parameter tool (ESP) [34,37], the optimization of objective functions such as the Global Score (GS) [38] and the F-measure [18,39] among others, with varying degrees of success. In the comparative study of Grybas et al. [23], the F-measure was found superior to the ESP and GS, potentially due to its sensitivity to over and under segmentation. The GS and F-measure assess spectral values within (i.e., Weighted Variance (WV)) and between (i.e., Global Moran's I (MI)) segments. Ideally, an accurate segmentation should minimize the spectral heterogeneity within segments and maximize the spectral heterogeneity between segments, so the TP that is found to maximize the aforementioned function is accredited to be optimal [40].

So far, the optimization of segment-creating algorithms (and in this study, the region growing one), has been attempted mainly through the use of global methods, either at single or multiple scales [36,37]. A global approach implies that the optimization of the TP is adequate using the whole extent of the study area or a subset which is assumed to be representative [15,33,41]. The vast majority of the developments in the past years operate on that assumption, a situation exaggerated from the relatively small study areas that are used (<3 $km^2$ in ~95% of the recent literature on object-based land cover mapping) as pointed out in the review of Ma et al. [42]. These approaches assume spatial stationarity—that the relationship between input data and the segment generating process is stable across space which is reflected by having a spatially invariant TP for the whole study area. However, this begs the question "Why is the extent of the study area in a remote sensing application

automatically assumed to be the most appropriate scale to optimize the segmentation algorithms?". This is of increasing importance as it has been recently demonstrated that partitioning the study area in smaller regions can provide significantly different results, highlighting the effect of geographic scale in remote sensing operations [43,44]. Spatial stationarity might hold for small homogenous regions, but perhaps is unsuitable for large and/or heterogenous scenes. It would be sensible to hypothesize that the optimal TP would intrinsically and significantly vary across space due to local variations in data structure, particularly for urban areas, which are known for their landscape variability even within the same LULC class. If a global approach would be used in such a case, it might only capture an average and potentially misleading impression of the situation and lead towards adding bias to the segmentation model, which could be reflected both in segmentation evaluation metrics and classification accuracy. In recent years, few studies have tackled this issue by employing more localized or regionalized procedures.

Johnson and Xie [36] refined their global segmentation results in a two-stage procedure by re-segmenting local outliers using geospatial metrics such as Local Moran's I. Cánovas-García and Alonso-Sarría [43] demonstrated improvements in segmentation quality by optimizing the TP independently in agricultural plots, instead of selecting a single parameter for the whole dataset. However, the spatial units were selected a priori by using land use parcel vectors, which requires ancillary data and expert knowledge of the study area. Recently, Kavzoglu et al. [35] proposed a regionalized multiscale approach for small, semi-urban environments where initial, broad scale segments derived from the coarse segmentation selection of the ESP tool, defined further areas for calibrating segmentation parameters. Classification results were shown to improve as the parametrization of the TP was performed regionally, rather than globally. The improvement local methods offer for urban LULC mapping has been recently demonstrated by Grippa et al. [44], where the study area was manually delineated into morphological zones that share similar built-up characteristics, and a separate USPO optimization was applied to each one of them. Nonetheless, the operational capabilities of such methods are either restricted computationally or require tedious manual labor and user expertise that is rarely available. These limitations are important given the advent of big data, which includes the use of VHR datasets at an increasing pace [45]. As such, our effort focuses on semi-automatically identifying and quantifying the degree of spatial non-stationarity and geographic scale dependency between the algorithm parameters for large and heterogeneous satellite images [1].

Our main hypothesis questions the use of global methods a priori, when heterogeneous and/or large datasets are employed. To do so, a discrimination between the observation and operating scales between the TP and USPO optimization must be made. The observation scale corresponds to the whole extent of the study area, whilst the operating scale can be a spatial delineation, which better reflects the optimization of a segmentation algorithm. In simpler words, we are asking the question: "Are the segmentation results better if we analyze the data locally rather than globally?".

In this paper, we present a methodological framework named Spatially Partitioned Unsupervised Segmentation Parameter Optimization (SPUSPO) in which optimization of the TP is performed in a localized manner. The proposed methods are automated and do not require reference information. The underlying rationale of SPUSPO is based on the first law of geography [46] that "all things are related but near things are more related", which suggests that objects being near each other (e.g., built-up characteristics of a neighborhood) have a higher degree of similarity than a set of objects far away. The results of the local optimizations are analyzed, mapped and quantified through spatial statistics, highlighting the variation of segmentation parameters as a function of location and spatial scale. The presented methods are evaluated both at the segmentation and classification level. As a proof of concept, we evaluated the procedure for the large, heterogenous city of Ouagadougou, capital of Burkina Faso. All of the analysis was performed using the GRASS open source GIS software along with open access processing chains suited for satellite VHR datasets [47].

## 2. Materials and Methods

### *2.1. Study Area and Data*

The study area covered the city of Ouagadougou, capital city of Burkina Faso in Sub-Saharan Africa (SSA). Ouagadougou comprises a complex and heterogenous urban landscape of planned and unplanned neighborhoods and buildings, of various sizes and materials [48]. The city has been undergoing extensive and partly unregulated urban growth (i.e., rural to urban migration) over the last decades [49,50]. To map the LULC of the city, we used a 4-band (R, G, B, NIR) WorldView-3 multispectral image (607 km$^2$, Figure 1) from October 2015, and a normalized Digital Surface Model (nDSM) derived from stereo image acquisitions on the same image date. The native spatial resolution of the Worldview-3 imagery is 0.30 cm but was resampled at 0.50 cm by the provider. The value of the elevation information was critical, as the built-up characteristics were very hard to visually discriminate from bare soil and artificial ground surfaces, due to the presence of dust on rooftops and the use of similar construction materials for roofs and artificial ground surfaces. Thus, this challenging study site provided a good stress test for our methods.

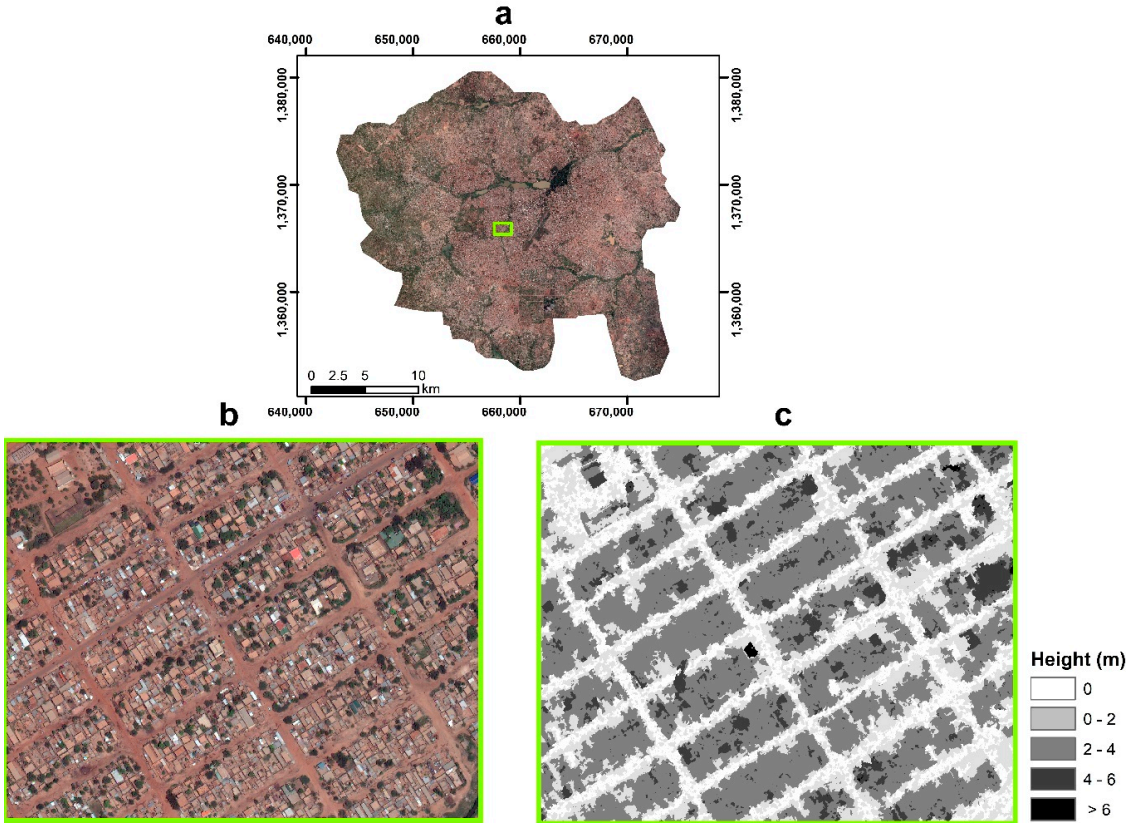


**Figure 1.** (**a**) Study area extent illustrated from a WorldView-3 RGB composite of Ouagadougou, (**b**) a typical built-up neighborhood of Ouagadougou and (**c**) Normalized Digital Surface Model for the region.

### *2.2. Segmentation and Unsupervised Segmentation Parameter Optimization*

The whole LULC classification framework was realized by employing and extending the semi-automated processing chain proposed by Grippa et al. [1]. The chain was implemented in a Jupyter Notebook format and integrated GRASS GIS functions with Python and R programming languages, framing a complete procedure from the input of initial datasets to final LULC map production. For segmentation, we utilized the RG algorithm implementation of GRASS GIS [51] with all four bands (VNIR) used as inputs. In the GRASS implementation, the TP ranges between 0 to

1, with 0 leading to the situation where each pixel represents a segment, while 1 unifies all image pixels in one object. As Böck et al. [52] pointed out, the USPO metrics are sensitive to the range of candidate segmentations used as input, so we empirically found a range that corresponded to cases of evident over- and under-segmentations to be used as minimum and maximum possible values, as commonly done in similar studies [18,53]. Thus, we evaluated 27 different segmentations starting with a TP of 4 and finishing at a TP of 31, guided by an incrementing step value of 1, as in previous studies, [54]. For reader convenience, all TP values were multiplied by 1000 in the illustrative and text materials.

To evaluate the quality of each of the different segmentations, we used the inter- and intra-segmentation heterogeneity metrics Moran's I (*MI*) and Weighted Variance (*WV*), respectively. MI calculates the degree of spatial autocorrelation present in the values of nearby geographic features, and it was used in our case (and in many other USPO studies) to calculate how spectrally heterogeneous segments are, on average, from their neighbors (i.e., in terms of the mean segment values calculated for each spectral band). For this reason, it can provide a measure of "oversegmentation goodness"; Low *MI* values for a segmentation layer indicate low spatial autocorrelation between segment spectral values, suggesting that most segments belong to a different ground feature (with different spectral reflectance properties) than its neighbors. *WV*, on the other hand, describes the average spectral variability within segments (weighted by each segment's area). *WV* can provide a measure of "undersegmentation goodness"; Low *WV* values indicate little internal variation in the spectral properties of segments, suggesting the segment does not contain a mixture of multiple ground features. *MI* and *WV* are given by:

$$WV = \frac{\sum_i^n a_i * v_i}{\sum_i^n a_i} \quad (1)$$

$$MI = \frac{n \sum_i^n \sum_j^n w_{ij} z_i z_j}{M \sum_i^n z_i^2} \quad (2)$$

where for Equation (1), $n$ is the number of segments, $v_i$ is the variance and $a_i$ the area for each segment, while in Equation (2), $n$ is the number of segments, $z_i = x_i - \overline{x}$, $\overline{x}$ is the mean value of segment $x$, $M = \sum_{i=1}^n \sum_{j=1}^n w_{ij}$ and $w_{ij}$ is the element of the matrix of spatial proximity $M$, which indicates the spatial connectivity for segments $i$ and $j$ [52,53].

To perform USPO, the oversegmentation and undersegmentation goodness values calculated for each segmentation layer need to be combined into a single value, e.g., through addition [38] or the F-measure [18]. We used the F-measure to combine *MI* and *WV* values in this study, as it was demonstrated to be less sensitive to excessive over- and undersegmentation than other combination approaches in Zhang et al. [39] and implemented in GRASS module "i.segment.uspo" [55]. To derive an F-measure from these two components, we first need to normalize them to a similar range (0–1) [38]:

$$MI_n = \frac{MI_{max} - MI}{MI_{max} - MI_{min}}, \quad (3)$$

$$WV_n = \frac{WV_{max} - WV}{WV_{max} - WV_{min}}, \quad (4)$$

where $WV_n$ is the normalized *WV* (or *MI*), $WV_{max}$ is the maximum *WV* (or *MI*) value of all candidate segmentations, $WV_{min}$ is the minimum *WV* (or *MI*) value of all candidate segmentations and *WV* is the *WV* (or *MI*) value of the current segmentation. The F-measure is a harmonic weighting of these two features:

$$F_{opt} = \left(1 + a^2\right) \frac{WV_{max} - WV}{a^2 * WV_{max} - WV_{min}}, \quad (5)$$

where $F_{opt}$ is the score of a candidate segmentation to be evaluated, ranging from 0 to 1, with higher values indicating higher quality; and $a$ is the relative weight factor that assigns different significance to one metric over the other [18]. In our case we used a relative weight of 1, indicating equal weighting of

the *MI* and *WV* components in calculating $F_{opt}$. The procedures were fully automated and parallelized due to the flexibility of GRASS GIS for applications including large raster datasets.

#### 2.2.1. Global USPO

The conventional global USPO approach involves using either the whole image extent as input to the USPO procedure, or a representative subset [43]. Since our image was very large (20 GB), we used the latter method, as depicted in Figure 2. The selected subset (10 km$^2$) contained planned, unplanned, and industrial built-up zones, with different kinds of vegetation, as well as bare soil, and thus, was deemed an appropriate candidate. The TP resulting from applying USPO to that region was 12, and we consequently used that value to segment all parts of the WorldView-3 image.

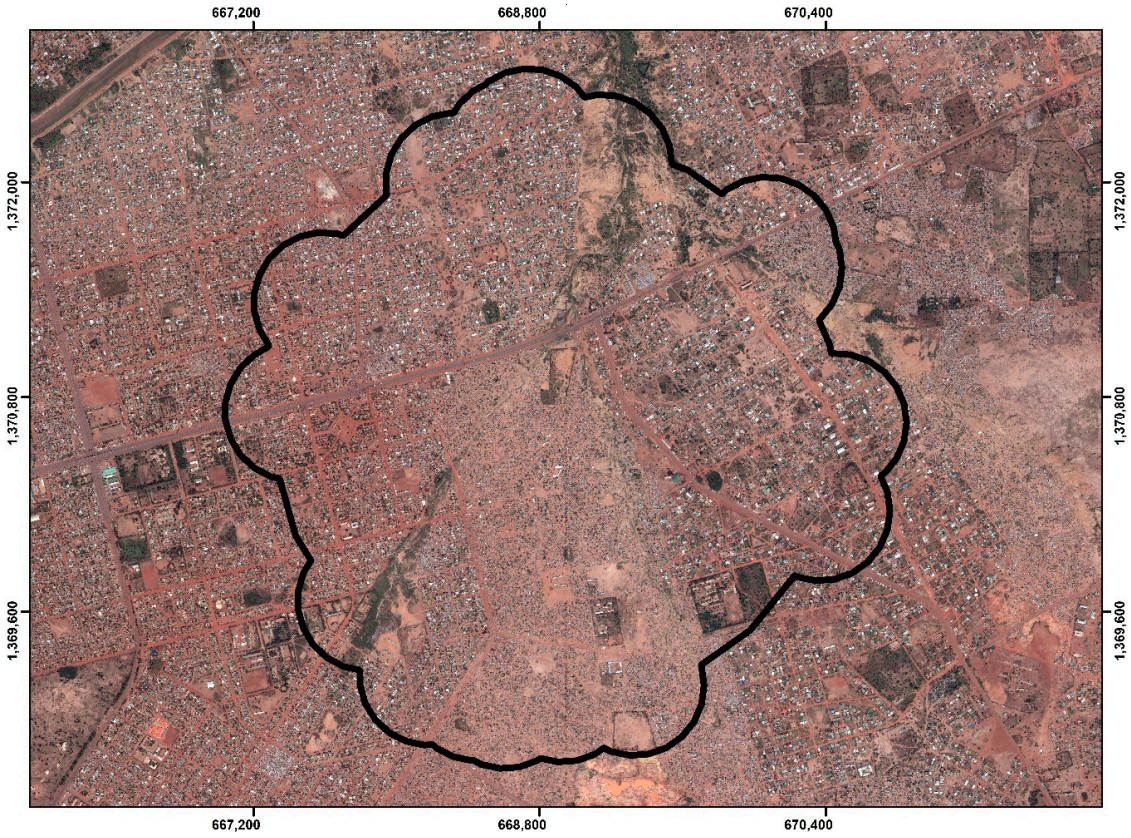


**Figure 2.** Subset of the WorldView-3 imagery (~10 km$^2$) where the RG's TP was optimized for use in the whole image. The selected area contains a distribution of land cover classes representative of the whole study area.

#### 2.2.2. Spatially Partitioned Unsupervised Segmentation Parameter Optimization (SPUSPO)

As mentioned in the introduction, a global optimization of the USPO might not be appropriate due to the spatial heterogeneity within the image. As such, an alternative approach would be to partition the study area into several subsets, and to apply the optimization procedure locally in each subset. If the segmentation level selected as optimal by a global USPO calculation approach differs significantly from the segmentation level selected locally (i.e., through local USPO calculation in each partition of the study area), a spatially non-stationary process is taking place, and thus a global model might not be the best candidate to use. To investigate this phenomenon, we partitioned the image in three automated ways. The first two methods for partitioning were done using regularly-shaped rectangular tiles of predefined sizes, and the third partitioning method involved automated delineation using a cutline creating algorithm. The predefined partition was based on splitting the WorldView-3 image, into tiles of equal area and for most cases, equal geometry. The area of the rectangular image

subsets for the first two partitioning approaches was 0.25 km$^2$ (P1) and 0.12 km$^2$ (P2), totaling to 2427 and 4887 subsets, respectively (Figure 3). Although the results of predefined partitioning can be fruitful for exploratory purposes, they suffer from edge effects at their borders. Since they are predefined and fixed in size, they arbitrarily partition the landscape, which can result in noisy/badly segmented objects along the boundaries of the rectangular subsets as artifacts (i.e., splitting building roofs or trees in half). To treat this issue, for the third and main partitioning approach (P3), we deployed a cutline creating algorithm using Laplacian zero-crossing edge detection [56–58], as implemented in the 'i.cutlines' module of GRASS GIS [59]. In that way, the created subsets would delineate the landscape in a more meaningful way, as they would follow linear patterns, such as roof edges and streets. The size of the cutline-created subsets can be decided by the user with respect to the application case. In our case, we created subsets closer to the P2 partition and as such, 4900 subsets were created. Examples of the different spatial partitioning methods are illustrated in Figure 3. In both global and local approaches, the minimum size of a created segment was preset at 14 pixels to avoid unnecessary oversegmentation.

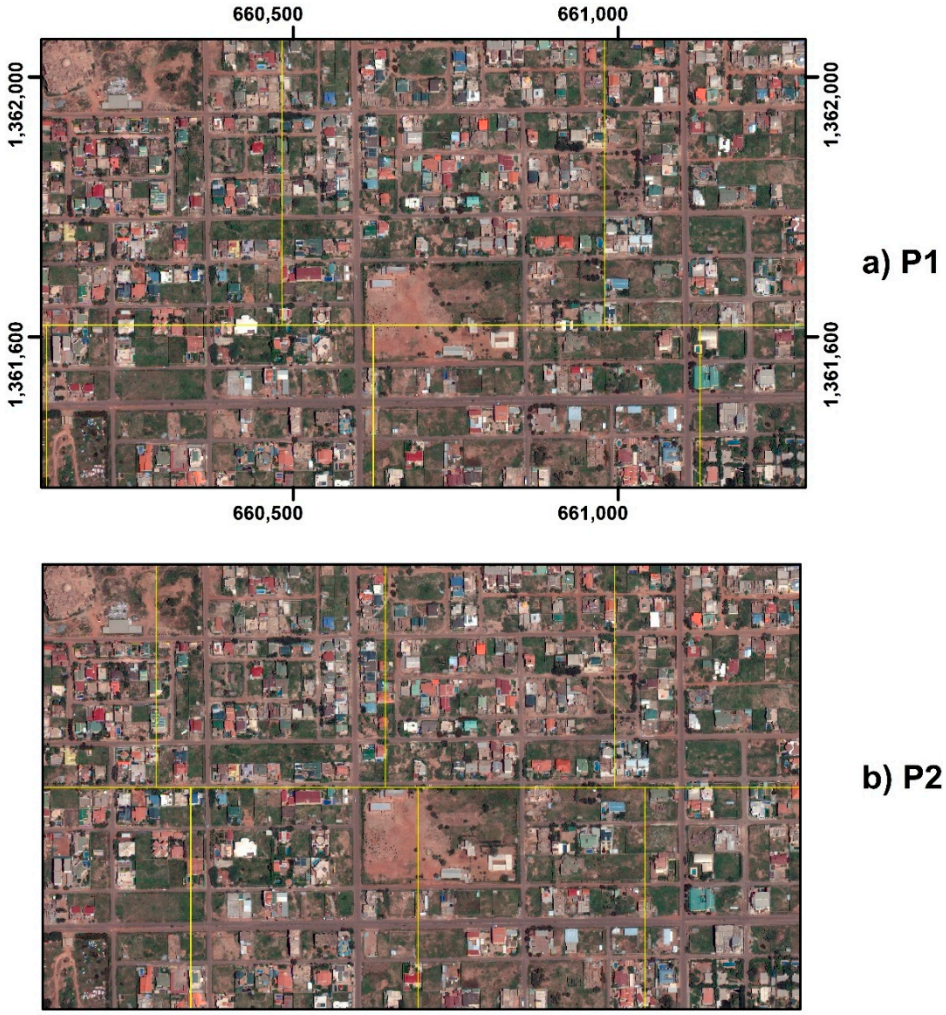


**Figure 3.** *Cont.*

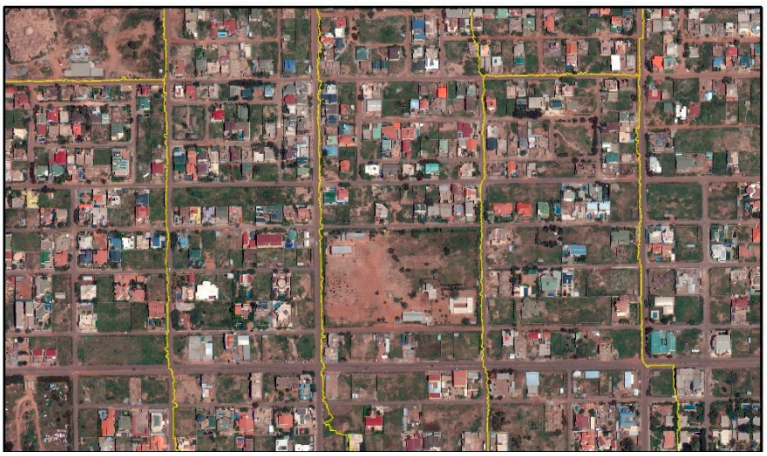


**Figure 3.** Partitioning the WorldView-3 image into spatial subsets for local USPO optimization. (**a**) Delineation by 0.250 km$^2$ area tiles, (**b**) delineation by 0.125 km$^2$ area tiles and (**c**) delineation based on zero crossing cutline algorithm.

#### 2.2.3. Spatially Partitioned Unsupervised Segmentation Parameter Optimization (SPUSPO)

One of the merits of carrying out a localized approach is that it allows for decomposing a global process, into a wide set of useful information which is mappable. Since USPO was applied locally, a unique TP was produced for each spatial subset. The variation of the local TP from the single TP value of the global USPO can be quantified to assess the degree of spatial non-stationarity. If there would be no unexpected variation in the TP, that would suggest that a global approach is indeed adequate, ceteris paribus. Along with mapping the results, we proposed a Segmentation Parameter Stationarity Index (*SPSI*), which was loosely based on the Stationarity Index of Osborne et al. [60] to assess spatial non-stationarity in gaussian models:

$$SPSI = \frac{IQR(TP_L)}{(TP_G + TP_{step}) \; - \; (TP_G - TP_{step})} \tag{6}$$

where $TP_G$ is the TP of the global USPO, $TP_{step}$ is the step parameter of the USPO procedure, and $IQR(TP_L)$ is the interquartile range of the distribution of the TP's from a local approach. The interquartile range was used to mask outlier TP values that could emerge from random variation. Values equal to or smaller than 1 imply stationarity, as the variation of the local TPs is not exceeding what one would expect from a random process. Values higher than 1 indicate that there is significant spatial variation.

### *2.3. Land Use and Land Cover Classification*

Ultimately, the segments were constructed with the aim of being labeled through a classification model. As such, another method to assess the local and global USPO methods is through the accuracy and performance of a LULC classification. The classification scheme and training data are presented below (Table 1). The training data were collected through random and stratified random sampling, and consisted of 2478 objects across the city, which were labeled through visual interpretation by two experts during the same period. The amount of training data was selected in such way that the addition of new data points did not significantly improve classification accuracy. Swimming pools were sampled manually due to their scarcity. To evaluate the results of the classification between the two methods, we used an expert-based manual delineation of Ouagadougou, based on building size and density [44] (Figure 4). In each one of these built-up types, we randomly sampled 150 points adding up to a total of 1650 points, and computed the Overall Accuracy (OA), as well as the F-score for each LULC class. No overlapping between training and testing data was allowed.

**Table 1.** Training objects for each LULC class and method.

| LULC | Description | Training Set Size |
|---|---|---|
| Buildings (BU) | | 400 |
| Swimming Pool (SP) | | 179 |
| Artificial Ground Surface (AS) | Asphalt, concrete, semi-built-up constructions | 216 |
| Bare Soil (BS) | | 399 |
| Tree (TR) | | 191 |
| Low Vegetation (LV) | Grass, bushes, dry vegetation | 702 |
| Inland Water (IW) | Lakes, ponds, rivers, wetlands | 205 |
| Shadow (SH) | | 186 |

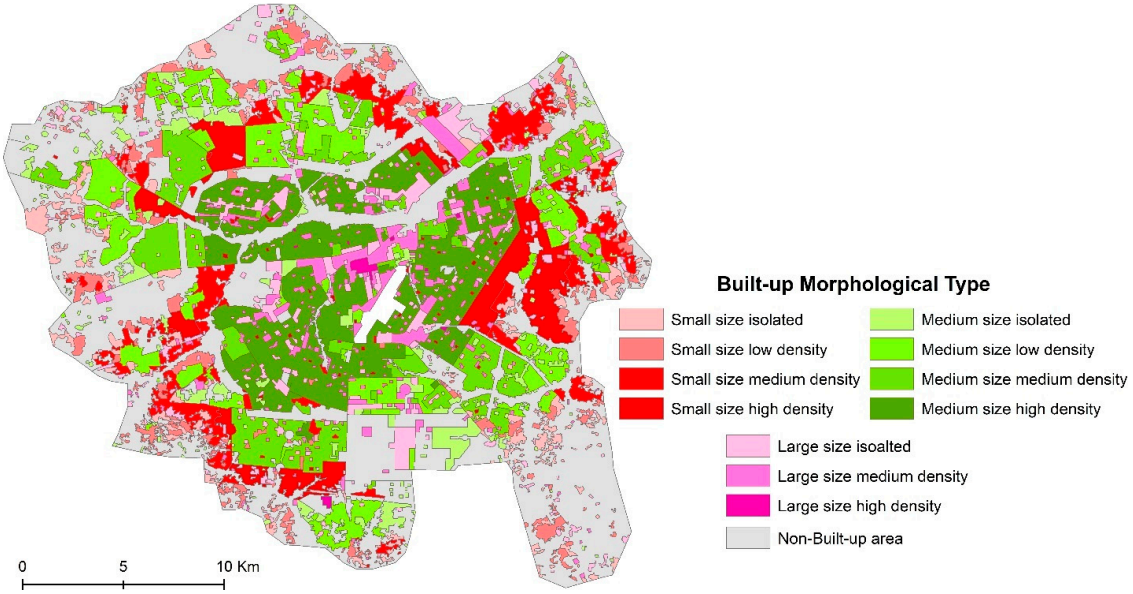


**Figure 4.** Morphological delineation of Ouagadougou based on built-up size and density categories.

To classify the whole image, we computed several descriptive statistics for segments, based on the values of the pixels located within the segment, i.e., the values of each spectral band, NDVI values, and nDSM values (min, median, mean, max, range, 1st and 3rd quantiles and sum) as well as geometrical covariates (fractal dimension, perimeter, area, compactness). An Extreme Gradient Boosting (XGBoost, R 3.5.1) classifier was used as it was recently shown to outperform benchmark classifiers such as Support Vector Machine in VHR LULC classifications [14]. XGBoost is an ensemble of Classification and Regression Trees that is based in the principle of boosting [61]. The parameters of the algorithm were tuned through Bayesian Optimization [14,62], to ensure the quality of the results. Finally, we performed feature selection to reduce the computational burden and potentially increase the predictive capabilities of the model by deploying the popular Variable Selection with Random Forests (VSURF) algorithm, which is suited for tree-based classifiers such as XGBoost [63,64]. Out of the initial 59 features, 18 were selected by VSURF to build the most discriminant, redundancy-free model.

### *2.4. Segmentation Goodness Metrics*

To evaluate the effect of SPUSPO on the segmentation of buildings, we compared the cutline-based segmentation and the global approach against reference data. In detail, we manually delineated 100 buildings that were randomly selected from the pool of training data used for the LULC classification. Finally, we computed the *Area Fit Index* (*AFI*) which is a commonly used joint index of over- and undersegmentation [31,32,53]:

$$AFI = \frac{area(x_i) - area(y_{imax})}{area(x_i)} \quad (7)$$

where $x_i$ is the reference object and $y_{imax}$ is the largest relevant segment intersecting $x_i$. Values closer to 0 suggest a better segmentation, values > 0 imply oversegmentation whereas values < 0 undersegmentation.

### *2.5. Computational Requirements and Data Availability*

The computing infrastructure used for the experiments consisted of two Intel® Xeon® CPU E5-2690 (2 processors of 2.90 GHz, 16 cores, 32 processing threads) and 96 GB of RAM. Segmenting the WorldView-3 image with a single TP parameter (tiled) required roughly 20 h of processing time while on average, a SPUSPO method required about 63 hours by exploiting the parallelization of the 'i.segment.uspo' module of GRASS [56]. The code, results and processed material is openly accessible in the following repository (https://zenodo.org/record/1341116#.W3FSUvZuJ_t) [65].

## 3. Results

### *3.1. Threshold Parameter Variation*

The spatial variation of the TP was a function of the size and geometry of the subsets used for local optimization. Figure 5 demonstrates that the variation follows patterns of the landscape. The locations where high TP values were selected as optimal were mainly clustered around unplanned, low elevated neighborhoods, whereas the locations where very low TP values were selected as optimal were mostly found in vegetated areas, potentially due to their unique spectral properties (high local variation in the NIR band). The local outputs of each metric used for the local USPO calculations can also be enlightening with respect to illustrating the level of spatial heterogeneity of the imagery. Figures 6 and 7 confirm that MI and WV have an inverse relationship, with MI being decisive in optimization in the central and eastern regions of unplanned areas, and vice-versa. The SPSI value was 1.5 for P1, and 2 for P2 and P3, indicating a non-stationary variation in optimal TP values.

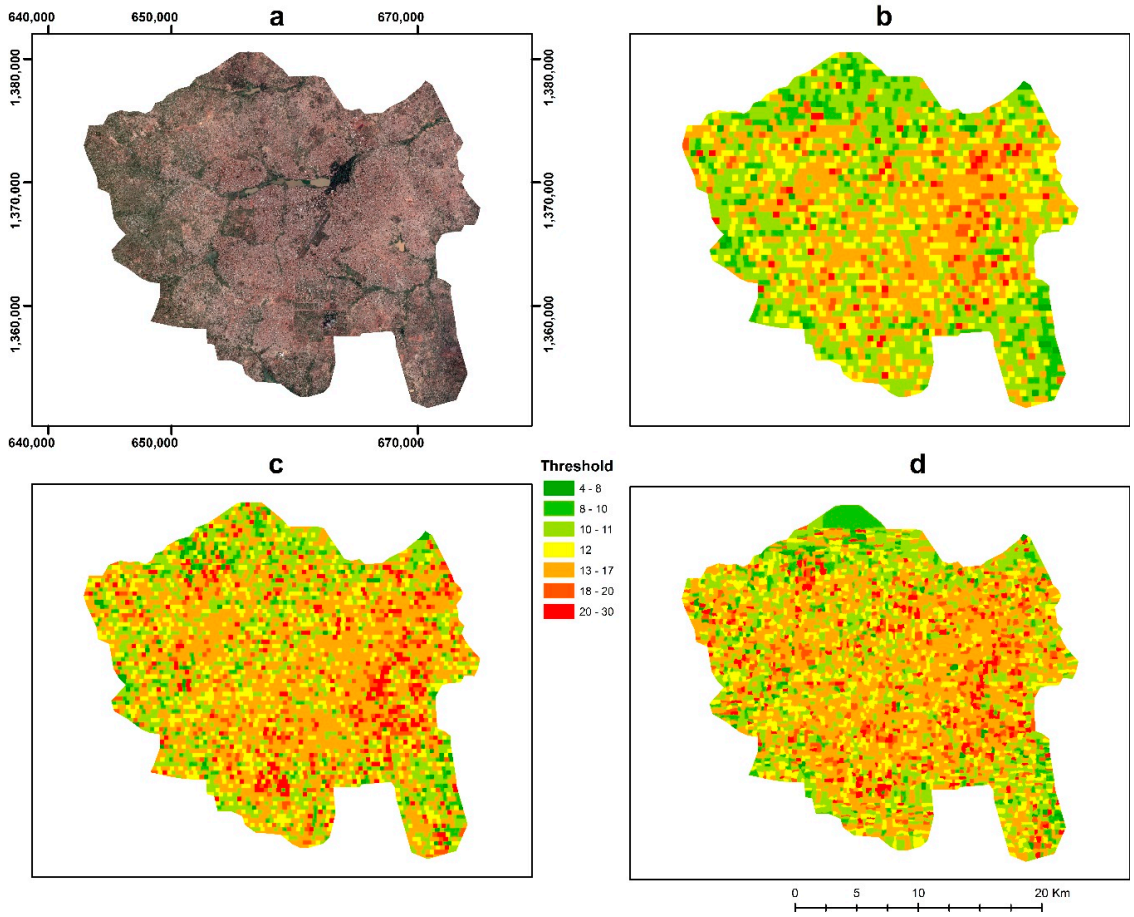


**Figure 5.** Spatial variation of the threshold parameter (TP) across Ouagadougou. (**a**) WorldView-**3** RGB composite, partitioning by (**b**) P1 (**c**) P2 and (**d**) P3 approaches, respectively. The TP controls the average size of the created segments.

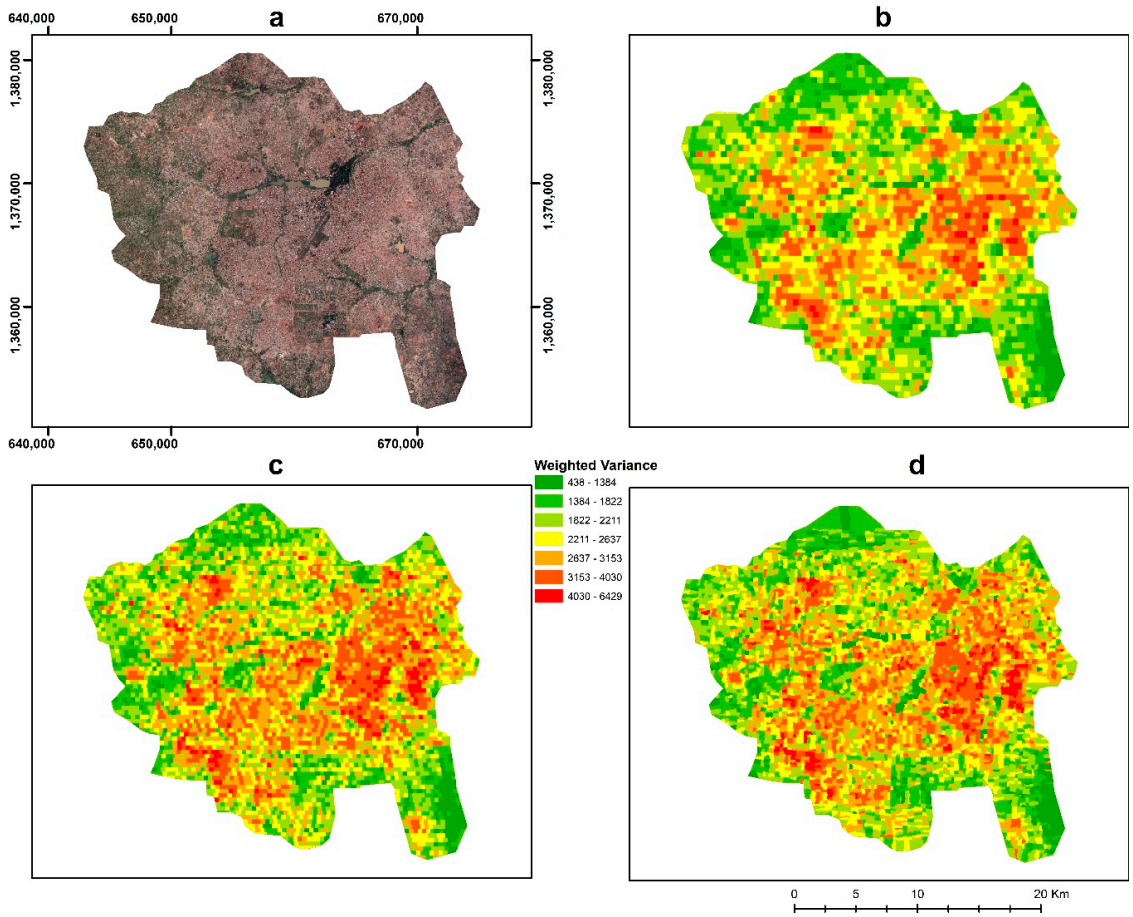


**Figure 6.** Spatial variation of weighted variance (WV) across Ouagadougou. (**a**) WorldView-3 RGB composite, partitioning by (**b**) P1, (**c**) P2 and (**d**) P3 approaches, respectively. High values of WV indicate large intra-segment variability while low values describe more homogenous objects.

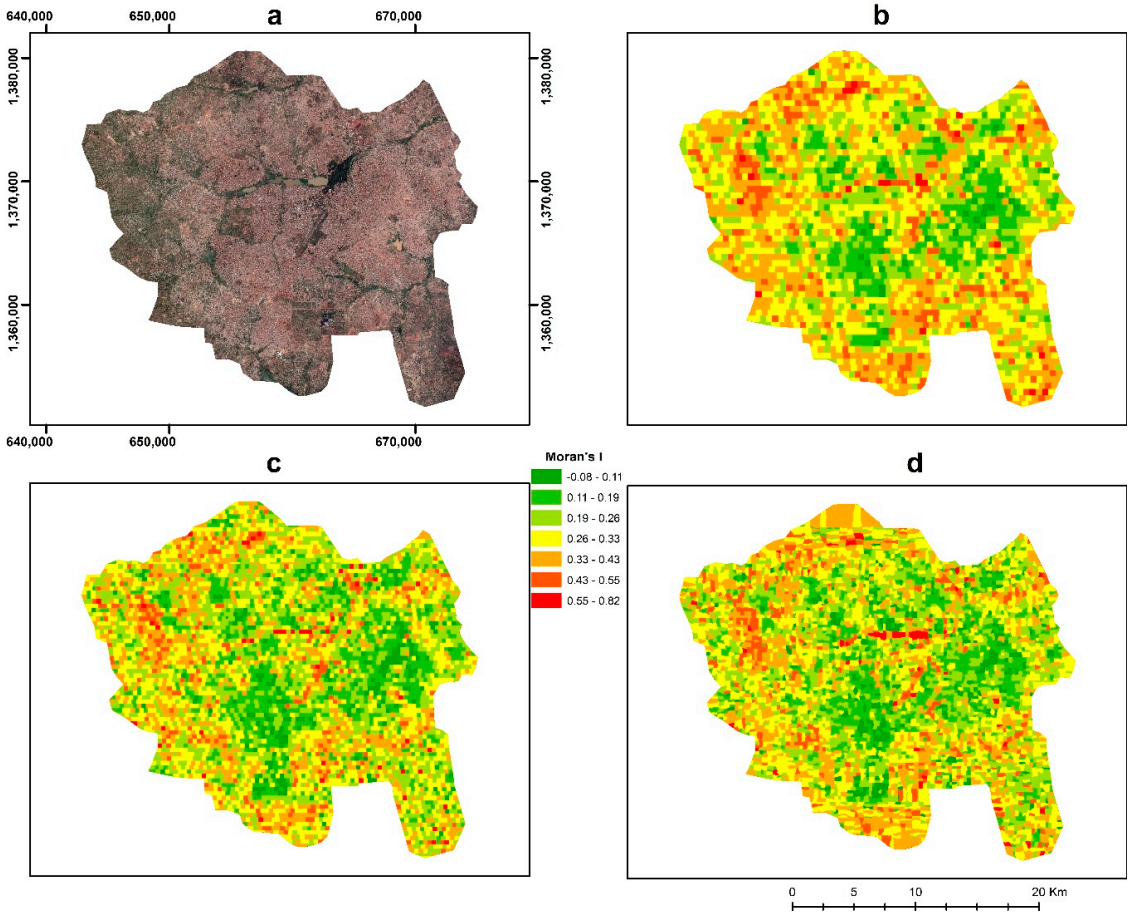


**Figure 7.** Spatial variation of Moran's I (MI) values across Ouagadougou. (**a**) WorldView-3 RGB composite, partitioning by (**b**) P1 (**c**) P2 and (**d**) P3 approaches, respectively. The higher the MI value, the stronger the effect of spatial autocorrelation between a created segment and its neighbors.

The variability of these parameters was also visualized in a set of boxplots in Figure 8. From this figure, the TP parameter variation is slightly smaller for the P1 approach than for the other two partitioning methods, possible because image partitions of P1 are larger than those of P2 and P3, and thus do not capture as much of the local heterogeneity in urban structure. Notably, when using smaller spatial partitions, MI tends to decrease (and WV tends to increase), which constitute the differences in TP among the different methods.

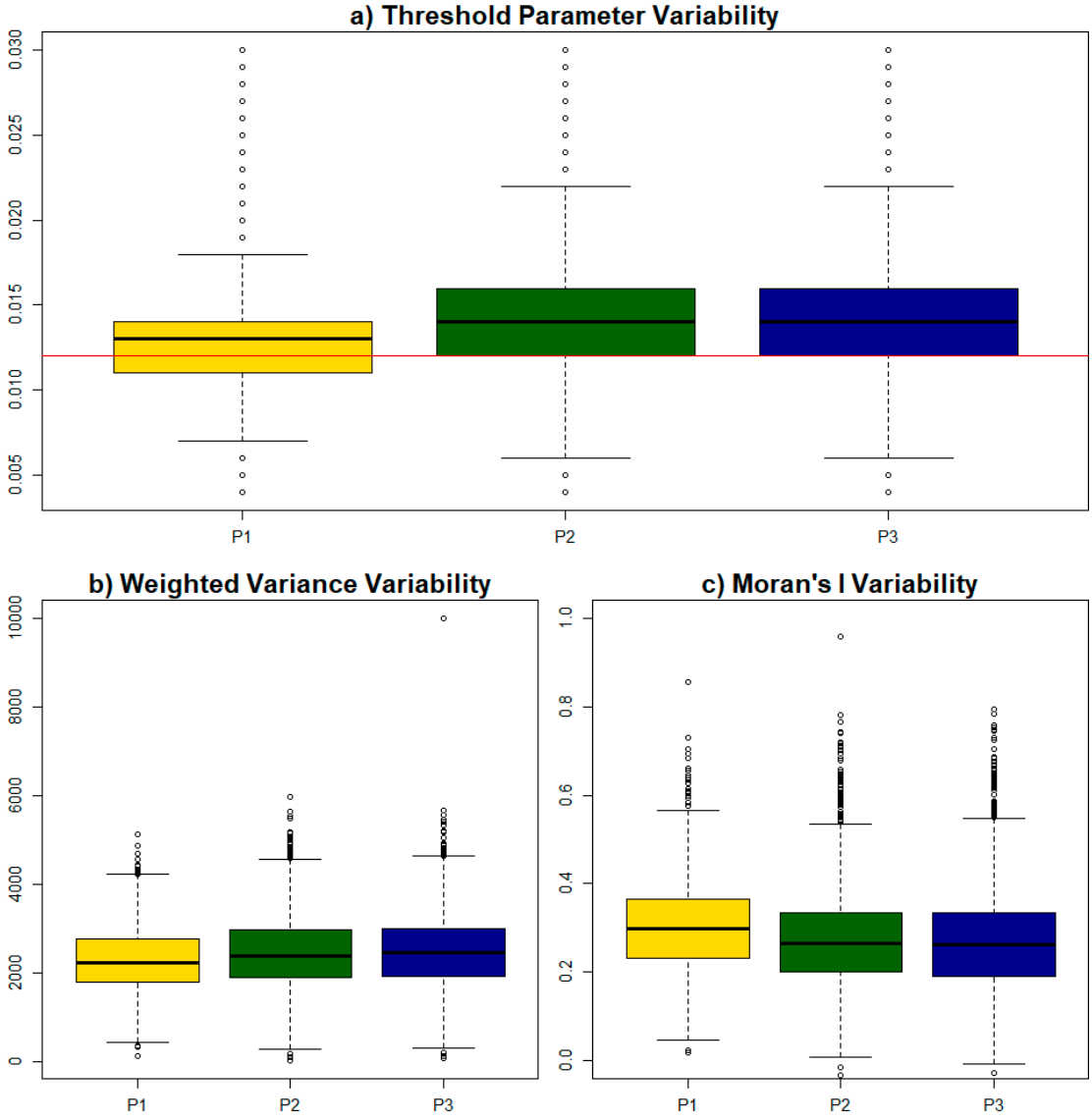


**Figure 8.** Boxplots demonstrating the variability of (**a**) the TP, (**b**) MI and (**c**) WV for the different partitioning approaches (P1, P2, P3).

### *3.2. Land-Use Land-Cover Classification*

The results of the LULC classification were found to be affected by the segmentation quality. Figures 9 and 10 show case how SPUSPO could enhance classification accuracy by producing segments better fitting the local environment, in various areas in Ouagadougou. Figure 9 demonstrates that in both planned and unplanned regions, the improvement in classification results was mainly due to the cutlines segmentation, delineating the buildings in a less oversegmenting fashion, avoiding overestimation of built-up near the borders due to the inconsistent and "patchy" nature of the nDSM as a predictor, that does not closely follow built-up boundaries.

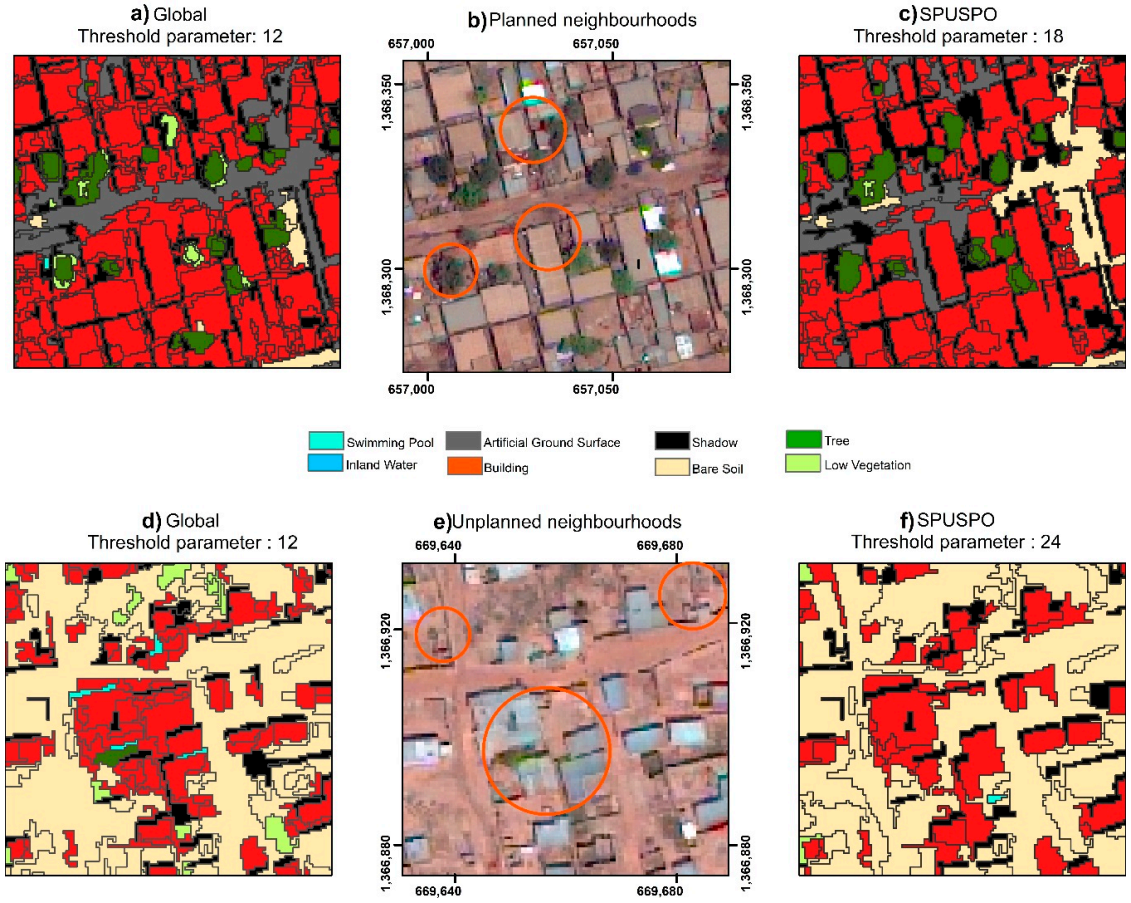


**Figure 9.** Example of the LULC map classification in a planned and unplanned built-up area. (**a**) LULC classification with a global approach in a planned neighborhood, (**b**) RGB Pleiades Composite, (**c**) LULC classification with a cutline approach in an unplanned neighborhood, and (**d**) LULC classification with a global approach in a planned neighborhood, (**e**) RGB Pleiades Composite, (**f**) LULC classification with a cutline approach in an unplanned neighborhood.

LULC classification based on SPUSPO was superior for vegetation and waterbodies of Ouagadougou. Figure 10 demonstrates cases of confusion between low and high vegetation, when using a global approach. Additionally, the misclassification of water as built-up is significantly less with SPUSPO. Notably, a scene might be segmented with intrinsically different thresholds (Figure 10f), which implies that the reason SPUSPO methods performed better is their incorporation of only the spatial information of the segmented region, and not information that comes from locations far away, which might not be useful at the local level.

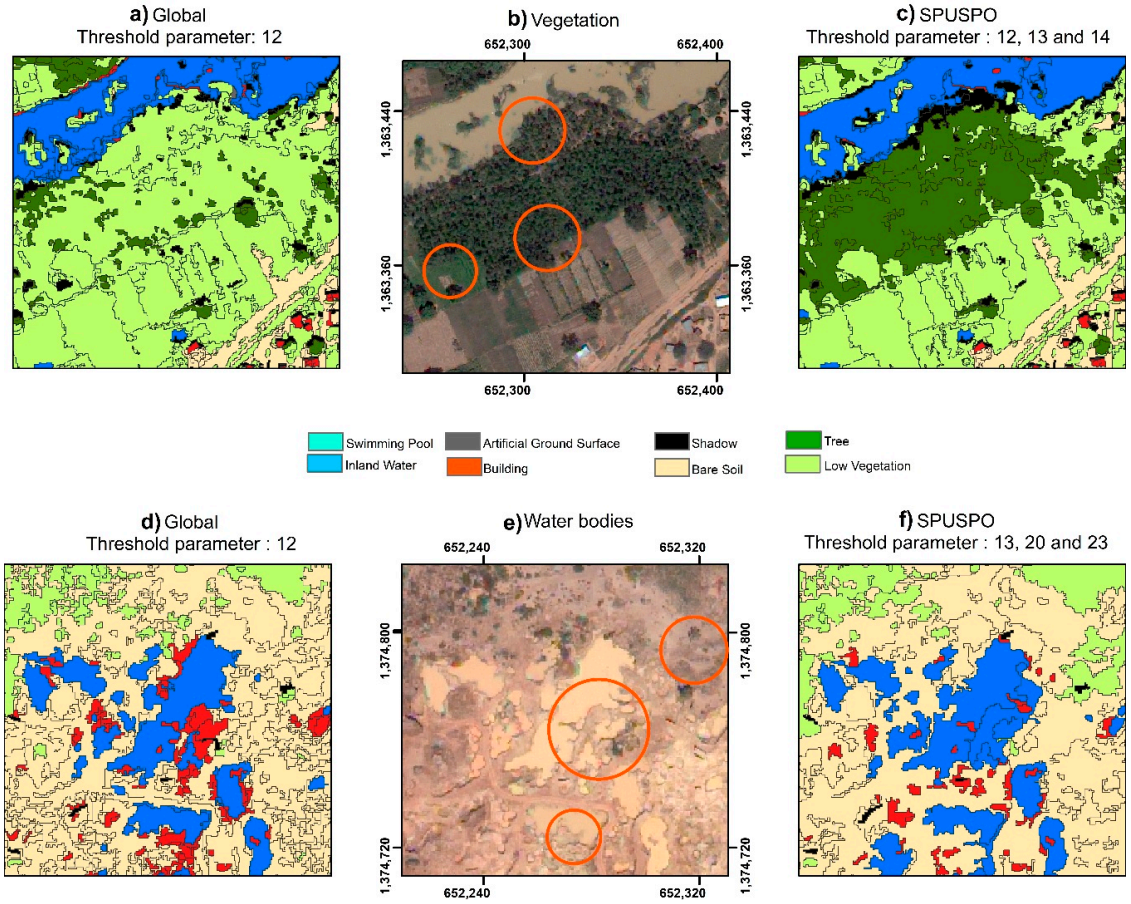


**Figure 10.** Example of the LULC map classification in a vegetated regions and inland water bodies. (**a**) LULC classification with a global approach in a forested area, (**b**) RGB Pleiades Composite, (**c**) LULC classification with a cutline approach in a forested area, (**d**) LULC classification with a global approach in water bodies, (**e**) RGB Pleiades Composite, and (**f**) LULC classification with a cutline approach in water bodies.

The Overall Accuracy for the SPUSPO and global optimization based on the reference set was 90.5% and 89%, respectively. Moreover, the differences among them were statistically significant, based on a two-tailed McNemar's test of similarity ($p < 0.05$). The local optimization was superior for most cases, both when concerning the OA and per-class evaluation metrics (Table 2). The largest improvements were found in the classification of inland water and shadows (+18% and +3% increase on the F1 score, respectively).

**Table 2.** Precision, Recall and F-score metrics for each LULC class with SPUSPO and global USPO, respectively.

| | **Precision** | | **Recall** | | **F1** | |
|---|---|---|---|---|---|---|
| Class | SPUSPO | Global | SPUSPO | Global | SPUSPO | Global |
| Building | 0.93 | 0.93 | 0.94 | 0.93 | 0.94 | 0.93 |
| Artificial Ground Surface | 0.83 | 0.83 | 0.88 | 0.86 | 0.85 | 0.84 |
| Bare Soil | 0.88 | 0.84 | 0.87 | 0.87 | 0.88 | 0.86 |
| Tree | 0.81 | 0.81 | 0.91 | 0.93 | 0.85 | 0.87 |
| Low veg | 0.94 | 0.94 | 0.89 | 0.86 | 0.91 | 0.90 |
| Inland Water | 0.86 | 0.73 | 0.66 | 0.47 | 0.75 | 0.57 |
| Shadow | 0.94 | 0.90 | 0.95 | 0.95 | 0.95 | 0.92 |

An additional, indirect way to assess the segmentation quality is to investigate the variable importance of the geometrical covariates. The geometrical covariates that were used in the classification model after VSURF feature selection took place were perimeter, area, and fractal dimension. Figure 11 illustrates the improved effect a local approach has on the importance of most of these variables, further supporting the merit of using SPUSPO. The interpretation of the results, refers to the gain in model accuracy when a feature is used in the splits of the XGBoost tree development. The importance of these covariates is varying, but in all cases, the local approach further enhances their predictive power for classification, since the segments fit better the variability of the local environment.

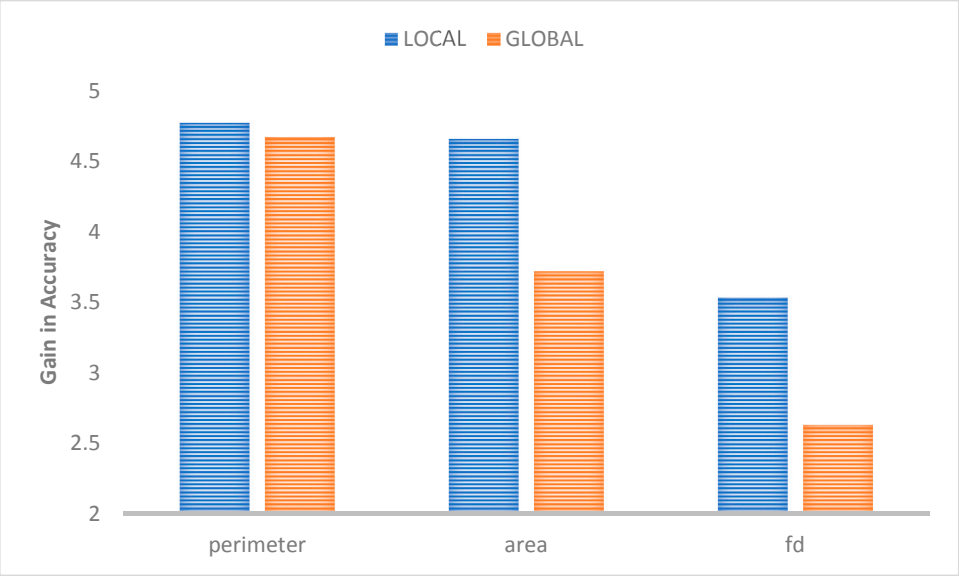


**Figure 11.** Feature importance of geometrical covariates, as derived from an XGBoost classifier, for the global and cutline segmentation-based approaches, respectively. The method used to derive importance is the gain in accuracy.

### *3.3. Segmentation Goodness Metrics*

The results of the AFI for buildings are depicted in Table 3 through several descriptive statistics. As expected, the building objects were less over segmented with SPUSPO, because the parameter was spatially adapting to characteristics of each built-up neighborhood in Ouagadougou (Figure 12). The AFI values of the local method were consistently closer to zero compared to their counterpart, further promoting the use of this approach.

**Table 3.** *Area Fit Index* for building objects in Ouagadougou. Values closer to 0 suggest a better segmentation, values > 0 imply over segmentation while values < 0 under segmentation.

| Descriptive Statistics | Area Fit Index (*AFI*) | |
|---|---|---|
| | SPUSPO | Global |
| 1st | 0.04 | 0.11 |
| Median | 0.22 | 0.38 |
| Mean | 0.28 | 0.36 |
| 3rd | 0.53 | 0.62 |

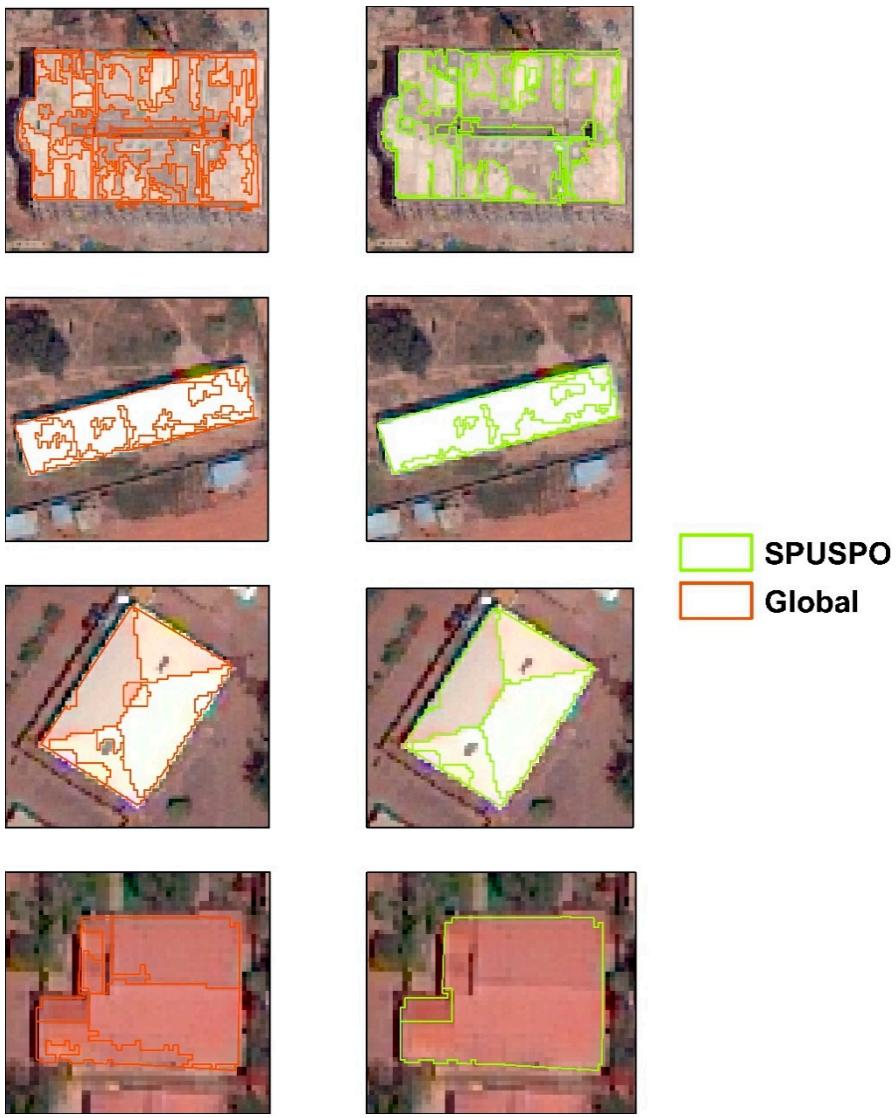


**Figure 12.** Example segmentations of buildings in Ouagadougou. Red color indicates segments created by a global approach, while green color indicates segments coming from SPUSPO. The decrease of over segmentation is evident in most cases, as the parameters are derived from neighboring locations, better fitting the data structure.

## 4. Discussion

The results suggested that the benefits of performing SPUSPO, are multiple. To start with, it allows for the local variations in spectral and spatial heterogeneity within an image to be incorporated into the segmentation parameter optimization approach, which is more intuitive because the optimization procedure is derived using the actual locations they are being applied to and not from locations situated afar. This supports the hypothesis that in large and heterogeneous areas, a single TP may be inadequate, as it is simply an average expression of several non-stationary processes. The results confirm prior analysis in another Sub-Saharan city of Dakar, where a semi-automated local approach outperformed classical optimization methods [54]. Moreover, several other studies have described how regionalized approaches can be of merit for urban, semi-rural, and agricultural environments [35,43,44]. Nonetheless, an important facet that has been neglected so far is how to partition the landscape in geographically large areas in conjunction with VHR imagery, and in the absence of reference data such as parcels or blocks. For a continuous LULC map, an appropriate delineation of the image is important, as it must be as adjustable to landscape patterns, such as streets or roofs, as much as

possible to avoid/reduce edge effects. Although all local approaches showed they can be of merit, the cutline-based partition helped to specifically address these issues. Undertaking SPUSPO, produced higher classification accuracy than using a traditional global optimization method (+1.5% increase in OA). The results are confirmed further using AFI as a segmentation goodness metric, which showed that building segments from applying SPUSPO are less oversegmented than their global counterparts, with mean values of 0.28 and 0.36 for SPUSPO and global USPO, respectively. The analysis validated our initial hypothesis that the way we look at the data can produce significantly different results, and is related to the importance of appropriate spatial scale selection in geography, which was largely signified through the work of Woodcock and Strahler [66] and Fotheringham et al. [67]. Additionally, a local segmentation optimization approach is not only linked to traditional GEOBIA analysis, but might be needed in large scale applications where deep learning classification is coupled with segments to achieve better object delineation/extraction as demonstrated recently in References [68–70]. Another important piece of information that we can extract from these methods is the ability to map intermediate and final results, which can be enlightening both as a general understanding of how spatial processes operate in the local scale, but also how to calibrate segmentation parameters in further processing if an unsupervised multi-scale framework is selected [18]. The LULC products in SSA cities are often used as inputs for fine scale population modelling, land use, and spatial planning, and consequently, effective policy making, given the extreme scarcity of reference information [2,71,72]. This is significant for the outcome of our analyses because there was better prediction of most classes by the SPUSPO approach; it presents an additional motivation to partake of a local method to reduce error propagation in secondary models.

The main limitation of SPUSPO is the increased computational time and experimentation to detect a satisfactory spatial level to analyze image information, which can vary depending on the image resolution and study area, leading to a trade-off between computational requirements and performance. Therefore, more sophisticated methods are needed to help establish an efficient framework to fully exploit the benefits of local optimization. Ideally, in large and heterogeneous areas, a spatial partition should not suffer from edge effects and should meaningfully delineate the landscape with a certain degree of intra-homogeneity. Cutline partitioning satisfies both criteria to some extent, but its effectiveness can only be determined post-hoc, which increases the computational and time demands as several cutline partitions may need to be evaluated. More adequate methods that can focus in a priori determination of a suitable scale using image statistics, such as spatial dependency among regions [73], could be of benefit to achieve this, particularly in a multi-scale context. Other research should explore the potential of multi-resolution imagery to define operational partitions using top down approaches. For instance, a low-medium resolution LULC product can define homogeneous regions to apply SPUSPO using finer resolution imagery. Moreover, noise additive models could help in better establishing a comparative framework among different segmentation approaches, particularly for SAR or hyperspectral data [74]. A lot of the limitations that come with involving local methods, can be significantly reduced (i) by utilizing GRASS GIS, which is highly parallelized in the USPO optimization module and more notably, performs all the operations in a raster format and does not require vector conversion at any moment, dramatically boosting its effectiveness for large-scale computing; and (ii) invoking state-of-the-art segmentation algorithms, with respect to their computational efficiency, as recently shown by Gu et al. [75].

## 5. Conclusions

In this study, the optimization of a region-growing segmentation algorithm was attempted using a spatially varying parameter model, named SPUSPO. The whole framework was developed with a focus on automation and large-scale analysis of VHR imagery. The results validated our hypothesis that in large and heterogeneous areas, using only a single set of parameters to optimize the region-growing algorithm was inadequate. Employing as a case study, the city of Ouagadougou, it was demonstrated that undertaking local optimization methods was of merit and led to significantly

better LULC classification results (+1.5% increase in OA), validated by a McNemar's test of similarity. Moreover, at the segmentation level, building delineation was improved with a mean Area Fit Index of 0.28 and 0.36 for SPUSPO and global USPO, respectively. Moreover, the feature importance of geometrical covariates is recommended as an indirect measure to assess the quality of a segmentation. We demonstrated that geometrical features were more important and predictive when using local approaches. Finally, GRASS GIS was heavily utilized and is promoted as an open source tool to handle large volumes of data with advanced analysis techniques.

**Author Contributions:** S.G. wrote the manuscript and performed the analysis. M.L. developed the cutline algorithm. T.G. provided technical assistance and helped develop the experiments. B.J., S.V. and E.W. provided valuable feedback and comments during the internal revisions of the manuscript.

**Acknowledgments:** This work was supported by BELSPO (Belgian Science Policy Office) in the frame of the STEREO III program—project REACT (SR/00/337). We would also like to thank the three reviewers for their useful and insightful comments and recommendations which significantly improved the quality of the manuscript. 

**Conflicts of Interest:** The authors declare no conflict of interest.

## References

1. Grippa, T.; Lennert, M.; Beaumont, B.; Vanhuysse, S.; Stephenne, N.; Wolff, E. An open-source semi-automated processing chain for urban object-based classification. *Remote Sens.* **2017**, *9*, 358. [CrossRef]
2. Kabaria, C.W.; Molteni, F.; Mandike, R.; Chacky, F.; Noor, A.M.; Snow, R.W.; Linard, C. Mapping intra-urban malaria risk using high resolution satellite imagery: A case study of Dar es Salaam. *Int. J. Health Geogr.* **2016**, *15*, 26. [CrossRef] [PubMed]
3. Linard, C.; Gilbert, M.; Snow, R.W.; Noor, A.M.; Tatem, A.J. Population distribution, settlement patterns and accessibility across Africa in 2010. *PLoS ONE.* **2012**, *7*, e31743. [CrossRef] [PubMed]
4. Taubenbock, H.; Wurm, M.; Setiadi, N.; Gebert, N.; Roth, A.; Strunz, G.; Birkmann, J.; Dech, S. Integrating remote sensing and social science. In Proceedings of the IEEE Joint Urban Remote Sensing Event, Shanghai, China, 20–22 May 2009.
5. Niehoff, D.; Fritsch, U.; Bronstert, A. Land-use impacts on storm-runoff generation: Scenarios of land-use change and simulation of hydrological response in a meso-scale catchment in SW-Germany. *J. Hydrol.* **2002**, *267*, 80–93. [CrossRef]
6. Otukei, J.R.; Blaschke, T. Land cover change assessment using decision trees, support vector machines and maximum likelihood classification algorithms. *Int. J. Appl. Earth Obs. Geoinf.* **2010**, *12*, 27–31. [CrossRef]
7. Manakos, I.; Braun, M. *Land Use and Land Cover Mapping in Europe*, 3rd ed.; Springer Nature: Heidelberg, Germany, 2014.
8. Iizuka, K.; Johnson, B.A.; Onishi, A.; Magcale-Macandog, D.B.; Endo, I.; Bragais, M. Modeling Future Urban Sprawl and Landscape Change in the Laguna de Bay Area, Philippines. *Land* **2017**, *6*, 26. [CrossRef]
9. Blaschke, T.; Hay, G.J.; Kelly, M.; Lang, S.; Hofmann, P.; Addink, E.; Queiroz Feitosa, R.; van der Meer, F.; van der Werff, H.; van Coillie, F.; et al. Geographic Object-Based Image Analysis—Towards a new paradigm. *ISPRS J. Photogramm. Remote Sens.* **2014**, *87*, 180–191. [CrossRef] [PubMed]
10. Chen, G.; Weng, Q.; Hay, G.J.; He, Y. Geographic Object-based Image Analysis (GEOBIA): Emerging trends and future opportunities. *GIScience Remote Sens.* **2018**, 55. [CrossRef]
11. Gu, H.; Li, H.; Yan, L.; Liu, Z.; Blaschke, T.; Soergel, U. An object-based semantic classification method for high resolution remote sensing imagery using ontology. *Remote Sens.* **2017**, *9*, 329. [CrossRef]
12. Blaschke, T. Object based image analysis for remote sensing. *ISPRS J. Photogramm. Remote Sens.* **2010**, *65*, 2–16. [CrossRef]
13. Rasanen, A.; Rusanen, A.; Kuitunen, M.; Lensu, A. What makes segmentation good? A case study in boreal forest habitat mapping. *Int. J. Remote Sens.* **2013**, *34*, 8603–8627. [CrossRef]

14. Georganos, S.; Grippa, T.; Vanhuysse, S.; Lennert, M.; Shimoni, M.; Wolff, E. Very high resolution object-based land use-land cover urban classification using extreme gradient boosting. *IEEE Geosci. Remote Sens. Lett.* **2018**, *15*, 607–611. [CrossRef]
15. Ma, L.; Li, M.; Blaschke, T.; Ma, X.; Tiede, D.; Cheng, L.; Chen, Z.; Chen, D. Object-based change detection in urban areas: The effects of segmentation strategy, scale, and feature space on unsupervised methods. *Remote Sens.* **2016**, *8*, 761. [CrossRef]
16. Srivastava, M.; Arora, M.K.; Raman, B. Selection of critical segmentation-A prerequisite for Object based image classification. In Proceedings of the 2015 National Conference on Recent Advances in Electronics & Computer Engineering (RAECE), Roorkee, India, 13–15 February 2015.
17. Lowe, S.H.; Guo, X. Detecting an optimal scale parameter in object-oriented classification. *IEEE J. Sel. Top. Appl. Earth Obs. Remote Sens.* **2011**, *4*, 890–895. [CrossRef]
18. Johnson, B.; Bragais, M.; Endo, I.; Magcale-Macandog, D.; Macandog, P. Image segmentation parameter optimization considering within- and between-segment heterogeneity at multiple scale levels: Test case for mapping residential areas using landsat imagery. *ISPRS Int. J. Geo-Inform.* **2015**, *4*, 2292–2305. [CrossRef]
19. Gao, Y.A.N.; Mas, J.F.; Kerle, N.; Navarrete Pacheco, J.A. Optimal region growing segmentation and its effect on classification accuracy. *Int. J. Remote Sens.* **2011**, *32*, 3747–3763. [CrossRef]
20. Yang, J.; Li, P.; He, Y. A multi-band approach to unsupervised scale parameter selection for multi-scale image segmentation. *ISPRS J. Photogramm. Remote Sens.* **2014**, *94*, 13–24. [CrossRef]
21. Zhang, Q.; Huang, X.; Zhang, L. An energy-driven total variation model for segmentation and classification of high spatial resolution remote-sensing imagery. *IEEE Geosci. Remote Sens. Lett.* **2013**, *10*, 125–129. [CrossRef]
22. Baatz, M.; Schape, A. Multiresolution Segmentation: An Optimization Approach for High Quality Multi-Scale Image Segmentation. 2000. Available online: https://www.semanticscholar.org/paper/Multiresolution-Segmentation-an-optimization-appro-Baatz-Sch%C3%A4pe/364cc1ff514a2e11d21a101dc072575e5487d17e (accessed on 20 December 2017).
23. Grybas, H.; Melendy, L.; Congalton, R.G. A comparison of unsupervised segmentation parameter optimization approaches using moderate- and high-resolution imagery. *GISci. Remote Sens.* **2017**, *54*, 515–533. [CrossRef]
24. Du, S.; Guo, Z.; Wang, W.; Guo, L.; Nie, J. A comparative study of the segmentation of weighted aggregation and multiresolution segmentation. *GISci. Remote Sens.* **2016**, *53*, 1–20. [CrossRef]
25. Mesner, N.; Oštir, K. Investigating the impact of spatial and spectral resolution of satellite images on segmentation quality. *J. Appl. Remote Sens.* **2014**, *8*, 83696. [CrossRef]
26. Zhong, Y.; Gao, R.; Zhang, L. Multiscale and multifeature normalized cut segmentation for high spatial resolution remote sensing imagery. *IEEE Trans. Geosci. Remote Sens.* **2016**, *54*, 6061–6075. [CrossRef]
27. Duro, D.C.; Franklin, S.E.; Dube, M.G. A comparison of pixel-based and object-based image analysis with selected machine learning algorithms for the classification of agricultural landscapes using SPOT-5 HRG imagery. *Remote Sens. Environ.* **2012**, *118*, 259–272. [CrossRef]
28. Zhang, H.; Fritts, J.E.; Goldman, S.A. Image segmentation evaluation: A survey of unsupervised methods. Comput. Vis. *Image Underst.* **2008**, *110*, 260–280. [CrossRef]
29. Flanders, D.; Hall-Beyer, M.; Pereverzoff, J. Preliminary evaluation of ecognition object-based software for cut block delineation and feature extraction. *Can. J. Remote Sens.* **2003**, *29*, 441–452. [CrossRef]
30. Belgiu, M.; Drăgut, L. Random forest in remote sensing: A review of applications and future directions. *ISPRS J. Photogramm. Remote Sens.* **2016**, *114*, 24–31. [CrossRef]
31. Clinton, N.; Holt, A.; Scarborough, J.; Yan, L.; Gong, P. Accuracy assessment measures for object-based image segmentation goodness. *Photogramm. Eng. Remote Sens.* **2010**, *76*, 289–299. [CrossRef]
32. Costa, H.; Foody, G.M.; Boyd, D.S. Supervised methods of image segmentation accuracy assessment in land cover mapping. *Remote Sens. Environ.* **2018**, *205*, 338–351. [CrossRef]
33. Belgiu, M.; Drăguţ, L. Comparing supervised and unsupervised multiresolution segmentation approaches for extracting buildings from very high resolution imagery. *ISPRS J. Photogramm. Remote Sens.* **2014**, *96*, 67–75. [CrossRef] [PubMed]
34. Drăguţ, L.; Tiede, D.; Levick, S.R. ESP: A tool to estimate scale parameter for multiresolution image segmentation of remotely sensed data. *Int. J. Geogr. Inf. Sci.* **2010**, *24*, 859–871. [CrossRef]

35. Kavzoglu, T.; Erdemir, M.Y.; Tonbul, H. Classification of semiurban landscapes from very high-resolution satellite images using a regionalized multiscale segmentation approach. *J. Appl. Remote Sens.* **2017**, *11*, 35016. [CrossRef]
36. Johnson, B.; Xie, Z. Unsupervised image segmentation evaluation and refinement using a multi-scale approach. *ISPRS J. Photogramm. Remote Sens.* **2011**, *66*, 473–483. [CrossRef]
37. Dragut, L.; Csillik, O.; Eisank, C.; Tiede, D. Automated parameterisation for multi-scale image segmentation on multiple layers. *ISPRS J. Photogramm. Remote Sens.* **2014**, *88*, 119–127. [CrossRef] [PubMed]
38. Espindola, G.M.; Camara, G.; Reis, I.A.; Bins, L.S.; Monteiro, A.M. Parameter selection for region-growing image segmentation algorithms using spatial autocorrelation. *Int. J. Remote Sens.* **2006**, *27*, 3035–3040. [CrossRef]
39. Zhang, X.; Feng, X.; Xiao, P.; He, G.; Zhu, L. Segmentation quality evaluation using region-based precision and recall measures for remote sensing images. *ISPRS J. Photogramm. Remote Sens.* **2015**, *102*, 73–84. [CrossRef]
40. Grippa, T.; Lennert, M.; Beaumont, B.; Vanhuysse, S.; Stephenne, N.; Wolff, E. An open-source semi-automated processing chain for urban obia classification. In Proceedings of the GEOBIA 2016: Solutions and Synergies, Enschede, The Netherlands, 14–16 September 2016.
41. Li, M.; Ma, L.; Blaschke, T.; Cheng, L.; Tiede, D. A systematic comparison of different object-based classification techniques using high spatial resolution imagery in agricultural environments. *Int. J. Appl. Earth Obs. Geoinf.* **2016**, *49*, 87–98. [CrossRef]
42. Ma, L.; Li, M.; Ma, X.; Cheng, L.; Du, P.; Liu, Y. A review of supervised object-based land-cover image classification. *ISPRS J. Photogramm. Remote Sens.* **2017**, *130*, 277–293. [CrossRef]
43. Cánovas-García, F.; Alonso-Sarría, F. A local approach to optimize the scale parameter in multiresolution segmentation for multispectral imagery. *Geocarto Int.* **2015**, *30*, 937–961. [CrossRef]
44. Grippa, T.; Georganos, S.; Vanhuysse, S.G.; Lennert, M.; Wolff, E. A local segmentation parameter optimization approach for mapping heterogeneous urban environments using VHR imagery. *Remote Sens. Technol. Appl. Urban Environ. II* **2017**, *10431*. [CrossRef]
45. Gorelick, N.; Hancher, M.; Dixon, M.; Ilyushchenko, S.; Thau, D.; Moore, R. Remote sensing of environment google earth engine: Planetary-scale geospatial analysis for everyone. *Remote Sens. Environ.* **2017**, *202*, 18–27. [CrossRef]
46. Tobler, W.R. A computer movie simulating urban growth in the detroit region. *Econ. Geogr.* **1970**, *46*, 234–240. [CrossRef]
47. Neteler, M.; Bowman, M.H.; Landa, M.; Metz, M. GRASS GIS: A multi-purpose open source GIS. *Environ. Model. Softw.* **2012**, *31*, 124–130. [CrossRef]
48. Grippa, T.; Georganos, S.; Zarougui, S.; Bognounou, P.; Diboulo, E.; Forget, Y.; Lennert, M.; Vanhuysse, S.; Mboga, N.; Wolff, E. Mapping urban land use at street block level using open street map, Remote Sensing Data, and Spatial Metrics. *ISPRS Int. J. Geo-Inform.* **2018**, *7*, 246. [CrossRef]
49. United Nations. *World Urbanization Prospects: The 2014 Revision, Highlights*, 3rd ed.; Population Division, United Nations: New York, NY, USA, 2014.
50. Schug, F.; Okujeni, A.; Hauer, J.; Hostert, P.; Nielsen Jonas Øand van der Linden, S. Mapping patterns of urban development in Ouagadougou, Burkina Faso, using machine learning regression modeling with bi-seasonal Landsat time series. *Remote Sens. Environ.* **2018**, *210*, 217–228. [CrossRef]
51. Momsen, E.; Metz, M.; GRASS Development TEAM. Module i.segment 2015. Available online: https://grass.osgeo.org/grass75/manuals/i.segment.html (accessed on 1 August 2018).
52. Böck, S.; Immitzer, M.; Atzberger, C. On the objectivity of the objective function—Problems with unsupervised segmentation evaluation based on global score and a possible remedy. *Remote Sens.* **2017**, *9*, 769. [CrossRef]
53. Georganos, S.; Lennert, M.; Grippa, T.; Vanhuysse, S.; Johnson, B.; Wolff, E. Normalization in unsupervised segmentation parameter optimization: A solution based on local regression trend analysis. *Remote Sens.* **2018**, *10*, 222. [CrossRef]
54. Georganos, S.; Grippa, T.; Lennert, M.; Vanhuysse, S.G.; Wolff, E. SPUSPO: Spatially Partitioned Unsupervised Segmentation Parameter Optimization for Efficiently Segmenting Large Heteregeneous Areas. In Proceedings of the 2017 Conference on Big Data from Space (BiDS'17), Toulouse, France, 28–30 November 2017.
55. Lennert, M.; GRASS Development TEAM. Module i.segment.uspo 2017. Available online: https://grass.osgeo.org/grass74/manuals/addons/i.segment.uspo.html (accessed on 1 August 2018).

56. Körting, T.S.; Castejon, E.F.; Fonseca, L.M.G. The divide and segment method for parallel image segmentation. In Proceedings of the International Conference on Advanced Concepts for Intelligent Vision Systems, Antwerp, Belgium, 18–21 September 2013.
57. Soares, A.R.; Körting, T.S.; Fonseca, L.M.G. Improvements of the divide and segment method for parallel image segmentation. *Rev. Bras. Cartogr.* **2016**, *68*.
58. Satnik, D.; GRASS Development TEAM. Module i.zc 2016. Available online: https://grass.osgeo.org/grass70/manuals/i.zc.html (accessed on 1 August 2018).
59. Lennert, M.; GRASS Development TEAM. Module i.cutlines 2018. Available online: https://grass.osgeo.org/grass74/manuals/addons/i.cutlines.html (accessed on 1 August 2018).
60. Osborne, P.E.; Foody, G.M.; Suárez-Seoane, S. Non-stationarity and local approaches to modelling the distributions of wildlife. *Divers. Distrib.* **2007**, *13*, 313–323. [CrossRef]
61. Chen, T.; Guestrin, C. XGBoost: Reliable large-scale tree boosting system. *arXiv* **2016**. [CrossRef]
62. Xia, Y.; Liu, C.; Li, Y.; Liu, N. A boosted decision tree approach using Bayesian hyper-parameter optimization for credit scoring. *Expert Syst. Appl.* **2017**, *78*, 225–241. [CrossRef]
63. Genuer, R.; Poggi, J.M.; Tuleau-Malot, C. VSURF: An R Package for variable selection using random forests. *R J.* **2015**, *7*, 19–33.
64. Georganos, S.; Grippa, T.; Vanhuysse, S.; Lennert, M.; Shimoni, M.; Kalogirou, S.; Wolff, E. Less is more: Optimizing classification performance through feature selection in a very-high-resolution remote sensing object-based urban application. *GISci. Remote Sens.* **2017**, 221–242. [CrossRef]
65. Georganos, S.; Grippa, T.; Lennert, M.; Johnson, B.A.; Vanhuysse, S.; Wolff, E. SPUSPO: Spatially Partitioned Unsupervised Segmentation Parameter Optimization for Efficiently Segmenting Large Heterogeneous Areas. Available online: https://zenodo.org/record/1341116#.W5S1oVKtZS0 (accessed on 31 August 2018).
66. Woodcock, C.E.; Strahler, A.H. The factor of scale in remote sensing. *Remote Sens. Environ.* **1987**, *21*, 311–332. [CrossRef]
67. Fotheringham, A.S.; Brunsdon, C.; Charlton, M. Geographically weighted regression: The analysis of spatially varying relationships. *Am. J. Agric. Econom.* **2004**, *86*, 554–556. [CrossRef]
68. Liu, T.; Abd-elrahman, A.; Jon, M.; Wilhelm, V.L.; Liu, T.; Abd-elrahman, A.; Jon, M.; Wilhelm, V.L. Comparing fully convolutional networks, random forest, support vector machine, and patch-based deep convolutional neural networks for object-based wetland mapping using images from small unmanned aircraft system. *GISci. Remote Sens.* **2018**, *55*, 243–264. [CrossRef]
69. Liu, T.; Abd-Elrahman, A. Deep convolutional neural network training enrichment using multi-view object-based analysis of Unmanned Aerial systems imagery for wetlands classification. *ISPRS J. Photogramm. Remote Sens.* **2018**, *139*, 154–170. [CrossRef]
70. Marmanis, D.; Schindler, K.; Wegner, J.D.; Galliani, S.; Datcu, M.; Stilla, U. Classification with an edge: Improving semantic image segmentation with boundary detection. *ISPRS J. Photogramm. Remote Sens.* **2018**, *135*, 158–172. [CrossRef]
71. Linard, C.; Tatem, A.J.; Gilbert, M. Modelling spatial patterns of urban growth in Africa. *Appl. Geogr.* **2013**, *44*, 23–32. [CrossRef] [PubMed]
72. Sandborn, A.; Engstrom, R.N. Determining the Relationship between Census Data and Spatial Features Derived From High-Resolution Imagery in Accra, Ghana. *IEEE J. Sel. Top. Appl. Earth Obs. Remote Sens.* **2016**, *9*, 1970–1977. [CrossRef]
73. Ming, D.; Li, J.; Wang, J.; Zhang, M. Scale parameter selection by spatial statistics for GeOBIA: Using mean-shift based multi-scale segmentation as an example. *ISPRS J. Photogramm. Remote Sens.* **2015**, *106*, 28–41. [CrossRef]
74. Yuan, Q.; Zhang, L.; Shen, H. Hyperspectral image denoising employing a spectral-spatial adaptive total variation model. *IEEE Trans. Geosci. Remote Sens.* **2012**, *50*, 3660–3677. [CrossRef]
75. Gu, H.; Han, Y.; Yang, Y.; Li, H.; Liu, Z.; Soergel, U.; Blaschke, T.; Cui, S. An efficient parallel multi-scale segmentation method for remote sensing imagery. *Remote Sens.* **2018**, *10*, 590. [CrossRef]


# Chapter 3

# Mapping the urban land use at street block level in data-poor context

**Grippa, Taïs**, Stefanos Georganos, Soukaina Zarougui, Pauline Bognounou, Eric Diboulo, Yann Forget, Moritz Lennert, Sabine Vanhuysse, Nicholus Mboga, and Eléonore Wolff. 2018. "**Mapping Urban Land Use at Street Block Level Using OpenStreetMap, Remote Sensing Data, and Spatial Metrics.**" ISPRS International Journal of Geo-Information 7 (7): 246. https://doi.org/10.3390/ijgi7070246.

International Journal of Geo-Information

MDPI

*Article*

# Mapping Urban Land Use at Street Block Level Using OpenStreetMap, Remote Sensing Data, and Spatial Metrics

**Taïs Grippa [1,*], Stefanos Georganos [1], Soukaina Zarougui [1], Pauline Bognounou [2], Eric Diboulo [3], Yann Forget [1], Moritz Lennert [1], Sabine Vanhuysse [1], Nicholus Mboga [1] and Eléonore Wolff [1]**

1 Department of Geoscience, Environment & Society, Université Libre De Bruxelles (ULB), 1050 Bruxelles, Belgium; sgeorgan@ulb.ac.be (S.G.); soukaina.zarougui@gmail.com (S.Z.); yann.forget@ulb.ac.be (Y.F.); mlennert@ulb.ac.be (M.L.); svhuysse@ulb.ac.be (S.V.); nmboga@ulb.ac.be (N.M.); ewolff@ulb.ac.be (E.W.)

2 Direction Générale des Impôts, Direction du Cadastre, 01 BP 119 Ouagadougou 01, Burkina Faso; bognounouoauline@gmail.com

3 Centre de Recherche en Santé de Nouna (CRSN), BP 02 Nouna, Burkina Faso; eric.diboulo@gmail.com

* Correspondence: tgrippa@ulb.ac.be; Tel.: +32-2-650-6803

Received: 1 June 2018; Accepted: 19 June 2018; Published: 22 June 2018


**Abstract:** Up-to-date and reliable land-use information is essential for a variety of applications such as planning or monitoring of the urban environment. This research presents a workflow for mapping urban land use at the street block level, with a focus on residential use, using very-high resolution satellite imagery and derived land-cover maps as input. We develop a processing chain for the automated creation of street block polygons from OpenStreetMap and ancillary data. Spatial metrics and other street block features are computed, followed by feature selection that reduces the initial datasets by more than 80%, providing a parsimonious, discriminative, and redundancy-free set of features. A random forest (RF) classifier is used for the classification of street blocks, which results in accuracies of 84% and 79% for five and six land-use classes, respectively. We exploit the probabilistic output of RF to identify and relabel blocks that have a high degree of uncertainty. Finally, the thematic precision of the residential blocks is refined according to the proportion of the built-up area. The output data and processing chains are made freely available. The proposed framework is able to process large datasets, given that the cities in the case studies, Dakar and Ouagadougou, cover more than 1000 km$^2$ in total, with a spatial resolution of 0.5 m.

**Keywords:** land use; street block; spatial metrics; landscape metrics; OpenStreetMap; machine learning; PostGIS; GRASS GIS; random forest

## 1. Introduction

As reported by the United Nations, urban areas currently contain more than 50% of the world's population. According to the latest estimates, this proportion will reach 60% by 2030 [1]. In developing countries, high urbanization rates and uncontrolled urban sprawl often lead to challenges such as inefficiency of transport systems, degradation of the environment, growth of informal settlements, and a proportion of the population living in deprived conditions. Availability of accurate and up-to-date information about the current situation of a city could help in defining and setting up adapted urban policies.

Among the set of potential geospatial information related to urban areas, population density and land use are probably the most important to an urban planner [2]. Unfortunately, they are limited

or not available at all in developing countries, as these lag behind the most developed countries in the adoption and use of geographic information systems (GIS) [3,4]. This is especially the case for Africa, which faces a critical need of geographic information [5–7]. For instance, a study showed that several important geographic datasets were still either unavailable or difficult to access in Africa [7]. Notwithstanding recent initiatives to alleviate this issue [8] and a stronger interest towards alternative data, such as volunteered geographic information (VGI) [9], more progress needs to be made.

In urban areas, land-use information can be mapped at different scales that range from cadastral plots to large neighborhoods. In this study, we chose to work at the street block level, as was the case in previous studies [2,10–12]. The street block, sometimes referred to as a "city block" or "land parcel", provides sufficient spatial detail to urban planners and have been depicted as the most fundamental and appropriate unit in which to map the urban structure [13–15]. Unfortunately, reference street block datasets were not accessible for our case studies, from either the local authorities and national mapping agencies or any other reliable source. We overcame this challenge by developing a semiautomated processing chain for the creation of street block geometries using OpenStreetMap (OSM) data [16]. OSM is open-data, meaning it can be accessed and used at no cost by anyone and for any purpose, which makes it an alternative source of data when the availability and access to geoinformation is limited. Disparaged during its early stages of development, the quality of OSM data has been improving rapidly, both in terms of completeness and of thematic accuracy. For that reason, it could become a key player in the coming decade for production and access to high-quality geoinformation in developing countries. As an example, a recent study proved the potential of OSM data to be used for increasing the thematic level of land-use/land-cover maps where there is a lack of official data [17].

To the best of our knowledge, few works [18,19] have proposed a methodology for the creation of street block geometries using OSM data. Long and Liu [18] proposed a method to automatically identify "land parcels" from OSM roads. They operated in the Chinese geographic context and developed a framework to address outdated, inexistent, or unavailable reference data. Their approach consists of using geometric operations to clear up the road network. Subsequently, land parcels are automatically created and defined as the remaining space when buffered roads are removed. Their approach proved to be a good approximation of the results obtain from conventional methods but suffered from incompleteness of the OSM road network, leading to the creation of large parcels in smaller cities. Their framework was used recently in other studies [20,21]. However, Long et al. [18] and Fan et al. [19] provided a theoretical framework without a ready-to-use computer code that limited the easy reproduction of their methods.

Studies aiming at mapping urban land use often make use of land-cover and/or ancillary reference geographic datasets, e.g., detailed cadastral datasets, socioeconomic datasets, or datasets that contain the location of urban facilities (schools, hospitals, shops, etc.) [11,20–22]. Despite their great potential for mapping land use at a fine scale, such exhaustive and detailed datasets are rarely available, especially in developing countries. Furthermore, the initial production and the process of keeping them updated are both costly and labor-intensive. Remote sensing solutions can be used as an alternative for creating and updating reliable land-use information on urban areas. The land use can be mapped directly from satellite imagery and/or from land-cover maps.

The latter approach usually relies on the computation of spatial metrics, also named "landscape metrics" [23]. These metrics have been widely used for the classification and characterization of urban or rural areas. They were first mainly used in the field of landscape ecology [24,25] for their ability to characterize landscapes as ecosystems according to the composition and spatial organization of the land cover classes they contain. Their use in urban areas dates back to the 2000s [26] for studying urban sprawl [27], urbanization gradient [28], or land-use changes [29].

More broadly, this study is part of two research projects, namely, MAUPP (maupp.ulb.ac.be) and REACT (react.ulb.be), aiming at improving urban population distribution models and urban malaria risk models, respectively. In these projects, the land-use and land-cover information will be used for disaggregating population counts available for administrative units, using dasymetric

modeling [30,31]. Consequently, emphasis is placed on having sufficient thematic details for residential use to allow for adequate reallocation of population counts and modeling of population density at the intraurban level. These projects focus on sub-Saharan African cities, which implies the development of solutions that consider the scarcity of ancillary reference data.

The present research proposes a complete, mostly automated, framework for mapping land use at the street block level, using only very-high resolution (VHR) land-cover maps and remote-sensing-derived data. It includes the extraction of the street blocks from OSM and their subsequent characterization using spatial, spectral, and morphological metrics, a feature selection step for discarding highly correlated and redundant information and supervised classification using fandom forest.

This research deploys great efforts for research reproducibility and open access to data and products. Consequently, implemented computer codes and resulting datasets are made available at no cost to any interested users (see Appendix B).

## 2. Materials and Methods

### 2.1. Study Areas

The methodology presented here was applied to two cities in Western Africa, namely Ouagadougou and Dakar, the capitals of Burkina Faso and Senegal, respectively. The areas of interests (AOI) were selected to cover both the core of the city and the peri-urban areas, as there is a lack of a well-established consensus for the definition and delineation of urban areas [32]. AOIs were selected through visual interpretation of VHR imagery and were not restricted to administrative units. This allowed for a wide capture of economic activities and urban sprawl. Figures 1 and 2 illustrate the extents of the AOIs, covering 615 km$^2$ for Ouagadougou and 418 km$^2$ for Dakar, superimposed with the administrative units.

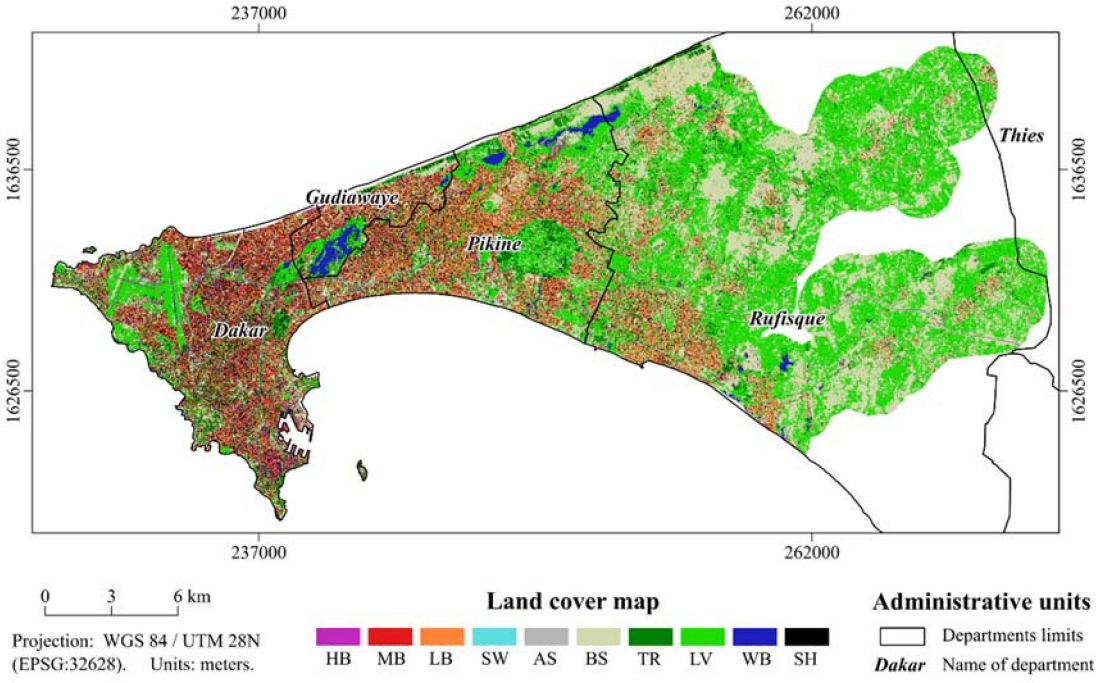


**Figure 1.** Land-cover map of Dakar superimposed with administrative units. HB: High buildings; MB: Medium buildings; LB: Low buildings; SW: Swimming pools; AS: Asphalt surfaces; BS: Bare soils; TR: Trees; LV: Low vegetation; WB: Water bodies; SH: Shadows.

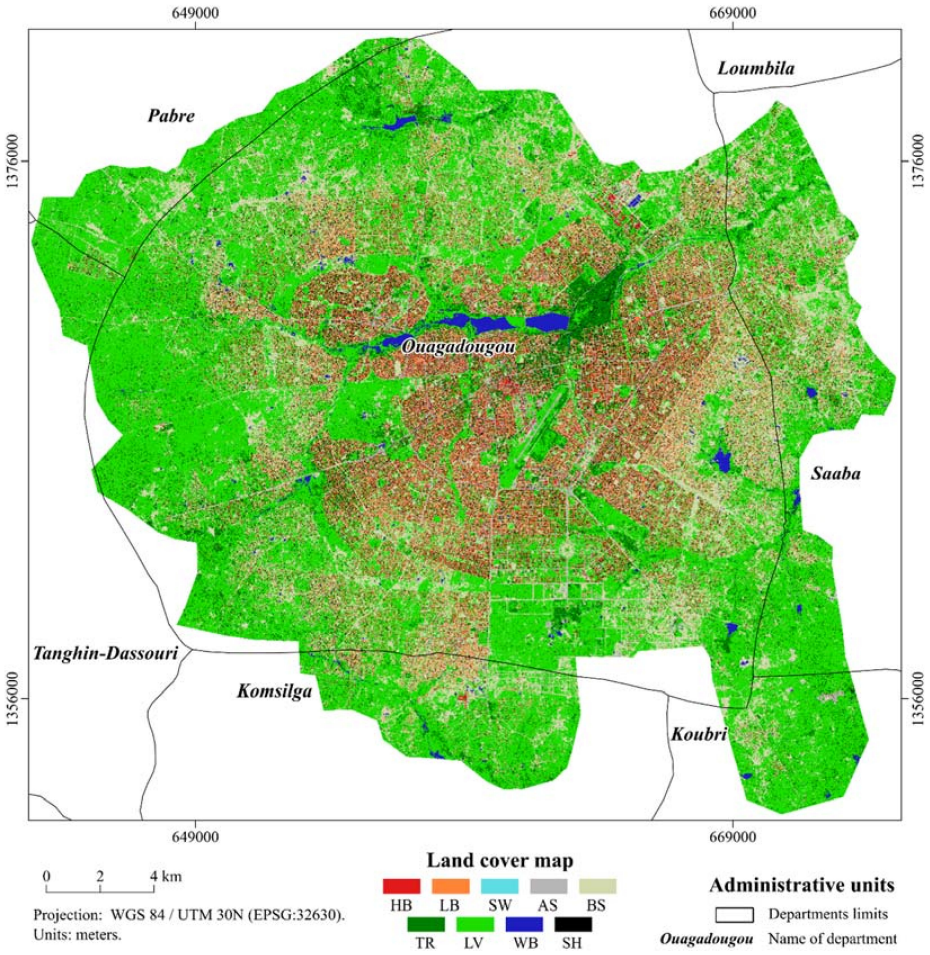


**Figure 2.** Land-cover map of Ouagadougou superimposed with administrative units. HB: High buildings; LB: Low buildings; SW: Swimming pools; AS: Asphalt surfaces; BS: Bare soils; TR: Trees; LV: Low vegetation; WB: Water bodies; SH: Shadows.

## 2.2. Input Data

The primary input data consisted of land-cover (LC) maps (Figures 1 and 2) derived from very-high resolution (VHR) satellite imagery, i.e., WorldView-3 and Pléiades for Ouagadougou and Dakar, respectively, with a spatial resolution of 0.5 m. These were produced using a semiautomated object-based image analysis (OBIA) [33] framework based on open-source solutions [34–37]. The overall accuracy (OA) of the LC products was 93.4% and 89.5% for Ouagadougou and Dakar, respectively. Their legends are presented in Table 1.

**Table 1.** Legend of the land-cover maps used as input to compute spatial metrics.

| Ouagadougou—Burkina Faso | | Dakar—Senegal | |
|---|---|---|---|
| **Class** | **Abbreviation** | **Class** | **Abbreviation** |
| High buildings (>3 m) | HB | High buildings (>10 m) | HB |
| Low buildings (<3 m) | LB | Medium buildings (5–10 m) | MB |
| - | - | Low buildings (<5 m) | LB |
| Swimming pools | SW | Swimming pools | SW |
| Asphalt surfaces | AS | Artificial ground surfaces | AS |
| Bare soils | BS | Bare soils | BS |
| Trees | TR | Trees | TR |
| Low vegetation | LV | Low vegetation | LV |
| Water bodies | WB | Inland waters | WB |
| Shadows | SH | Shadows | SH |

Additionally, normalized digital surface models (nDSM), i.e., datasets that contain the height of above-ground objects, were used. The nDSMs were derived from photogrammetric digital surface models (DSM) generated from a stereo triplet for Dakar and a stereo couple for Ouagadougou. Vegetation and water indices, i.e., normalized difference vegetation index (NDVI) and normalized difference water index (NDWI), respectively, were also used.

### *2.3. Extraction of Street Block Geometries Using OpenStreetMap*

In OSM data, roads are the map features mostly associated with the highest completeness. A recent study [38] estimates that the OSM roads have reached more than 80% of completeness at a global scale. Although this high score hides important variations at regional or national scales, it encourages the use of this global dataset to develop solutions that can be applied worldwide.

In this research, we propose an approach similar to [19]. Our method is a semiautomated workflow exploiting the OpenStreetMap data for the creation of urban street blocks geometries, to be used as a fundamental urban landscape unit to map land use [16]. Different from proprietary solutions (ESRI ArcGIS) proposed in [19], it takes advantage of the open-source software PostGIS for storage, management, and processing of large vector datasets. The programming language is Python and the code is implemented in a "Jupyter notebook" [39] accessible under an open license on a dedicated online repository (Appendix B). It can be easily adapted to suit further research needs. The main steps are illustrated in Figure 3.

To map the land use at the street block level implies that blocks should have a high intrahomogeneity of the urban function. Indeed, it is important to get meaningful spatial units, according to the process investigated (here, the land use). Otherwise, the spatial metrics will be meaningless [40] and the classification task would be more complex, with more confusions between classes and lower confidence in the land-use maps produced.

The OSM road network alone could not adequately meet our needs. Indeed, in some situations, the edges of the blocks could be defined better using line segments of a river, hill, or other manmade structures [19]. Actual land use is often a mix of uses, and thus it is difficult to reach a situation where all street blocks extracted would be homogenous in terms of land use. However, incorporating other extra map features (e.g., rivers, water bodies, railways, military camps, cemeteries, residential areas, farmlands, etc.) allowed for these problems to be reduced. Consequently, the blocks that were produced were not street blocks stricto sensu, but they met the needs of our analysis. Moreover, vector data such as administrative city sectors or functional zones could be used as ancillary datasets in addition to OSM data.

The script starts by taking as input a polygon shapefile corresponding to the AOI and optionally some ancillary vector layers. Then, the bounding box of the AOI is created and subdivided into tiles and OSM data are automatically downloaded using the OSM extended overpass API [41]. Next, map features of interest are filtered according to their "key = value" pairs in the OSM tagging scheme [42,43]. The map features (i.e., lines and polygons) are then intersected with the extent of the AOI and the polygons are converted into linear features. At this point, some lines that cross each other without being connected, e.g., because they do not share a common node at their intersection, are processed to obtain a stack of fully connected lines. Owing to coregistration inaccuracies and/or nearly redundant road geometries in OSM [44] or between OSM and ancillary data, many sliver polygons are created. This is overcome by using the PostGIS topological functions to merge neighboring nodes according to a user-provided snapping tolerance. The snapping tolerance should not be too large because it is likely to distort the accurately digitized road sections and make further steps more difficult [44]. After this procedure, the street blocks polygons are extracted from the stack of lines. Similar to [19], two kinds of polygons are generated: (i) urban blocks and (ii) undesirable polygons (sliver polygons) resulting from multilane roads, functional roads near crossroads, or highway ramps. These sliver polygons are usually easily identifiable based on criteria of shape and size since they are thin and small. The user is here in charge of adapting the preset criteria to be used for identification of probable sliver polygons.

The sliver polygons are then eliminated by merging them with their neighboring nonsliver polygon with which they shared the larger border. This latest step iterates until no sliver polygons remain, resulting in final block geometries.

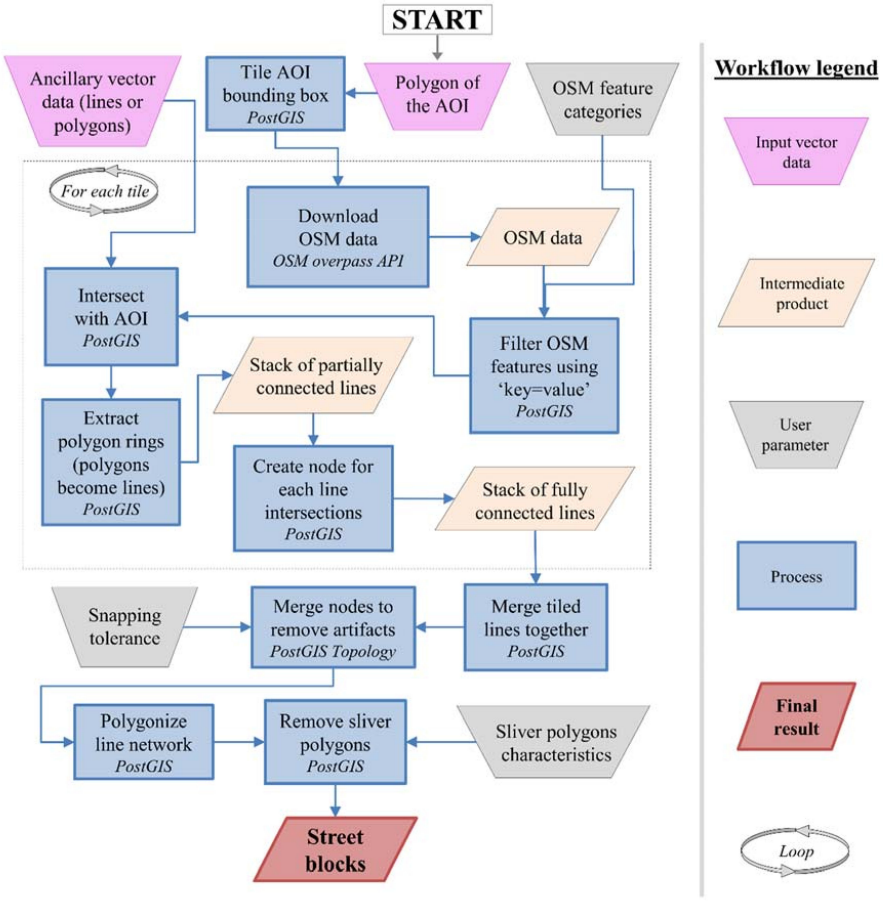


**Figure 3.** Flowchart of the semiautomated processing chain for the extraction of street blocks from OpenStreetMap and ancillary vector data.

### *2.4. Computing Street Block Features*

In this research, street block features used to classify land use can be separated in two groups. The first relates to spatial metrics computed based on the land-cover maps available. The other group include additional information, such as block morphology or features derived directly from the spectral values. In total, 116 and 97 features were computed for Ouagadougou and Dakar, respectively. All metrics were computed in GRASS GIS, using an automated script coded in Python [45] which is available on a dedicated repository (see Appendix B).

#### 2.4.1. Street Blocks' Spatial Metrics (Patch-Based Metrics)

In this paper, the spatial metrics used are all related to the "patch mosaic" paradigm [40,46], whereby the landscape is viewed as a mosaic of land-cover patches. A patch could be defined as a group of neighboring pixels that belong to the same class. In that way, it acts as an abstraction level that masks some information of the actual landscape. For instance, in urban areas, a coalescence of hundreds of small individual buildings can form one single patch and could have the same size as a patch corresponding to a single large building, such as a commercial center. Amongst other things, this paradigm makes the use and interpretation of patch-based metrics difficult for nonexperts. According to [40], the behavior of spatial metrics are theoretically not well understood and their

interpretation could be very challenging. There is a profusion of different patch-based metrics but all aiming at describing a landscape either on its composition/diversity or the spatial configuration of the patches it contains.

Different software can be used for computing spatial metrics and the best known is probably FRAGSTAT [23]. Unfortunately, its use is limited by the size of the dataset that can be handled [40] and offers limited automation. As an alternative, we used the "r.li" suite of modules, available in GRASS GIS [47]. These modules provide a set of landscape indices that can be found in FRAGSTATS and are designed not to overload the computer memory (i.e., the RAM), thus having the capacity to process large datasets [48]. Besides, GRASS GIS is built as a collection of hundreds small programs, enabling all common GIS operations to be handled in the same environment in a computationally efficient manner. Importantly, the process could be automated thanks to the Python application programming interface (API) [49]. The list of metrics computed is presented in Table A1 (see Appendix A).

#### 2.4.2. Additional Street Block's Features

In addition to the spatial metrics described above, features related to the shape of the street blocks were computed, as well as key features aggregated from spectral data, e.g., the median and standard deviation of NDVI and NDWI, for their ability in the characterization of nonbuilt landscapes. Those additional features were computed using "i.segment.stats" add-on of GRASS GIS [50]. Moreover, as information on the height of above-ground objects was available from the nDSMs, we computed the mean height of the building pixels. Table A2 (see Appendix A) summarizes the additional block features that are used in complement to spatial metrics.

### *2.5. Land Use Scheme and Sampling*

The choice of the land-use classes constituting the legend scheme was made after a visual interpretation of the different types of urban structures and uses. Both cities are characterized by several types of land use such as industrial, commercial and services, administrative, or residential. In the land-use legend scheme (see Table 2), a clear focus is made on having a better thematic precision for residential areas than for other classes. It includes two residential classes enabling the distinction between planned (usually richer and with lower density) and unplanned/deprived (usually poorer and with higher density). The nonresidential built-up land uses, such as commercial, administrative, or services, were all grouped together in one single class. This was done because we intend to utilize the land-use information for further research regarding fine-scale modeling of population density.

Moreover, as we aimed at mapping the whole extent of the AOI, which encompasses peri-urban areas, we also included classes related to natural elements, e.g., vegetated or bare areas. Urban land use is often mixed because of the presence of multiple urban activities on the same block. However, our aim here was to map the dominant activity in the block. This explains the absence of "mixed" classes in the legends.

While urban patterns in Ouagadougou present a clear distinction between planned and unplanned neighborhoods (as visible in Figure 4a), in Dakar, the difference is less straightforward. There, some neighborhoods look more deprived than most of the residential areas, even if they present a semblance of regular street pattern (see Figure 4b). Previous research, integrating remote sensing and socioeconomic census data, proved that they are inhabited by a poorer population [51].

First, a set of 1648 and 1500 street blocks were randomly sampled for Dakar and Ouagadougou, respectively, for training a supervised classification algorithm and for validation. Each sampled block was then assigned a label by visual interpretation according to its supposed dominant land-use class. In the case of Dakar, the resulting training/test set was highly imbalanced, between "Planned residential" and "Deprived residential". The same was true for "Agricultural vegetation" and "Natural vegetation". For that reason, we manually sampled an extra 344 blocks to obtain a more balanced training/validation set. Next, for both case studies, a split in a 75%/25% ratio was made to get a training set and an independent validation set. During the process, the interpreter was asked

about his confidence in giving an adequate label without any doubt. Finally, samples for which the interpretation decision was not certain, i.e., the experts were undecided about the land-use class to be attributed, were removed from the validation set (41 and 76 blocks removed for Dakar and Ouagadougou, respectively). This explains why the number of validation samples do not reach the 25% previously mentioned for some classes (see Table 1).

**Table 2.** Legend scheme of land use for Ouagadougou and Dakar and size of training and test sets (number of street block polygons).

| Class | Abbreviation | Training Set Size | Test Set Size |
|---|---|---|---|
| **Ouagadougou—Burkina Faso** | | | |
| Vegetation | VEG | 122 | 41 |
| Bare soils | BARE | 173 | 57 |
| Non-residential built-up (administrative, commercial, services, etc.) | ACS | 220 | 68 |
| Planned residential built-up | PLAN | 268 | 83 |
| Unplanned residential built-up | UNPLAN | 302 | 90 |
| **Dakar—Senegal** | | | |
| Agricultural vegetation | AGRI | 93 | 42 |
| Natural vegetation | VEG | 86 | 30 |
| Bare soils | BARE | 57 | 18 |
| Non-residential built-up (administrative, commercial, services, etc.) | ACS | 153 | 46 |
| Planned residential built-up | PLAN | 872 | 277 |
| Deprived residential built-up | DEPR | 209 | 68 |

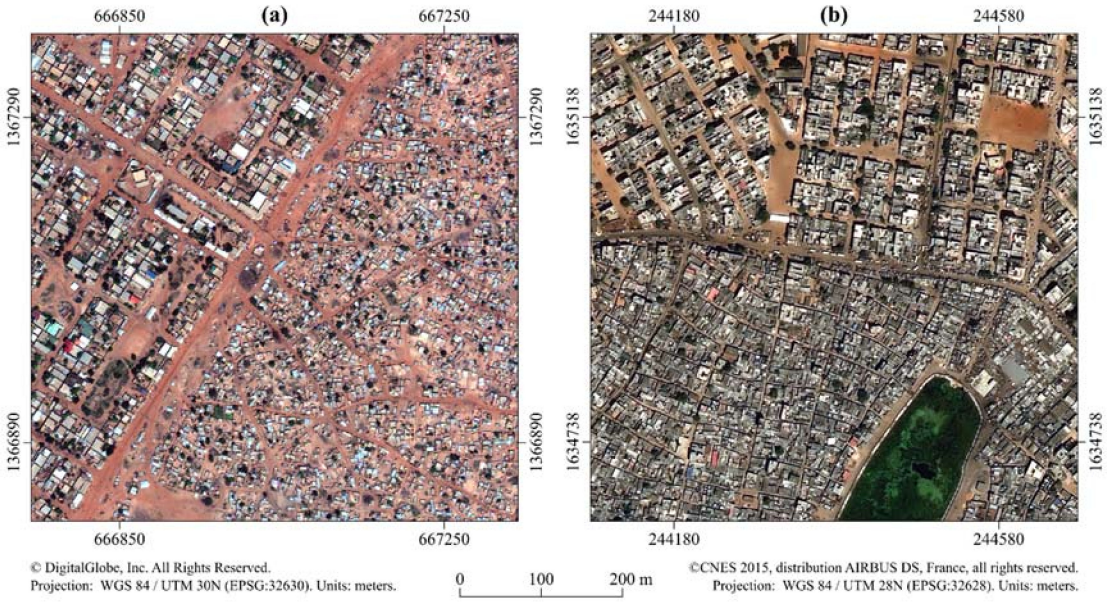


**Figure 4.** (**a**) Opposition between planned residential neighborhoods and unplanned ones in Ouagadougou. (**b**) Opposition between planned residential areas and deprived (poorer) neighborhoods in Dakar.

### *2.6. Feature Selection and Classification Using Machine Learning*

A supervised random forest classifier (RF) was used for the classification step. RF is an ensemble of Classification and Regression Decision Trees (CARTs) [52], where each tree is trained on a random

bootstrapped sample of the training data (about two-thirds of the data). In the end, a label is assigned, as derived from the combined predictions (majority voting) of each tree. Since RF is an aggregation of several individual and independent trees, it has been very commonly used in RS studies due to its high prediction accuracy and relative immunity to overfitting [53]. To maximize performance, two parameters are usually fine-tuned in RF, the number of trees to grow and the number of randomly selected features at each decision point (split) within a tree. The former is commonly suggested to be set as high as computationally efficient [52], while the value of the latter is identified through cross-validation of the out-of-sample training data, known as Out of Bag (OOB) error.

As already mentioned, many features were computed for both case studies. A large proportion were spatial metrics which are inherently highly correlated and redundant since they are all dependent on a small amount of basic patch metrics for their computation, e.g., area, perimeter, patch, and neighboring patch type [54]. This kind of dataset could result in an underperforming and unnecessarily complex classification model. Consequently, we performed a feature selection (FS) procedure prior to the classification step with the aim of constructing smaller, more predictive and parsimonious models [55]. The "Variable Selection Using Random Forest" (VSURF) algorithm, a popular automated method for FS selection developed by [56], was used. The salient features of VSURF are categorized in defining three types of feature subsets: (i) removing useless features, (ii) finding the most predictive set of features which may contain a great amount of redundancy, and (iii) retaining the accuracy while removing redundant features through a stepwise search.

Feature selection and classification were performed using the R software, version 3.5.0 [57]. The R code has been made available in R markdown format [58] on a dedicated repository (see Appendix B).

## 3. Results

### *3.1. Extraction of Street Block Geometries*

Our processing chain was used to create the street block geometries using a large amount of input data thanks to the capabilities of PostGIS. To give an order of magnitude, in Ouagadougou, more than 47,000 blocks were extracted from a set of more than 180,000 segments. The number of sliver polygons present after this initial extraction was quite impressive: 32.6% and 31.5% for Ouagadougou and Dakar, respectively. Sliver polygons were removed to produce a final layer containing nearly 32,000 street blocks geometries for Ouagadougou and 23,000 for Dakar. In Ouagadougou, an existing ancillary layer produced in a previous study [35], whereby the city had been delineated into local morphological zones, was used.

Figure 5 illustrates the results from different main steps of the processing chain. The initial stack of linear elements coming from OSM and ancillary data is quite chaotic (see Figure 5a). Snapping all nodes (here, with a snapping threshold of 7 m), enables efficient cleaning of the initial errors but some sliver polygons remain (see Figure 5b). The final geometries after the removal of sliver polygons are presented on Figure 5c.

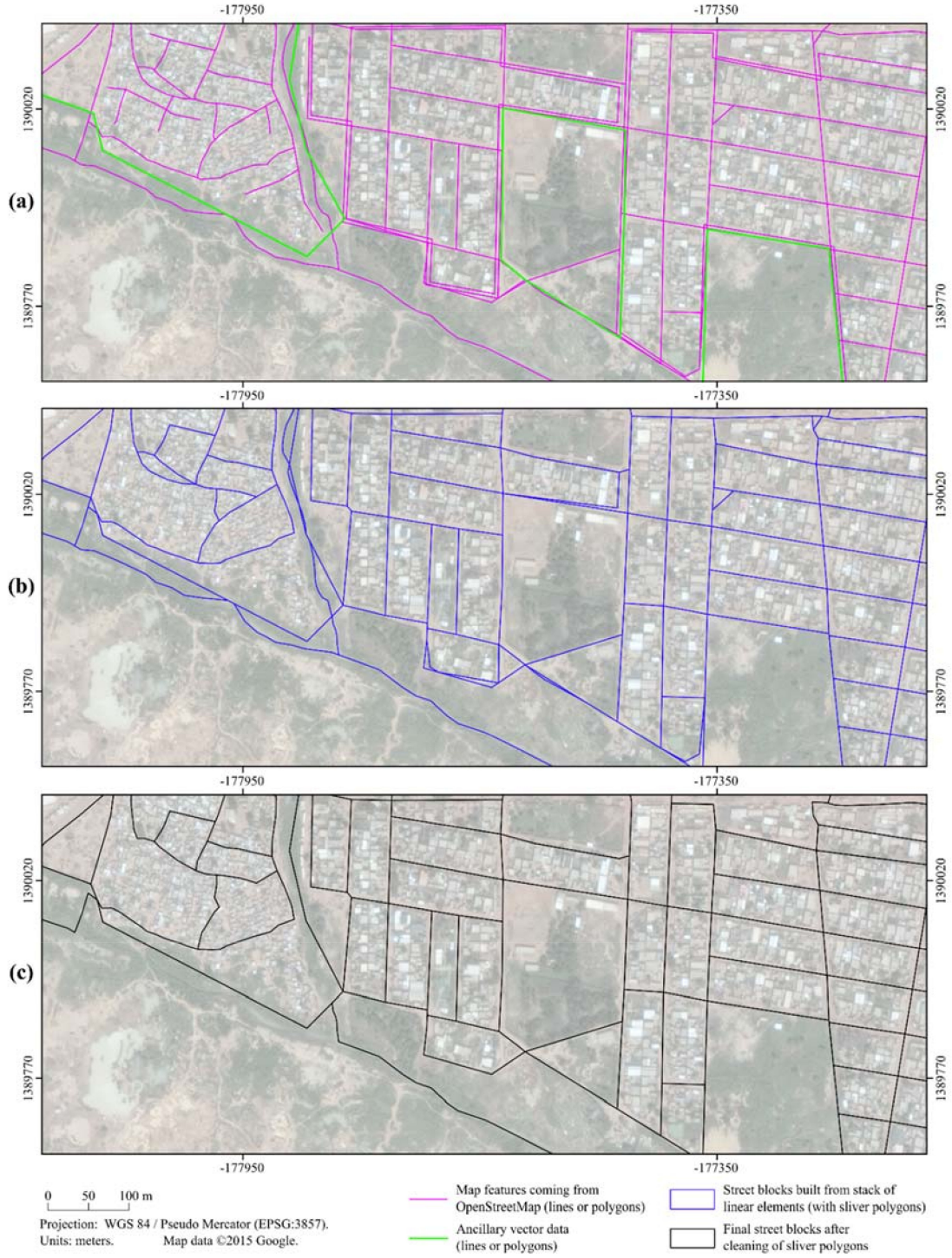


**Figure 5.** Extraction of street blocks from OSM data and ancillary vector data. (**a**) Lines and polygons coming from OSM and ancillary vector layer; (**b**) Street blocks that contain several undesired polygons (sliver polygons); (**c**) Final street blocks extracted.

### *3.2. Automated Feature Selection*

Feature selection was performed on the initial set of features computed and resulted in an impressive reduction of 81.9% (from an initial set of 116 features to 21 remaining features) and 86.6% (from 97 initial features to 13 remaining) for Ouagadougou and Dakar, respectively. The list of selected features is presented in Table 3. Globally, spatial metrics relative to almost all land-cover

classes are present in the set of selected features. However, it appears that classes related to different building heights are more represented, which is unsurprising. Moreover, features related to landscape composition, street block morphology, and remote sensing indices are also present, which proves their added-value in the classification model.

**Table 3.** Blocks features selected by feature selection using "VSURF". These are the remaining features at the "prediction" step.

| | Case Studies | |
|---|---|---|
| **Street Block Features** | **Ouagadougou** | **Dakar** |
| *Landscape composition* | | |
| Shannon | X | X |
| Dominance | X | |
| *Features relative to building class* | | |
| High buildings mean patch size | X | |
| SD of high buildings patch area | X | |
| Proportion of high buildings pixels in the block | X | |
| Proportion of medium buildings | NA | X |
| Proportion of low building pixels in the block | X | X |
| SD of low building patch area | X | |
| Low building patch density | X | X |
| Low building patch number | X | |
| Count of built pixels | | X |
| Mean height of built pixels | X | X |
| *Features relative to shadow class* | | |
| Proportion of shadows pixels in the block | | X |
| Shadows patch density | X | X |
| Shadows patch number | X | |
| *Features relative to other land-cover classes* | | |
| Artificial surface shape index | | X |
| Range of artificial surfaces patch area | | X |
| SD of asphalt surface patch area | X | |
| Bare soils patch density | X | |
| *Features relative to vegetation classes* | | |
| Low vegetation patch density | X | |
| Range of low vegetation patch area | | X |
| Range of trees patch area | X | |
| Trees mean patch size | X | |
| *Remote sensing indices* | | |
| NDVI median | X | X |
| NDWI SD | X | |
| *Features relative to block morphology* | | |
| Block perimeter | | X |
| Compactness relative to a circle | X | |
| Compactness relative to a square | X | |
| *Total* | 21 | 13 |

### 3.3. Land-Use Classification Using Random Forest

The reduced set of features was then used as an input dataset of a supervised classification using RF. The predictions of the model were evaluated using an independent validation set and overall accuracies of 84% and 79% were achieved for Ouagadougou and Dakar, respectively. However, these values hide disparities between classes. The F-score, e.g., a synthetic accuracy metric, is used here to compare the classification performance at the class level [59].

The class "Planned residential" performed similarly in both case studies with F-scores of 0.88 and 0.84 for Dakar and Ouagadougou, respectively. However, the class "Deprived residential"/"Unplanned residential" showed a strongly lower accuracy in Dakar, with an F-score of 0.68, while in Ouagadougou it was the best-performing class, reaching an impressive score of 0.92. The inspection of confusion matrices (Tables 4 and 5) revealed that while some confusions were present

between the residential classes in Ouagadougou, they were of a larger magnitude in Dakar. In both cases, most of the confusion occurred between the "Plan residential" and "Nonresidential built-up" classes. Moreover, misclassifications appeared between "Bare soils" and "Low vegetation", as was expected, since many nonbuilt street blocks present a mix of vegetated and bare soil elements.

The analysis of the RF feature importance reveals that, for both cases studies, the most important features are those related to the built environment (see Tables 6 and 7). They are in the top-five features in Ouagadougou and in the top four in Dakar (assuming shadows are a proxy of the built-up patterns).

**Table 4.** Confusion matrix of land-use classification for Ouagadougou. VEG: Vegetation; BARE: Bare soils; ACS: Nonresidential built-up (administrative, commercial, services, etc.); PLAN: Planned residential; UNPLAN: Unplanned residential.

| | | Reference | | | | |
|---|---|---|---|---|---|---|
| | **Classes** | **VEG** | **BARE** | **ACS** | **PLAN** | **UNPLAN** |
| **Prediction** | VEG | 36 | 7 | 0 | 0 | 2 |
| | BARE | 5 | 47 | 4 | 0 | 2 |
| | ACS | 0 | 0 | 47 | 7 | 0 |
| | PLAN | 0 | 2 | 14 | 79 | 2 |
| | UNPLAN | 0 | 1 | 3 | 4 | 77 |
| | F-score | 0.84 | 0.82 | 0.77 | 0.84 | 0.92 |

**Table 5.** Confusion matrix of land-use classification for Dakar. AGRI: Agricultural vegetation; VEG: Natural vegetation; BARE: Bare soils; ACS: Nonresidential built-up (administrative, commercial, services, etc.); PLAN: Planned residential; DEPR: Deprived residential.

| | | Reference | | | | | |
|---|---|---|---|---|---|---|---|
| | **Classes** | **AGRI** | **VEG** | **BARE** | **ACS** | **PLAN** | **DEPR** |
| **Prediction** | AGRI | 34 | 3 | 0 | 1 | 1 | 0 |
| | VEG | 6 | 17 | 2 | 4 | 3 | 0 |
| | BARE | 1 | 3 | 12 | 0 | 0 | 0 |
| | ACS | 1 | 4 | 1 | 24 | 8 | 1 |
| | PLAN | 0 | 3 | 2 | 15 | 253 | 25 |
| | DEPR | 0 | 0 | 1 | 1 | 12 | 42 |
| | F-score | 0.84 | 0.55 | 0.71 | 0.57 | 0.88 | 0.68 |

**Table 6.** Ouagadougou—Per class feature importance from the random forest classifier (mean decrease in accuracy). Only the 10 most important are presented. "SD" refers to standard deviation. The color-ramp indicates the feature importance for each land-use classes, with darker green corresponding to the top feature for each class (number in bold). ACS: Nonresidential built-up (administrative, commercial, services, etc.); BARE: Bare soils; PLAN: Planned residential; UNPLAN: Unplanned residential; VEG: Vegetation.

| | Land Use Classes | | | | | |
|---|---|---|---|---|---|---|
| **Street Blocks Features** | **PLAN** | **UNPLAN** | **ACS** | **BARE** | **VEG** | **Overall** |
| Mean height of built pixels | 0.078 | **0.137** | **0.106** | 0.061 | 0.034 | **0.091** |
| Proportion of high buildings patch | **0.124** | 0.089 | 0.065 | 0.082 | 0.071 | 0.090 |
| Low building patch density | 0.085 | 0.120 | 0.024 | 0.045 | 0.165 | 0.084 |
| Proportion of Low building patch | 0.071 | 0.077 | 0.010 | **0.089** | 0.150 | 0.072 |
| High buildings mean patch size | 0.061 | 0.030 | 0.065 | 0.048 | 0.051 | 0.051 |
| Low vegetation patch density | 0.048 | 0.047 | 0.048 | −0.004 | 0.032 | 0.038 |
| NDVI median | 0.006 | 0.030 | 0.007 | 0.015 | **0.257** | 0.042 |
| Shadows patch density | 0.024 | 0.087 | 0.018 | 0.076 | −0.011 | 0.043 |
| SD of high buildings patch area | 0.039 | 0.047 | 0.055 | 0.042 | 0.043 | 0.045 |
| Trees mean patch size | 0.023 | 0.010 | 0.063 | 0.008 | 0.003 | 0.023 |

**Table 7.** Dakar—Per class feature importance from the random forest classifier (mean decrease in accuracy). Only the 10 most important are presented. The color-ramp indicates the feature importance for each land-use classes, with darker green corresponding to the top feature for each class (number in bold). ACS: Nonresidential built-up (administrative, commercial, services, etc.); AGRI: Agricultural vegetation; BARE: Bare soils; DEPR: Deprived residential; PLAN: Planned residential; VEG: Natural vegetation.

| | Land Use Classes | | | | | | |
|---|---|---|---|---|---|---|---|
| **Street Blocks Features** | **PLAN** | **DEPR** | **ACS** | **BARE** | **AGRI** | **VEG** | **Overall** |
| Proportion of low buildings patch | 0.070 | **0.164** | 0.017 | 0.100 | 0.259 | 0.122 | **0.098** |
| Shadows patch density | **0.080** | 0.055 | 0.032 | 0.039 | 0.047 | 0.097 | 0.069 |
| Low buildings patch density | 0.044 | 0.075 | 0.029 | 0.008 | 0.248 | 0.018 | 0.061 |
| Mean height of built pixels | 0.067 | 0.056 | 0.037 | 0.064 | 0.020 | 0.092 | 0.060 |
| NDVI median | 0.065 | 0.030 | 0.016 | 0.020 | 0.181 | **0.193** | 0.072 |
| Proportion of shadows patch | 0.050 | 0.095 | 0.004 | 0.051 | 0.080 | 0.066 | 0.055 |
| Range of low vegetation patch area | 0.024 | 0.016 | −0.001 | 0.010 | **0.389** | 0.010 | 0.049 |
| Count of built pixels | 0.036 | 0.022 | 0.025 | **0.115** | 0.037 | 0.097 | 0.040 |
| Range of artificial surfaces patch area | 0.025 | 0.018 | **0.132** | 0.006 | 0.012 | 0.021 | 0.033 |
| Proportion of medium buildings patch | 0.065 | 0.002 | 0.002 | 0.025 | 0.088 | 0.013 | 0.047 |

For the built-up classes, height is an important element, as witnessed by the selection of proportions of high and low buildings. It is interesting to notice the importance of shadows patch density as a top feature in Dakar for "Planned residential" which is not the case in Ouagadougou. This could be explained by the fact that residential buildings are more often multi-stories in Dakar than in Ouagadougou. Thereby, this shadow-related feature could be considered as a proxy of the presence of highly elevated built-up structures. Unsurprisingly, the vegetation index (NDVI) is the best feature for the vegetated land-use classes. Bare soils also present a feature related to the built land-cover classes. We assume it should be an inverse relation, i.e., characterizing the blocks as having no presence of built-up.

### *3.4. Introduction of Uncertainty and Thematic Improvement of Final Products*

Errors and uncertainty are inherent in any classification problem. Even if the classifier provides a class label for each item, predictions could be affected by a high level of uncertainty. RF natively provides the class probability for each street block [60]. We take the decision to use this essential information to reclassify street blocks for which the prediction was highly uncertain. We compute the difference between the probabilities of the most probable and the second most probable class. Street blocks having a difference of less than 5 percentage points were then relabeled as "Uncertain" (see Figure 6c). It concerns 3.7% and 4.1% of the available street blocks for Ouagadougou and Dakar, respectively. For the convenience of the users, all class probabilities are included in the product releases.

Residential built-up density is usually a good indicator of population densities. For that reason, we use the information about blocks' percentage of built-up patches to discriminate between different densities of built-up. (Figure 6d). In both case studies, street blocks classified as "Planned residential" were relabeled as "Planned residential (low density)" if their built-up percentage was lower than 30% and 40% for Ouagadougou and Dakar, respectively. In Ouagadougou, the same approach was used to distinguish two classes of built-up density for the "Unplanned residential" class, with a threshold fixed at 15% of built-up, and to enable a split between peri-urban settlements and slum-like patterns. The choice of these thresholds was made through trial-and-error, relying on visual assessment of the land-cover map. The final land-use maps are visible in Figures 7 and 8. For the convenience of the reader, they can be visualized online along with the land-cover information (https://tgrippa.github.io/Landuse_from_landcover_webmap/).

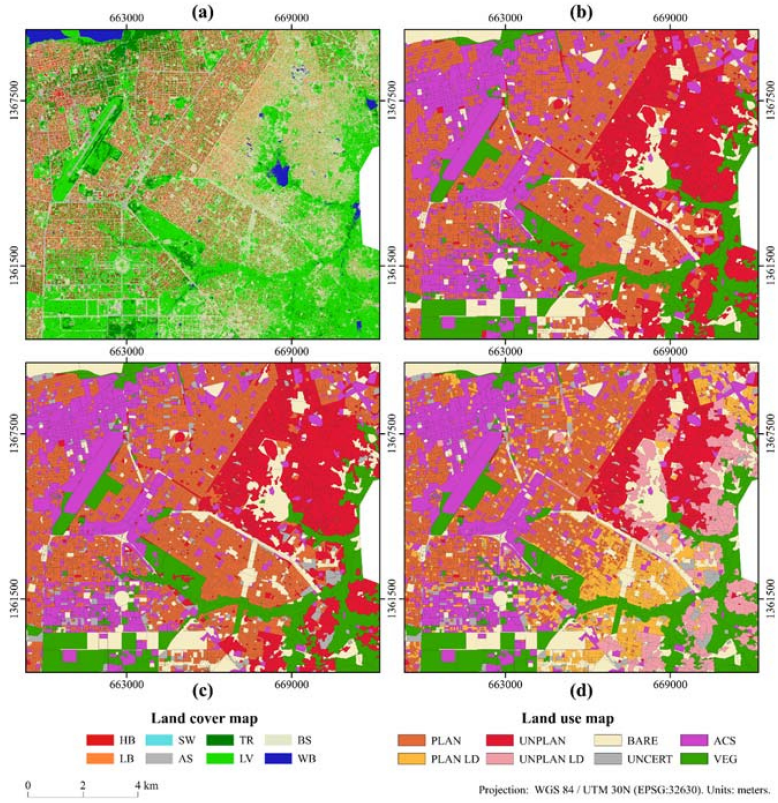


**Figure 6.** Addition of uncertainty and built-up density to refine the thematic precision of the maps for Ouagadougou. (**a**) Land cover map for comparison purpose; (**b**) Most probable class from the random forest classifier; (**c**) Introducing "Uncertain" class; (**d**) Thematic refinement of residential classes according to the computed proportion of buildings. Land-cover classes (**a**) HB: High buildings; LB: Low buildings; SW: Swimming pools; AS: Asphalt surfaces; BS: Bare soils; TR: Trees; LV: Low vegetation; WB: Water bodies; SH: Shadows. Land-use classes (**b**–**d**) VEG: Vegetation; BARE: Bare soils; ACS: Nonresidential built-up (administrative, commercial, services, etc.); PLAN: Planned residential; PLAN LD: Planned residential (low density); UNPLAN: Unplanned residential; UNPLAN LD: Unplanned residential (lox density); UNCERT: Uncertain prediction.

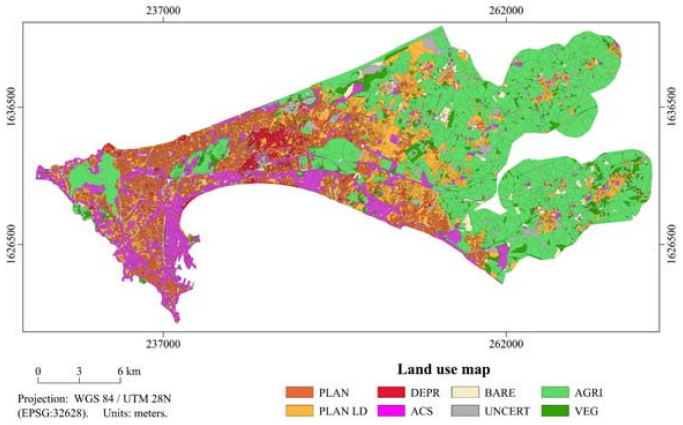


**Figure 7.** Land-use map of Dakar. AGRI: Agricultural vegetation; VEG: Natural vegetation; BARE: Bare soils; ACS: Nonresidential built-up (administrative, commercial, services, etc.); PLAN: Planned residential; PLAN LD: Planned residential (low density); DEPR: Deprived residential; UNCERT: Uncertain prediction.

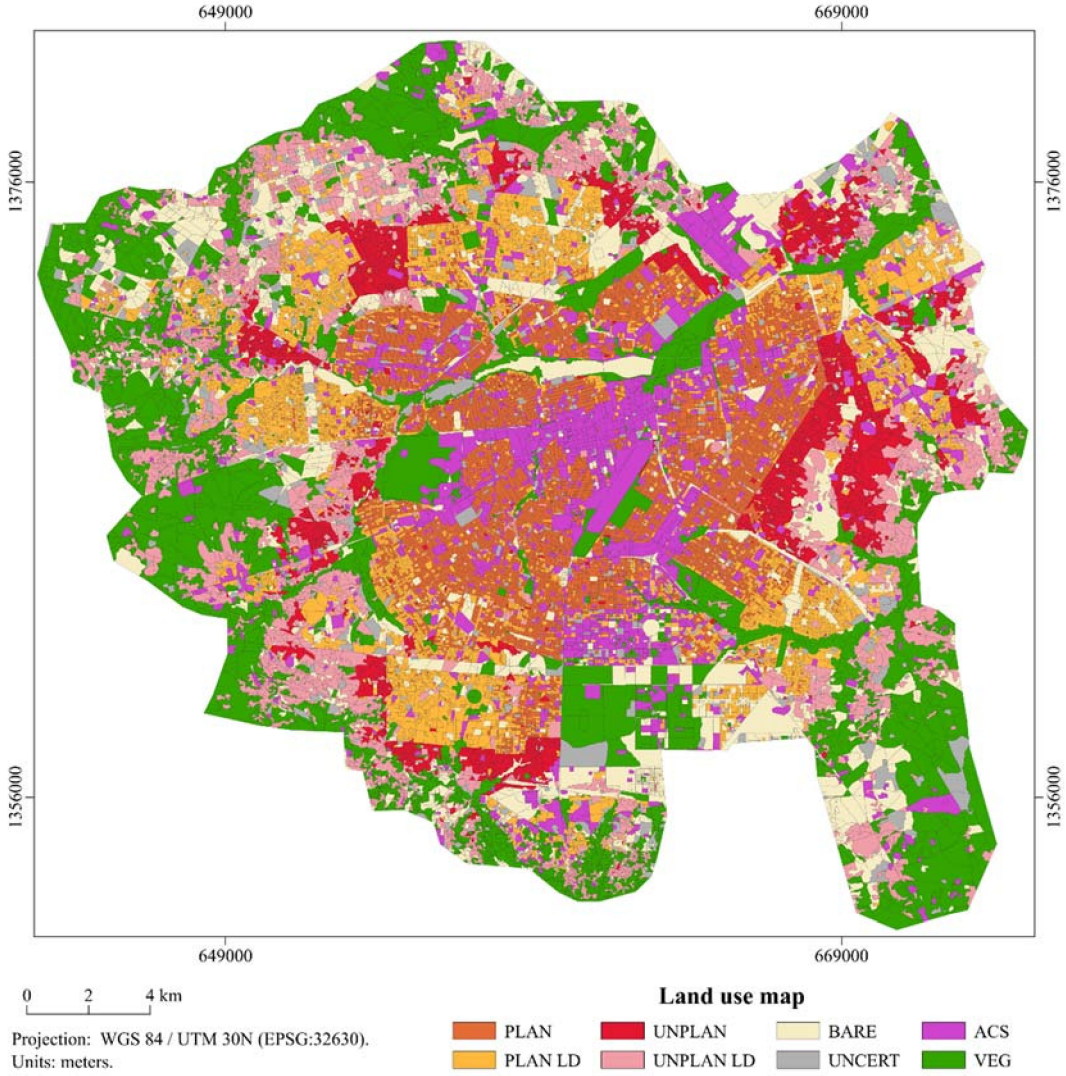


**Figure 8.** Land-use map of Ouagadougou. VEG: Vegetation; BARE: Bare soils; ACS: Nonresidential built-up (administrative, commercial, services, etc.); PLAN: Planned residential; PLAN LD: Planned residential (low density); UNPLAN: Unplanned residential; UNPLAN LD: Unplanned residential (lox density); UNCERT: Uncertain prediction.

## 4. Discussion

The solution proposed in this paper proved to be operational for processing very large areas, as our case studies datasets cover more than 1000 km$^2$ in total, with a spatial resolution of 0.5 m. However, some limitations can be highlighted.

The first limitation relates to the completeness of OSM data. A quantitative evaluation of the geometric and semantic quality of the street blocks is out of the scope of this article, but some aspects can be discussed. A qualitative visual assessment shows that the consistency is more evident in the core urban areas, where the street network is denser and OSM data generally more complete. From several tests that were carried out, we concluded that the resulting street blocks may not be as detailed as expected, e.g., presence of polygons that are too large and encompass multiple distinct land uses. This is mostly related to the fact that the OSM database is not complete enough for certain locations, especially in peri-urban areas. To solve this issue, time was dedicated to the digitization of additional map features in OSM (e.g., roads, tracks, natural elements, etc.) at the periphery of our AOIs (peri-urban areas) to meet our requirements. This also contributed to the completion of the OSM

database, which is a positive outcome. Since the OSM data completeness is increasing, it is likely that such issues will become less prevalent in the future. However, the performance of the proposed framework is likely to decrease as the landscape becomes more rural. Further research could look for other strategies for the automated extraction of meaningful landscape units for mapping the land use in rural and peri-urban areas.

The second limitation is linked to the spatial metrics. The selection of relevant spatial metrics for the phenomenon under investigation and the interpretation of their behaviors can be a challenging task in itself [40]. Moreover, it is likely that some metrics that perform well in one case study are less discriminant for another. It was the case in our results and this could be interpreted because of differences in terms of urban landscapes. As a solution, computing many metrics and feeding them into a feature selection procedure allows for the unsupervised selection of a parsimonious set of features.

Thirdly, the labelling procedure for creating the training and validation sets may clearly be a bottleneck if automation is mandatory. Further research could explore the possibility of taking advantage of the OSM database for the automatic selection and labeling of these samples, as OSM contains some information on land use and Point of Interest (POI).

Next, future studies aiming at implementing the same kind of workflow that we present here should consider the possibility of improving efficiency by computing the metrics for the street blocks belonging to the training samples only. Since they are sufficient for performing the feature selection step, this would save processing time and storage space [61]. Only the most discriminant features could then be computed for the whole AOI. This approach would allow for computing a very large number of features without creating computational and storage issues.

Finally, as previously mentioned (see Section 2.4.1), the "patch mosaic" paradigm hides some aspects of the urban structures, which is likely to limit the ability of spatial metrics to adequately characterize urban land use. Possible future work should investigate a broader workflow that would include explicit information derived from the OBIA segmentation process. For example, information on individual segments could be computed, e.g., area, compactness, and fractal dimension, and then summarized either at the class or at the landscape level.

Prediction errors and the corollary uncertainty of the produced maps are important points that any classification framework should consider. In this study, we used the class-probability output from the RF model to identify street blocks for which the prediction was affected by an important level of uncertainty. In addition to the land-use maps where labels correspond to the most probable class, we also provide the class-probability values for each street block. This information is useful especially when classification products are used as input data to other classification or modeling tasks since it is well known that errors propagate to the derived products. In the future, we plan to carry out sensitivity analysis to assess how errors and uncertainty of land-cover maps affect the derived land use and the models of spatial distribution of population densities.

## 5. Conclusions

While availability of up-to-date and reliable geographical information on urban areas is sorely missing in developing countries, new sources of information such as VGI can overcome existing challenges. This research presented a workflow, mostly automated, for mapping urban land use at the street block level, with a focus on residential use. The proposed framework proved its ability to efficiently handle large datasets, since the two case studies, Ouagadougou and Dakar, covering more than 1000 $km^2$ in total, achieved 84% and 79%, respectively. All of the computer codes developed and the resulting datasets have been released in open-access to any interested users.

**Author Contributions:** T.G. is the main author of the study who wrote the manuscript, analyzed the results, developed the code for street blocks extraction and the final version of the code for spatial metrics computation. S.G. extracted the street blocks and performed the classification using R software. S.Z. initiated an exploratory analysis in the early stages of this study and assessed the ability of GRASS GIS to meet the needs. M.L. provided

support in programming. Y.F. developed the online map for visualization of the results. T.G., S.G., N.M., P.B., and E.D. contributed to the visual interpretation for creation of training/validation sets. S.G., M.L., S.V., N.M., and E.W. revised the manuscript and helped to improve it.

**Funding:** This research was funded by BELSPO (Belgian Federal Science Policy Office) in the frame of the STEREO III program, as part of the MAUPP (SR/00/304) and REACT (SR/00/337) project (http://maupp.ulb.ac.be and http://react.ulb.be/).

**Acknowledgments:** WorldView-3 data is copyrighted under the mention "©COPYRIGHT 2015 DigitalGlobe, Inc. (Westminster, CO, USA), Longmont CO USA 80503. DigitalGlobe and the DigitalGlobe logos are trademarks of DigitalGlobe, Inc. The use and/or dissemination of this data and/or of any product in any way derived there from are restricted. Unauthorized use and/or dissemination is prohibited". OpenStreetMap data are copyrighted under the mention "©OpenStreetMap contributors, CC BY-SA". The authors greatly thank Hugo Perilleux-Sanchez and Augustin Martinet for their contribution on improving the completeness of OSM data on both case studies. The authors greatly thank the reviewers for their relevant comments which helped to improve this manuscript.

**Conflicts of Interest:** The authors declare no conflict of interest.

## Appendix A

Hereafter are presented the tables containing the list of street block features computed.

**Table A1.** Spatial metrics computed.

| Level of Computation | Metric |
|---|---|
| Landscape level<br>All land-cover classes together | Dominance<br>Pielou<br>Renyi<br>Richness<br>Shannon<br>Simpson |
| Class level<br>On binary maps (for each land-cover class separately) | Patch number<br>Patch density<br>Mean patch size<br>SD of patch size<br>Patch size coef. of variation<br>Range of patch size<br>Shape index<br>Proportion |

**Table A2.** Additional block features computed.

| Source of Information | Blocks Feature |
|---|---|
| Spectral | NDVI median<br>NDVI mean<br>NDWI median<br>NDWI mean |
| nDSM models Built-up mask (from land-cover map) | Mean height of built pixels<br>Number of built pixels |
| Block morphology (shape features) | Area<br>Perimeter<br>Compactness relative a to square<br>Compactness relative a to circle<br>Fractal dimension |

## Appendix B

Hereafter are referenced the dataset, pieces of computer code, and processing chains used in this research. These are all made available under Creative Common License (CC-BY).

The land-cover maps used as input data for the computation of landscape metrics:

- Ouagadougou land-cover map [62] is referenced and available on https://doi.org/10.5281/zenodo.1290653. The version used in this research is referred as v1.0 (10.5281/zenodo.1290654).
- Dakar land-cover map [63] is referenced and available on https://doi.org/10.5281/zenodo.1290799. The version used in this research is referred as v1.0 (10.5281/zenodo.1290800).

The results of the land use classification and the street blocks extracted:

- Ouagadougou land-use map [64] is referenced and available on https://doi.org/10.5281/zenodo.1291384. The version produced in this research is referred as v1.0 (10.5281/zenodo.1291385).
- Dakar land-use map [65] is referenced and available on https://doi.org/10.5281/zenodo.1291388. The version produced in this research is referred as v1.0 (10.5281/zenodo.1291389).

The R code used for the feature selection and RF classification steps, belonging to the dataset of features used and training/test sets, is available in the following Github repository: https://github.com/ANAGEO/R_stuff/tree/master/VSURF_FeatureSelection_RF_Optimization.

The semiautomated processing chain for extraction of street block from OSM using PostGIS is available in the following Github repository: https://github.com/ANAGEO/OSM_Streetblocks_extraction.

The semiautomated processing chain for computation of spatial metrics using GRASS GIS is available in the following Github repository: https://github.com/tgrippa/Street_blocks_features_computation.

The piece of Python code used for computing uncertainty form the probabilistic output of RF: https://github.com/ANAGEO/RFprob_to_uncertainty.

## References


1. UN DESA. *World Urbanization Prospects: The 2018 Revision*, Online ed; United nations, Department of Economic and Social Affairs: New York, NY, USA, 2018.
2. Novack, T.; Kux, H.; Feitosa, R.; Costa, G. Per block urban land use interpretation using optical VHR data and the knowledge-based system Interimage. *Int. Arch. Photogramm. Remote Sens. Spat. Inf. Sci.* **2010**, *38*, 6.
3. Mennecke, B.E.; West, L.A., Jr. Geographic Information Systems in Developing Countries: Issues in Data Collection, Implementation and Management. *J. Glob. Inf. Manag.* **2001**, *9*, 44–54. [CrossRef]
4. Eria, S. The State of GIS in Developing Countries: A Diffusion and GIS & Society Analysis of Uganda, and the Potential for Mobile Location-Based Services. Ph.D. Thesis, University of Minnesota, Minneapolis, MN, USA, 2012.
5. Tumba, A.G.; Ahmad, A. Geographic information system and spatial data infrastructure: A developing societies' perception. *Univers. J. Geosci.* **2014**, *2*, 85–92. [CrossRef]
6. Schwabe, C.A. The geoinformation industry in Africa: Prospects and potentials. In Proceedings of the Fourth Meeting of the Committee on Development Information (CODI IV), Addis Ababa, Ethiopia, 23–28 April 2005.
7. Schwabe, C. *Getting Geoinformation and SDI to Work for Africa–Part 2*; PositionIT: Gauteng, South Africa, 2010.
8. Economic Commission for Africa, United Nations. *Geospatial Information for Sustainable Development in Africa: African Action Plan on Global Geospatial Information Management*; Economic Commission for Africa, United Nations: Addis Ababa, Ethiopia, 2017.
9. Goodchild, M.F. Citizens as sensors: The world of volunteered geography. *GeoJournal* **2007**, *69*, 211–221. [CrossRef]
10. Walde, I.; Hese, S.; Berger, C.; Schmullius, C. From land cover-graphs to urban structure types. *Int. J. Geogr. Inf. Sci.* **2014**, *28*, 584–609. [CrossRef]
11. Vanderhaegen, S.; Canters, F. Mapping urban form and function at city block level using spatial metrics. *Landsc. Urban Plan.* **2017**, *167*, 399–409. [CrossRef]
12. Voltersen, M.; Berger, C.; Hese, S.; Schmullius, C. Object-based land cover mapping and comprehensive feature calculation for an automated derivation of urban structure types at block level. *Remote Sens. Environ.* **2014**, *154*, 192–201. [CrossRef]
13. Siksna, A. The effects of block size and form in North American and Australian city centres. *Urban Morphol.* **1997**, *1*, 19–33.

14. Almeida, C.M.D.; Monteiro, A.M.V.; Câmara, G.; Soares-Filho, B.S.; Cerqueira, G.C.; Pennachin, C.L.; Batty, M. GIS and remote sensing as tools for the simulation of urban land-use change. *Int. J. Remote Sens.* **2005**, *26*, 759–774. [CrossRef]
15. Bochow, M.; Taubenbock, H.; Segl, K.; Kaufmann, H. An automated and adaptable approach for characterizing and partitioning cities into urban structure types. In Proceedings of the 2010 IEEE International Geoscience and Remote Sensing Symposium, Honolulu, HI, USA, 25–30 July 2010; pp. 1796–1799. [CrossRef]
16. Grippa, T. Osm Street Blocks Extraction (Version V1.0). *Zenodo* **2018**. [CrossRef]
17. Fonte, C.; Minghini, M.; Patriarca, J.; Antoniou, V.; See, L.; Skopeliti, A. Generating Up-to-Date and Detailed Land Use and Land Cover Maps Using OpenStreetMap and GlobeLand30. *ISPRS Int. J. Geo-Inf.* **2017**, *6*, 125. [CrossRef]
18. Long, Y.; Liu, X. Automated identification and characterization of parcels (AICP) with OpenStreetMap and Points of Interest. *Environ. Plan. B Plan. Des.* **2016**, *43*, 341–360.
19. Fan, H.; Yang, B.; Zipf, A.; Rousell, A. A polygon-based approach for matching OpenStreetMap road networks with regional transit authority data. *Int. J. Geogr. Inf. Sci.* **2016**, *30*, 748–764. [CrossRef]
20. Simwanda, M.; Murayama, Y. Integrating Geospatial Techniques for Urban Land Use Classification in the Developing Sub-Saharan African City of Lusaka, Zambia. *ISPRS Int. J. Geo-Inf.* **2017**, *6*, 102. [CrossRef]
21. Hu, T.; Yang, J.; Li, X.; Gong, P. Mapping Urban Land Use by Using Landsat Images and Open Social Data. *Remote Sens.* **2016**, *8*, 151. [CrossRef]
22. Aubrecht, C.; Steinnocher, K.; Hollaus, M.; Wagner, W. Integrating earth observation and GIScience for high resolution spatial and functional modeling of urban land use. *Comput. Environ. Urban Syst.* **2009**, *33*, 15–25. [CrossRef]
23. McGarigal, K.; Marks, B.J. *FRAGSTATS: Spatial Pattern Analysis Program for Quantifying Landscape Structure*; U.S. Department of Agriculture, Forest Service, Pacific Northwest Research Station: Portland, OR, USA, 1995.
24. Turner, M.G.; Gardner, R.H. *Landscape Ecology in Theory and Practice*; Springer: New York, NY, USA, 2015; ISBN 978-1-4939-2793-7.
25. Urban, D.L.; O'Neill, R.V.; Shugart, H.H. Landscape Ecology. *BioScience* **1987**, *37*, 119–127. [CrossRef]
26. Uuemaa, E.; Mander, Ü.; Marja, R. Trends in the use of landscape spatial metrics as landscape indicators: A review. *Ecol. Indic.* **2013**, *28*, 100–106. [CrossRef]
27. Lowry, J.H.; Lowry, M.B. Comparing spatial metrics that quantify urban form. *Comput. Environ. Urban Syst.* **2014**, *44*, 59–67. [CrossRef]
28. Luck, M.; Wu, J. A gradient analysis of urban landscape pattern: A case study from the Phoenix metropolitan region, Arizona, USA. *Landsc. Ecol.* **2002**, *17*, 327–339. [CrossRef]
29. Herold, M.; Scepan, J.; Clarke, K.C. The use of remote sensing and landscape metrics to describe structures and changes in urban land uses. *Environ. Plan. A* **2002**, *34*, 1443–1458. [CrossRef]
30. Petrov, A. One Hundred Years of Dasymetric Mapping: Back to the Origin. *Cartogr. J.* **2012**, *49*, 256–264. [CrossRef]
31. Mennis, J. Generating Surface Models of Population Using Dasymetric Mapping. *Prof. Geogr.* **2003**, *55*, 31–42. [CrossRef]
32. Gisbert, F.J.G.; Martí, I.C.; Gielen, E. Clustering cities through urban metrics analysis. *J. Urban Des.* **2017**, *22*, 689–708. [CrossRef]
33. Blaschke, T.; Hay, G.J.; Kelly, M.; Lang, S.; Hofmann, P.; Addink, E.; Queiroz Feitosa, R.; van der Meer, F.; van der Werff, H.; van Coillie, F.; et al. Geographic Object-Based Image Analysis—Towards a new paradigm. *ISPRS J. Photogramm. Remote Sens.* **2014**, *87*, 180–191. [CrossRef] [PubMed]
34. Grippa, T.; Lennert, M.; Beaumont, B.; Vanhuysse, S.; Stephenne, N.; Wolff, E. An Open-Source Semi-Automated Processing Chain for Urban Object-Based Classification. *Remote Sens.* **2017**, *9*, 358. [CrossRef]
35. Grippa, T.; Georganos, S.; Vanhuysse, S.G.; Lennert, M.; Wolff, E. A local segmentation parameter optimization approach for mapping heterogeneous urban environments using VHR imagery. In Proceedings of the Remote Sensing Technologies and Applications in Urban Environments II, Warsaw, Poland, 4 October 2017; Volume 10431. [CrossRef]
36. Georganos, S.; Grippa, T.; Lennert, M.; Vanhuysse, S.; Wolff, E. SPUSPO: Spatially Partitioned Unsupervised Segmentation Parameter Optimization for efficiently segmenting large heterogeneous areas. In Proceedings of the 2017 Conference on Big Data from Space (BiDS'17), Toulouse, France, 28–30 November 2017.

37. Vanhuysse, S.; Grippa, T.; Lennert, M.; Wolff, E.; Idrissa, M. Contribution of nDSM derived from VHR stereo imagery to urban land-cover mapping in Sub-Saharan Africa. In Proceedings of the 2017 Joint Urban Remote Sensing Event (JURSE), Dubai, UAE, 6–8 March 2017.
38. Barrington-Leigh, C.; Millard-Ball, A. The world's user-generated road map is more than 80% complete. *PLoS ONE* **2017**, *12*, e0180698. [CrossRef] [PubMed]
39. Kluyver, T.; Ragan-Kelley, B.; Pérez, F.; Granger, B.; Bussonnier, M.; Frederic, J.; Kelley, K.; Hamrick, J.; Grout, J.; Corlay, S.; et al. Jupyter Notebooks—A publishing format for reproducible computational workflows. In Proceedings of the 20th International Conference on Electronic Publishing; Göttingen, Germany, 7–9 June 2016; pp. 87–87. [CrossRef]
40. McGarigal, K. FRAGSTATS help v.4.2 2015. Available online: https://www.umass.edu/landeco/research/fragstats/documents/fragstats.help.4.2.pdf (accessed on 1 June 2018).
41. OpenStreetMap Wiki contributors Overpass API—OpenStreetMap Wiki. 2018. Available online: https://wiki.openstreetmap.org/wiki/Overpass_API (accessed on 1 June 2018).
42. Davidovic, N.; Mooney, P.; Stoimenov, L.; Minghini, M. Tagging in Volunteered Geographic Information: An Analysis of Tagging Practices for Cities and Urban Regions in OpenStreetMap. *ISPRS Int. J. Geo-Inf.* **2016**, *5*, 232. [CrossRef]
43. Vandecasteele, A.; Devillers, R. Improving Volunteered Geographic Information Quality Using a Tag Recommender System: The Case of OpenStreetMap. In *OpenStreetMap in GIScience*; Arsanjani, J.J., Zipf, A., Mooney, P., Helbich, M., Eds.; Lecture Notes in Geoinformation and Cartography; Springer: Basel, Switzerland, 2015; pp. 59–80. ISBN 978-3-319-14279-1.
44. Li, Q.; Fan, H.; Luan, X.; Yang, B.; Liu, L. Polygon-based approach for extracting multilane roads from OpenStreetMap urban road networks. *Int. J. Geogr. Inf. Sci.* **2014**, *28*, 2200–2219. [CrossRef]
45. Grippa, T. Street Blocks Features Computation (Version V1.0). *Zenodo* **2018**. [CrossRef]
46. McGarigal, K.; Tagil, S.; Cushman, S.A. Surface metrics: An alternative to patch metrics for the quantification of landscape structure. *Landsc. Ecol.* **2009**, *24*, 433–450. [CrossRef]
47. Porta, C.; Spano, L.D.; Metz, M.; GRASS Development Team. Module r.li.*. 2017. Available online: https://grass.osgeo.org/grass74/manuals/r.li.html (accessed on 1 June 2018).
48. Neteler, M.; Mitasova, H. *Open Source GIS—A GRASS GIS Approach*; Springer: New York, NY, UISA, 2008.
49. Neteler, M.; Beaudette, D.E.; Cavallini, P.; Lami, L.; Cepicky, J. Grass gis. In *Open Source Approaches in Spatial Data Handling*; Springer: Berlin/Heidelberg, Germany, 2008; pp. 171–199. ISBN 978-3-540-74831-1.
50. Lennert, M.; GRASS Development Team. *Addon i.segment.stats. Geographic Resources Analysis Support System (GRASS) Software, Version 7.3.*; Open Source Geospatial Foundation: Chicago, IL, USA, 2016.
51. Borderon, M.; Oliveau, S.; Machault, V.; Vignolles, C.; Lacaux, J.-P.; N'Donky, A. Qualifier les espaces urbains à Dakar, Sénégal. *Cybergeo Eur. J. Geogr.* **2014**. [CrossRef]
52. Breiman, L. Random forests. *Mach. Learn.* **2001**, *45*, 5–32. [CrossRef]
53. Belgiu, M.; Drăgut, L. Random forest in remote sensing: A review of applications and future directions. *ISPRS J. Photogramm. Remote Sens.* **2016**, *114*, 24–31. [CrossRef]
54. Cushman, S.A.; McGarigal, K.; Neel, M.C. Parsimony in landscape metrics: Strength, universality, and consistency. *Ecol. Indic.* **2008**, *8*, 691–703. [CrossRef]
55. Guyon, I.; Elisseeff, A. An introduction to variable and feature selection. *J. Mach. Learn. Res.* **2003**, *3*, 1157–1182.
56. Genuer, R.; Poggi, J.-M.; Tuleau-Malot, C. VSURF: An R Package for Variable Selection Using Random Forests. *R J.* **2015**, *7*, 19–33.
57. R Development Core Team. *R: A Language and Environment for Statistical Computing*; Version 3.5.0; R Foundation for Statistical Computing: Vienna, Austria, 2008; ISBN 3-900051-07-0.
58. Baumer, B.; Cetinkaya-Rundel, M.; Bray, A.; Loi, L.; Horton, N.J. R Markdown: Integrating a reproducible analysis tool into introductory statistics. *arXiv*, 2014.
59. Sokolova, M.; Lapalme, G. A systematic analysis of performance measures for classification tasks. *Inf. Process. Manag.* **2009**, *45*, 427–437. [CrossRef]
60. Chunyang, L. Probability Estimation in Random Forests. Master's Thesis, Department of Mathematics and Statistics, Utah State University, Logan, UT, USA, 2013.

61. Georganos, S.; Grippa, T.; Vanhuysse, S.; Lennert, M.; Shimoni, M.; Kalogirou, S.; Wolff, E. Less is more: Optimizing classification performance through feature selection in a very-high-resolution remote sensing object-based urban application. *GISci. Remote Sens.* **2017**, *1*. [CrossRef]
62. Grippa, T.; Georganos, S. Ouagadougou Very-High Resolution Land Cover Map (Version V1.0) [Data set]. *Zenodo* **2018**. [CrossRef]
63. Grippa, T.; Georganos, S. Dakar Very-High Resolution Land Cover Map (Version V1.0) [Data set]. *Zenodo* **2018**. [CrossRef]
64. Grippa, T.; Georganos, S. Ouagadougou Land Use Map at Street Block Level (Version V1.0) [Data set]. *Zenodo* **2018**. [CrossRef]
65. Grippa, T.; Georganos, S. Dakar Land Use Map at Street Block Level (Version V1.0) [Data set]. *Zenodo* **2018**. [CrossRef]

# Chapter 4

# Assessing the contribution of VHRRS for dasymetric mapping

**Grippa Tais**, Linard Catherine, Lennert Moritz, Georganos Stefanos, Mboga Nicholus, Vanhuysse Sabine, Gadiaga Assane and Wolff Eleonore. "**Improving Urban Population Distribution Models with Very-High Resolution Satellite Information.**" Data 4, no. 1 (January 16, 2019): 13. https://doi.org/10.3390/data4010013.

*data*

MDPI

*Article*

# Improving Urban Population Distribution Models with Very-High Resolution Satellite Information

**Taïs Grippa [1,*], Catherine Linard [2], Moritz Lennert [1], Stefanos Georganos [1], Nicholus Mboga [1], Sabine Vanhuysse [1], Assane Gadiaga [2] and Eléonore Wolff [1]**

[1] Department of Geoscience, Environment & Society, Université Libre De Bruxelles (ULB), 1050 Bruxelles, Belgium; mlennert@ulb.ac.be (M.L.); sgeorgan@ulb.ac.be (S.G.); nmboga@ulb.ac.be (N.M.); svhuysse@ulb.ac.be (S.V.); ewolff@ulb.ac.be (E.W.)

[2] Department of Geography, University of Namur, 5000 Namur, Belgium; catherine.linard@unamur.be (C.L.); assanegadiaga@gmail.com (A.G.)

* Correspondence: tgrippa@ulb.ac.be; Tel.: +32-2-650-6803

Received: 5 December 2018 ; Accepted: 14 January 2019; Published: 16 January 2019

**Abstract:** Built-up layers derived from medium resolution (MR) satellite information have proven their contribution to dasymetric mapping, but suffer from important limitations when working at the intra-urban level, mainly due to their difficulty in capturing the whole range of variation in terms of built-up densities. In this regard, very-high resolution (VHR) remote sensing is known for its ability to better capture small variations in built-up densities and to derive detailed urban land use, which plead in favor of its use when mapping urban populations. In this paper, we compare the added value of various combinations of VHR data sets, compared to a MR one. A top-down dasymetric mapping strategy is applied to reallocate population counts from administrative units into a regular 100 × 100 m grid, according to different weighting layers. These weighting layers are created from MR and/or VHR input data, using simple built-up proportion or reallocation "weights", obtained from a set of multiple ancillary data used to train a Random Forest regression model. The results reveal that (1) a built-up mask derived from VHR can improve the accuracy of the reallocation by roughly 13%, compared to MR; (2) using VHR land-use information alone results in lower accuracy than using a MR built-up mask; and (3) there is a clear complementarity between VHR land cover and land use.

**Keywords:** population modelling; dasymetric mapping; top-down approach; very-high resolution data; remote sensing; random forest; African city

## 1. Introduction

The less developed regions of the world have reached a symbolic milestone: Half of the population is now living in urban areas [1]. Even though this ratio is much lower in the least developed countries, most of which are located in sub-Saharan Africa (SSA), urbanization rates are increasing rapidly (where about 33% of the population is urban and are expected to face the highest growth rates during the next decades). It is expected that 40% of the population will live in urban areas by 2030 and 50% by 2050 [1]. As a consequence of these rapid transformations, SSA cities are exposed to increasing urban poverty and intra-urban inequalities [2], while a large part of the urban population is extremely vulnerable to health and disaster risks. In this context, detailed population data is essential in improving evidence-based decision-making by relevant authorities and organizations [3–5], as well as for any application relying on a human population denominator, such as estimating the population at risk, assessing vulnerability, and deriving health or development goals indicators [6–8]. However, this knowledge is often very limited in SSA and population data are regularly outdated and criticized regarding their reliability [6,7]. While collected at a household or individual level,

census data are generally aggregated and released in administrative units for privacy reasons [5,9], and do not match the requirements for different fields of research [4]. With regards to population data aggregated in administrative units, we can further mention some issues related to the fact that (1) the real spatial patterns of the population distribution are blurred by an impression of homogeneity within entities [10], (2) the aggregated values and subsequent analysis are very dependent on the choice of the administrative limits, which is also known as the modifiable areal unit problem (MAUP) [11], and (3) administrative units create subjective spatial discontinuities that sometimes change from one census to another [9,10].

When the spatial extension of a phenomenon does not correspond to any existing administrative limits, official population data are often unexploitable. In such a situation, a gridded population product—a raster layer where the pixel value refers to the (estimated) number of inhabitants—can provide a more useful estimate of population counts [12], by summing up all the pixels falling into the area under investigation. Creation of these population grid products is usually achieved using dasymetric mapping [9,13]. This modeling technique relies on the assumption that the knowledge of the territory—places more densely populated than others—can be used to spatially disaggregate the official census data provided at the administrative level to a finer scale [5]. Ancillary geoinformation data, such as land cover (LC) and land use (LU) maps, can provide valuable information for estimating the potential of different locations within the administrative units to be inhabited. Even though they are different by nature—LC is related to the physical characteristics of earth surface elements (e.g., vegetation, water, built-up, ...), while LU refers to the functions and activities that humans decided to carry out in certain locations (e.g., agricultural land, residential area, industrial area, ...)—they can provide complementary information valuable for population modelling purposes; for example, by combining building density (from LC) with the distinction between residential and commercial areas (from LU). For example, the built-up density and the land use information of a location can be combined and used as proxies for population density.

The major challenge in dasymetric mapping resides in the determination, from a set of ancillary data, of the relative distribution of the population within the administrative units. This information can be seen as spatial reallocation "weights", which are used in dasymetric mapping to disaggregate (redistribute) the population count known for the administrative units into a finer subunit level. When a simple built-settlement layer is available, a common strategy is to homogeneously allocate the population counts of the administrative unit within areas identified as built-up (binary dasymetric method). When the ancillary data are thematically more detailed than just a binary built-up layer—e.g., with a distinction between urban core, periurban, and rural areas—the weights can be adjusted to better correspond with the expected relative distribution of the population. For a long time, these weights were subjectively determined based on expert knowledge, or according to existing information [12], such as land-use information or household characteristics, combined with the use of quantitative methods, such as correlation analysis and multivariate regression [13]. Recent research has shifted this paradigm by taking advantage of the power and the efficiency of machine learning algorithms to model the distribution of population densities, without any prior knowledge. In the case of the WorldPop project, the popular Random Forest (RF) algorithm [14] is used to predict the weights for reallocation of population in 100 $\times$ 100 m grid layers [15]. In this work, the RF algorithm is used in a similar fashion.

Irrespective of the approach (expert-based or using machine-learning), built-settlement layers are consistently among the most important predictors for population models [16]. These layers are typically extracted from satellite imagery, and have been commonly used to estimate population densities at large spatial scales. However, both the quality [5] and the spatial resolution [4] of ancillary information have a strong influence on the accuracy of the predictions. In an urban context, the potential of finer resolution products for population redistribution is largely unexplored. We hypothesize that, by utilizing high and very-high resolution information (i.e., land cover and land use), the accuracy of the dasymetric reallocation might be significantly improved.

In this paper, we compare the contribution of three data sets with different spatial and thematic resolutions (built-up mask, land cover, and land use) for disaggregating population counts into 1 hectare grid cells. The availability of extremely detailed census data for the city of Dakar (Senegal) enables the assessment of the added value of very-high resolution (0.5 m) data, compared to medium resolution (10 m) data, in the context of a top-down dasymetric approach. Different levels of information are extracted from these data sets to create different weighting layers and perform dasymetric mapping. While very-high resolution data are expected to increase the accuracy of the dasymetric mapping procedure, their acquisition and processing costs might hinder their applicability for large-scale population mapping in Africa. It is, therefore, important to evaluate the loss in accuracy when using freely-available medium resolution data.

## 2. Materials and Methods

### 2.1. General Workflow

A visual representation of the different administrative levels and geographical scales used in this study as well, as the major steps of the workflow, is provided in Figure 1. Level 1 represents the finest level available with the reference population count (census data). It is reserved for validation purposes, and is kept completely independent from the dasymetric mapping procedure itself. It is important to understand that the total volume of the population of each administrative level is maintained during the disaggregation, meaning that, if the predictions at grid level are re-aggregated back to the original units, the initial population count is preserved (pycnophylactic property, [17]). As a consequence, the population counts and administrative units in level 1 cannot be used directly for dasymetric mapping, since they are the finest official level at which a validation is possible. In order to keep level 1 units available for validation purposes, the first step aims at creating coarser administrative units, hereafter referred to as 'level 0', by aggregating level 1 units (more details about this aggregation procedure are provided in Section 2.4). The second step consists of the dasymetric reallocation of population counts from level 0 units to a regular grid layer of 100 × 100 m. The different tests performed as well as the procedure for the creation of weighting layers used for dasymetric reallocation are further described in Section 2.5. The purpose of the third step is validation. The grid level predictions are summed for each of the level 1 units, in order to compare them against the reference count kept available at this level. More details about the validation procedure is provided in Section 2.6.

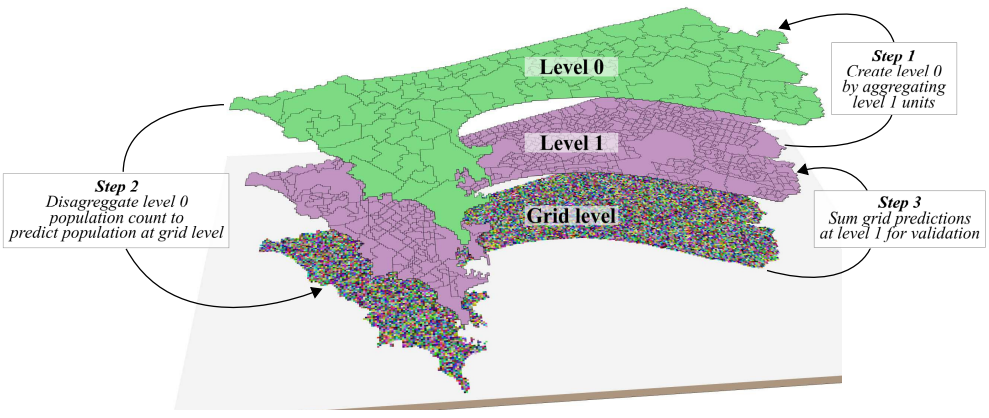


**Figure 1.** Representation of the major steps of the workflow presented and the different scales used in the analysis. A population count at level 0 is reallocated at grid level using weighting layers. For accuracy assessment, the predictions at grid level are aggregated to reach level 1 boundaries, and are compared with the official reference data available at this level.

### 2.2. Remote Sensing Derived Data

We used three ancillary data sets, to design different approaches for creating weighting layers to be used for the reallocation of population counts at a finer-scale using dasymetric mapping. All were derived from earth observation (EO) data, but are different regarding their spatial and thematic resolution. These data sets were previously produced in the context of the MAUPP (http://maupp.ulb.ac.be) and REACT (http://react.ulb.be/) projects, and are publicly available (see Appendix A).

The first data set consists of a binary built-up mask (see Figure 2A), recently published in [18]. It was derived from Landsat 8 and Sentinel-1 imagery from 2015, processed using a recently developed automated pixel-based fusion framework [19,20]. The main advantage of this product is that it is accessible and reproducible at no cost, since the EO data it relies on are free of cost. This built-up mask has a spatial resolution of 10 m and, with regards to its accuracy, an F1-score of 0.92. As its resolution could be described as medium, this product is referred to hereafter as "MR-BU".

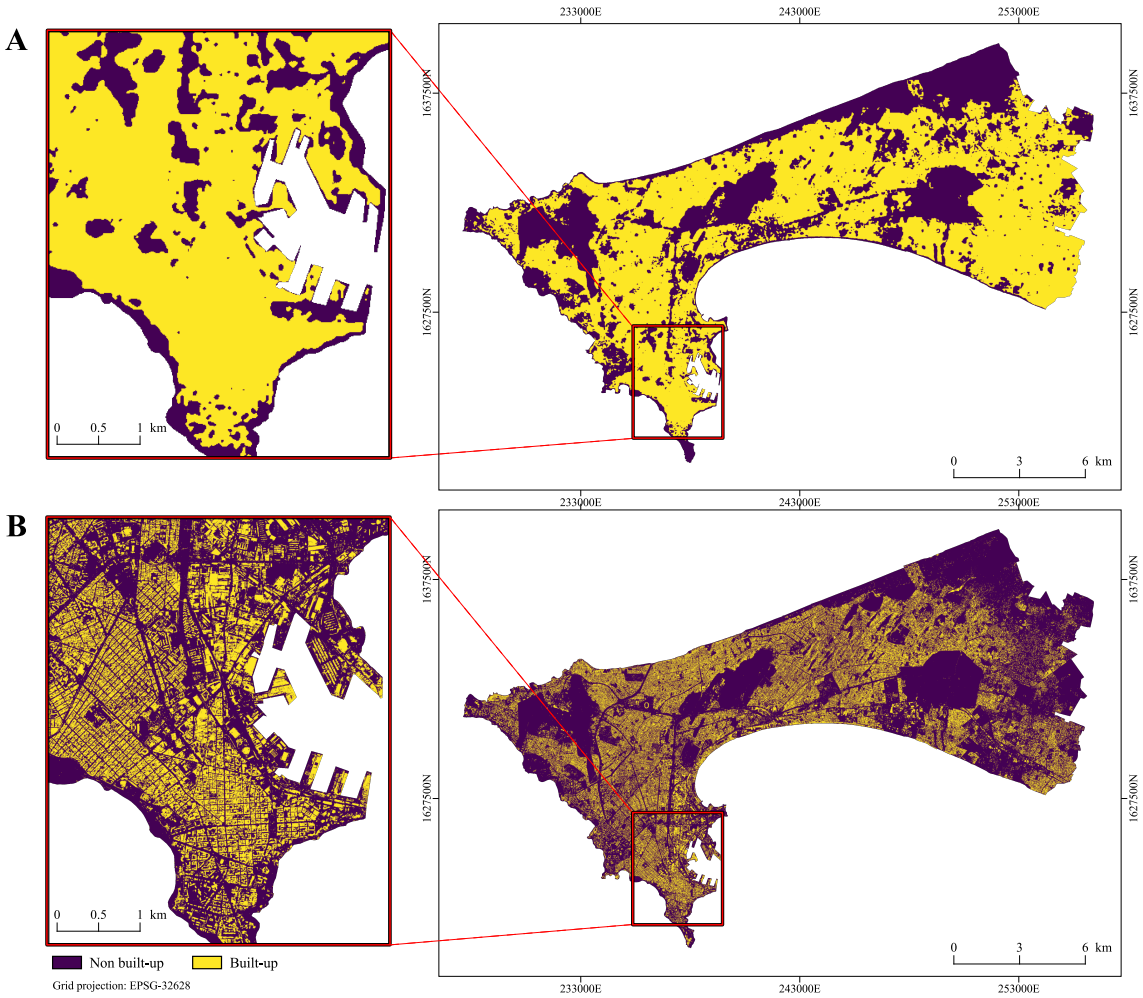


**Figure 2.** Built-up masks used: (**A**) Medium resolution (10 m), derived from freely available satellite images (MR-BU). (**B**) Very-high resolution (0.5 m), derived from commercial satellite images (VHR-BU).

The second data set consists of a very-high resolution land-cover map, derived from the Pleiades pan-sharpened tri-stereo images of 2015, with a spatial resolution of 0.5 m (see Figure 3). This map was previously produced thanks to a semi-automated open-source framework for object-based image analysis and supervised classification [21–23]. The overall accuracy (OA) of this product achieved 89.5%, and the building class reached 94% and 97% for user and producer accuracy, respectively (more details about the validation of this product are provided in [24]). A post-processing step was used, to further reclassify the built-up class into three classes of buildings by applying a threshold on the

height information provided by a photogrammetricaly-derived normalized digital surface model (nDSM). From the land-cover product, we extracted different combinations of land-cover classes in order to produce three very-high resolution layers for the analysis: (1) The land-cover map itself, including all the classes, as illustrated in Figure 3 (referred to as "VHR-LC"), (2) a built-up mask (referred to as "VHR-BU") (see Figure 2B), and (3) a layer containing three building classes, categorized by height (referred to as "VHR-3BU").

The last data set used in this study consists of a map providing the dominant land use at the street block level (see Figure 4). This map, reaching an OA of 79%, was produced in a recent study [25], in which street blocks were automatically created using OpenStreetMap data, and were further classified based on spatial metrics (also called 'landscape metrics') allowing characterization according to their composition and organization, in terms of land cover. This data set is an important complement to the land-cover or built-up masks, as it provides a distinction between residential and non-residential areas (e.g., commercial areas). Moreover, the map used here contains several residential classes that should help better estimate intra-urban population distribution. This product is referred to hereafter as "VHR-LU".

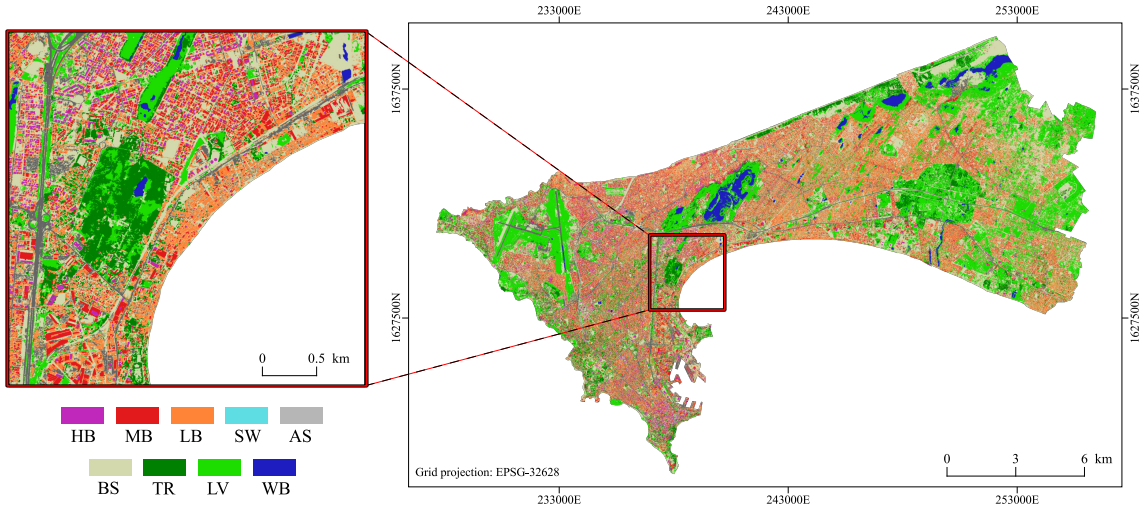


**Figure 3.** The very-high resolution land-cover map derived from commercial satellite images. Legend classes: HB: High buildings (>10 m); MB: Medium buildings (5–10 m); LB: Low buildings (<5 m); SW: Swimming pools; AS: Artificial ground surfaces; BS: Bare soils; TR: Trees; LV: Low vegetation; WB: Inland waters.

### *2.3. Population Data*

Population data used in this research comes from the most recent national census, performed in 2013 [26], and provided by the National Agency for Statistics and Demography of Senegal (ANSD). A limited temporal shift of 2 years exists between census data and the imagery used. Here, we are working under the assumption that the urban expansion and/or densification that occurred during this two-year period is marginal and should not impact the main findings. Population counts are available at the 'neighborhood' level (admin-5 in the Senegalese scheme), consisting of 1347 administrative units for the whole extent of the Dakar agglomeration. The spatial extent of the population data was reduced, in order to only keep administrative units fully covered by the different map products to be used for the dasymetric mapping. This resulted in dropping 154 units (1193 remaining).

### *2.4. Creation of Validation and Training Levels*

For this research, we had the opportunity to access population data at a very detailed scale. Figure 5A illustrates how fine this administrative level is, in terms of spatial resolution. It is important to point out that accessing such a fine-scaled population data, linked with the delineation

of the corresponding administrative units (i.e., polygon geometries provided as Shapefile), is rather exceptional for SSA cities, as the connection between population data and the finest administrative units is usually limited [6]. In this research, we take advantage of a citywide coverage with spatially detailed data, to implement a top-down dasymetric approach and perform fine-scale validation in an intra-urban environment.

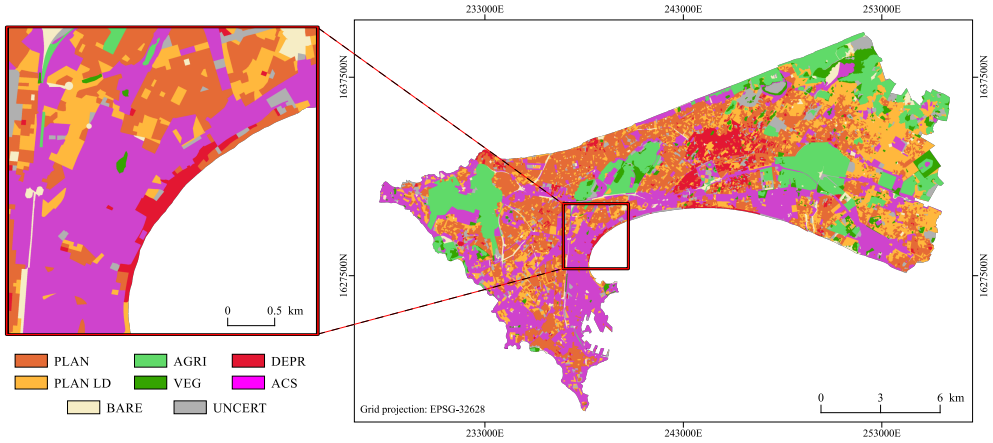


**Figure 4.** The very-high resolution land-use map derived from the VHR land-cover map. Legend classes: AGRI: Agricultural vegetation; VEG: Natural vegetation; BARE: Bare soils; ACS: Non-residential built-up (administrative, commercial, services, etc.); PLAN: Planned residential built-up; DEPR: Deprived residential built-up.

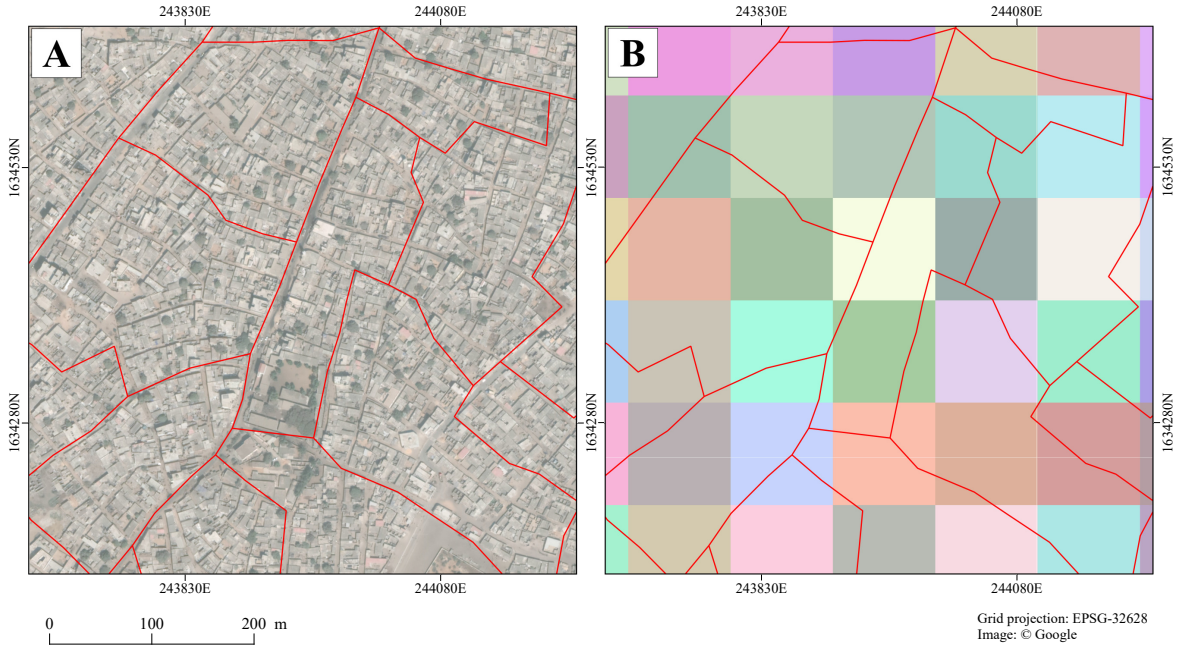


**Figure 5.** The administrative units (neighborhoods of level admin-5) are very small. Administrative unit limits (in red) are superimposed on (**A**) Google Map imagery, and (**B**) a 100 × 100 m grid.

In the core urban area, some administrative units are so small that they include only portions of a few 100 × 100 m grid cells, as illustrated in Figure 5B. This could create some issues when summing (aggregating) the predicted values from grid level to unit level. To mitigate these potential issues and ensure that units at level 1 cover a sufficient number of grid cells, a simple procedure was performed in order to automatically merge administrative units smaller than 8 hectares with the neighbor with which they share the longest border. This minimum size was chosen as a compromise between keeping enough administrative units at the finest level and having sufficiently big units to avoid potential

issues during the validation procedure. The resulting layer, referred to as "level 1", consisted of 677 units and was used in our analysis as the validation level. Figure 6A gives an overview of the population density at this level.

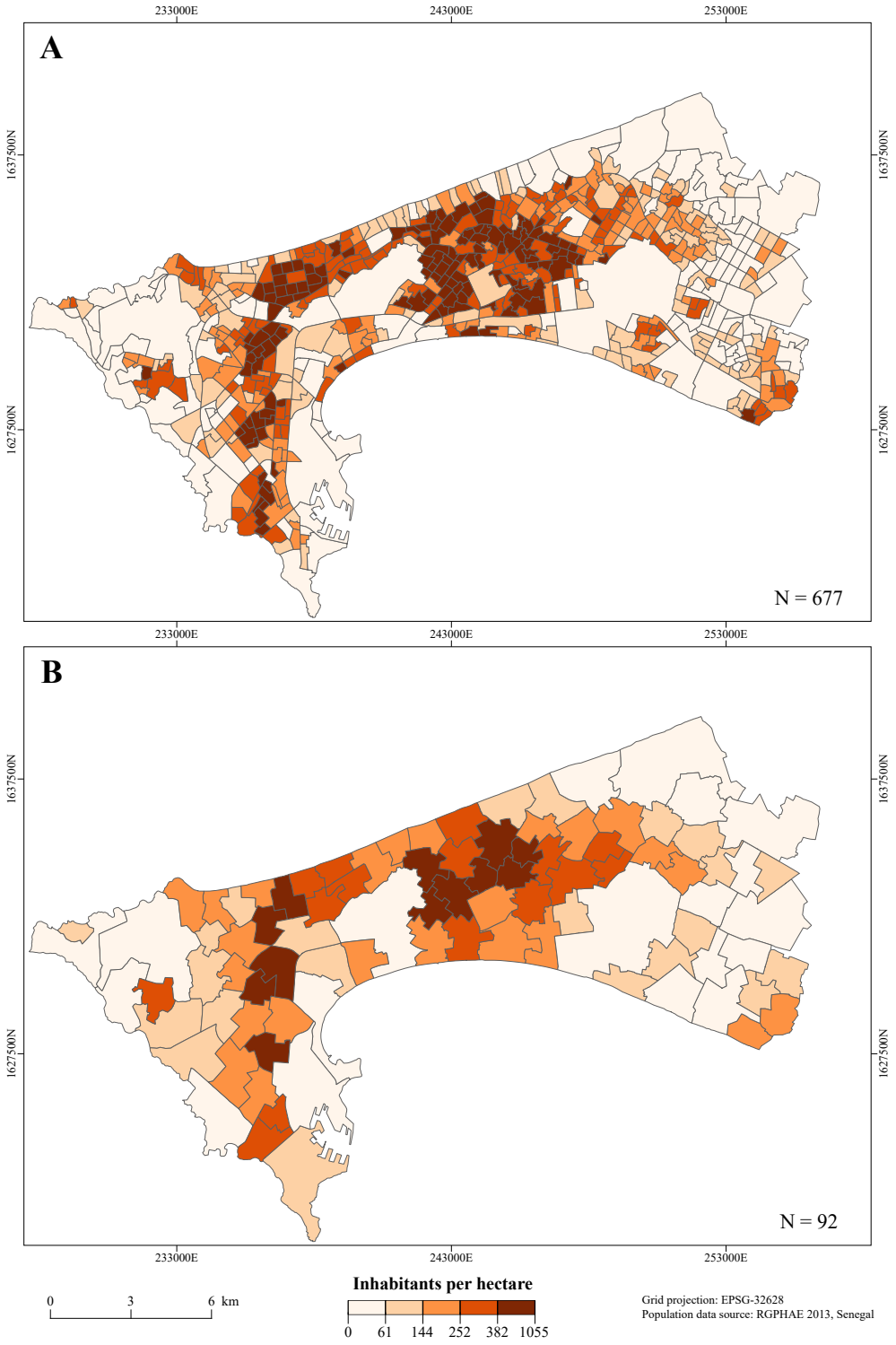


**Figure 6.** Reference population densities. (**A**) Level 1: Finest level reference population data, used here for validation purposes. (**B**) Level 0: A coarser level, created by aggregating contiguous level 1 units together. This level is used as a basis for dasymetric mapping and for training the RF model.

The official admin-4 level in the Senegalese administrative scheme could have been used to create a coarser base level for the dasymetric mapping procedure . However, only 40 admin-4 units were completely included in our area of interest, which would have dramatically affected the ability to train the RF model properly. Instead, we aggregated the level 1 administrative units to create a coarser level, to be used as basis for the disaggregation procedure (represented as step 1 in Figure 1). It was performed using K-means unsupervised clustering on the $X/Y$ coordinates of the polygons' centroid. The desired number of clusters is specified by the user. Further refinement was performed to guarantee that the level 0 units consisted of at least 4 contiguous units from level 1. This procedure allowed for reduction of the 677 units available for validation (level 1) to 92 units, composing the level 0 on which to perform dasymetric mapping procedures. The reason of this drastic reduction is double: Firstly, the access to such spatially detailed data is quite rare for SSA cities. Therefore, having a limited number of units at level 0 gives a more realistic point of view regarding the data that are usually available. Secondly, the aim of the validation procedure is to assess the accuracy of the population reallocation from level 0 to level 1. With respect to the relevance of the validation scheme, it is important to have a sufficient ratio between the number of administrative units at the training and validation level. The average size of level 0 units and level 1 units are 167.42 hectares and 16.49 hectares, respectively (see Table 1).

**Table 1.** Descriptive statistics of both administrative levels used in the analysis.

| Level | Area (ha.) | Population Density (inhab./ha.) | | |
|---|---|---|---|---|
| | Mean | Minimum | Median | Maximum |
| Level 1 (677 units) | 16.49 | 0.81 | 184.59 | 1047.23 |
| Level 0 (92 units) | 167.42 | 5.89 | 164.04 | 541.99 |

### *2.5. Analysis Design and Weighting Layer Creation*

The aim of this study is to assess the contribution of very-high resolution land-cover and land-use products, in comparison to a medium resolution (10 m) built-up mask. Table 2 gives a snapshot of the different test layouts. When single binary built-up/non-built-up information is used as ancillary data, the built-up proportion is computed and directly used as weights for dasymetric mapping (tests A and B). On the other hand, when a larger amount of ancillary information is used, weights are derived through the use of a RF model, such as in tests C to J. Because they are derived from the same single source and consequently represent redundant information, a combination of VHR-BU, VHR-3BU, and/or VHR-LC layers are not used together in the same test.

**Table 2.** Layout of the different tests performed. The "X" marks inform about which layer(s) is used in each test.

| Test | Weights Creation | MR-BU | VHR-BU | VHR-3BU | VHR-LC | VHR-LU |
|---|---|---|---|---|---|---|
| A | Simple proportion | X | | | | |
| B | Simple proportion | | X | | | |
| C | RF-derived weights | | | X | | |
| D | RF-derived weights | | | | X | |
| E | RF-derived weights | | | | | X |
| F | RF-derived weights | X | | | | X |
| G | RF-derived weights | | X | | | X |
| H | RF-derived weights | | | X | | X |
| I | RF-derived weights | | | | X | X |
| J | RF-derived weights | X | | | X | X |

Expert knowledge could be sufficient for identifying evident trends in a data set, or for pointing out specific proxies for a well-known phenomenon. However, when numerous non-linear input data

are used to derive a weighting layer, as in dasymetric mapping strategies, it can become very difficult to rely on expert knowledge. In this context, advantage can be taken from machine learning methods which have proved their efficiency in finding relevant relationships between data for predicting a response variable (e.g., the population density), as is in the WorldPop project that utilises the Random Forest (RF) regression algorithm [15].

RF is a non-parametric supervised machine learning algorithm, which is efficient in handling noisy and highly correlated input data, in addition to its relative resistance to overfitting. It belongs to the category of "ensemble learning" strategies, and consists of an aggregation of several individual and independent trees (CART), each of them trained on a random bootstrapped sample of the training data. RF has a low number of (hyper-)parameters to be set when looking for model optimization. Usually, the number of trees to grow and the number of randomly selected features at each node within a tree are the most common. In the procedure we developed, these parameters are automatically fine-tuned, using a grid search procedure that considers all possible combinations from a range of potential parameter values, to train different models and assess their performance through a k-fold cross-validation. It should be noted that the RF algorithm can be used either for classification or, as in the case in this paper, for regression tasks. Interested readers can refer to the original publication of the RF algorithm [14] for a deeper understanding of its principles.

From the different ancillary data sets, we compute the proportion of each available class available in the different layers. This refers to the built-up proportion for the two binary mask products (MR-BU and VHR-BU), the proportions of three built-up classes categorized by elevation for the VHR-3BU layer, the proportion of each of the land cover classes for the VHR-LC layer, and the proportion of each land-use class provided by the VHR-LU layer. These results constitute the set of covariates used to train the RF model, according to the layout of the different tests designed (see Table 2). The proportions are computed at two levels: For each polygon at the administrative unit level, and for each pixel of the $100 \times 100$ m grid layer. After training on administrative unit level, the fitted model is used to predict the population density for each pixel of the grid layer. This means that this modeling strategy relies on the assumption that the relations that exist between the covariates and the response variable at the administrative unit level (training level) are the same that exist at the grid level (prediction level), which is unlikely to be completely true and is very dependent on the importance of the scale factor between these levels (MAUP effect). The natural log of the population density is used as response variable of the RF model, as previous research suggested it improved the quality of the weight prediction [15], and a back-transformation is applied on the predicted values to retrieve population densities. The values predicted by RF can only be in the range of the response variable it was trained on. It is, thus, incapable of predicting zero values (there are no zero densities in our population data, but even if there were, the log transformation requires the removal of all units with zero population count). Prior to using the predicted weights for dasymetric mapping, we make the choice to force all the grid pixels with a 0% built proportion (in case of a test using LC information) or with 0% potentially inhabited areas (in case of a test using only LU), to have a zero weight value for the grid. This strategy was already used in previous studies [15,27].

### *2.6. Validation Scheme*

The prime rationale for performing dasymetric mapping is to estimate population distribution at a finer scale than the one at which official reference data are released. Usually, when the finest reference data is not sufficiently detailed, validation procedures to assess the accuracy of the spatial reallocation are not performed. Here, we take advantage of the sufficient details of the population data (see description in Section 2.3) to systematically assess the contribution of input data with different spatial and thematic resolution in a dasymetric reallocation procedure.

As already mentioned in Section 2.1, the validation design consists in aggregating the grid-level predictions to get the total estimates (sum) for each of the level 1 units, and comparing them against the reference population count available at this level. It is important to note that this validation procedure

only assesses the efficiency of the different weighting layers for reallocating the population count from level 0 to level 1. The validation of the grid level predictions cannot be achieved here, since official population counts do not exists at this level.

Two different metrics are used to evaluate the performance of the dasymetric models by confronting the population count estimates at level 1 against the reference counts: (1) The normalized version of the commonly used metric root-mean-square error (%RMSE), which uses the mean reference population of administrative units for normalization [15]; and (2) the relative total absolute error (RTAE), which is the ratio between the sum of all absolute errors and the total reference population [28]. These metrics are computed as follows:

$$\%RMSE = \frac{\sqrt{\frac{1}{n}\Sigma_{i=1}^{n}\left(pred_i - ref_i\right)^2}}{\frac{1}{n}\Sigma_{i=1}^{n} ref_i} * 100, \text{ and} \quad (1)$$

$$RTAE = \frac{\Sigma_{i=1}^{n} \mid pred_i - ref_i \mid}{\Sigma_{i=1}^{n} ref_i} * 100, \quad (2)$$

where $ref_i$ is the reference population count of the administrative unit $i$, and $pred_i$ is the sum (aggregation) of all the predictions at grid level that fall within the administrative unit $i$.

### *2.7. Software Environment and Computer Code Availability*

All the analyses were performed in Python, using common libraries for the manipulation of geospatial data (GeoPandas, Fiona, Shapely) and machine learning (Scikit-learn [29]). In addition, the "GRASS Python scripting library" enabled us to take advantage of the efficiency of the open-source software GRASS GIS [30] for raster processing and manipulation. All computer codes produced for the analysis are distributed in a "Jupyter notebook" format [31] and are available from a dedicated repository (see Appendix A). Where possible, the code was designed to support parallel processing on multiple cores, to save computing time.

## 3. Results

The analysis of the results, hereafter, is based on the validation performed by comparing the reference data against the aggregated estimates at administrative level 1. Several conclusions can be drawn, when analyzing the results (see Table 3). First, when relying only on built-up/non-built-up masks, the impact of the very-high resolution data is notable, since it allows the RTAE to decrease by 13% (from 36.7 to 31.7). As highlighted in Figure 7, VHR-BU also leads to an important reduction of extreme relative errors of prediction. It is consistent with recent research which shows that VHR settlement layers systematically have better feature importance than lower resolution layers, in a RF-based dasymetric approach [27].

Second, when taking advantage of the detailed spatial and thematic information provided by the VHR-LC layer, the accuracy of the dasymetric reallocation is significantly improved, with the RTAE reduced to 0.308; corresponding to a drop by 16%, relative to the results obtained using only the built-up mask at medium resolution (MR-BU). Third, when considered as a single source of ancillary data, the VHR-LU layer performs poorly, compared to VHR-LC alone, and is even worse than when only using the binary information provided by the VHR-BU layer. Regarding the data used, it is probable that the lower spatial resolution (characterization of land use at the street block level) and lower classification accuracy of the VHR-LU, compared to VHR-LC and VHR-BU, have a strong influence on this result. Fourth, combined use of VHR-LC and VHR-LU provides better result than when using either of them alone, which confirms that these data are complementary. Figure 8 depicts the feature importance provided by the RF model for the best-performing test (J). It supports the conclusion that VHR-LC and VHR-LU are complementary, since there is a clear alternation of land-cover and land-use variables in the sixth most important features. In addition, it is interesting to

see that both the building classes from the LC layer ("Low buildings (> 5 m)" and "Medium buildings (5 to 10 m)") appear in the most important variable, as well as the distinction between planned residential areas and deprived residential areas from the LU layer.

**Table 3.** Accuracy assessment for the different tests performed. RF internal OOB score refers to the Out-Of-Bag score, computed during the internal cross-validation of the Random Forest. External validation refers to the validation scheme described in the methods section. As tests A and B did not use RF for the creation of the weighting layer, an OOB score is not available ("NA").

| Test | Input Data | RF Internal OOB Score | | External Validation | |
|---|---|---|---|---|---|
| | | Level 0 | Level 1 | %RMSE | RTAE |
| A | MR-BU | NA | NA | 61.00 | 36.7 |
| B | VHR-BU | NA | NA | 54.54 | 31.7 |
| C | VHR-3BU | 0.767 | 0.715 | 52.22 | 33.9 |
| D | VHR-LC | 0.759 | 0.759 | 49.31 | 30.8 |
| E | VHR-LU | 0.789 | 0.757 | 54.37 | 33.5 |
| F | MR-BU, VHR-LU | 0.808 | 0.766 | 47.59 | 29.7 |
| G | VHR-BU, VHR-LU | 0.842 | 0.768 | 46.21 | 28.2 |
| H | VHR-3BU, VHR-LU | **0.850** | 0.802 | 45.22 | 28.8 |
| I | VHR-LC, VHR-LU | 0.833 | **0.815** | 45.24 | 28.4 |
| J | MR-BU, VHR-LC, VHR-LU | 0.836 | 0.813 | **44.40** | **27.9** |

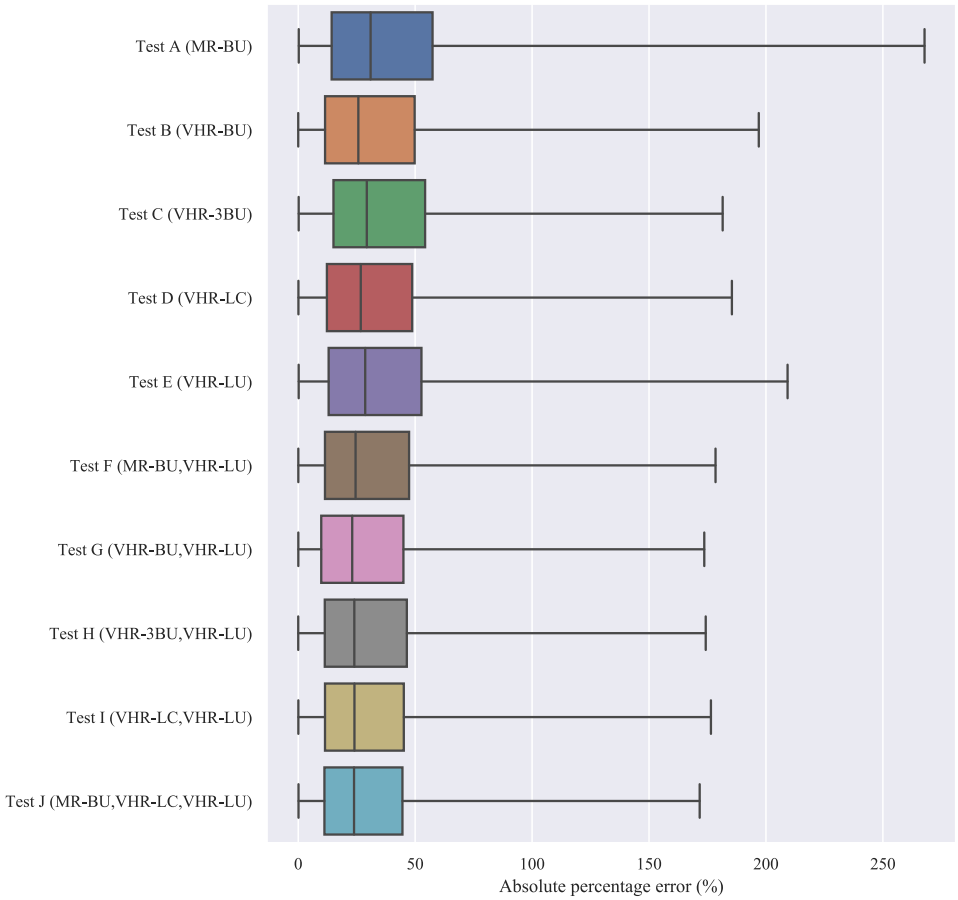


**Figure 7.** Boxplots representing the distribution of the absolute errors of prediction for level 1 units. The values refer to the percentage of absolute prediction error. The vertical line in the box corresponds to the median value. The left and right limits of the boxes refer to the first and third quartile, respectively. The right limit of the whiskers corresponds to the last observation whose value is below the 95th percentile. Observations with higher values are considered as outliers and are not represented here.

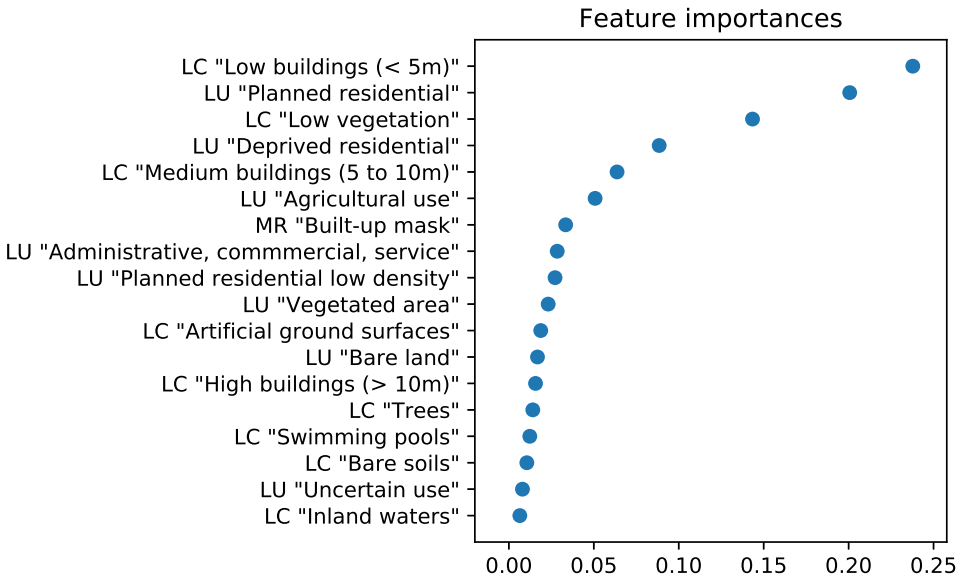


**Figure 8.** Feature importances from the Random Forest model for test J.

Finally, in our analysis, the best-performing dasymetric reallocation was obtained when using all available data; that is, test J, whose predictions at the grid level are illustrated in Figure 9. Surprisingly, the accuracy is improved when using MR-BU in addition to VHR-LC and VHR-LU. As shwon in Figure 10, the majority of the large relative errors (in terms of percentage of the reference population) are located, not surprisingly, in less populated administrative units.

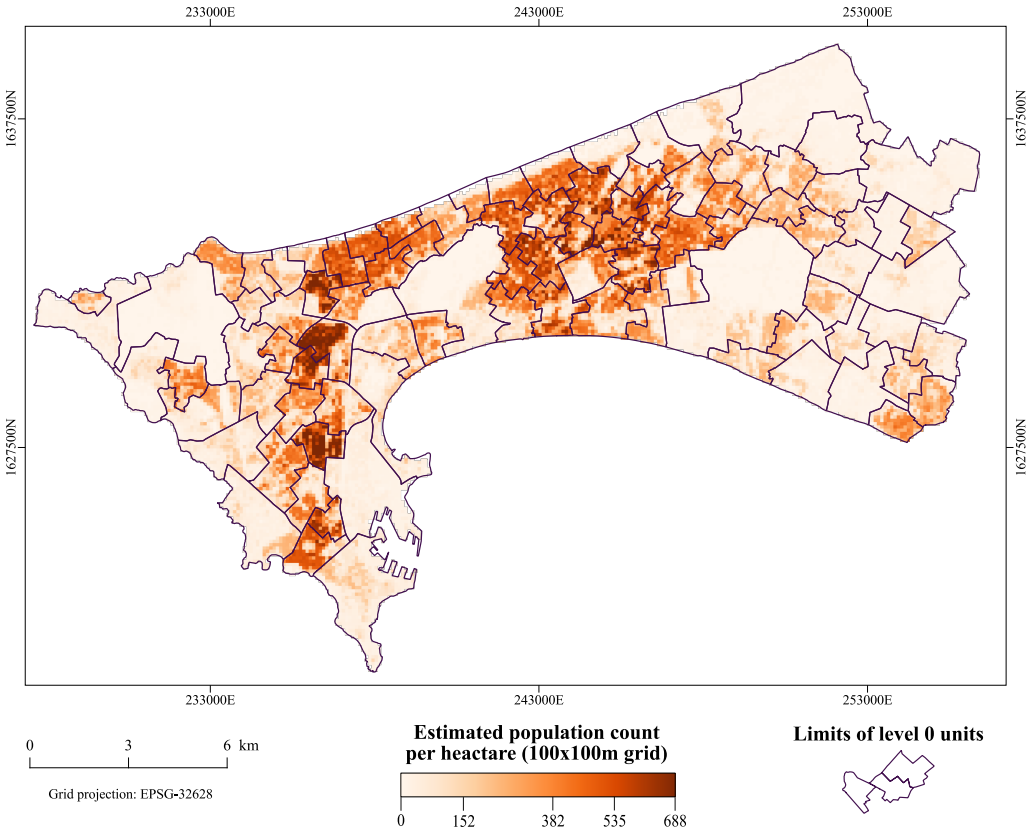


**Figure 9.** Test J—Prediction of population count at grid level (100 × 100 m), superimposed with the limits of units of level 0.

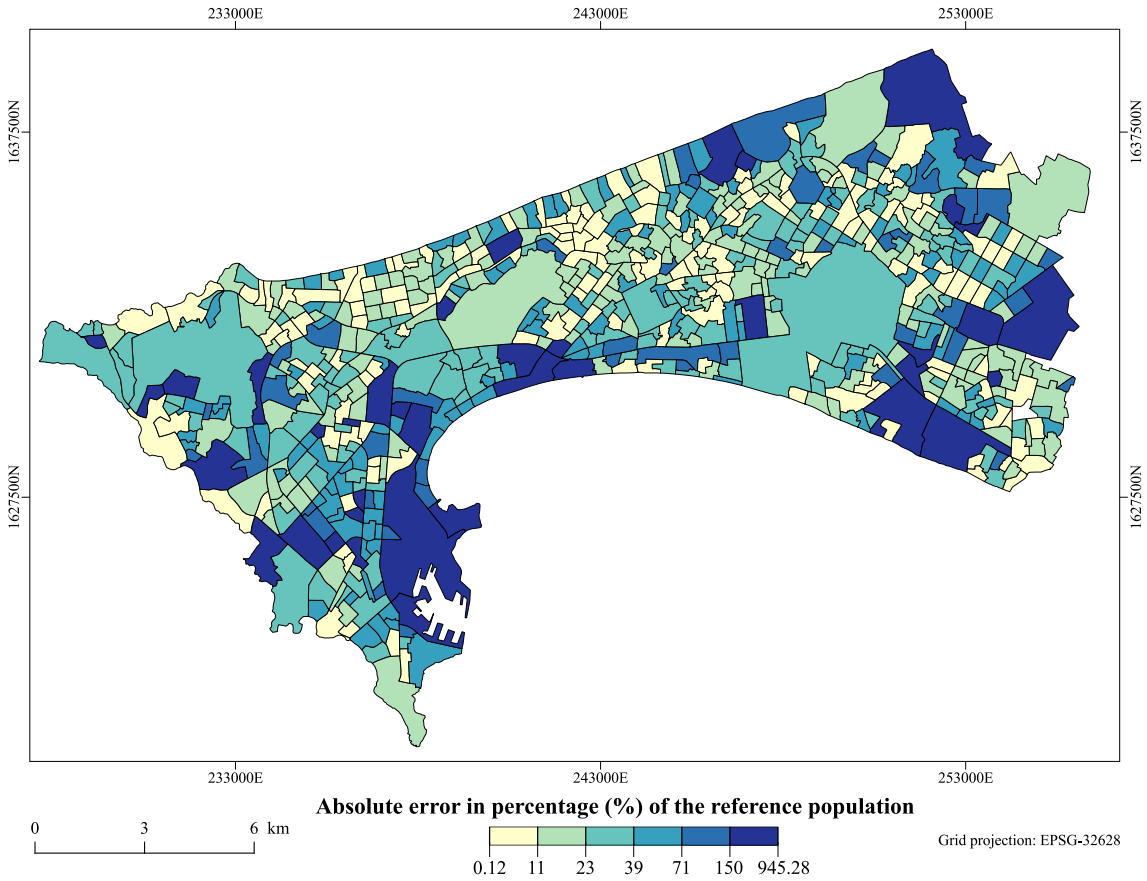


**Figure 10.** Errors of prediction, aggregated to level 1 in absolute percentage of the reference population.

Another interesting point, that can be highlighted from our analysis, is related to the validity of the Out-Of-Bag (OOB) score as a validation metric in dasymetric mapping. The OOB-score (or error) is an accuracy assessment metric, computed during the fitting of the Random Forest model. It is computed from the internal cross-validation procedure, and can be interpreted as an average goodness measure of the ability of the model to predict on unseen data in the training set. Since the training set is composed of administrative units of level 0, this metric could be seen as a measure of the ability of the model to predict on unseen units at the same specific level. Inversely, the external validation used here, as described in the "methods" section, is designed to assess the ability of the dasymetric mapping procedure to accurately redistribute population counts from one geographic scale to a finer one. When studies suffer from the lack of spatially detailed population data, external validations can not be systematically performed. In such contexts, it may be tempting to consider the OOB-score as a measure of the performance of the dasymetric reallocation. Nevertheless, our results show that there is no straightforward relationship between the external validation metrics and the internal OOB-score. Indeed, as visible in Table 3, the best-performing combination of input data (covariates) appears to be in the case of test H (OOB of 0.85 for a RF model built at level 0). However, when considering the RTAE or %RMSE, test J is identified to be the best-performing one. Furthermore, fitting RF models on both administrative levels revealed that the best-performing set of covariates identified at one scale is not obviously the one that performs best at another scale, which could be interpreted as a result of the MAUP effect.

The gridded population layer resulting of the dasymetric mapping procedure presented in this paper is available for anyone interested and for any purposes. The reference is provided in Appendix A.

## 4. Discussion

Medium resolution built-up settlement layers have been commonly used in population modeling [15,32]. They present the advantage of being free and providing global coverage, even though their spatial resolution is limited. However, high or very-high spatial resolution data are usually preferred for applications covering a relatively small geographic extent, as they allow the counting of dwelling units or the interpretation of residential land-use types, despite their expensive costs. To date, little research has explored the potential of built-settlement layers at different spatial resolutions for urban population mapping.

Even if the price of VHR remote sensing data tends to drop slowly, it is still an important limiting factor and reduces the merits of large-scale applications. Usually, the acquisition of VHR imagery is firstly dedicated to the production of detailed LC and LU maps, which are useful pieces of information by themselves. The gains that these VHR-LC and VHR-LU information could provide to the performance of a dasymetric mapping approach is important information regarding the cost effectiveness of these data. In this regard, our results show that there is a clear positive impact of using VHR products for population modeling, as well as a complementarity between VHR-LC and VHR-LU products. Future research could involve integrating low-cost imagery, such as SPOT-6/7 (1.5 m of spatial resolution for pan-sharpened images), which could provide an interesting cost-efficient compromise between MR and VHR.

Regarding the performance of the dasymetric mapping procedure presented here, it is important to mention that the accuracy of the predictions at the grid layer are probably lower than the one presented here (with a validation at level 1, after reaggregation of grid level estimates). Since grid population products tend to be commonly used in different fields of research, it is essential to inform end-users about the confidence and limitations of such products, as much as about their advantages. When using such population models, the end-user should always keep in mind that *"The most that can be expected from any model is that it can supply a useful approximation to reality: All models are wrong; some models are useful"* [33] (p. 440).

With regard to top-down dasymetric approaches, such as the one presented here, we should mention that they are completely dependent on official censuses which are frequently criticized regarding their reliability [6]. Furthermore, in the best case, official censuses are usually organized once in a decade, but in developing countries this rate is not systematically respected. This often forces studies to deal with population data that are asynchronous with ancillary geoinformation, used as covariates. When the official population data are not available or are outdated, remotely-sensed data can be used to support bottom-up approach [6,7]. The latter uses population counts coming from micro-census surveys—i.e., the collection of census information through field surveys on a limited portion of the territory—to extrapolate the population count on the rest of the territory, thus allowing implementation with limited human and financial capacity, compared to a regular census [6].

Additionally, we highlighted that, in a RF-based dasymetric mapping procedure, the OOB-score is not guaranteed to effectively help in the identification of the best-performing combination of input layers, in terms of reallocation accuracy. Therefore, a recommendation is made for future studies to exercise caution when using the OOB-score as an indicator of the performance of dasymetric mapping. More generally, the sensitivity of RF-based top-down population models to the scale factor and the MAUP effect is poorly explored in the literature. It would be beneficial for the field to further investigate the impact of the quantity and the spatial resolution of the administrative units used to train the RF model, and the impact of the difference of spatial resolutions between training and prediction (grid) levels.

## 5. Conclusions

Dasymetric mapping has been used to provide estimation of population densities at a finer scale than the available official data released in administrative units. To this end, this method relies on the use of ancillary data—such as settlement layers, land cover, or land use maps—that are used

as proxies of the real spatial distribution of the population within the administrative units. On one hand, MR satellite imagery can be used to derive such ancillary data at no cost. Unfortunately, when working at the intra-urban level, these data often fail to provide sufficient details in the population model. On the other hand, VHR satellite imagery can provide very detailed information and thus improve the quality of the population models, but their acquisition is much more expensive. In this research, we assessed the added value of VHR remote-sensing derived products, compared to MR products, when used as ancillary data in a dasymetric mapping procedure. When using a simple binary built-up/non-built-up mask, we showed that the use of VHR resulted in a drop of 13% in the error (RTAE). Moreover, our results showed that the use of the spatially and thematically detailed information, which can be derived from VHR land cover and land use maps, which are useful pieces of information by themselves, enabled significant improvement in the dasymetric reallocation accuracy, compared to what can be achieved using a MR built-up mask alone.

**Author Contributions:** Conceptualization, methodology, T.G. and C.L.; formal analysis and validation, T.G.; resources, A.G.; data curation, S.G. and T.G.; writing and editing, T.G., N.M., S.G., S.V., and M.L.; supervision, M.L. and E.W.; project administration, funding acquisition, C.L., S.V., and E.W.

**Funding:** This research was funded by BELSPO (Belgian Federal Science Policy Office) in the frame of the STEREO III program, as part of the MAUPP (http://maupp.ulb.ac.be) (SR/00/304) and REACT (http://react.ulb.be/) (SR/00/337) projects.

**Acknowledgments:** The authors gratefully thanks the ASSESS project (http://assess-sn.org/), funded by the ARES-CDD (https://www.ares-ac.be), which provided the access to the population data. The authors sincerely acknowledge the reviewers for their relevant comments which helped to improve this manuscript.

**Conflicts of Interest:** The authors declare no conflict of interest.

## Appendix A

All the computed code that supported this research is available from the following repository: https://github.com/tgrippa/Dasymetric_mapping_using_GRASSGIS.

The gridded population layer produced in this study is accessible in a dedicated repository (CC-BY license): https://doi.org/10.5281/zenodo.2525671

The data sets used as input for the analysis presented in this paper are as follows. These are all available under CC-BY license.

- The MR built-up layer is available from https://doi.org/10.5281/zenodo.1450931.
- The VHR land-cover map is available from https://doi.org/10.5281/zenodo.1290799.
- The VHR land-use map is available from https://doi.org/10.5281/zenodo.1291388.

## References

1. UN DESA. *World Urbanization Prospects: The 2018 Revision, Online Edition*; United Nations Department of Economic and Social Affairs: New York, NY, USA, 2018.
2. United Nations Human Settlements Programme (UN-Habitat). *The State of African Cities, 2014: Re-Imagining Sustainable Urban Transitions*; UN-Habitat: Nairobi, Kenya, 2014.
3. Steiner, P.; Paulus, G. Dasymetric mapping for public health planning. In Proceedings of the 10th AGILE International Conference on Geographic Information Science, Aalborg, Denmark, 8–11 May 2007.
4. Ehrlich, D.; Lang, S.; Laneve, G.; Mubareka, S.; Schneiderbauer, S.; Tiede, D. Can Earth Observation help to improve information on population? Indirect Population Estimations from EO Derived Geo-Spatial Data: Contribution from GMOSS. In *Remote Sensing from Space: Supporting International Peace and Security*; Springer: Dordrecht, The Netherlands, 2009; pp. 211–237.
5. Su, M.D.; Lin, M.C.; Hsieh, H.I.; Tsai, B.W.; Lin, C.H. Multi-layer multi-class dasymetric mapping to estimate population distribution. *Sci. Total Environ.* **2010**, *408*, 4807–4816.
6. Wardrop, N.A.; Jochem, W.C.; Bird, T.J.; Chamberlain, H.R.; Clarke, D.; Kerr, D.; Bengtsson, L.; Juran, S.; Seaman, V.; Tatem, A.J. Spatially disaggregated population estimates in the absence of national population and housing census data. *Proc. Natl. Acad. Sci. USA* **2018**, *115*, 3529–3537.

7. Weber, E.M.; Seaman, V.Y.; Stewart, R.N.; Bird, T.J.; Tatem, A.J.; McKee, J.J.; Bhaduri, B.L.; Moehl, J.J.; Reith, A.E. Census-independent population mapping in northern Nigeria. *Remote Sens. Environ.* **2018**, *204*, 786–798.
8. United Nations Economic and Social Council. *Report of the Inter-Agency and Expert Group on Sustainable Development Goal Indicators*; United Nations Economic and Social Council: New York, NY, USA, 2016.
9. Langford, M. Rapid facilitation of dasymetric-based population interpolation by means of raster pixel maps. *Comput. Environ. Urban Syst.* **2007**, *31*, 19–32.
10. Langford, M.; Unwin, D.J. Generating and mapping population density surfaces within a geographical information system. *Cartogr. J.* **1994**, *31*, 21–26.
11. Openshaw, S. The modifiable areal unit problem. *Concepts Tech. Mod. Geogr.* **1984**, *38*.
12. Mennis, J. Generating Surface Models of Population Using Dasymetric Mapping. *Prof. Geogr.* **2003**, *55*, 31–42.
13. Wu, S.; Qiu, X.; Wang, L. Population Estimation Methods in GIS and Remote Sensing: A Review. *GISci. Remote Sens.* **2005**, *42*, 80–96.
14. Breiman, L. Random Forests. *Mach. Learn.* **2001**, *45*, 5–32.
15. Stevens, F.R.; Gaughan, A.E.; Linard, C.; Tatem, A.J. Disaggregating census data for population mapping using random forests with remotely-sensed and other ancillary data. *PLoS ONE* **2015**, doi:10.1371/journal.pone.0107042.
16. Nieves, J.J.; Stevens, F.R.; Gaughan, A.E.; Linard, C.; Sorichetta, A.; Hornby, G.; Patel, N.N.; Tatem, A.J. Examining the correlates and drivers of human population distributions across low- and middle-income countries. *J. R. Soc. Interface* **2017**, *14*, 20170401.
17. Tobler, W.R. Smooth pycnophylactic interpolation for geographical regions. *J. Am. Stat. Assoc.* **1979**, *74*, 519–530.
18. Forget, Y.; Shimoni, M.; Gilbert, M.; Linard, C. Complementarity Between Sentinel-1 and Landsat 8 Imagery for Built-Up Mapping in Sub-Saharan Africa. *Preprints* **2018**, doi:10.20944/preprints201810.0695.v1.
19. Forget, Y.; Linard, C.; Gilbert, M. Automated supervised classification of Ouagadougou built-up areas in Landsat scenes using OpenStreetMap. In Proceedings of the 2017 Joint Urban Remote Sensing Event (JURSE), Dubai, UAE, 6–8 March 2017; pp. 1–4.
20. Forget, Y.; Linard, C.; Gilbert, M.; Shimoni, M.; Lopez, J. Fusion Scheme for Automatic and Large-Scaled Built-up Mapping. In Proceedings of the IGARSS 2018—2018 IEEE International Geoscience and Remote Sensing Symposium, Valencia, Spain, 22–27 July 2018; pp. 2072–2075.
21. Grippa, T.; Lennert, M.; Beaumont, B.; Vanhuysse, S.; Stephenne, N.; Wolff, E. An Open-Source Semi-Automated Processing Chain for Urban Object-Based Classification. *Remote Sens.* **2017**, *9*, 358.
22. Grippa, T.; Georganos, S.; Vanhuysse, S.; Lennert, M.; Wolff, E. A local segmentation parameter optimization approach for mapping heterogeneous urban environments using VHR imagery. In *Remote Sensing Technologies and Applications in Urban Environments II*; International Society for Optics and Photonics: Bellingham, WA, USA, 2017.
23. Georganos, S.; Grippa, T.; Lennert, M.; Vanhuysse, S.; Wolff, E. SPUSPO: Spatially Partitioned Unsupervised Segmentation Parameter Optimization for efficiently segmenting large heterogeneous areas. In Proceedings of the 2017 Conference on Big Data from Space (BiDS'17), Toulouse, France, 28–30 November 2017.
24. Brousse, O.; Georganos, S.; Demuzere, M.; Vanhuysse, S.; Wouters, H.; Wolff, E.; Linard, C.; van Lipzig, N.P.M.; Dujardin, S. Using Local Climate Zones in Sub-Saharan Africa to tackle urban health issues. *Urban Clim.* **2019**, *27*, 227–242.
25. Grippa, T.; Georganos, S.; Zarougui, S.; Bognounou, P.; Diboulo, E.; Forget, Y.; Lennert, M.; Vanhuysse, S.; Mboga, N.; Wolff, E. Mapping Urban Land Use at Street Block Level Using OpenStreetMap, Remote Sensing Data, and Spatial Metrics. *ISPRS Int. J. Geo-Inf.* **2018**, *7*, 246.
26. Agence Nationale de la Statistique et de la Démographie (ANSD). *Rapport définitf du RGPHAE 2013*; ANSD: Dakar, Senegal, 2013.
27. Reed, F.; Gaughan, A.; Stevens, F.; Yetman, G.; Sorichetta, A.; Tatem, A. Gridded Population Maps Informed by Different Built Settlement Products. *Data* **2018**, *3*, 33.
28. Batista e Silva, F.; Gallego, J.; Lavalle, C. A high-resolution population grid map for Europe. *J. Maps* **2013**, *9*, 16–28.

29. Pedregosa, F.; Varoquaux, G.; Gramfort, A.; Michel, V.; Thirion, B.; Grisel, O.; Blondel, M.; Prettenhofer, P.; Weiss, R.; Dubourg, V.; et al. Scikit-learn: Machine Learning in Python. *J. Mach. Learn. Res.* **2011**, *12*, 2825–2830.
30. Neteler, M.; Bowman, M.H.; Landa, M.; Metz, M. GRASS GIS: A multi-purpose open source GIS. *Environ. Model. Softw.* **2012**, *31*, 124–130.
31. Kluyver, T.; Ragan-Kelley, B.; Pérez, F.; Granger, B.; Bussonnier, M.; Frederic, J.; Kelley, K.; Hamrick, J.; Grout, J.; Corlay, S.; et al. Jupyter Notebooks—A publishing format for reproducible computational workflows. In Proceedings of the 20th International Conference on Electronic Publishing, Göttingen, Germany, 7–9 June 2016; pp. 87–90.
32. Linard, C.; Tatem, A.J.; Gilbert, M. Modelling spatial patterns of urban growth in Africa. *Appl. Geogr.* **2013**, *44*, 23–32.
33. Box, G.E.P.; Hunter, J.S.; Hunter, W.G. *Statistics for Experimenters: Design, Innovation, and Discovery*, 2nd ed.; Wiley Series in Probability and Statistics; Wiley-Interscience: Hoboken, NJ, USA, 2005.

# Chapter 5

# Conclusion

The first objective of this thesis was to develop open-source solutions for mapping SSA cities. However, advantage have been taking from the geoinformation produced with these frameworks to evaluate the contribution of VHRRS data to improve the quality of intra-urban population models. To achieve these objectives and answer research questions, new efficient strategies were developed and leveraged into semi-automated processing chains providing a framework allowing to generate a complete and complementary set of geoinformation - i.e., land cover, land use and population estimation.

This chapter aims to summarize the outcomes, discuss the limitations of the proposed solutions and open perspectives for future research.

## 5.1 Summary of the outcomes

The major outcome of this thesis consists of the semi-automated OBIA land cover mapping framework that went through several stages of development and improvement. It led to three scientific publications (**papers 1,2,3**) presented in detail in chapter 2. In order to process VHRRS data covering large-scale areas, we had to push existing state-of-the-art methods up to their limits. Our methodological developments allow for the processing of VHR imagery covering very large and heterogeneous urban scenes, through local unsupervised segmentation parameter optimization for different automatically subdivided partitions of a satellite image. On top of that, this framework is implemented in a semi-automated processing chain published under an open license. It relies on open-source software and is computationally efficient since it was designed to allow for parallel processing. This new approach, overcoming the limitations that marred existing methods by providing efficient solutions, opens a door toward big data processing.

The framework for mapping the urban land use constitutes another important outcome of this thesis. As highlighted in chapter 3 (**paper 4**), the proposed solution

is designed to respond to the lack of ancillary data on which fine-scale land-use classification usually rely on. It takes advantage of OSM data for the creation of street block geometries and of existing land cover maps for the characterization and classification of these blocks, all in a highly automated fashion. For these reasons, we consider the proposed framework as an important contribution to land use mapping in data-poor contexts which could be reused for many applications in SSA or in other developing countries.

Finally, the last achievement that should be mentioned refers to the assessment of the contribution of VHR to the improvement of existing population density estimates in SSA. The research presented in chapter 4 (**paper 5**) confirmed that VHR-derived geoinformation was highly valuable for population modeling. Using our dasymetric mapping framework, we were able to model the distribution of population densities for the city of Dakar, Senegal, and we produced a gridded population layer with unprecedented spatial details. A systematic validation was performed to measure the gain in accuracy for the population reallocation procedure. The results showed that, when relying only on a binary built-up mask alone, VHR (0.5m) allowed to decrease the error rate by 13% compared to HR (10m). Furthermore, the complementarity of VHR-derived land-cover and land-use maps for the population modeling was confirmed by model features importance. Used together, it allowed us to increase even more the quality of population models and to decrease the error rates by 22% compared to a model based on an HR built-up mask.

Moreover, in addition to these cutting-edge methodological developments, this thesis contributed to the geographical knowledge of SSA cites. Indeed, the frameworks implemented were used to produce key geographic information - i.e., land cover, land use and fine-scaled population maps - for Dakar and Ouagadougou, covering respectively 418 $km^2$ and 615 $km^2$. To our knowledge, there are no other maps currently available that provide such recent and spatially detailed LC and LU information for these cities. These could serve for future research and LC information has already been used in research aiming to map local climate zones in Dakar [89].

In addition, all the methods were developed with a particular focus on automation and transferability. Thanks to these efforts, the frameworks developed in this thesis to map the land cover and land use at the intra-urban level are already being used in another research project called REACT which aims at mapping other SSA cities and model urban climate in support to malaria risk assessment [89]. The OBIA land-cover framework proved its ability to be transferred to other case studies and sources of VHR images with minimal adaptation efforts [90]. Moreover, the WALOUS project is currently taking advantage of the lessons learned in this thesis to go further in the automation and scaling of methods and processing of big data sets with the aim of mapping the whole Walloon region in Belgium (>16.000 $km^2$),

based on VHR airborne images with a spatial resolution of 0.25m.

Also, open-source and open-access were important governing principles in this thesis. For this reason, the mapping frameworks and other computer code developed as well as the final maps (land cover, land use and gridded population estimates) are made available through different public repositories, at no cost, for anybody and for any purpose:

- Data sets repositories: zenodo.org
- Frameworks and computer code: github.com/tgrippa and github.com/anageo

## 5.2 Limitations of the proposed solutions

Even though the methods proposed in this thesis provide highly valuable contributions in the field of remote sensing, they remain affected by some limitations. We present below a summary of the main limitations that have been previously addressed in chapter 2, 3 and 4.

For both land-cover and land-use mapping, a important limitation of the proposed solutions is that the implemented supervised classification requires the creation of training and validation samples. For the moment, we do not propose any automated solution for the labeling of these samples. This remains a challenge to be overcome by future research, especially in the context of SSA where reference databases are often not available. OpenStreetMap data could be used for that purpose but their quality is often inconsistent. Issues of co-registration with VHR imagery might also arise when using such data sets.

Regarding the computational efficiency of the framework, some limitation has been highlighted regarding processing time and storage space required for the features used for the classification. More complex strategies could be implemented to compute many classification features (NDVI, band ratios, GLCM textures, spatial metrics on land cover maps for land use mapping, etc...) only for the segments included in the training/validation samples. Then, by using feature selection algorithm, it would be possible to identify which are the most important predictive features for the specific data set under investigation. Only the most discriminant features could then be computed for the whole AOI. This approach would allow for computing a very large number of features without creating computational and storage issues.

Another limitation is related to the use of SPUSPO. Even if this approach achieves better segmentation and classification results, it also increases the computational time. In order to reduce the required processing time, several solutions could be explored. For example, superpixels that run faster could be used in the early stages of the segmentation and used as seeds to the main region-growing algo-

rithm. An add-on has recently been implemented in GRASS GIS for this functionality. Another possibility could be to experiment massive parallel computing for the segmentation step, but an adequate infrastructure needs to be accessible such as a High-performance computing (HPC) system.

Regarding to the land use mapping framework, the main limitation relates to the completeness of OSM data. Indeed, the OSM database is not complete enough in certain locations, especially in peri-urban areas. However, the completeness of OSM is increasing and it is likely that such issues will become less prevalent in the future. Still, the performance of the proposed framework is likely to decrease as the landscape becomes more rural, because the density of roads in OSM will be lower. For this reason, other strategies should be investigated in order to try to automatically extract meaningful landscape units in rural environments.

Another limitation of the land use framework is the use of landscape metrics. These belong to the "patch mosaic" paradigm [91] and may hide some aspects of the urban structures. Future research could investigate to use of information derived from the OBIA segments. For example, information on individual segments could be computed, e.g., area, compactness, and fractal dimension, and then summarized either at the class or at the landscape level.

Finally, a limitation also exists for the population framework and with regard to top-down dasymetric approaches, such as the one presented here. The main and most obvious limitation is that this approach is completely dependent on official censuses which are frequently criticized regarding their reliability. Furthermore, in the best of cases, official censuses are usually organized once in a decade, but in developing countries this frequence is not systematically respected.

More general limitations and criticisms of the proposed solutions, not yet addressed in the published papers, are discussed below.

First of all, we implemented a top-down dasymetric mapping as population modeling strategy. The major limitation of this approach is that it relies completely on the official population data provided in administrative units. If the latter are highly outdated or if they suffer from a lack of reliability, population estimates will be directly affected. As shown in the introduction (chapter 1), a bottom-up approach should be preferred in this kind of situation. Also, since dasymetric models depend on official census data which count the population by usual place of residence (night-time population), they fail to provide useful information for abrupt hazard event that could happen during daytime. Again, a bottom-up approach could be used to get daytime estimates ("ambient" population).

Second, all the proposed frameworks have been developed to be used with VHRRS data. While access to these data is usually not a problem in rich coun-

tries[1], their acquisition is more difficult for countries faced with a lack of financial resources. This could inhibit the use of VHR data in remote sensing applications in poor countries. However, in order to limit acquisition costs, fine-scaled maps could be created using VHR acquired only over urban areas, while the rest of the national territory could be mapped using coarser but free HR data[2]. Moreover, it should be noted that the acquisition costs only represent a small proportion of the total financial resources needed which also include personnel cost, hardware acquisition and often the expensive licensing cost of proprietary GIS and image processing software. By providing entirely free and open-source solutions, this thesis tries to slightly reduce the gap that exists between research conducted in rich and poor countries. In future research, it would be very interesting to analyse and compare the total financial means - i.e., image acquisition, personnel cost, hardware, training, etc. . . - required to perform a national mapping campaign using our approach and the approach currently used by national authorities.

Next, one limitation of the frameworks proposed here is related to the level of expertise required to reuse them. Indeed, even if they are semi-automatized and if important efforts have been made for making them easily understandable and reusable, their implementations remain quite complex and users should be skilled in geomatics and in basic computer programming for employing them in their own research. In this regard, there is still a technical lag in SSA compared to the developed world. Several algorithms developed in this thesis were translated into ready-to-use GRASS GIS modules, which is a first step toward making the proposed solutions reusable by a larger audience.

Finally, another potential criticism is related to the effective use of the proposed solutions. Aside from scientific aspects, a pending question is if the new geoinformation produced in this thesis - i.e., land-cover and land-use maps as well as gridded population estimates - will reach their target and serve as evidence-based support for decision-making processes for public policy, e.g., for poverty reduction programs or access to healthcare infrastructure or sanitation equipment. This is, of course, very difficult to answer, especially because it depends on the political will and financial capacities. It is unlikely that the geoinformation produced here will serve directly as a decision tool. However, this key information is likely to be used in the analyses of other research aiming at providing valuable specific indicators in direct support to political decision-making.

Besides, it should be kept in mind that modeled population layers could be misused. For example, the end users could consider the population estimation as real

[1]Acquisition cost remains relatively limited compared to personal costs, for example. Also, more and more countries provide national coverage with VHR images accessible at no cost for research purpose.

[2]Obviously, the high level of accuracy achieved through the use of VHR would be affected.

counts if they are not sufficiently informed that they only provide an approximation of the reality. Also, it may be tempting to compute specific indicators (e.g., population at risk of flooding), at the same resolution as the gridded population product. However, the accuracy of estimated population count is likely to be low at the grid-cell level[3]. The appropriate use would be to derive indicators at a coarser resolution instead (e.g., proportion of the population who are at risk of flooding in a larger area), because it would enable the mitigation of extreme errors and then increase the confidence that one can have in the indicator. For this reason, it is important to inform end users about product limitations and good practices for its use.

## 5.3 Perspectives for future research

As research never stops, there are obviously many perspectives for future research linked with topics tackled in this thesis. Some of them are presented below.

As aforementioned, a bottom-up approach should be preferred to top-down dasymetric mapping when population data are outdated or considered unreliable. Future research using a bottom-up approach could investigate how VHR may be used to improve population estimates obtained by using HR data. One idea is to use VHR-derived geoinformation to improve the selection of the locations where to carry out the micro-surveys to make them more representative of the diversity of the AOI, which might result in an improvement of the quality of the population estimates.

Another perspective of research is to tackle the issues related to the acquisition cost of VHRRS images, which could reduce their potential for regional and national scale application applications. Future research could assess the potential of remote sensing data with slightly coarser spatial resolution as cost-effective alternatives to VHR in dasymetric mapping. For example, SPOT satellites providing images with a spatial resolution of 1.5m but at a lower cost than VHR, could be used to map the land cover and land use at the intra-urban level. While we expect that it could not provide such detailed and accurate geographic information as sub-metric data used in this thesis, it would be very interesting to carry out a comparative study to quantify the loss of accuracy in population estimates induced by the use of LC and LU maps produced from coarser resolution data. In this context, it would be interesting to see how the frameworks proposed in this thesis could be adapted to coarser resolution.

An important point that was not covered in this thesis and that is worth investigating in future studies is related to uncertainty. Indeed, land-cover and land-use

[3]Actually, the main reason to provide gridded population layer with grid cells of 100*100m is to mitigate the loss of spatial precision when performing spatial analysis.

maps are never produced with an accuracy of 100% and are thus affected to a certain level by classification uncertainties. The main issue, from a modeling point of view, is that errors in ancillary data are likely to impact the output of the model. Future research could aim at analyzing and quantifying the influence of the uncertainty in input data on the quality of population estimations with dasymetric mapping.

Last but not least, we could not conclude this thesis without raising the perspective provided by the recent development of Deep Learning (DL). As it reaches many aspects of our society, these methods affect more and more fields of research leading to scientific breakthroughs and paradigm changes. Potentially, many remote sensing and modeling applications could be treated with DL approaches. It opens doors to a considerable amount of future research. With regards to the topics addressed in this thesis, it would be interesting to see how far DL approaches can go in replacing "classical" methods as the one proposed here that proved their efficiency.

# Bibliography


[1] Philippe Antoine. *L'urbanisation en Afrique et ses perspectives*. Aliments et Villes. FAO, 1997. URL: http://www.fao.org/docrep/003/x6988f/x6988f07.htm (visited on 09/23/2016).

[2] Pierre Vennetier. "Que faire des villes d'Afrique tropicale? Ou: les problèmes d'une urbanisation galopante". In: *Bulletin de la Société géographique de Liège* 26 (1990), pp. 63–75. URL: http://popups.ulg.ac.be/0770-7576/index.php?id=3702&file=1 (visited on 08/04/2015).

[3] Catherine Coquery-Vidrovitch. "The Process of Urbanization in Africa (From the Origins to the Beginning of Independence)". In: *African Studies Review* 34.1 (Apr. 1991), p. 1. ISSN: 00020206. DOI: 10.2307/524256. (Visited on 10/08/2015).

[4] UN DESA. *World Urbanization Prospects: The 2018 Revision, Online Edition*. New York, NY, USA: United nations, Department of Economic and Social Affairs, 2018.

[5] Daniel Hoornweg and Kevin Pope. "Population predictions for the world's largest cities in the 21st century". en. In: *Environment and Urbanization* 29.1 (Apr. 2017), pp. 195–216. ISSN: 0956-2478, 1746-0301. DOI: 10.1177/0956247816663557.

[6] Jérôme Chenal. *The West African city: urban space and models of urban planning*. eng. 1. ed. Lausanne: EPFL Press [u.a.], 2014. ISBN: 978-2-940222-82-7.

[7] A. Ambrose. "A Tale of Two African cities: Hyper Growth, Sprawl and Compact city development". In: *Proceeding of the 48th ISOCARP Congress*. 2012. URL: http://www.isocarp.net/Data/case_studies/2172.pdf.

[8] Catherine Coquery-Vidrovitch. "De la ville en Afrique noire". In: *Annales. Histoire, Sciences Sociales* 61e Année.No. 5 (2006), pp. 1087–1119.

[9] United Nations Human Settlements Programme (UN-Habitat). *The state of African cities, 2014: re-imagining sustainable urban transitions*. OCLC: 896908610. United Nations Human Settlements Programme, UN-Habitat, 2014. ISBN: 978-92-1-132598-0.

[10] Francisco J. Goerlich Gisbert, Isidro Cantarino Martí, and Eric Gielen. "Clustering cities through urban metrics analysis". In: *Journal of Urban Design* 22.5 (2017), pp. 689–708. DOI: 10.1080/13574809.2017.1305882.

[11] Taïs Grippa et al. "Mapping Urban Land Use at Street Block Level Using OpenStreetMap, Remote Sensing Data, and Spatial Metrics". In: *ISPRS International Journal of Geo-Information* 7.7 (June 22, 2018), p. 246. ISSN: 2220-9964. DOI: 10.3390/ijgi7070246.

[12] Lei Ma et al. "A review of supervised object-based land-cover image classification". en. In: *ISPRS Journal of Photogrammetry and Remote Sensing* 130 (Aug. 2017), pp. 277–293. ISSN: 09242716. DOI: 10.1016/j.isprsjprs.2017.06.001.

[13] Stefanos Georganos et al. "Scale Matters: Spatially Partitioned Unsupervised Segmentation Parameter Optimization for Large and Heterogeneous Satellite Images". In: *Remote Sensing* 10.9 (Sept. 9, 2018), p. 1440. ISSN: 2072-4292. DOI: 10.3390/rs10091440.

[14] Franz Schug et al. "Mapping patterns of urban development in Ouagadougou, Burkina Faso, using machine learning regression modeling with bi-seasonal Landsat time series". en. In: *Remote Sensing of Environment* 210 (June 2018), pp. 217–228. ISSN: 00344257. DOI: 10.1016/j.rse.2018.03.022. (Visited on 04/12/2018).

[15] Direction générale des impôts. Burkina Faso, ed. *Recensement de la population de la commune de Ouagadougou*. 2012.

[16] Agence Nationale de la Statistique et de la Démographie (ANSD). *Rapport définitf du RGPHAE 2013*. 2013. URL: http://anads.ansd.sn/index.php/catalog/51.

[17] Jean-Paul Deroin et al. "Integrated non-invasive remote-sensing techniques and field survey for the geoarchaeological study of the Sud Lípez mining district, Bolivia". In: *Journal of Geophysics and Engineering* 9.4 (Aug. 2012), S40–S52. ISSN: 1742-2132, 1742-2140. DOI: 10.1088/1742-2132/9/4/S40.

[18] Maggi Kelly et al. "Terrestrial Remotely Sensed Imagery in Support of Public Health: New Avenues of Research Using Object-Based Image Analysis". en. In: *Remote Sensing* 3.11 (Oct. 2011), pp. 2321–2345. ISSN: 2072-4292. DOI: 10.3390/rs3112321.

[19] T. Blaschke. "Object based image analysis for remote sensing". In: *ISPRS Journal of Photogrammetry and Remote Sensing* 65.1 (Jan. 2010), pp. 2–16. ISSN: 0924-2716. DOI: 10.1016/j.isprsjprs.2009.06.004.

[20] Robert M. Haralick and Linda G. Shapiro. "Image segmentation techniques". In: *Computer Vision, Graphics, and Image Processing* 29.1 (Jan. 1985), pp. 100–132. ISSN: 0734-189X. DOI: 10.1016/S0734-189X(85)90153-7.

[21] Taïs Grippa et al. "An Open-Source Semi-Automated Processing Chain for Urban Object-Based Classification". In: *Remote Sensing* 9.4 (Apr. 11, 2017), p. 358. DOI: 10.3390/rs9040358.

[22] Lennert M. and GRASS Development Team. *Addon i.segment.uspo*. 2016. URL: https://grass.osgeo.org/grass70/manuals/addons/i.segment.uspo.html (visited on 11/25/2016).

[23] F. Cánovas-García and F. Alonso-Sarría. "A local approach to optimize the scale parameter in multiresolution segmentation for multispectral imagery". In: *Geocarto International* 30.8 (Sept. 2015), pp. 937–961. ISSN: 1010-6049. DOI: 10.1080/10106049.2015.1004131. (Visited on 05/06/2016).

[24] Taïs Grippa et al. “A local segmentation parameter optimization approach for mapping heterogeneous urban environments using VHR imagery”. In: *Proceedings Volume 10431, Remote Sensing Technologies and Applications in Urban Environments II*. IEEE, Oct. 4, 2017. DOI: 10.1117/12.2278422.

[25] S. Vanhuysse et al. “Contribution of nDSM derived from VHR stereo imagery to urban land-cover mapping in Sub-Saharan Africa”. In: *2017 Joint Urban Remote Sensing Event (JURSE)*. Mar. 2017. DOI: 10.1109/JURSE.2017.7924570.

[26] T Novack et al. “Per block urban land use interpretation using optical VHR data and the knowledge-based system Interimage”. In: *The International Archives of the Photogrammetry, Remote Sensing and Spatial Information Sciences* 38.4/C7 (2010), p. 6. URL: https://urlz.fr/975E.

[27] Michael Voltersen et al. “Object-based land cover mapping and comprehensive feature calculation for an automated derivation of urban structure types at block level”. In: *Remote Sensing of Environment* 154 (Nov. 2014), pp. 192–201. ISSN: 0034-4257. DOI: 10.1016/j.rse.2014.08.024. (Visited on 02/13/2015).

[28] Irene Walde et al. “From land cover-graphs to urban structure types”. In: *International Journal of Geographical Information Science* 28.3 (Mar. 2014), pp. 584–609. ISSN: 1365-8816. DOI: 10.1080/13658816.2013.865189. (Visited on 01/13/2017).

[29] Sven Vanderhaegen and Frank Canters. “Mapping urban form and function at city block level using spatial metrics”. en. In: *Landscape and Urban Planning* 167 (Nov. 2017), pp. 399–409. ISSN: 01692046. DOI: 10.1016/j.landurbplan.2017.05.023. (Visited on 12/21/2017).

[30] T. Hermosilla Gómez et al. “EFFICIENCY OF CONTEXT-BASED ATTRIBUTES FOR LAND-USE CLASSIFICATION OF URBAN ENVIRONMENTS”. en. In: *ISPRS - International Archives of the Photogrammetry, Remote Sensing and Spatial Information Sciences* XXXVIII-4/W19 (Sept. 2012), pp. 105–110. ISSN: 1682-1777. DOI: 10.5194/isprsarchives-XXXVIII-4-W19-105-2011. (Visited on 04/25/2016).

[31] T. Hermosilla et al. “Assessing contextual descriptive features for plot-based classification of urban areas”. In: *Landscape and Urban Planning* 106.1 (May 2012), pp. 124–137. ISSN: 0169-2046. DOI: 10.1016/j.landurbplan.2012.02.008. (Visited on 05/19/2016).

[32] Txomin Hermosilla. “Automatic building detection and land-use classification in urban areas using multispectral high-spatial resolution imagery and LiDAR data”. eng. In: *ELCVIA : Electronic Letters on Computer Vision and Image Analysis* 13.2 (2014), pp. 0004–6. URL: http://ddd.uab.cat/record/118703/ (visited on 05/19/2016).

[33] Arnis Siksna. “The effects of block size and form in North American and Australian city centres”. In: *Urban morphology* 1.1 (1997), pp. 19–33. URL: https://urlz.fr/975P.

[34] Cláudia Maria De Almeida et al. "GIS and remote sensing as tools for the simulation of urban land-use change". en. In: *International Journal of Remote Sensing* 26.4 (Feb. 2005), pp. 759–774. ISSN: 0143-1161, 1366-5901. DOI: 10.1080/01431160512331316865. (Visited on 05/27/2018).

[35] Mathias Bochow et al. "An automated and adaptable approach for characterizing and partitioning cities into urban structure types". In: *Proceedings of IGARSS 2010 conference*. IEEE, July 2010, pp. 1796–1799. ISBN: 978-1-4244-9565-8. DOI: 10.1109/IGARSS.2010.5652972. (Visited on 05/24/2018).

[36] Jamal Jokar Arsanjani et al., eds. *OpenStreetMap in GIScience*. Lecture Notes in Geoinformation and Cartography. Cham: Springer International Publishing, 2015. ISBN: 978-3-319-14280-7. DOI: 10.1007/978-3-319-14280-7. (Visited on 05/23/2018).

[37] Matamyo Simwanda and Yuji Murayama. "Integrating Geospatial Techniques for Urban Land Use Classification in the Developing Sub-Saharan African City of Lusaka, Zambia". en. In: *ISPRS International Journal of Geo-Information* 6.4 (Mar. 2017), p. 102. DOI: 10.3390/ijgi6040102. (Visited on 04/27/2017).

[38] Jeremiah J. Nieves et al. "Examining the correlates and drivers of human population distributions across low- and middle-income countries". en. In: *Journal of The Royal Society Interface* 14.137 (Dec. 2017), p. 20170401. ISSN: 1742-5689, 1742-5662. DOI: 10.1098/rsif.2017.0401.

[39] Frank Tanser, Peter Gething, and Peter Atkinson. "Location-allocation Planning". In: *A companion to health and medical geography*. Ed. by Tim Brown, Sara McLafferty, and Graham Moon. Blackwell companions to geography 8. Chichester, West Sussex, U.K. ; Malden, MA: Wiley-Blackwell, 2009. ISBN: 978-1-4051-7003-1. URL: http://doi.wiley.com/10.1002/9781444314762.ch28.

[40] Mohammad H. Vahidnia, Ali A. Alesheikh, and Abbas Alimohammadi. "Hospital site selection using fuzzy AHP and its derivatives". In: *Journal of Environmental Management* 90.10 (July 2009), pp. 3048–3056. ISSN: 03014797. DOI: 10.1016/j.jenvman.2009.04.010.

[41] Shams-ur Rahman and David K. Smith. "Use of location-allocation models in health service development planning in developing nations". en. In: *European Journal of Operational Research* 123.3 (June 2000), pp. 437–452. ISSN: 03772217. DOI: 10.1016/S0377-2217(99)00289-1.

[42] Sara L. McLafferty. "GIS and Health Care". In: *Annual Review of Public Health* 24.1 (Jan. 2003), pp. 25–42. ISSN: 0163-7525, 1545-2093. DOI: 10.1146/annurev.publhealth.24.012902.141012.

[43] Inuwa Barau et al. "Improving Polio Vaccination Coverage in Nigeria Through the Use of Geographic Information System Technology". en. In: *The Journal of Infectious Diseases* 210.suppl_1 (Nov. 2014), S102–S110. ISSN: 0022-1899, 1537-6613. DOI: 10.1093/infdis/jiu010.

[44] Doctor without border. *DRC: Saving lives with remote mapping*. July 7, 2016. URL: https://www.msf.org.uk/article/drc-saving-lives-with-remote-mapping.

[45] N. A. Wardrop et al. "Spatially disaggregated population estimates in the absence of national population and housing census data". en. In: *Proceedings of the National Academy of Sciences* 115.14 (Apr. 2018), pp. 3529–3537. ISSN: 0027-8424, 1091-6490. DOI: 10.1073/pnas.1715305115.

[46] Caroline Michellier et al. "Contextualizing vulnerability assessment: a support to geo-risk management in central Africa". In: *Natural Hazards* 82 (S1 May 2016), pp. 27–42. ISSN: 0921-030X, 1573-0840. DOI: 10.1007/s11069-016-2295-z.

[47] S. Wegscheider et al. "Generating tsunami risk knowledge at community level as a base for planning and implementation of risk reduction strategies". In: *Natural Hazards and Earth System Science* 11.2 (Feb. 1, 2011), pp. 249–258. ISSN: 1684-9981. DOI: 10.5194/nhess-11-249-2011.

[48] Gordon McGranahan, Deborah Balk, and Bridget Anderson. "The rising tide: assessing the risks of climate change and human settlements in low elevation coastal zones". en. In: *Environment and Urbanization* 19.1 (Apr. 2007), pp. 17–37. ISSN: 0956-2478, 1746-0301. DOI: 10.1177/0956247807076960.

[49] Pinki Mondal and Andrew J. Tatem. "Uncertainties in Measuring Populations Potentially Impacted by Sea Level Rise and Coastal Flooding". In: *PLoS ONE* 7.10 (Oct. 24, 2012). Ed. by Abdisalan Mohamed Noor, e48191. ISSN: 1932-6203. DOI: 10.1371/journal.pone.0048191.

[50] Sanjiv Kumar, Neeta Kumar, and Saxena Vivekadhish. "Millennium development goals (MDGS) to sustainable development goals (SDGS): Addressing unfinished agenda and strengthening sustainable development and partnership". en. In: *Indian Journal of Community Medicine* 41.1 (2016), p. 1. ISSN: 0970-0218. DOI: 10.4103/0970-0218.170955.

[51] Economic United Nations and Social Council. *Report of the inter-agency and expert group on sustainable development goal indicators (No. E/CN.3/2016/2/Rev.1).* 2016. URL: http://undocs.org/E/CN.3/2016/2/Rev.1.

[52] Diana M Liverman. "Geographic perspectives on development goals: Constructive engagements and critical perspectives on the MDGs and the SDGs". en. In: *Dialogues in Human Geography* 8.2 (July 2018), pp. 168–185. ISSN: 2043-8206, 2043-8214. DOI: 10.1177/2043820618780787.

[53] Mitchel Langford. "Rapid facilitation of dasymetric-based population interpolation by means of raster pixel maps". In: *Computers, Environment and Urban Systems* 31.1 (Jan. 2007), pp. 19–32. ISSN: 01989715. DOI: 10.1016/j.compenvurbsys.2005.07.005.

[54] Ming-Dawa Su et al. "Multi-layer multi-class dasymetric mapping to estimate population distribution". In: *Science of The Total Environment* 408.20 (Sept. 2010), pp. 4807–4816. ISSN: 00489697. DOI: 10.1016/j.scitotenv.2010.06.032.

[55] S. Openshaw. "The modifiable areal unit problem". In: *Concepts and Techniques in Modern Geography* (1984).

[56] Florence Fournet, Aude Meunier-Nikiema, and Gérard Salem. *Ouagadougou (1850-2004) : Une urbanisation différenciée*. Petit atlas urbain. Montpellier: IRD Éditions, 2008. 143 pp. URL: http://books.openedition.org/irdeditions/870.

[57] M. Langford and D. J. Unwin. "Generating and mapping population density surfaces within a geographical information system". In: *The Cartographic Journal* 31.1 (June 1994), pp. 21–26. ISSN: 0008-7041, 1743-2774. DOI: 10.1179/000870494787073718.

[58] Florent Bédécarrats, Jean-Pierre Cling, and François Roubaud. "Révolution des données et enjeux de la statistique en Afrique". fr. In: *Afrique contemporaine* 258.2 (2016), pp. 9–23. ISSN: 0002-0478. URL: https://urlz.fr/976w.

[59] Ehrlich and Lang. "Can Earth Observation help to improve information on population? Indirect Population Estimations from EO Derived Geo-Spatial Data: Contribution from GMOSS". In: *Remote Sensing from Space: Supporting International Peace and Security*. Springer Netherlands, 2009, pp. 211–237. DOI: 10.1007/978-1-4020-8484-3_14.

[60] Statistics Division. United Nations. *Census dates for all countries*. May 27, 2016. URL: https://unstats.un.org/unsd/demographic/sources/census/censusdates.htm.

[61] Pierre Vennetier. *Les villes d'Afrique tropicale*. 2. éd., revue et complétée. Collection géographie. Paris: Masson, 1991. ISBN: 978-2-225-82259-9.

[62] Alain Dubresson and Jean Pierre Raison. *L'Afrique subsaharienne: une géographie du changement*. 2e éd. entièrement mise à jour. Collection U. Géographie. Paris: A. Colin, 2003. ISBN: 978-2-200-26588-5.

[63] Shantayanan Devarajan. "Africa's Statistical Tragedy". en. In: *Review of Income and Wealth* 59.S1 (2013), S9–S15. ISSN: 1475-4991. DOI: 10.1111/roiw.12013.

[64] George E. P. Box and Norman Richard Draper. *Empirical model-building and response surfaces*. Wiley series in probability and mathematical statistics. New York: Wiley, 1987. ISBN: 978-0-471-81033-9.

[65] George E. P. Box, J. Stuart Hunter, and William Gordon Hunter. *Statistics for experimenters: design, innovation, and discovery*. 2nd ed. Wiley series in probability and statistics. Hoboken, N.J: Wiley-Interscience, 2005. ISBN: 978-0-471-71813-0.

[66] Cory L. Eicher and Cynthia A. Brewer. "Dasymetric mapping and areal interpolation: Implementation and evaluation". In: *Cartography and Geographic Information Science* 28.2 (2001), pp. 125–138. DOI: 10.1559/152304001782173727.

[67] Andrey Petrov. "One Hundred Years of Dasymetric Mapping: Back to the Origin". In: *The Cartographic Journal* 49.3 (Aug. 2012), pp. 256–264. ISSN: 0008-7041, 1743-2774. DOI: 10.1179/1743277412Y.0000000001.

[68] Jeremy Mennis and Torrin Hultgren. "Intelligent Dasymetric Mapping and Its Application to Areal Interpolation". en. In: *Cartography and Geographic Information Science* 33.3 (Jan. 2006), pp. 179–194. ISSN: 1523-0406, 1545-0465. DOI: 10.1559/152304006779077309.

[69] Jeremy Mennis. "Generating Surface Models of Population Using Dasymetric Mapping". In: *The Professional Geographer* 55.1 (Feb. 2003), pp. 31–42. ISSN: 0033-0124. DOI: 10.1111/0033-0124.10042.

[70] Jeremy Mennis. "Dasymetric Mapping for Estimating Population in Small Areas". en. In: *Geography Compass* 3.2 (Mar. 2009), pp. 727–745. ISSN: 1749-8198. DOI: 10.1111/j.1749-8198.2009.00220.x.

[71] Shuo-sheng Wu, Xiaomin Qiu, and Le Wang. "Population Estimation Methods in GIS and Remote Sensing: A Review". In: *GIScience & Remote Sensing* 42.1 (Mar. 2005), pp. 80–96. ISSN: 1548-1603, 1943-7226. DOI: 10.2747/1548-1603.42.1.80.

[72] Van Huyen Do, Christine Thomas-Agnan, and Anne Vanhems. "Spatial reallocation of areal data – another look at basic methods". en. In: *Revue d'Économie Régionale & Urbaine* mai.1 (June 2015), pp. 27–58. ISSN: 0180-7307. DOI: 10.3917/reru.151.0027.

[73] Filipe Batista e Silva, Javier Gallego, and Carlo Lavalle. "A high-resolution population grid map for Europe". en. In: *Journal of Maps* 9.1 (Mar. 2013), pp. 16–28. ISSN: 1744-5647. DOI: 10.1080/17445647.2013.764830. (Visited on 11/15/2017).

[74] Uwe Deichmann, Deborah Balk, and Greg Yetman. "Transforming population data for interdisciplinary usages: from census to grid". In: *Washington (DC): Center for International Earth Science Information Network* 200.1 (2001). URL: https://urlz.fr/977n.

[75] DL Balk et al. "Determining global population distribution: methods, applications and data". In: *Advances in parasitology* 62 (2006), pp. 119–156. DOI: 10.1016/S0065-308X(05)62004-0.

[76] Sergio Freire et al. "Development of new open and free multi-temporal global population grids at 250 m resolution". In: *Geospatial data in a changing world*. New York, NY: Springer Berlin Heidelberg, 2016. ISBN: 978-3-319-33782-1. URL: https://urlz.fr/977H.

[77] Christopher T. Lloyd, Alessandro Sorichetta, and Andrew J. Tatem. "High resolution global gridded data for use in population studies". In: *Scientific Data* 4 (Jan. 2017), p. 170001. ISSN: 2052-4463. DOI: 10.1038/sdata.2017.1.

[78] Jerome E Dobson et al. "LandScan: a global population database for estimating populations at risk". In: *Photogrammetric engineering and remote sensing* 66.7 (2000), pp. 849–857. URL: https://urlz.fr/977Q.

[79] Forrest R Stevens et al. "Disaggregating census data for population mapping using random forests with remotely-sensed and other ancillary data". In: *Plos One* (Feb. 2015). DOI: 10.1371/journal.pone.0107042.

[80] Derek Azar et al. "Generation of fine-scale population layers using multi-resolution satellite imagery and geospatial data". en. In: *Remote Sensing of Environment* 130 (Mar. 2013), pp. 219–232. ISSN: 00344257. DOI: 10.1016/j.rse.2012.11.022. (Visited on 08/20/2015).

[81] Waldo R. Tobler. "Smooth pycnophylactic interpolation for geographical regions". In: *Journal of the American Statistical Association* 74.367 (1979), pp. 519–530. DOI: 10.1080/01621459.1979.10481647.

[82] Alexis Comber, Chris Proctor, and Steve Anthony. "A combined pycnophylactic - dasymetric method for disaggregating spatial data: the example of agricultural land use". In: *Proceedings of the Geographical Information Science Research UK Conference, National Centre for Geocomputation, National University of Ireland: Maynooth*. Citeseer, 2007, pp. 445–450. URL: https://urlz.fr/9786.

[83] Tobias Lung et al. "Human population distribution modelling at regional level using very high resolution satellite imagery". en. In: *Applied Geography* 41 (July 2013), pp. 36–45. ISSN: 01436228. DOI: 10.1016/j.apgeog.2013.03.002.

[84] Yann Forget et al. "Complementarity Between Sentinel-1 and Landsat 8 Imagery for Built-Up Mapping in Sub-Saharan Africa". In: *Preprints* (Oct. 2018). DOI: 10.20944/preprints201810.0695.v1.

[85] Taïs Grippa et al. "Improving Urban Population Distribution Models with Very-High Resolution Satellite Information". en. In: *Data* 4.1 (Jan. 2019), p. 13. ISSN: 2306-5729. DOI: 10.3390/data4010013. (Visited on 01/17/2019).

[86] Monya Baker. "1,500 scientists lift the lid on reproducibility". In: *Nature* 533.7604 (May 2016), pp. 452–454. ISSN: 0028-0836, 1476-4687. DOI: 10.1038/533452a.

[87] Erin C McKiernan et al. "How open science helps researchers succeed". en. In: *eLife* 5 (July 2016). ISSN: 2050-084X. DOI: 10.7554/eLife.16800. URL: https://elifesciences.org/articles/16800 (visited on 03/08/2019).

[88] Andreas Neuhold. *Open Science - Principles*. URL: https://commons.wikimedia.org/w/index.php?curid=33542838.

[89] Oscar Brousse et al. "Using Local Climate Zones in Sub-Saharan Africa to tackle urban health issues". en. In: *Urban Climate* 27 (Mar. 2019), pp. 227–242. ISSN: 22120955. DOI: 10.1016/j.uclim.2018.12.004.

[90] Benjamin Beaumont et al. "Toward an operational framework for fine-scale urban land-cover mapping in Wallonia using submeter remote sensing and ancillary vector data". In: *Journal of Applied Remote Sensing* 11.3 (Aug. 19, 2017), p. 1. ISSN: 1931-3195. DOI: 10.1117/1.JRS.11.036011.

[91] Kevin McGarigal, Sermin Tagil, and Samuel A. Cushman. "Surface metrics: an alternative to patch metrics for the quantification of landscape structure". In: *Landscape Ecology* 24.3 (Mar. 2009), pp. 433–450. ISSN: 1572-9761. DOI: 10.1007/s10980-009-9327-y. URL: https://doi.org/10.1007/s10980-009-9327-y.